New Approaches to the Chemotherapy of Glioblastoma: investigations on doxorubicin nanoparticles, inhibition of PDGF receptors and kinesin Eg5, with emphasis on confocal laser-scanning microscopy

Dissertation

zur Erlangung des Doktorgrades der Naturwissenschaften (Dr. rer. nat.)

der Naturwissenschaftlichen Fakultät IV - Chemie und Pharmazie -

der Universität Regensburg

vorgelegt von

Dietmar Gross

aus Schwäbisch Gmünd

2006

Die vorliegende Arbeit entstand in der Zeit von Juli 2002 bis August 2006 unter der Leitung von Herrn Prof. Dr. A. Buschauer sowie von Herrn Prof. Dr. G. Bernhardt am Institut für Pharmazie der Naturwissenschaftlichen Fakultät IV - Chemie und Pharmazie - der Universität Regensburg.

Das Promotionsgesuch wurde eingereicht im August 2006.

Tag der mündlichen Prüfung: 24. August 2006.

Prüfungsausschuss:

Prof. Dr. O. Reiser (Vorsitzender)
Prof. Dr. A. Buschauer (Erstgutachter)
Prof. Dr. G. Bernhardt (Zweitgutachter)
Prof. Dr. S. Elz (Drittprüfer)

Für meine Eltern

“It is easier to work hard, than to undo the testimony of laziness.”

J. Bachmann

Mein Dank geht an:

Herrn Prof. Dr. A. Buschauer, für das Ermöglichen dieser Arbeit in seinem Arbeitskreis, für sein großes Engagement in der Förderung meiner Arbeit, für seine stetige persönliche Unterstützung und sein stets offenes Ohr für alle vorgebrachten Anliegen während der Promotionszeit.

Herrn Prof. Dr. G. Bernhardt, für seine wissenschaftliche Anleitung, für seine Anregungen und auch für konstruktive Kritik, sowie für seine ständige und geduldige Hilfsbereitschaft bei vielen Problemstellungen der täglichen Laborarbeit.

Herrn Prof. Dr. J. Kreuter (Universität Frankfurt) und seinen Mitarbeitern, für die Bereitstellung der PBCA Nanopartikel und damit verbundener Messdaten, sowie für die wissenschaftliche Zusammenarbeit.

Herrn Prof. Dr. A. Giannis (Universität Leipzig) und seinen Mitarbeitern, für die Bereitstellung der Monastrol-Analoga, sowie für die wissenschaftliche Zusammenarbeit.

Herrn Prof. Dr. F. Böhmer (Universität Jena), für das Bereitstellen der Swiss 3T3 Zellen, sowie Herrn Dr. R. Gastpar (Klinikum der Universität Regensburg), für das Bereitstellen der K-562 Zellen.

Herrn Prof. Dr. A. Göpferich und seinen Mitarbeitern, für die Bereitstellung von Messgeräten, insbesondere des Konfokalmikroskops.

Herrn Prof. Dr. O. Wolfbeis und seinen Mitarbeitern, sowohl für die Bereitstellung des Aminco Bowman Fluorimeters, als auch für die wissenschaftliche Beratung.

Herrn O. Merkel, Herrn Dr. C. Lottner, sowie Herrn Dr. C. Scherübl, für das Bereitstellen von Lokalisationsvektoren und Fluoreszenzfarbstoffen.

Frau S. Bollwein für die Einweisung in Zellkulturarbeiten, für die Durchführung der Mykoplasmentests, sowie für die Durchführung von Chemosensitivitätstests.

Frau E. Schreiber, für die Hilfe und Beratung bei der Durchführung von Kalzium-Assays, für die Mitbetreuung von Zellkulturen, sowie für die angenehme Laborgesellschaft über einen wesentlichen Teil der Promotionsdauer.

Frau S. Heinrich, Frau M. Luginger und Herrn P. Richthammer, die durch ihre Hilfe bei Organisation und bei der Lösung von technischen Problemen meine Arbeit oft wesentlich erleichtert haben.

Herrn Dr. R. Ziemek und Frau E. Hofinger, für ihre beratende Unterstützung bei gentechnischen Arbeiten, an Frau C. Müller und Frau Dr. M. Hubensack, für die Unterstützung und Durchführung von Calcein-AM- sowie Mitoxantron-Assays, sowie an Herrn H. Preuss, für seine Hilfe bei der Bearbeitung und Erstellung von Molekül-Darstellungen.

Meinen Studienkollegen Herrn Dr. E. Schneider, der mir in mannigfacher Hinsicht eine wissenschaftliche sowie persönliche Unterstützung über die gesamte Dauer der Promotion gewesen ist.

Alle meine Kollegen, für ihre Geduld, die sie manchmal im Umgang mit mir aufbringen mussten.

Weiterhin geht mein besonderer Dank an:

Meinen Labor- und Studienkollegen Herrn Peter Jarzyna, der den Laboralltag auf seine ganz persönliche Art nie hat langweilig werden lassen, und mir oft mit Rat zur Seite gestanden hat.

Meinen Studienkollegen Herrn Dr. Marc Kunze, der mir in der Promotionszeit stets eine wichtige persönliche Stütze war.

Meinen Studienkollegen Herrn Christian Becker, der meinen Laboralltag oft aufgehellt hat.

Frau Nathalie Pop, die mir insbesondere im letzten Abschnitt der Promotion ein Licht im Universitätsalltag gewesen ist.

Mister and Misses Keith Klaus, Mister and Misses John Radank, and Mister and Misses Erick Elkins, for their help in personal and spiritual growth (Pr 27:17).

Meine Familie, die mich während der Promotionszeit beständig und selbstlos getragen und unterstützt hat.

Miss Stefanie S. Pappas. Her love kept me going through all highs and lows.

Abstracts and Publications

Results of this work were in part published or presented as posters or short lecture prior to submission of the thesis:

Publications:

- Gross D, Bernhardt G and Buschauer A (**2005**). Platelet-derived growth factor receptor independent proliferation of human glioblastoma cells. *Turkish Journal of Cancer* **35**: 40-49 (Poster abstract).

- Müller C, Gross D, Sarli V, Gartner M, Giannis A, Bernhardt G and Buschauer A (**2006**). Inhibitors of kinesin Eg5: antiproliferative activity of monastrol analogues against human glioblastoma cells. *Cancer Chemother Pharmacol.*

- Gross D, Bernhardt G and Buschauer A (**2006**). Platelet-derived growth factor receptor independent proliferation of human glioblastoma cells: selective tyrosine kinase inhibitors lack antiproliferative activity. *J Cancer Res Clin Oncol* **132**: 589-99.

Posters and short lecture:

- Annual Meeting of the German Pharmaceutical Society (DPhG) in Regensburg, October 6-8, **2004:** Platelet-Derived Growth Factor Receptor Mediated Proliferation of Human Glioblastoma Cells: Imatinib lacks Antiproliferative Activity (Poster contribution).

- European High-Grade Glioma Meeting Regensburg, February 25–26, **2005**: Platelet-Derived Growth Factor Receptor Independent Proliferation of Human Glioblastoma Cells (Short lecture).

- Annual Meeting of the German Pharmaceutical Society (DPhG) in Mainz, October 5-8, **2005**: Monoaster Formation in Human Glioblastoma Cells: Investigations on New Monastrol Derivatives (Poster contribution).

Contents

Chapter 1
General Introduction

1.1 Primary malignant brain tumors

Primary malignant brain tumors originate in the brain itself. They often spread into other sites in the central nervous system, such as the spinal cord, but rarely metastasize to other parts of the body. These tumors show a high biological diversity, and can be named and classified according to the normal brain tissue from which they have derived. A major part of all primary brain tumors are collectively known as gliomas. They are malignant forms of glial cells, which primarily constitute the connective and supportive tissue in the central nervous system. Several glial cell types are known from which gliomas can derive:

- Astrocytomas are primary brain tumors derived from astrocytes, which serve supportive functions for nerve cells, and their foot processes encapsulate the brain capillaries.
- Oligodendrogliomas originate from oligodendrocytes, which surround nerve cells and thereby provide a protective coating. Pure oligodendrogliomas however are rare, and in most cases malignant oligodendroglioma cells occur in mixed gliomas.
- Ependymomas are derived from ependymal cells. These cells line the brain ventricles and the central canal of the spinal cord.
- Mixed gliomas consist of a mixture of different malignant glioma cells, mostly malignant oligodendrocytes and astrocytes.

In adults astrocytomas amount to about 75 % of all primary malignant brain tumors. The most commonly used World Health Organization (WHO) classification system for astrocytomas distinguishes four different grades, whereas three of them are considered as malignant tumors. The grade I tumors break ranks, due to their low incidence of brain infiltration and distant spreading. The other grades comprise the low-grade astrocytomas (WHO grade II), anaplastic astrocytomas (WHO grade III), and glioblastomas (WHO grade IV). By now, the survival of patients with WHO grade II–IV gliomas is poor, despite various multimodal clinical treatment approaches. According to the Central Brain Tumor Registry of the United States, the 5-year survival rate for anaplastic astrocytoma is 29.7 %, and 3.4 % for glioblastoma (Central Brain Tumor Registry of the United States 2004).

1.2 Biological peculiarities of astrocytomas

Astrocytomas can infiltrate normal brain tissue, and thus even extensive resections are unlikely to eradicate the entire malignant tissue. Burger et al. disclosed a great variability in the geometry, extent, and character of the peripheral infiltrating margin of glioblastomas (Burger et al. 1988). The regional histological heterogeneity within each tumor poses a diagnostic problem. In many cases the first diagnosis from the biopsy has to be changed when the tumors have been removed by resection (Jackson et al. 2001). Furthermore, when a low-grade glioma is diagnosed, transformation to another, higher malignant grade is very probable. Nigro et al. ascribed this to a progressive genetic instability, linked to the loss of chromosome 10 in the tumor cells (Nigro et al. 2005).

The further detailed genetic profiling of tumors, using gene expression arrays, is currently evaluated in order to establish a molecular classification system as shown for an epidermal growth factor receptor-associated molecular signature in glioblastoma multiforme (Mischel et al. 2003). This approach may also provide the basis for a more accurate and histology-independent classification system in the future. Freije et al. reported on a list of 44 genes, which reliably classify gliomas into previously unrecognized biological and prognostic groups, and revealed heterogeneity of tumors and prognosis-related gene expression (Freije et al. 2004). Fig. 1-1 gives an overview of the most frequent genetic abnormalities in astocytomas, reviewed by Gonzalez and Gilbert (Gonzalez and Gilbert 2005). The genetic profiling and molecular analysis of tumors is suggested to allow optimized individual

treatment. Generally, tumor treatment can include tumor resection, radiation treatment, and chemotherapy.

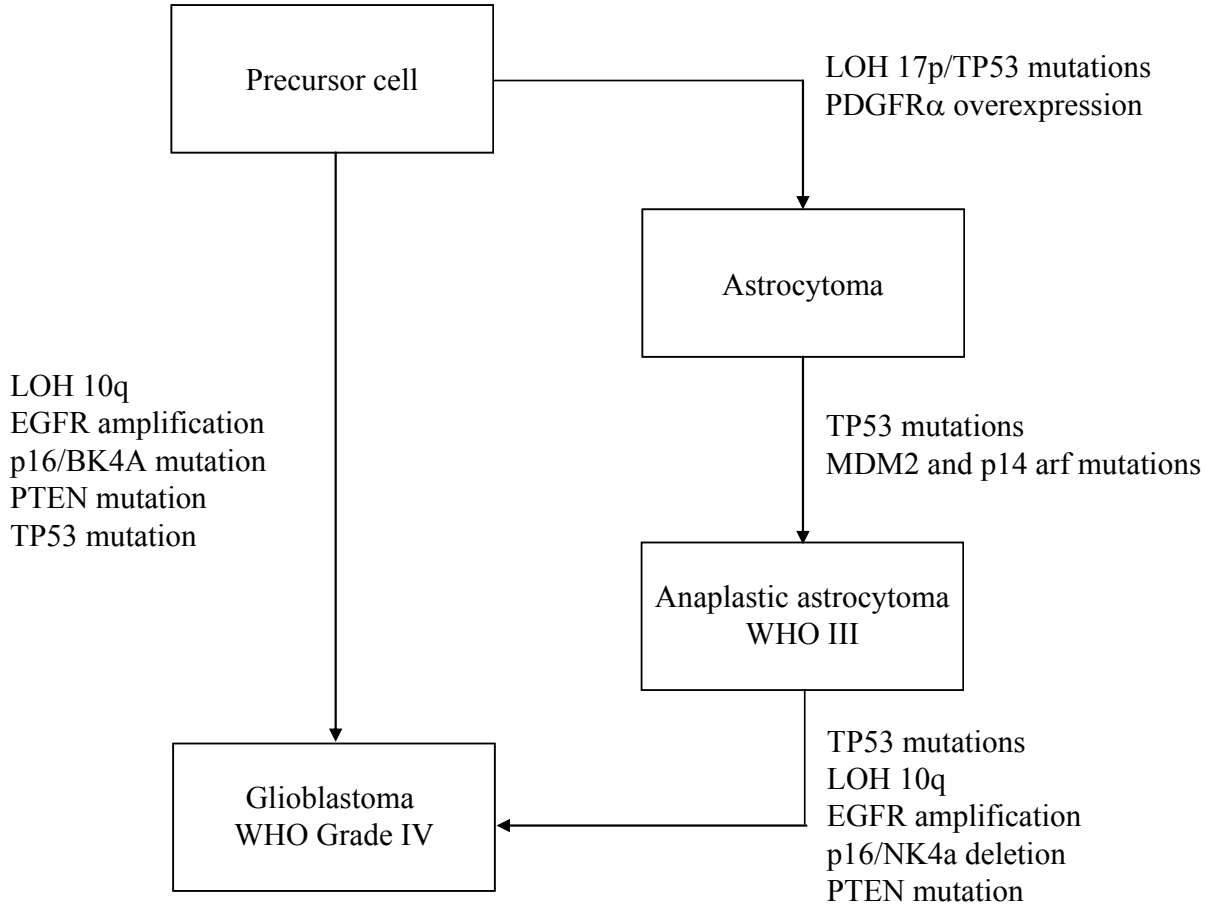

Figure 1-1: Pathways from normal precursor cells to gliomas. Several genetic abnormalities have been associated with the development of glioblastoma via different WHO grades, or by direct transformation into WHO grade IV (from Gonzalez et al. 2005, modified).

1.3 Tumor resection

Surgical resection can achieve rapid symptom control, which is of primary relevancy for patients with large tumors, causing life-threatening situations. Moreover, resection provides tissue for histological diagnosis. Even though a complete eradication of the tumor is rather unlikely, extensive tumor resection has an impact on survival. As reported by Lacroix et al., a significant advantage in patients' survival was associated with the resection of 98 % or more of the tumor volume (median survival of 13 months) compared to resections of less than 98 % (median survival of 8.8 months) (Lacroix et al. 2001). However, in many cases surgical

removal to the abovementioned extent is not possible due to the highly invasive growth of the tumor.

1.4 Irradiation

Nearly all treatment regimens for newly diagnosed tumors include radiation treatment. It represents one of the most effective forms of treatment for gliomas. Also the postoperative radiation therapy plays an important role in patients´ survival. This has been shown in several studies, e.g. for anaplastic astrocytoma (Walker et al. 1978) and for glioblastoma multiforme patients (Deutsch et al. 1989). The optimal radiation dose is estimated as 60 Gy, whereas a further increase in the dose does not appear to provide any additional benefit (Nelson et al. 1988). Hyperfractionation of the dose does not improve the outcome significantly, as shown in patients suffering from WHO grade III and grade IV tumors (Ludgate et al. 1988).

Another variant in radiotherapy involves the use of radiosensitizers, chemotherapeutic agents, which are supposed to increase the sensitivity of the tumors against radiation. Several compounds have been evaluated for this therapeutic purpose, e.g. misonidazole (Huncharek 1998; Prados et al. 1999), carmustin (BCNU), lomustin (CCNU), and vincristine, with or without bromdesoxyuridine (Prados et al. 1999). To date, no clear clinical benefit compared to the standard radiation regimen has been demonstrated. The stereotactic radiosurgery (SRS) also has been considered as a promising treatment approach. However, a study by Souhami et al. revealed that SRS, followed by conventional radiation therapy in combination with BCNU, showed no improved outcome in the treated glioblastoma multiforme patients (Souhami et al. 2004). Finally, the interstitial brachytherapy of glioma has been evaluated, also with no decisive success. Laperriere et al. concluded from their studies with stereotactic radiation implants, that this approach does not provide a statistically significant improvement in survival in the initial management of patients with malignant astrocytoma (Laperriere et al. 1998).

1.5 Chemotherapy

The treatment of malignant gliomas with pharmacologically active compounds has been studied for several decades, and up to now no curative chemotherapy for malignant gliomas exists. Due to the poor penetration from the blood to the brain after systemic administration, the choice of applicable chemotherapeutic agents for the therapy of malignant brain tumors is

limited to a few compounds. Amongst them are the alkylating nitrosoureas carmustin (BCNU), lomustine (CCNU), procarbazine, and temozolomide. Most of the present chemotherapy regimens are involved in adjuvant therapy after tumor resection or irradiation therapy.

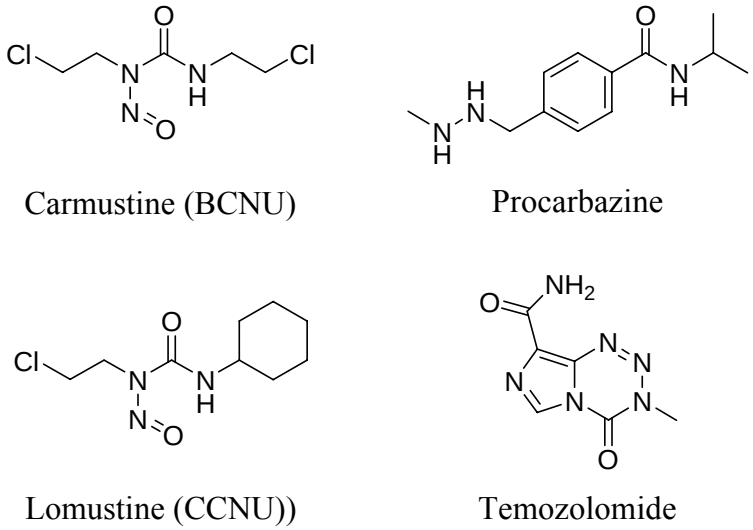

Figure 1-2: Structures of carmustine, lomustine, procarbazine and temozolomide.

Since 1970 several randomized trials have been conducted on the combined radiotherapy and chemotherapy. Some studies failed to demonstrate a significant increase in survival when chemotherapy was added to radiation treatment (Walker et al. 1978; Walker et al. 1980; Medical Research Council Brain Tumor Working party 2001). However, meta-analysis of several randomized clinical trials demonstrated some benefit for the adjuvant chemotherapy. Fine et al. used the results from 16 randomized clinical trials and reported on an absolute increase in patients survival of 10.1 % at 1 year and 8.6 % at 2 years after treatment with combined radiation and chemotherapy (Fine et al. 1993). Another meta-analysis with the data from 12 randomized controlled trials was performed by Stewart (Stewart 2002). The results showed a significant increase of 6 % in the 1-year survival, and an increase of two months in the median survival. Despite the positive results from the meta-analysis, individual trials failed to provide a significant therapeutic advantage. As mentioned in a review on the treatment of astrocytomas by Gonzalez and Gilbert (Gonzalez and Gilbert 2005), much of the controversy on the administration of adjuvant chemotherapy was the concern about toxic side effects associated with the use of nitrosoureas in classical adjuvant chemotherapy.

1.5.1 Temozolomide

The introduction of the alkylating agent temozolomide (Temodal®) renewed the interest in chemotherapy for glioma treatment, especially due to its almost 100 % oral bioavailability and its ability to pass the blood-brain barrier (BBB). Ostermann et al. reported on a cerebrospinal fluid concentration of temozolomide of 20 % of the plasma concentration in patients with newly diagnosed or recurrent glioma (Ostermann et al. 2004). In a phase II trial with patients suffering from recurrent glioblastoma at first relapse, temozolomide was compared to procarbazine (Yung et al. 2000). A significantly improved progression-free survival (PFS) rate at 6 months was observed for temozolomide (21 % versus 8 % with procarbazine treatment). Moreover the median PFS was increased (12.4 versus 8.3 weeks), and a higher 6-month survival rate was observed (60 % versus 44 %). Despite a current lack of a direct clinical comparison temozolomide has largely replaced the nitrosoureas in the treatment primary malignant brain tumors, and is considered as the mainstay of chemotherapy of high-grade gliomas. A recent study showed that the combined irradiation and temozolomide treatment in newly diagnosed glioblastoma multiforme patients improved median survival by 3 months, compared to radiotherapy alone, with acceptable levels of severe side effects (Stupp et al. 2005). The results from these trials were encouraging, since no single chemotherapeutic agent has demonstrated an improvement in patients survival to such an extent before. The use of temozolomide in the chemotherapy of brain tumors has been reviewed in detail by van den Bent et al. (van den Bent et al. 2006).

Table 1-1: Median 1- and 2-year survival of patients with high-grade glioma after various postoperative adjuvant treatment (from van den Bent et al. 2006, modified).

Reference	Treatment	Median survival	1-year survival (%)	2-year survival (%)
Walker et al. 1987	Supportive care	3 mo	3	0
	BCNU	4 mo	12	0
	RT	8 mo	24	1
	RT + BCNU	8 mo	32	5
Glioma Meta-analysis Trialists Group 2002	RT		40	15
	RT + CTX		46	20
EORTC 26981	RT	12 mo	51	10
Stupp et al. 2005	RT + temozolomide	15 mo	61	27

RT: radiotherapy; CT: chemotherapy; BCNU: carmustine; mo: months

1.5.2 Modulation of O^6-methylguanine-DNA methyltransferase

Since temozolomide produces cytotoxicity by methylation of DNA (O^6-methylation of guanine), the activity of DNA repair mechanisms has been suggested to stand against temozolomide efficacy, and may cause poor response to temozolomide treatment. Especially the O^6-methylguanine-DNA methyltransferase (MGMT) represents the most important and clinically relevant resistance mechanism. Friedman et al. found a significant negative correlation between the MGMT expression in newly diagnosed glioblastoma, and the response to temozolomide treatment (Friedman et al. 1998). Similar results were reported on the relationship between the intracellular MGMT concentration, estimated by immunohistochemistry and the response to BCNU (Esteller et al. 2000). Moreover, Esteller et al. showed that hypermethylation of the MGMT gene promoter inhibits the transcription and finally MGMT synthesis (Esteller et al. 1999). Two studies published by Hegi et al. (Hegi et al. 2004; Hegi et al. 2005) demonstrated a clear relationship between the methylation status of the MGMT promoter, MGMT expression, response to chemotherapy, and clinical outcome. Especially in the study from 2005, the 2-year survival rate was 46 % in patients with MGMTpromotor hypermethylation, compared to 2 % in patients suffering from tumors with unmethylated MGMT-promoter. Due to the results from these studies, the modulation of MGMT activity has been investigated in order to enhance response to chemotherapeutic treatment with alkylating agents. A specific MGMT-inhibitor, O^6-benzylguanine (O6BG), was demonstrated to almost quantitatively suppress MGMT activity in gliomas (Friedman et al. 1998). After phase I dose evaluation for the combined treatment with BCNU and O6BG (Friedman et al. 2000) a first phase II study was performed in patients with progressive or recurrent malignant glioma, resistant to nitrosourea treatment. However, none of the 18 patients showed a partial or complete response (Quinn et al. 2002). By now, another clinical phase II trial is recruiting patients for the evaluation of this concept in recurrent childhood brain stem gliomas and recurrent childhood brain tumors (US National Institutes of Health 2006).

1.5.3 Inhibitors of signal transduction

Since up to now temozolomide is the only single agent with promising efficacy in the treatment of high-grade gliomas, there is great interest in the identification of new targets for pharmacotherapy, such as particular elements of signal transduction pathways. Currently,

several signal transduction inhibitors are subject to clinical evaluation, e.g. the epidermal growth factor receptor (EGFR) inhibitor gefitinib (Iressa®). As reviewed by Halatsch et al. preclinical data strongly supported that the inhibition of the EGFR tyrosine kinase by gefitinib might be an attractive approach to the chemotherapy of gliomas (Halatsch et al. 2006). However, the data from phase I and phase II clinical trials of gefitinib appear to conflict the promising preclinical experiences. Treatment with gefitinib was generally well tolerated, but in two phase II single agent therapy trials patients with newly diagnosed glioblastoma multiforme (Uhm 2004) and patients with recurrant glioblastoma (Rich et al. 2004) failed to objective response. In contrast, in another phase I/II trial application of gefitinib led to response in patients with recurrent glioma which had progressed after radiotherapy. However, the observed response was not accompanied by an increase in the progression-free survival compared with historical controls (Lieberman 2004). Despite these rather disappointing results, another phase I/II trial of gefitinib, in combination with radiotherapy in patients with newly diagnosed glioblastoma multiforme is ongoing (US National Institutes of Health 2006).

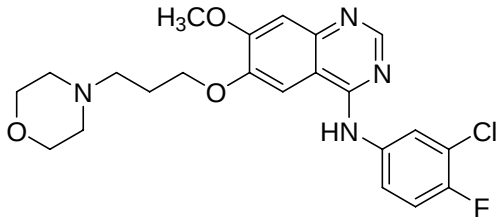

Gefitinib (Iressa®)

Figure 1-3: Structure of the EGFR tyrosine kinase inhibitor gefitinib.

1.6 Summary

Taken together, after more than three decades of intensive research efforts the median survival of 12 to 15 months in glioma patients has not changed markedly since the introduction of radiation therapy, and an effective chemotherapy regimen for glioblastoma multiforme does not exist. Despite advances in surgery, irradiation treatment, and some advances in chemotherapy, only modest therapy improvements were achieved, and no improved long-term survival for most patients with malignant glioma was accomplished. Among the recent clinical therapy approaches, only the combined therapy of temozolomide and radiation treatment produced encouraging clinical results in long term survival of patients suffering from malignant glioma. Furthermore, the identification of biological peculiarities of

gliomas and advances in the techniques to discover and to study genetic alterations may provide new opportunities in the development of more effective treatment in the future, and eventually may allow individualized treatment of patients.

There is still a great need to develop new therapy approaches, including the evaluation of new potential pharmacological targets, and new classes of pharmacologically active compounds, capable of penetrating into the brain after standard drug administration. Furthermore, since the expression of drug resistance-mediating proteins at the BBB (such as the p-glycoprotein 170) causes poor penetration of many registered anticancer drugs from the blood to the brain, new approaches to the overcome of the BBB and of the drug-resistance mechanisms are of particular interest in order to enlarge the variety of applicable anticancer drugs in the treatment of malignant brain tumors.

Bibliography

Burger P C, Heinz E R, Shibata T and Kleihues P (1988). Topographic anatomy and CT correlations in the untreated glioblastoma multiforme. *J Neurosurg* **68**: 698-704.

Central Brain Tumor Registry of the United States (2004). Statistical Report: primary brain tumors in the United States, 1997-2001.

Deutsch M, Green S B, Strike T A, Burger P C, Robertson J T, Selker R G, Shapiro W R, Mealey J, Jr., Ransohoff J, 2nd, Paoletti P and et al. (1989). Results of a randomized trial comparing BCNU plus radiotherapy, streptozotocin plus radiotherapy, BCNU plus hyperfractionated radiotherapy, and BCNU following misonidazole plus radiotherapy in the postoperative treatment of malignant glioma. *Int J Radiat Oncol Biol Phys* **16**: 1389-96.

Esteller M, Garcia-Foncillas J, Andion E, Goodman S N, Hidalgo O F, Vanaclocha V, Baylin S B and Herman J G (2000). Inactivation of the DNA-repair gene MGMT and the clinical response of gliomas to alkylating agents. *N Engl J Med* **343**: 1350-4.

Esteller M, Hamilton S R, Burger P C, Baylin S B and Herman J G (1999). Inactivation of the DNA repair gene O6-methylguanine-DNA methyltransferase by promoter hypermethylation is a common event in primary human neoplasia. *Cancer Res* **59**: 793-7.

Fine H A, Dear K B, Loeffler J S, Black P M and Canellos G P (1993). Meta-analysis of radiation therapy with and without adjuvant chemotherapy for malignant gliomas in adults. *Cancer* **71**: 2585-97.

Freije W A, Castro-Vargas F E, Fang Z, Horvath S, Cloughesy T, Liau L M, Mischel P S and Nelson S F (2004). Gene expression profiling of gliomas strongly predicts survival. *Cancer Res* **64**: 6503-10.

Friedman H S, McLendon R E, Kerby T, Dugan M, Bigner S H, Henry A J, Ashley D M, Krischer J, Lovell S, Rasheed K, Marchev F, Seman A J, Cokgor I, Rich J, Stewart E, Colvin O M, Provenzale J M, Bigner D D, Haglund M M, Friedman A H and Modrich P L (1998). DNA mismatch repair and O6-alkylguanine-DNA alkyltransferase analysis and response to Temodal in newly diagnosed malignant glioma. *J Clin Oncol* **16**: 3851-7.

Friedman H S, Pluda J, Quinn J A, Ewesuedo R B, Long L, Friedman A H, Cokgor I, Colvin O M, Haglund M M, Ashley D M, Rich J N, Sampson J, Pegg A E, Moschel R C, McLendon R E, Provenzale J M, Stewart E S, Tourt-Uhlig S, Garcia-Turner A M, Herndon J E, 2nd, Bigner D D and Dolan M E (2000). Phase I trial of carmustine plus O6-benzylguanine for patients with recurrent or progressive malignant glioma. *J Clin Oncol* **18**: 3522-8.

Gonzalez J and Gilbert M R (2005). Treatment of astrocytomas. *Curr Opin Neurol* **18**: 632-8.

Halatsch M E, Schmidt U, Behnke-Mursch J, Unterberg A and Wirtz C R (2006). Epidermal growth factor receptor inhibition for the treatment of glioblastoma multiforme and other malignant brain tumours. *Cancer Treat Rev* **32**: 74-89.

Hegi M E, Diserens A C, Godard S, Dietrich P Y, Regli L, Ostermann S, Otten P, Van Melle G, de Tribolet N and Stupp R (2004). Clinical trial substantiates the predictive value of O-6-methylguanine-DNA methyltransferase promoter methylation in glioblastoma patients treated with temozolomide. *Clin Cancer Res* **10**: 1871-4.

Hegi M E, Diserens A C, Gorlia T, Hamou M F, de Tribolet N, Weller M, Kros J M, Hainfellner J A, Mason W, Mariani L, Bromberg J E, Hau P, Mirimanoff R O, Cairncross J G, Janzer R C and Stupp R (2005). MGMT gene silencing and benefit from temozolomide in glioblastoma. *N Engl J Med* **352**: 997-1003.

Huncharek M (1998). Meta-analytic re-evaluation of misonidazole in the treatment of high grade astrocytoma. *Anticancer Res* **18**: 1935-9.

Jackson R J, Fuller G N, Abi-Said D, Lang F F, Gokaslan Z L, Shi W M, Wildrick D M and Sawaya R (2001). Limitations of stereotactic biopsy in the initial management of gliomas. *Neuro-oncol* **3**: 193-200.

Lacroix M, Abi-Said D, Fourney D R, Gokaslan Z L, Shi W, DeMonte F, Lang F F, McCutcheon I E, Hassenbusch S J, Holland E, Hess K, Michael C, Miller D and Sawaya R (2001). A multivariate analysis of 416 patients with glioblastoma multiforme: prognosis, extent of resection, and survival. *J Neurosurg* **95**: 190-8.

Laperriere N J, Leung P M, McKenzie S, Milosevic M, Wong S, Glen J, Pintilie M and Bernstein M (1998). Randomized study of brachytherapy in the initial management of patients with malignant astrocytoma. *Int J Radiat Oncol Biol Phys* **41**: 1005-11.

Lieberman F S, Cloughesy, T., Fine, H., Kuhn, J., Lamborn, K., Malkin, M., Robbins, H. I., Yung, W. A., Wen, P., Prados, M. (2004). NABTC phase I/II trial of ZD-1839 for recurrent malignant gliomas and unresectable meningiomas. *J Clin Oncol* **22**: 1510.

Ludgate C M, Douglas B G, Dixon P F, Steinbok P, Jackson S M and Goodman G B (1988). Superfractionated radiotherapy in grade III, IV intracranial gliomas. *Int J Radiat Oncol Biol Phys* **15**: 1091-5.

Medical Research Council Brain Tumor Working party (2001). Randomized trial of procarbazine, lomustine, and vincristine in the adjuvant treatment of high-grade astrocytoma: a Medical Research Council trial. *J Clin Oncol* **19**: 509-18.

Mischel P S, Shai R, Shi T, Horvath S, Lu K V, Choe G, Seligson D, Kremen T J, Palotie A, Liau L M, Cloughesy T F and Nelson S F (2003). Identification of molecular subtypes of glioblastoma by gene expression profiling. *Oncogene* **22**: 2361-73.

Nelson D F, Diener-West M, Horton J, Chang C H, Schoenfeld D and Nelson J S (1988). Combined modality approach to treatment of malignant gliomas--re-evaluation of RTOG 7401/ECOG 1374 with long-term follow-up: a joint study of the Radiation Therapy Oncology Group and the Eastern Cooperative Oncology Group. *NCI Monogr*: 279-84.

Nigro J M, Misra A, Zhang L, Smirnov I, Colman H, Griffin C, Ozburn N, Chen M, Pan E, Koul D, Yung W K, Feuerstein B G and Aldape K D (2005). Integrated array-comparative genomic hybridization and expression array profiles identify clinically relevant molecular subtypes of glioblastoma. *Cancer Res* **65**: 1678-86.

Ostermann S, Csajka C, Buclin T, Leyvraz S, Lejeune F, Decosterd L A and Stupp R (2004). Plasma and cerebrospinal fluid population pharmacokinetics of temozolomide in malignant glioma patients. *Clin Cancer Res* **10**: 3728-36.

Prados M D, Scott C, Sandler H, Buckner J C, Phillips T, Schultz C, Urtasun R, Davis R, Gutin P, Cascino T L, Greenberg H S and Curran W J, Jr. (1999). A phase 3 randomized study of radiotherapy plus procarbazine, CCNU, and vincristine (PCV) with or without BUdR for the treatment of anaplastic astrocytoma: a preliminary report of RTOG 9404. *Int J Radiat Oncol Biol Phys* **45**: 1109-15.

Quinn J A, Pluda J, Dolan M E, Delaney S, Kaplan R, Rich J N, Friedman A H, Reardon D A, Sampson J H, Colvin O M, Haglund M M, Pegg A E, Moschel R C, McLendon R E, Provenzale J M, Gururangan S, Tourt-Uhlig S, Herndon J E, 2nd, Bigner D D and Friedman H S (2002). Phase II trial of carmustine plus O(6)-benzylguanine for patients with nitrosourea-resistant recurrent or progressive malignant glioma. *J Clin Oncol* **20**: 2277-83.

Rich J N, Reardon D A, Peery T, Dowell J M, Quinn J A, Penne K L, Wikstrand C J, Van Duyn L B, Dancey J E, McLendon R E, Kao J C, Stenzel T T, Ahmed Rasheed B K, Tourt-Uhlig S E, Herndon J E, 2nd, Vredenburgh J J, Sampson J H, Friedman A H,

Bigner D D and Friedman H S (2004). Phase II trial of gefitinib in recurrent glioblastoma. *J Clin Oncol* **22**: 133-42.

Souhami L, Seiferheld W, Brachman D, Podgorsak E B, Werner-Wasik M, Lustig R, Schultz C J, Sause W, Okunieff P, Buckner J, Zamorano L, Mehta M P and Curran W J, Jr. (2004). Randomized comparison of stereotactic radiosurgery followed by conventional radiotherapy with carmustine to conventional radiotherapy with carmustine for patients with glioblastoma multiforme: report of Radiation Therapy Oncology Group 93-05 protocol. *Int J Radiat Oncol Biol Phys* **60**: 853-60.

Stewart L A (2002). Chemotherapy in adult high-grade glioma: a systematic review and meta-analysis of individual patient data from 12 randomised trials. *Lancet* **359**: 1011-8.

Stupp R, Mason W P, van den Bent M J, Weller M, Fisher B, Taphoorn M J, Belanger K, Brandes A A, Marosi C, Bogdahn U, Curschmann J, Janzer R C, Ludwin S K, Gorlia T, Allgeier A, Lacombe D, Cairncross J G, Eisenhauer E and Mirimanoff R O (2005). Radiotherapy plus concomitant and adjuvant temozolomide for glioblastoma. *N Engl J Med* **352**: 987-96.

Uhm J H, Ballman, K. V., Giannini, C., Krauss, J. C., Buckner, J. C., James, D., Scheithauer, B. W., O'Fallon, J. R., Jaeckle, K. A. (2004). Phase II study of ZD1839 in patients with newly diagnosed grade 4 astrocytoma. *J Clin Oncol* **22**: 1505.

US National Institutes of Health (2006). O6-Benzylguanine and Temozolomide in Treating Young Patients With Recurrent or Progressive Gliomas or Brain Stem Tumors.

US National Institutes of Health (2006). Phase I/II Study of Gefitinib and Radiotherapy in Patients With Glioblastoma Multiforme.

van den Bent M J, Hegi M E and Stupp R (2006). Recent developments in the use of chemotherapy in brain tumours. *Eur J Cancer* **42**: 582-8.

Walker M D, Alexander E, Jr., Hunt W E, MacCarty C S, Mahaley M S, Jr., Mealey J, Jr., Norrell H A, Owens G, Ransohoff J, Wilson C B, Gehan E A and Strike T A (1978). Evaluation of BCNU and/or radiotherapy in the treatment of anaplastic gliomas. A cooperative clinical trial. *J Neurosurg* **49**: 333-43.

Walker M D, Green S B, Byar D P, Alexander E, Jr., Batzdorf U, Brooks W H, Hunt W E, MacCarty C S, Mahaley M S, Jr., Mealey J, Jr., Owens G, Ransohoff J, 2nd, Robertson J T, Shapiro W R, Smith K R, Jr., Wilson C B and Strike T A (1980). Randomized comparisons of radiotherapy and nitrosoureas for the treatment of malignant glioma after surgery. *N Engl J Med* **303**: 1323-9.

Yung W K, Albright R E, Olson J, Fredericks R, Fink K, Prados M D, Brada M, Spence A, Hohl R J, Shapiro W, Glantz M, Greenberg H, Selker R G, Vick N A, Rampling R, Friedman H, Phillips P, Bruner J, Yue N, Osoba D, Zaknoen S and Levin V A (2000). A phase II study of temozolomide vs. procarbazine in patients with glioblastoma multiforme at first relapse. *Br J Cancer* **83**: 588-93.

Chapter 2
Scope and Objectives

The poor accessibility of the brain for many clinically well evaluated anticancer drugs constitutes a major problem in the treatment of malignant brain tumors. Especially the p-glycoprotein 170 (pgp)-mediated classical multi-drug resistance plays an important role, not only in the poor penetration of compounds from the blood into the brain, but it also can cause resistance of the tumors themselves. One approach to overcome the pgp-mediated resistance against the DNA intercalating agent and pgp substrate doxorubicin is the use of polybutylcyanoacrylate (PBCA) nanoparticles, which have been evaluated as targeted drug delivery systems by different workgroups (see Introduction of Chapter 3). However, little is known about the mechanism of the enhanced drug penetration into the brain across the blood-brain barrier (BBB) and about how the pgp-efflux mechanism is circumvented, respectively.

Thus, the objective of the first part of this work was to investigate whether PBCA nanoparticles are suitable carriers for doxorubicin in order to overcome pgp-mediated multi-drug resistance in vitro, and if so, to elucidate the mechanism of the enhanced antiproliferative activity of nanoparticle-bound doxorubicin compared to the efficacy of the dissolved drug (Chapter 3). The experiments comprised the determination of the chemosensitivity of pgp-overexpressing KBv1 cells to different doxorubicin nanoparticle formulations as an in vitro model for the classical multi-drug resistance. Furthermore, flow cytometric and confocal laser-scanning microscopic (CLSM) studies were performed to determine uptake and distribution of doxorubicin into pgp-negative human glioblastoma cells and pgp-overexpressing KBv1 cells, and to investigate whether PBCA nanoparticles permeate into the cells in vitro.

The second part of this thesis was concerned with the concept of selective inhibition of the platelet-derived growth factor (PDGF) receptor as a new approach to the treatment of glioblastoma (Chapter 4). The autocrine activation of PDGF receptors by PDGF has been commonly suggested to be of major importance for the maintenance and malignancy of glioblastoma, and has been considered as an extremely promising pharmacological target (see Introduction of Chapter 4). The inhibition of tumor growth by selective PDGF receptor tyrosine kinase inhibitors would provide a selective and non-cytotoxic chemotherapeutic approach to the treatment of human glioblastoma. Therefore, the expression of PDGF receptors in human glioblastoma cells was determined as well as the chemosensitivity of human glioblastoma cell variants to various PDGF receptor tyrosine kinase inhibitors. Further experiments included the determination of the activity of PDGF receptors in human glioblastoma cells, and the effect of PDGF on glioblastoma cell proliferation.

Besides the classical cytotoxic anticancer drugs (alkylating agents, DNA intercalators, microtubule-interfering agents) and the non-cytotoxic signal transduction inhibitors, new compounds targeting the action of a mitotic motor protein, the Eg5 kinesin, are currently preclinically evaluated (see Introduction of Chapter 5). Eg5 inhibition causes mitotic arrest and is supposed to leave quiescent cells unaffected. Since cytotoxicity and especially neurotoxicity of the classical microtubule-interfering agents such as paclitaxel or vinblastine are mainly ascribed to their effect on microtubule-dependent processes, the development of potent and selective Eg5 inhibitors is suggested to lead to a new class of well tolerated anticancer drugs. In the last part of this work the effects of new analogs of the first identified selective Eg5 inhibitor monastrol on the spindle formation and the cytoskeleton of human glioblastoma cells were investigated by confocal laser-scanning microscopy.

Chapter 3

Investigations on doxorubicin-loaded poly-butylcyanoacrylate nanoparticle formulations as an approach to overcome p-glycoprotein-mediated drug efflux

3.1 Introduction

3.1.1 Nanoparticle carrier systems

The use of biodegradable polymeric nanoparticles as drug delivery systems has been evaluated over the last few decades. Compared to other drug application modes they offer some particular advantages. They can increase stability of drugs or proteins and can provide controlled drug release. Up to now, various polymers have been investigated for their suitability for targeted drug delivery to the particular site of interest. Those studies included controlled drug release, targeting of particular organs and tissues, carriers for DNA in gene therapy, and delivery of peptides and DNA by oral administration (Langer 2000; Soppimath et al. 2001). Compared to standard drug formulations the nanoparticle drug formulations have been anticipated to provide an optimized therapeutic effect while minimizing drug side effects.

Nanoparticles are colloidal polymeric particles with a size of up to 1000 nm. Depending on the method of preparation nanospheres or nanocapsules are obtained. Most reports on the development and evaluation of nanoparticle drug carriers deal with the polymers poly(D,L-lactide), poly(lactic acid), poly(D,L-glycolide), poly(lactide-co-glycolide), poly(lactic-co-glycolic acid) (PLGA), and poly(cyanoacrylate). Nanoparticles have also been prepared from poly(methylidenemalonate) (Lescure et al. 1994), gelatin (Farrugia and Groves 1999), chitosan (Fernandez-Urrusuno et al. 1999; Janes et al. 2001), and sodium alginate (Soppimath

et al. 2001). In general, compounds to be delivered by nanoparticles can be bound to the nanoparticle matrix by sorption, incorporation, or chemical binding (Kreuter 1994). The drug release depends on desorption of the surface-bound drug, the diffusion through the nanoparticle matrix, the erosion of the nanoparticle matrix, and on combined diffusion/erosion processes. Thus, except for diffusion, biodegradation makes the major contribution to the controlled drug release from nanoparticles (Soppimath et al. 2001).

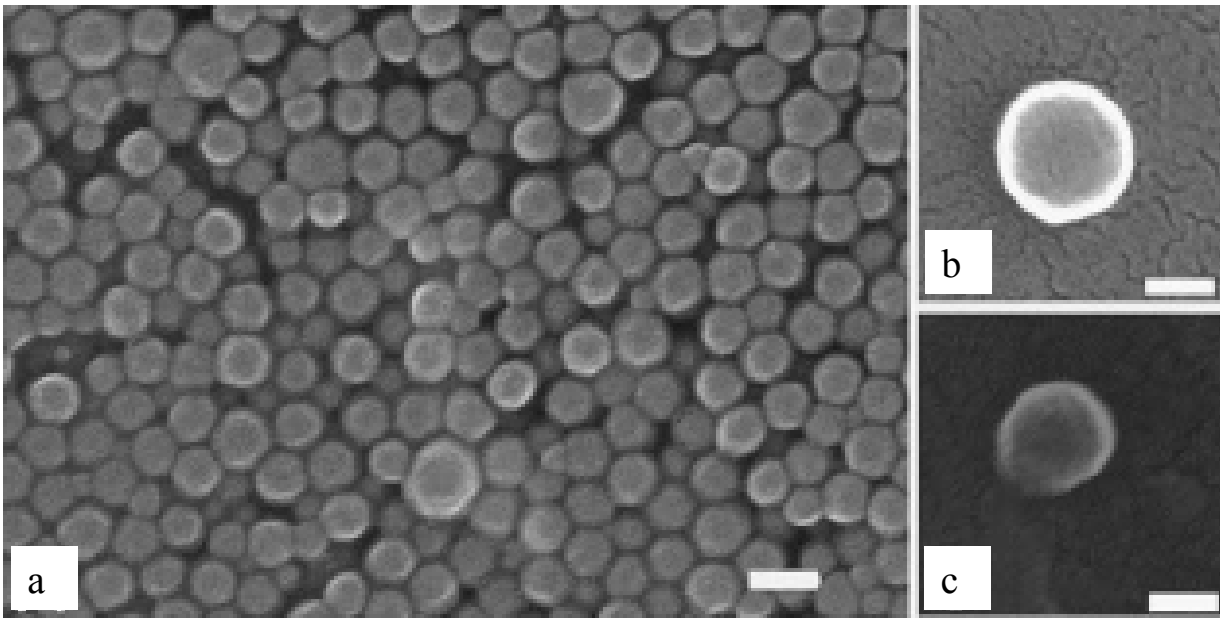

Figure 3-1: Morphology of polybutylcyanoacrylate (PBCA) nanoparticles (originally in water), determined by scanning electron microscopy (SEM). a: densely packed particles; b and c: isolated particles; bar: 200 nm (a), 100 nm (b and c) (from Bootz et al. 2004, modified).

After intravenous injection, the nanoparticles adsorb blood components of which the amount and composition depend on the size and on the hydrophobicity of the nanoparticle surface. This determines their distribution into the organs, particularly of the reticulo-endothelial system (RES: liver, spleen, lung, and bone marrow), whereas phagocytosis plays a major role in the elimination of the nanoparticles from the blood circulation. Surface modifications have been shown to drastically change the binding of plasma proteins to the nanoparticles. For example, the coating of PLGA microspheres with poly(L-lysine)-poly(ethylene glycol) reduced protein binding to the surface by two orders of magnitude compared to uncoated microspheres (Müller et al. 2003). Therefore, modified protein adsorption has been suggested to protect nanoparticles from phagocytosis and thus from fast elimination by the RES. This has been shown for polystyrene microspheres and other colloidal carriers, coated with poloxamer 338 (Illum and Davis 1983; Illum et al. 1987). The influence of surface

composition on phagocytosis has been basically described and reviewed by van Oss (van Oss 1978). Several studies reviewed by Soppimath et al. suggested surface-dependent body distribution of various biodegradable nanoparticle systems (Soppimath et al. 2001), whereas the most intensively investigated surface modifications involved coatings with hydrophilic polymers (surfactants) such as polyethylene glycol, polyethylene oxide, poloxamer, poloxamine, lauryl ethers, and polysorbate 80 (Tween 80®).

The successful targeted drug delivery to particular tissues and organs, in many cases, would also imply the overcome of certain drug resistance mechanisms such as the p–glycoprotein 170 (pgp)-mediated multi-drug resistance. Since the pgp basically contributes to the physiological blood-brain barrier (BBB) function, the overcome of the BBB by the use of nanoparticle carrier systems would provide enhanced accessibility of the brain with pharmacologically active compounds, and might improve the treatment of diseases of the central nervous system (CNS), such as primary malignant brain tumors.

3.1.2 The blood-brain barrier

In order to treat diseases within the CNS with pharmacologically active compounds the administered drugs must reach their biological target in therapeutic concentrations. Despite high blood perfusion the brain is one of the least accessible organs for the delivery of pharmacologically active molecules. For the entry into as well as for the exit from the brain endogenous and exogenous compounds have to pass two physiological barriers. Those are the BBB and the blood-cerebrospinal fluid barrier (BCSFB). Both barriers separate the brain from the systemic blood circulation and control the interchange of biomolecules. However the contribution of the BCSFB to the regulation of drug concentrations in the brain is considered negligibly small (Rautioa and Chikhale 2004).

The particular cytoarchitecture of the BBB was elucidated by electron microscopic studies. The BBB is formed by the microvasculature of the brain, consisting of a monolayer of polarized brain capillary endothelial cells, which are connected with tight junctions (zonulae occludentes). These are formed by a number of transmembrane proteins such as occludin and claudin (Kniesel and Wolburg 2000), and effectively block paracellular aqueous diffusion, sealing the brain off from free diffusion of polar solutes from the blood. Hence, the brain capillary endothelium maintains a high expression of transporters in order to supply the brain with essential nutrients, e.g. glucose and amino acids. The brain capillaries are

embedded in astrocyte end feet, pericytes, and nerve endings, forming altogether a network on the abluminal surface of the capillaries. The differentiation of the endothelial cells to a polarized blood-brain barrier is thought to be a result of close association of the endothelial cells with astrocytes and pericytes (Kacem et al. 1998; Dore-Duffy 2003).

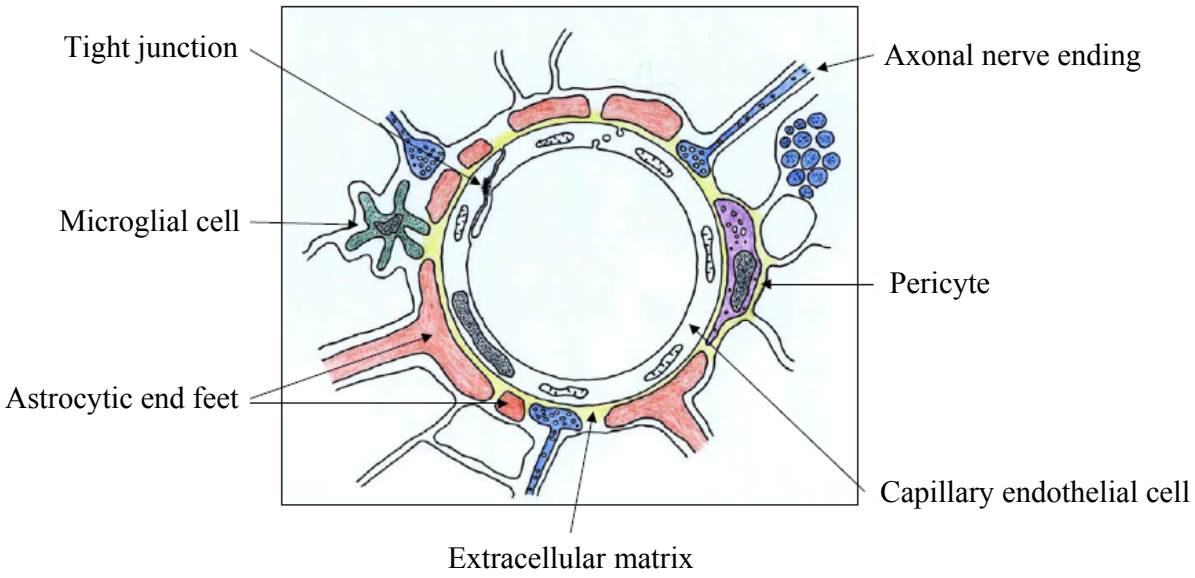

Figure 3-2: Schematic drawing of the BBB cytoarchitecture (from Begley 2004, with modifications). The brain capillaries are lined by endothelial cells which are connected via tight junctions at their adjacent cell membranes. The abluminal side of the endothelium is covered by a network of numerous astrocytic end feet and discontinuously distributed pericytes maintaining the structural integrity of the BBB. The cellular environment of the endothelium is completed by immunocompetent cells of the brain, perivascular macrophages (microglial cells), which are derived from systemic circulating monocytes and macrophages.

The BBB serves two major physiological functions. First, the composition of the interstitial fluid and the cerebrospinal fluid have to be controlled within very close limits to maintain the integrative neuronal function. For example, the availability of the potent CNS neurotransmitters glycine and glutamic acid, which are present at high concentrations in the blood, has to be controlled precisely in the brain extracellular fluid. The second basic function is the protection of the brain against the exposure to toxic endogenous metabolites. Since neuronal replacement in the mammalian CNS after cell damage or cell death is considered to be minimal or absent the BBB is of major importance.

3.1.3 Regulation of drug uptake into the brain across the blood-brain barrier

The uptake of a drug into the brain across the BBB depends on the sum of uptake and efflux processes regulated by the BBB. Thus the net uptake is influenced by various factors. One of them is the drug plasma concentration characterized by the area under the curve (AUC) and the maximal systemic blood concentration (C_{max}). These parameters represent the amount of drug available for crossing the BBB, and determine the concentration gradient between the blood and the brain. Since a paracellular drug transport normally does not occur due to the tight junctions, the permeability of the BBB is primarily controlled by the properties of the endothelium cells, whereas the permeability and metabolic capacity basically contribute to the regulation of influx and efflux processes. The endothelial cells contain several enzymes implicated in first and second pass metabolism processes, e.g. NADH-cytochrom P-450 reductase, epoxide hydrolase, and UDP glucuronosyltransferase (Ghersi-Egea et al. 1994). Thus, these enzymes may metabolize drugs and alter their ability to permeate the BBB and to penetrate into the brain, respectively.

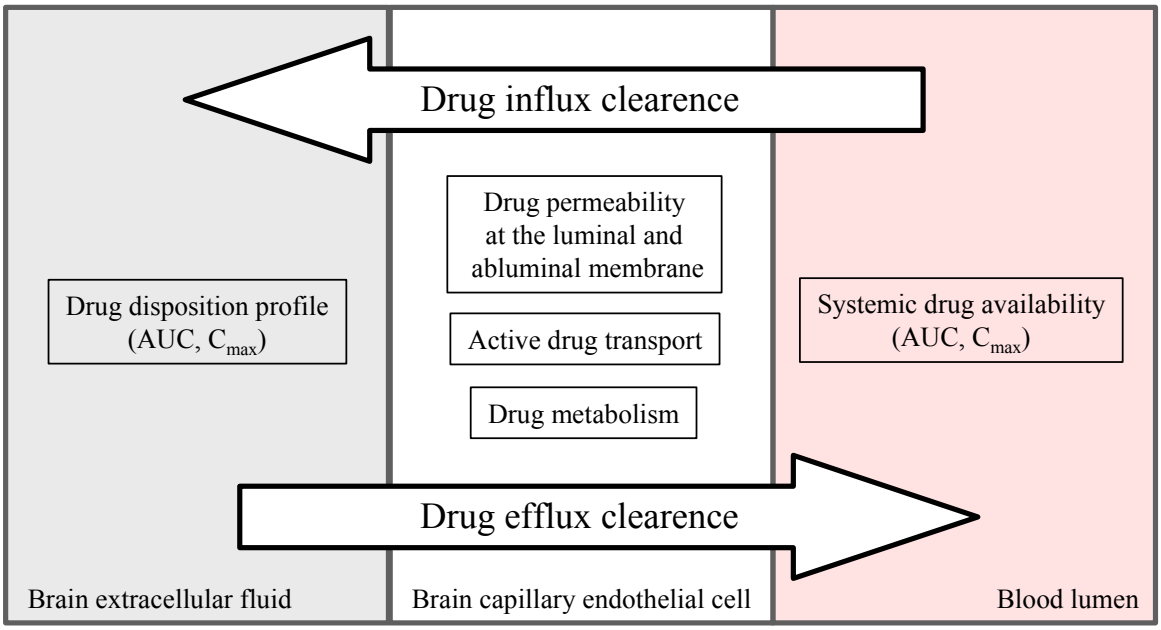

Figure 3-3: The sum of uptake and efflux processes determines the net uptake of compounds from the blood into the brain through the capillary endothelial cells (modified from Scherrmann 2002).

According to Levin small lipophilic molecules with a molecular weight below 600 Da are capable of passing the plasma membrane of the endothelial cells (Levin 1980). The passive diffusion of the drugs depends on their concentration gradient between the blood and the

brain, and its octanol-water partition coefficient ($P_{o/w}$) which has been determined to be optimal between $logP_{o/w}$ values of 1.5 and 2.5 (Madrid et al. 1991). Furthermore, the diffusion is inversely related to the ionization degree of the drug at physiological pH (7.4). Moreover, non-diffusible compounds such as hydrophilic drugs, peptides and proteins can cross the BBB via carrier-mediated transport and via endocytotic mechanisms. Due to the polarized expression of ion channels, bidirectional transporters, energy-dependent pumps, and endocytosis-mediative receptors in the luminal and abluminal membrane of the endothelium, these highly specialized transport pathways provide a capacity of asymmetric transport of certain compounds across the BBB.

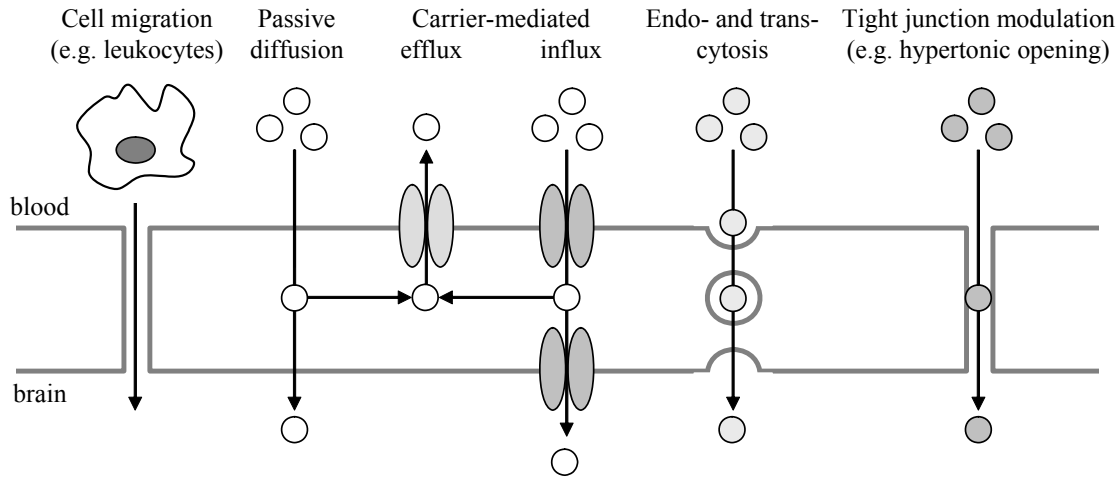

Figure 3-4: Transport routes across the blood brain barrier (from Begley et al. 2003, modified). Besides permeation of the BBB via cell migration or paracellular crossing by tight junction modulation, all molecules must pass the membranes and the cytosol of the capillary endothelial cells. Thereby, permeation of substances depends on passive diffusion, carrier-mediated efflux and influx processes, and receptor- or adsorptive-mediated endo- and transcytosis. Moreover, the permeation of a compound may also depend on more than one of the schematically drawn mechanisms.

Several transmembrane transport proteins, located in the luminal and in the abluminal membrane of the brain capillary endothelium, are involved in the regulation of the uptake of numerous drugs into the brain. Many amphipathic cationic compounds are substrates for at least one of these proteins, the pgp, which is expressed at the luminal pole of the brain capillary endothelium (Cordon-Cardo et al. 1989). Drion et al. provided solid evidence for a major contribution of pgp to the BBB function (Drion et al. 1996). In perfusion studies with rat brains the uptake of the pgp substrates colchicine and vinblastine was enhanced to the 8.5- and 9.0-fold, respectively, after the pretreatment with valspodar (PSC 833), a second generation pgp inhibitor. Thus, pgp and other transport proteins are considered to mediate the

efflux of many pharmacologically active molecules from the brain to the blood. As a consequence this leads to poor accessibility of the brain for various drugs after systemic administration, making several CNS diseases refractory to treatment.

3.1.4 Targeted drug delivery to the brain

Several approaches to circumvent the blood-brain barrier via targeted drug delivery have been evaluated:

- the use of prodrugs and chemical delivery systems
- carrier- and receptor-mediated transport across the BBB
- liposomal drug carriers
- nanoparticle drug carriers

3.1.4.1 Prodrugs and chemical delivery systems

Since the lipophilicity of a compound improves its permeability with respect to biomembranes, the use of lipophilic prodrugs may be considered as a rather non-selective enhancement of drug delivery from the blood to the brain. After crossing the BBB the prodrugs are usually metabolized to more hydrophilic compounds, incapable of permeating the BBB towards the blood. In general such compounds have to be expected to accumulate not only in the brain, but also in other organs and tissues, resulting in an increased systemic toxicity and a decreased efficiency of the intended drug delivery.

Similar problems occur with chemical drug delivery systems. For this concept, developed from the prodrug approach, drugs are provided with several additional chemical moieties in order to improve their pharmacokinetic properties. The moieties increase lipophilicity and permeation of the drug through lipid membranes, they protect certain pharmacologically important functional groups from metabolic degradation, and target the compounds to the tissue of interest. Brewster et al. introduced 1-methyl-1,4-dihydronicotinic acid as a moiety providing various benefits for drug delivery to the brain, when covalently linked to drugs by esterification. Due to the enhanced lipophilicity the esterified compound passes the BBB followed by enzymatic oxidation of the targeting moiety to the quarternary ammonium salt in the brain parenchyma. Consequently, the charged metabolite is trapped inside the CNS and ester hydrolysis separates the pharmacologically active compound from the delivery moiety.

This drug delivery principle has been successfully applied to zidovudine in rabbits (Brewster et al. 1991). The administration of the 1-methyl-1,4-dihydronicotinic acid ester generated higher and more sustained levels of zidovudine in the brain tissue than unchanged zidovudine. The increase in the area under the brain concentration-time curve occurred with lower systemic zidovudine concentrations. Yet, various chemical delivery systems have been established, comprising chemotherapeutic agents (Bodor and Buchwald 1999) and steroids (Bodor and Buchwald 2002).

3.1.4.2 Carrier- and receptor-mediated transport across the BBB

A large number of endogenous solute transporters at the BBB can be utilized for targeted drug delivery from the blood to the brain (Begley 2003). The physiological role of many of those transport mechanisms is to carry polar metabolites into the brain. The directed transport across the BBB towards to brain side is further enhanced by the polarized expression of the transporters at the cerebral endothelium membrane. Thus, drugs designed as pseudosubstrates for these transport proteins can be carried across the BBB (Tab. 3-1). However, in several cases the stereochemical requirements for the carrier-mediated transport are very stringent, and consequently the number of applicable compounds is limited. For example, since the nucleoside carriers do not accept a broad variety of substrates, many antiviral and cytostatic drugs, according to the nucleoside analog approach, do not permeate the BBB to a sufficient extent.

Another transport route across the BBB involves endocytotic pathways, which can be accessed by peptides and proteins, leading to a transcytotic uptake into the brain. It has to be distinguished between receptor-mediated and adsorption-induced transcytosis. Since many drugs are not substrates, neither for receptor-mediated nor adsorption-induced endocytotic pathways, the linkage to targeting molecules provides a useful approach to create pseudosubstrates, capable of accessing transcytotic mechanisms. In experiments in rats, Bickel et al. showed uptake into the brain of a monoclonal anti-transferrin receptor antibody coupled to colloidal gold particles (OX26-Au) via transcytosis (Bickel et al. 1994). Furthermore, the linkage to the OX26 antibody led to the uptake of vasoactive intestinal peptide, nerve growth factor, glial cell line-derived neurotrophic factor, and brain derived neurotrophic factor into the brain (Begley 2003). It has been suggested that binding of the anti-transferrin receptor antibody to the transferrin receptor induces endocytosis of the antibody-peptide construct, which is then entirely or in part translocated through the capillary endothelial cell and released into the brain. Further examples for vector-mediated delivery

across the BBB have been reviewed by Pardridge (Pardridge 1999). Moreover, vesicle formation and internalization at the luminal membrane of brain capillary endothelial cells can be induced by electrostatic interactions between the membrane surface and charged peptides or proteins from the blood circulation. This mechanism has been used for the delivery of cationized rat albumin to the rat brain (Pardridge et al. 1990), and furthermore has been suggested to be applicable to other highly positively charged compounds.

Table 3-1: Examples for drug delivery to the brain via endogenous transport mechanisms (from Begley 2003 with modifications).

Endogenous transporter	Carried drug
Medium chain fatty acid carrier	Valproic acid Docosahexanoic acid (DHA)–paclitaxel
Large neutral amino acid carrier (L-system)	L-dopa α-methyl-dopa Melphalan Baclophen Gabapentin
Monocarboxylic acid carrier	Active metabolites of simvastatin and lovastatin (carboxylic acid form)
Organic cation transporter	Mepyramine Diphenhydramine Diphenylpyraline Lidocaine Imipramine Propranolol
Purine carrier	Oxazolamine COR3224
Nucleoside carrier	Abacivir
Hexose carrier	Dehydroascorbic acid Glycosylated morphine

3.1.4.3 Liposomal drug carriers

Liposomes, which have a size of up to 500 nm, represent a drug carrier system, exhibiting various benefits compared to conventional dosage forms. Drugs can be encapsulated into the lumen of the liposomes or incorporated into the liposomal matrix. Thereby the drugs are protected from degradation and the liposomes can be targeted to the site of pharmacodynamic action by various modifications of the liposomal surface. The high lipophilicity enables the liposomes to cross the BBB, and drug release starts with the degradation of the liposomes.

Surface modifications of liposomes, e.g. the incorporation of monoclonal antibodies into the liposomal matrix, can enhance targeting and delivery efficiency of pgp substrates to the brain. Huwyler et al. demonstrated the overcome of pgp-mediated drug efflux by the use of targeted liposomes in vitro (Huwyler et al. 2002). After the modification of the liposomal surface with the monoclonal anti-transferrin receptor antibody OX26, radiolabeled liposomal digoxin permeated into cells, which were coexpressing pgp and transferrin receptors. Since digoxin is a substrate of the pgp, this study demonstrated the validity not only of antibodies as targeting vectors, but also of immunoliposomes for drug delivery across the BBB.

Despite of several benefits of liposomes as drug carrier systems, the progress in the development of more efficient liposomal drug formulations has been limited due to several immanent problems, e.g. low encapsulation efficiency, rapid leakage of hydrophilic drugs in the presence of blood components, and low stability of liposomal drug formulations in storage.

3.1.4.4 Tween 80®-coated polybutylcyanoacrylate nanoparticles

The first drug transport across the BBB using Tween 80®-coated PBCA nanoparticles (NP) has been demonstrated for the hexapeptide dalargin, a leu-enkephalin analog with opioid activity, which is not capable of passing the BBB when applied in solution. The degree of dalargin transport into the brain was indirectly measured by its analgesic effect in mice using the tail flick test (Kreuter et al. 1995) and the hot plate test (Schroeder et al. 1998). An analgesic effect was only observed after the application of the Tween 80®-coated dalargin-loaded nanoparticles, whereas uncoated dalargin PBCA NP or a simple mixture of PBCA NP, Tween 80®, and dalargin had no effect. Coating with other surfactants, such as polysorbate 20, 40, and 60 led to lower antinociceptive effects, whereas no effect was observed with various poloxamers, poloxamine 908, Cremophor EL® and Cremophor® RH 40, and polyoxyehtylene-(23)-laurylether (Brij® 35) (Kreuter et al. 1997). Analogous experiments with the dipeptide kytorphin (Schroeder et al. 1998) and loperamide (Alyautdin et al. 1997) led to similar results. Compared to the simple mixture of drug-loaded nanoparticles and surfactant, a significantly higher and dose-dependent analgesic effect was only observed when the compounds were bound to Tween 80®-, respectively Tween 85®-coated PBCA nanoparticles. Furthermore, in brain perfusion studies with rats, tubocurarine-loaded Tween 80®-coated PBCA NP led to frequent severe spikes in the EEG, as observed after intraventricular injection of the dissolved drug. The drug in solution or a mixture of drug, PBCA NP, and the surfactant did not cause any changes in the EEG (Alyautdin et al. 1998).

Another non-peptidic compound, delivered by Tween 80®-coated PBCA NP is the NMDA receptor antagonist MRZ 2/576 (Friese et al. 2000). This compound is excluded from the CNS by efflux pump-mediated processes. In mice with electroshock-induced convulsions the anticonvulsive effect of the short acting MRZ 2/576 (5-15 minutes) was prolonged (up to 210 minutes) after the compound was applied as the Tween 80® coated PBCA NP formulation.

3.1.4.5 Delivery of doxorubicin to the brain via Tween 80®-coated PBCA nanoparticles

Gulyaev et al. investigated the pharmacokinetics of doxorubicin-loaded Tween 80®-coated PBCA NP after intravenous injection to rats, by the basis of HPLC determination of doxorubicin plasma concentrations (Gulyaev et al. 1999). Compared to the standard drug application in solution, the plasma half-life of doxorubicin, when applied as the nanoparticle-bound formulation, was 4-fold higher, and the mean residence time was increased to the 6-fold. Furthermore, compared to the drug in solution and to the simple combination of doxorubicin with Tween 80® and empty PBCA NP, the Tween 80®-coated nanoparticles led to the highest initial plasma concentration, whereas the differences in the body distribution were not large, but in some organs statistically significant. In previous studies by Couvreur et al. (Couvreur et al. 1982) the coated as well as the uncoated nanoparticle formulations led to a drastically decreased doxorubicin concentration in the heart. Since the therapeutical use of doxorubicin is known to be limited by its cardiotoxicity, PBCA NP-bound doxorubicin may provide an alternative therapeutic doxorubicin administration. The most important observation of Gulyaev et al. was that doxorubicin was delivered into the brain after administration of Tween 80®-coated doxorubicin PBCA nanoparticles (Gulyaev et al. 1999). While with all other drug formulations concentrations were below the detection limit (0.1 µg/g), the coated doxorubicin PBCA nanoparticles yielded a doxorubicin concentration of 6 µg/g within the brain. Steiniger et al. were able to show that this application mode of doxorubicin is suitable to affect tumor growth in vivo (Steiniger et al. 2004). Rats bearing intracranially implanted glioblastoma showed significantly higher survival times when they were treated with Tween 80®-coated doxorubicin-loaded nanoparticles, accordant to a total dose of 2.5 mg/kg doxorubicin. Over 20 % of this animal group showed long term remission (100-180 days), whereas animals in all other groups, treated with vehicle, drug in solution, or with combinations of doxorubicin with Tween 80® or empty PBCA NP, died within 50 days. Interestingly, no doxorubicin-related neurotoxicity was observed (Steiniger et al. 2004), being a controversially discussed issue for several years. Neuwelt et al. concluded from their

experiments on osmotic opening of the BBB and intracarotid drug application in rodent and canine models that even small amounts of doxorubicin or its metabolites cause neurotoxicity (Neuwelt et al. 1981). However, in clinical trials liposomal doxorubicin and daunorubicin, another anthracycline, exhibited no significant neurotoxic effects, even though both drugs were successfully delivered to the brain after i.v. injection (Boiardi et al. 1999; Lippens 1999; Koukourakis et al. 2000). A more detailed study on the toxicity of doxorubicin formulations was performed by Gelperina et al. (Gelperina et al. 2002). When applied to healthy rats and to rats with intracranial glioma, nanoparticle-bound doxorubicin showed lower toxicity compared to the drug in solution. These findings were confirmed by the results of Steiniger et al., who further demonstrated that, compared to the uncoated doxorubicin PBCA NP, the coating with Tween 80® did not lead to increased, but to alleviated systemic drug-related toxicity (Steiniger et al. 2004).

In summary, Tween 80®-coated PBCA NP are considered as a very promising therapeutic system for the delivery of doxorubicin and possibly also other antitumor drugs across the BBB to the brain, and consequently a promising approach to overcome the pgp-mediated multi-drug resistance. In view of the reported minimized systemic toxicity and the lack of short-term neurotoxicity, the surfactant-coated doxorubicin-loaded PBCA nanoparticles may provide an efficient non-invasive, and probably well tolerated chemotherapeutic approach to the treatment of CNS malignancies, such as glioblastoma multiforme.

3.2 Objective

The chemotherapy of malignant brain tumors by the systemic application of anticancer drugs is strongly restricted by physiological barriers between the systemic blood circulation and the near tumor environment. Amongst those barriers the BBB bears several physiological resistance mechanisms against toxins and toxic metabolites. Those mechanisms are responsible for the strictly limited penetration of many registered drugs and experimental compounds into the brain as the primary step for drug delivery after systemic administration. The pgp efflux transporter consists one of the main representatives of these resistance mechanisms, responsible for absence of a successful pharmacological treatment. Doxorubicin, a registered anticancer drug, is a good substrate for pgp, and thus hardly enters the brain. Biodegradable PBCA NP, coated with the surfactant polysorbate 80 (Tween 80®) have been evaluated as a carrier system for this compound in studies with glioma in rats, showing a significant transport of doxorubicin into the brain (Gulyaev et al. 1999).

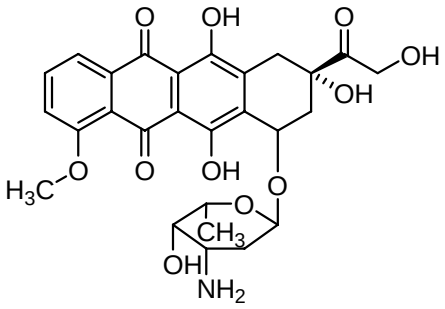

Figure 3-5: Chemical structure of the anthracycline derivative doxorubicin (adriamycin). Due to its planar anthracycline partial structure the compound intercalates into double stranded DNA, causing inhibition of the topoisomerase II enzyme. The DNA transcription is perturbed, and as a consequence also the DNA/RNA synthesis. Doxorubicin is registered for the treatment of various malignancies (Adriblastin®, Caelyx®, DOXO-Cell®, and others). Since it does not penetrate into the CNS after systemic administration, it is not registered for the chemotherapy of any type of CNS tumor. Targeted doxorubicin delivery to certain body compartments is not only anticipated to provide an increased therapeutic efficacy against tumors, but also to minimize the common side effects, like bone marrow suppression, cardiotoxicity, and the development of secondary neoplasia.

However, up to now, the mechanism of the enhanced drug delivery to the brain, by the use of the Tween 80®-coated PBCA NP carrier system, has not been sufficiently elucidated. The transport across the BBB has been suggested to occur due to various single or combined mechanisms (Kreuter 2001):

- passive diffusion of the drug after binding of nanoparticles to the inner endothelial lining of the brain capillaries, and thereby creating a concentration gradient of nanoparticle-released drug at the BBB.
- drug uptake by endocytosis of nanoparticles by the brain endothelial cells, followed by the intracellular drug release and delivery to the brain.
- transcytosis of drug-loaded nanoparticles through the endothelial cells.
- the tight junctions could be opened by the nanoparticles, allowing paracellular transport of released drug or of whole drug-loaded nanoparticles.
- a general effect of the surfactant Tween 80® on the endothelial cell membrane fluidity, e.g. by membrane solubilization.
- Tween 80® could modulate the function of membranous efflux transporters such as pgp.

The objective of this work was to evaluate the efficacy of the polybutylcyanoacrylate nanoparticles as a carrier for the registered anticancer drug doxorubicin against pgp-overexpressing cells. Since the pgp largely contributes to drug resistance of most of the primary malignant brain tumors in adults, such as glioblastoma multiforme, the aim of the performed experiments was to investigate the possibility of breaking through the pgp efflux mechanism with the doxorubicin-loaded nanoparticles in vitro. Therefore, cells with pgp-overexpression were included in a major part of the described investigations. The presented work includes the determination of pgp expression in KB wild type and KBv1 cells, and in the human glioblastoma cell variants U-87 MG, U-118 MG, and U-373 MG. Moreover, the determination of the chemosensitivity of KB wild type and KBv1 cells to doxorubicin and doxorubicin nanoparticle formulations was subject to this work. The effect of different drug formulations on the doxorubicin uptake was investigated flow cytometrically, using the abovementioned cell types. A major emphasis was put on microscopic investigations on the uptake and the intracellular distribution of doxorubicin and of doxorubicin nanoparticle formulations. Therefore, new glioblastoma cell lines were established and used in confocal laser-scanning microscopic studies of cellular drug distribution and localization.

3.3 Materials and methods

3.3.1 Drugs and chemicals

If not especially stated, chemicals were of analytical grade and purchased from Merck (Darmstadt, Germany). Doxorubicin was purchased from Sigma (Deisenhofen, Germany); a 1 mM stock solution was made in 70 % ethanol. Vinblastine (Sigma) was kept as a 1 mM stock solution in 70 % ethanol. SDZ PSC 833 (Valspodar®) was a gift from Novartis (Nürnberg, Germany); a 1 mM stock solution was prepared in 70% ethanol. All stock solutions were stored at -20 °C. The following selection antibiotics were used: ampicillin (Amp, 100 µg/µl, Sigma), kanamycin (Kan, 50 µg/µl, Sigma), geneticin (G418, 400 µg/µl, PAA Laboratories, Cölbe, Germany) and puromycin (Pur, 10 µg/µl, Sigma). All antibiotics were kept as aliquoted stock solutions in millipore water at -20 °C.

3.3.2 Preparation of polybutylcyanoacrylate nanoparticle formulations

All nanoparticles were prepared in the workgroup of Prof. Kreuter (Institute for Pharmaceutical Technology, Johann Wolfgang Goethe Universität, Frankfurt, Germany). To a solution of 2 % dextran 70,000 in 0.01 N hydrochloric acid adjusted to pH 2.0, monomeric butylcyanoacrylate was added, yielding a final monomer concentration of 1 % (weight per volume). After stirring on a magnetic stirrer at 500 rpm for 4 hours, the mixture was neutralized with 0.1 N sodium hydroxide solution, filtered through a G2 glass filter, and afterwards aliquoted into 2 ml vials for lyophilization (3 % mannitol served as cryoprotector). For the preparation of doxorubicin-loaded nanoparticles (DoxoNP) the total stirring time was 2.5 hours instead of 4 hours, and after the first 30 minutes a solution of doxorubicin (10 mg/ml in 0.9 % NaCl saline) was added in order to yield a final concentration of 0.25 %. Prior to the experiments the nanoparticles of one lyophilized aliquot were freshly resuspended in 0.9 % saline or in the appropriate culture medium, respectively. Surfactant-coated nanoparticles were prepared by resuspending lyophilized PBCA nanoparticles in 0.9 % saline containing 1 % Tween 80®, followed by stirring at room temperature for 15 minutes. With respect to the performed experiment, the nanoparticle stock suspensions were further diluted using 0.9 % NaCl solution or serum free culture medium, respectively.

3.3.3 Cell lines and culture conditions

The human U-87 MG (HTB 14, passage 126), the U-118 MG (HTB 15, passage 448) and the U-373 MG (HTB-17, passage 182) glioblastoma/astrocytoma cell lines (Beckman et al. 1971) were obtained from the American Type Culture Collection (ATCC). Cell banking and quality control were performed according to the "seed stock concept" (Hay 1988). U-87 MG and U-373 MG cells were grown in Eagle´s minimum essential medium (EMEM, Sigma,) containing L-glutamine, 2.2 g/l $NaHCO_3$, 110 mg/l sodium pyruvate, and 5 % fetal calf serum (FCS, Biochrom, Berlin, Germany), whereas the U-118 MG cells were maintained in Dulbecco´s minimum essential medium (DMEM, Sigma) which was also supplemented with 5 % FCS. The human KB wild type (KBwt) cells (ATCC CCL-17) were cultured in DMEM with 10 % FCS supplement, and the pgp-overexpressing KBv1 variant was maintained in DMEM 10 % FCS, containing 300 ng/ml vinblastine. All cells were cultured in a water-saturated atmosphere of 95 % air and 5 % carbon dioxide at 37 °C in 75-cm² culture flasks (Nunc, Wiesbaden, Germany) and were serially passaged following trypsinization using trypsin (0.05 %)/EDTA(0.02 %) (Roche Diagnostics, Mannheim, Germany).

3.3.4 Chemosensitivity assay

The assays were performed according to Bernhardt et al. (Bernhardt et al. 1992). In brief: tumor cell suspensions (100 µl/well) were seeded into 96-well flat bottomed microtitration plates (Greiner, Frickenhausen, Germany) at a density of ca. 15 cells/microscopic field (magnification 320x). After 2-3 days the culture medium was removed by suction and replaced by fresh medium (200 µl/well) containing varying drug concentrations, different nanoparticle formulations, or vehicle, respectively. Drugs and nanoparticle formulations were added as 1000-fold concentrated feed solutions. On every plate 16 wells served as controls and 16 wells were used per drug concentration. After various times of incubation the cells were fixed with glutardialdehyde (Merck, Darmstadt, Germany) and stored in a refrigerator. At the end of the experiment all plates were stained with crystal violet (Serva, Heidelberg, Germany) simultaneously. Absorbance was measured at 578 nm using a Biotek 309 Autoreader (Tecnomara, Fernwald, Germany). Growth curves were created using SigmaPlot analysis software (Systat Software GmbH, Erkrath, Germany). When necessary for data

illustration, the absorbance values were further transformed into corrected T/C values, expressing the net growth of the treated cells, relative to the growth of the vehicle control.

3.3.5 Immunostaining

The expression of pgp in KBwt, KBv1, and the human glioblastoma cell variants was investigated by immunostaining and confocal fluorescence microscopy. The cells were seeded into chamberslides (Nunc, Wiesbaden, Germany). At an appropriate density, the cells were fixed with 4 % paraformaldehyde (PFA) solution in phosphate buffered saline (PBS) for 20 minutes at room temperature. After discarding the fixative the cells were washed three times with 300 µl of PBS containing 0.5 % bovine serum albumin (BSA, Serva, Heidelberg, Germany). Cells were permeabilized by incubation with 0.1 % Triton X-100 solution in PBS containing 0.5 % BSA (PBS/BSA) for 10 minutes at room temperature (150 µl per well). The cells were washed three times with 300 µl of PBS/BSA and incubated with 125 µl of a 1:200 dilution of the monoclonal mouse anti-human pgp Ab2 primary antibody Clone F4 (Dianova, Hamburg, Germany) for 1 hour at room temperature. After removing the excess primary antibody and washing three times with PBS/BSA, the cells were incubated with 125 µl of 1:200 diluted fluorescein isothiocyanate (FITC)-conjugated polyclonal rabbit anti-mouse IgG secondary antibody (F0261, DAKO, Hamburg, Germany) for 1 hour at room temperature. For pgp staining after incubation of cells with doxorubicin, an Alexa (Panchuk-Voloshina et al. 1999) Fluor® 546-conjugated anti-mouse secondary antibody (A11030, Molecular Probes, Eugene, USA) was used at a dilution of 1:200. The cells were washed three times with PBS/BSA and with millipore water. After air drying and mounting with Fluoromount mounting medium (Serva, Heidelberg, Germany) the cells were inspected with a Carl Zeiss Axiovert 200M confocal laser-scanning microscope, equipped with a LSM510 scanning unit.

3.3.6 UV-vis and fluorescence spectroscopy

For the determination of the doxorubicin stock concentrations, UV absorption spectra of doxorubicin were acquired in 96 % ethanol. UV-vis absorption difference spectra of doxorubicin/DNA were recorded using a set of matched tandem cuvettes (Hellma, No. 230-QS, Müllheim, Germany), containing two compartments of equal pathlength (4.375 mm). DNA concentrations of 10 µg/ml, 20 µg/ml and 60 µg/ml were added to a 20 µM doxorubicin

solution in CS buffer (10 mM tri-sodium citrate, 150 mM NaCl). All absorption spectra were measured using a Cary 100 conc. spectrophotometer (Varian, Darmstadt, Germany) at room temperature. Different concentrations of DNA (from calf thymus, Sigma, final concentrations: 0.5, 1.0, 3.0, 5.0, 10.0, 30.0, and 50.0 µg/ml) were added to a 1 µM doxorubicin solution in CS buffer and fluorescence excitation (λ_{ex} = 488 nm) and emission spectra (λ_{em} = 589 nm) were acquired five times and averaged using an AMINCO-Bowman AB2 spectrofluorometer (workgroup of Prof. Wolfbeis, University of Regensburg). All spectra were corrected for the wavelength dependent photomultiplier sensitivity by using an internal calibration feature of the instrument. After that, excitation and emission spectra were normalized to 100 arbitrary units of relative fluorescence excitation respectively emission.

3.3.7 Flow cytometry

Confluent cells were trypsinized and harvested from 75-cm² culture flasks (Nunc, Wiesbaden, Germany). The cell suspension was washed one time with PBS and adjusted to a cell number of $5 \cdot 10^5$ cells/ml PBS. 1 ml aliquots were dispensed into 1.5 ml reaction vessels (Eppendorf, Wesseling-Berzdorf, Germany), the cells were centrifuged at 300 g for 5 minutes, and the supernatant was discarded. The cell pellets were resuspended in 200 µl of PBS containing the respective drug formulation: dissolved doxorubicin 500 nM, PBCA NP suspension (blank), PBCA NP suspension containing the equivalent concentration of doxorubicin, Tween 80®-coated PBCA NP suspension, Tween 80®-coated PBCA NP suspension containing the equivalent concentration of doxorubicin. The cells were incubated for 2 hours or 4 hours, respectively, at 37 °C in the dark. For flow cytometric analysis with a FACSCalibur™ (Becton Dickinson, Heidelberg, Germany) the samples were filled up with PBS to a final volume of 500 µl. Cell-associated doxorubicin fluorescence was detected in the FL2 detection channel. For each measurement data were acquired for 30,000 events gated from a FSC/SSC dotplot. Instrument settings: E^{-1} for FSC, 260 for SSC and 474 for FL2. Data were analyzed by the WinMDI 2.8 FACS analysis software.

3.3.8 Amplification and purification of localization vectors

3.3.8.1 Localization vectors

The following localization vectors were used: pECFP-ER (Takara Bio Europe/Clontech, Saint-Germain-en-Laye, France), pECFP-Golgi (Clontech), pECFP-Mem (Clontech) and pECFP-Mito (Clontech), whereas the latter two vectors were modified by subcloning into the retroviral expression vector pQCXIP (Clontech). For restriction maps of all used localization vectors see Fig. 3-6. For amplification of all vectors, competent *E. coli* (strain TOP10, Invitrogen GmbH Karlsruhe, Germany) were transformed with 1 ng of plasmid DNA.

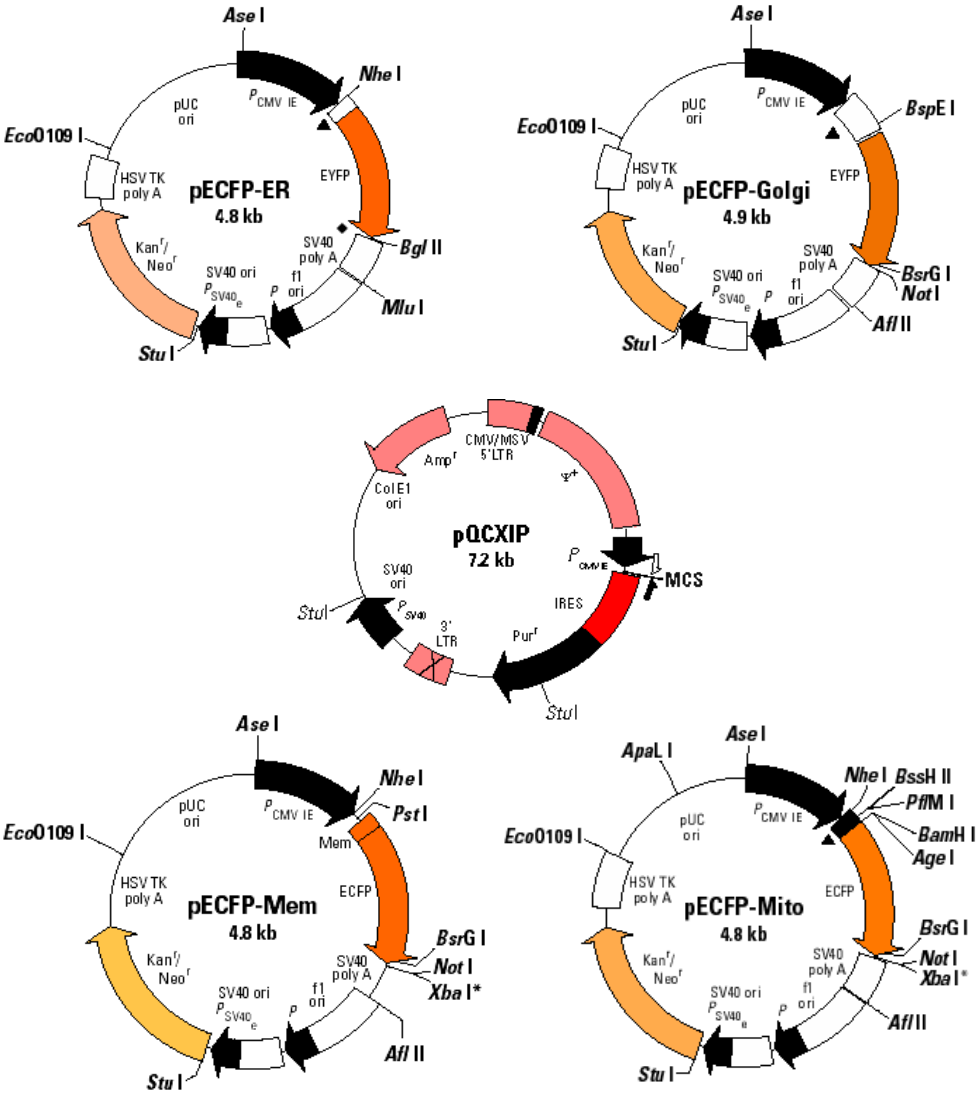

Figure 3-6: Restriction maps of localization vectors. The sequences encoding the fluorescent fusion proteins for plasma membrane and mitochondria localization were subcloned into the multiple cloning site (MCS) of the retroviral expression vector pQCXIP.

3.3.8.2 Culture media and selection agar

E. coli cells were cultured in Luria Bertani (LB) medium, which was prepared by dissolving 10 g of NaCl (Merck, Darmstadt, Germany), 10 g of tryptone (Difco, Detroit, USA), and 5 g of yeast extract (Roth, Karlsruhe, Germany) in 1 l of millipore water, adjusted to pH 7.0. After autoclaving, the selective media were prepared by adding Amp (Kan) to a final concentration of 100 mg/l (50 mg/l). For the preparation of selective agar plates 20 g of agar agar (Roth, Karlsruhe, Germany) were dissolved in 1 l of LB medium, followed by autoclaving. The sterilized medium was cooled down to 55–60 °C, and Amp (Kan) was added to a final concentration of 100 mg/l (50 mg/l). The agar plates were poured immediately (20 ml solution per plate) and stored at 4 °C. The salt optimized + carbon (SOC) medium was prepared by dissolving KCl (2.5 mM $MgCl_2$ [10 mM] and$MgSO_4$ [10 mM] in LB medium. After autoclaving, glucose was added to yield a concentration of 20 mM.

3.3.8.3 Preparation of competent bacteria

For the preparation of competent *E. coli* cells, 5 ml of LB medium were inoculated with *E. coli* TOP10 (glycerol stock) and incubated overnight at 37 °C on a shaker (200 rpm). 200 ml of LB medium were inoculated with 2 ml from an overnight culture and grown for 2-2.5 hours until the bacteria had reached an optical density (OD_{600} nm) of 0.2. The bacterial suspension was cooled on ice for 10 minutes, centrifuged for 7 minutes at 3000 rpm (4 °C), and the supernatant was discarded. The pellet was resuspended in 32 ml of ice-cold $CaCl_2$ solution (60 mM $CaCl_2 \cdot 2\ H_2O$, 10 mM PIPES, 15 % glycerol, pH 7.0, sterilized by autoclaving) and incubated on ice for 30 minutes. Again the bacteria were centrifuged (7 minutes, 2500 rpm, 4 °C) and the pellet was resuspended in 6.4 ml of ice-cold $CaCl_2$ solution. The suspension was portioned into 200 µl aliquots (1.5 ml reaction vessels, Eppendorf), and after incubation on ice for 2 hours the aliquots were frozen in liquid nitrogen and stored in a -80 °C freezer.

3.3.8.4 Transformation of *E. coli* cells

For each transformation one aliquot (200 µl) of competent bacteria (*E. coli* TOP10) was thawn on ice, and then the plasmid DNA (dissolved in 10 mM HEPES, pH 8.5) was added. After incubation on ice for 30 min, the bacteria were put onto a 42 °C water bath for 90 seconds and immediately put back on ice for 5 minutes. 1 ml of SOC medium was added, and the bacteria were incubated for 45 minutes at 37 °C (shaker, 200 rpm) to obtain a starting culture. Then, 20-100 µl of the bacterial suspension were plated on selective agar and the

plates were incubated at 37 °C until single colonies appeared. When no colonies had appeared after 48 hours transformation was repeated. The resistant colonies were used for the inoculation of LB medium for plasmid DNA preparations from overnight cultures.

3.3.8.5 Plasmid DNA maxipreparation and determination of plasmid DNA

For each plasmid DNA maxipreparation 200 ml of LB medium, supplemented with the appropriate selection antibiotic (Amp 100 µg/ml, Kan 50 µg/ml), were inoculated with a single colony from a selection agar plate. The culture was grown overnight at 37 °C (shaker, 200 rpm). Next day, the DNA was isolated using the Qiagen Plasmid Purification Kit (Qiagen, Hilden, Germany) after taking a sample from the bacterial culture for the preparation of a glycerol stock culture (800 µl of bacterial suspension, 200 µl 85 % glycerol), which was stored at -80 °C. The isolation of the DNA was performed according to the manufacturer´s instructions (Qiagen-tip 500 column).

3.3.8.6 Restriction digest

The following enzymes were used for restriction analysis of plasmid DNA: *Bam*HI (20 U/µl, New England Biolabs GmbH [NEB], Frankfurt am Main, Germany), *Eco*RI (10 U/µl, MBI Fermentas GmbH, St. Leon-Rot, Germany), *Not*I (10 U/µl, Fermentas), *Nhe*I (10 U/µl, NEB); *Stu*I (10 U/µl, Amersham Pharmacia Biotech, Piscataway, NJ, USA). Normally, 1 µl of the enzyme stock solution was mixed with 2 µl of the appropriate 10x reaction buffer from the respective manufacturer. After addition of 1 µg of DNA the samples were diluted to a final volume of 20 µl with millipore water, and incubated for 60 minutes at 37 °C. The samples were cooled to room temperature and either processed immediately for agarose gel electrophoresis or stored at -20 °C.

3.3.8.7 Agarose gelelectrophoresis

5x TBE buffer contained 445 mM tris-base (USB, Cleveland, USA), 445 mM boric acid and 10 mM EDTA (Titriplex III). The 5x TBE buffer stock was diluted by 1:5 with millipore water to obtain 1x TBE for preparation of agarose gels. 0.375 g of agarose (peqGOLD Universal-Agarose; Peqlab, Erlangen, Germany) were dissolved in 50 ml of 1x TBE buffer under heating on a magnetic stirrer, then 2 µl of ethidium bromide solution (10 mg/ml H_2O, Janssen Chimica, Beerse, Belgium) were added. The mixture was cooled at room temperature

for an appropriate period of time and poured into the gel chamber. The solidified gel was covered with 1x TBE buffer up to the denoted fill line. The DNA samples were prepared from the restriction digest products, whereas 10 µl of digested DNA solution were mixed with 2 µl of 6x gel loading buffer. The gel pockets were filled with 5 µl of the DNA/loading buffer mixture immediately before the electrophoresis was started. On each gel one or two pockets were filled with 5 µl of the MassRuler™ DNA Ladder High Range (1.5-10 kb, Fermentas) ready-to-use DNA standard (grading: 1.5, 2.0, 2.5, 3.0, 4.0, 5.0, 6.0, 8.0, and 10.0 bp). Electrophoresis was run at a voltage of 90 V, resulting in a total duration of 80–120 minutes. After electrophoresis, the gels were inspected in a gel analysis and documentation system (Gel-Doc, Bio-Rad Laboratories, Munich, Germany) with UV excitation of 254 nm. The acquired data were analyzed with the Quantity One software (Bio-Rad).

3.3.9 Transient and stable transfection of human glioblastoma cells

For transient transfection, cells were seeded into LabTek® chambered coverglasses (8 well, Nunc, Wiesbadenm, Germany) in the appropriate culture medium, 350 µl of cell suspension per well. At 50 % confluency, at least 48 hours after seeding, the cells were transfected with the respective localization vector DNA, using the FuGene® 6 transfection reagent (Roche, Mannheim, Germany). The DNA/FuGene®-complex was prepared prior to the transfection, according to the manufacturers instructions. For each well 0.25 µg of plasmid DNA were used. Controls were run without FuGene® and without the DNA/FuGene®-complex, respectively. After 36-48 hours the transiently transfected cells were prepared for microscopic examination. In order to obtain stably transfected cell lines, wild-type cells were seeded in 6-well plates (Greiner, Frickenhausen, Germany) and transfected as described for the transient transfection, whereas 1 µg of DNA was used for each well. 48 hours after transfection the culture medium was exchanged by medium containing the respective selection antibiotic. G418 (Geneticin, PAA Laboratories) was used at concentrations ranging from 400 to 800 µg/ml and puromycin (Sigma) at concentrations from 1 to 3 µg/ml. After the first passage cells were maintained in 25-cm² culture flasks (Nunc, Wiesbaden, Germany).

3.3.10 Image acquisition of living cells by confocal laser-scanning microscopy

Living cells were seeded into 8-well LabTek® chambered cover slides (Nunc, Wiesbaden, Germany). After 48 hours respectively at the appropriate cell density, the culture medium was exchanged with Leibovitz L15 medium (Sigma), supplemented with 5 % FCS. DRAQ5™ (Biostatus Limited, Leicestershire, UK) was used as nuclear counterstain for multifluorescence CLSM imaging at a final concentration of 5 µM. All cell variants were imaged with a Carl Zeiss Axiovert 200M LSM510 confocal laser-scanning microscope (CLSM), surrounded by a tempered incubation chamber (37 °C). The proper instrument settings were evaluated for all used fluorophor combinations, with respect to excitation and emission crosstalk between the fluorophors. The particular instrument settings (laser excitation wavelengths, beam paths, filter combinations) for the acquisition of each image of fluorophore combination are described in the legends of the respective figures. When required, images were processed with the Carl Zeiss LSM Image Examiner or LSM Image Browser software.

3.3.11 Preparation of fixed samples for confocal laser-scanning microscopy

Cells were fixed with 400 µl of paraformaldehyde solution (PFA, 4 % in PBS, 20 min, room temperature) for each well of a chambered coverglass and chamberslide, respectively. When the cells had been grown on chambered coverglasses the fixative was removed, the cells were washed with PBS, supplemented with 0.5 % BSA, and 400 µl of PBS was added, followed by immediate image acquisition. After fixation of cells grown on chamberslides the cells were washed with PBS 0.5 % BSA and air dried for 5 min. The microscopic slides were mounted with either Confocal-Matrix® (Micro-Tech-Lab, Graz, Austria) or Fluoromount mounting medium (Serva, Heidelberg, Germany).

3.4 Results

3.4.1 Expression of pgp by human glioblastoma cells and by KBwt and KBv1 cells

Figure 3-7 shows the results of the immunostaining with the anti-pgp antibody. While KBv1 cells showed the expected high membranous expression, pgp was not detected in the glioblastoma variants. These results are in agreement with the RT-PCR results (Chapter 4).

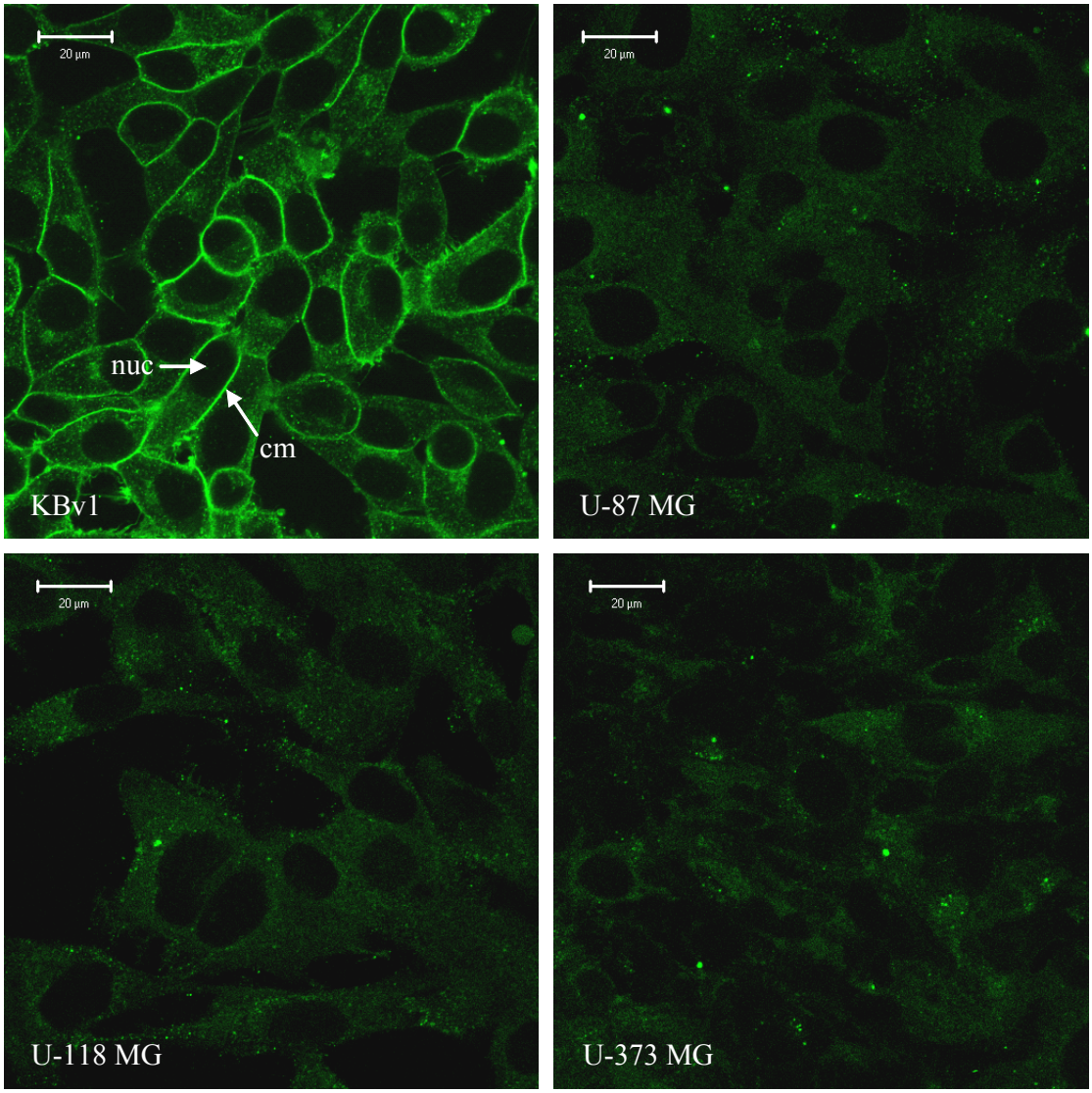

Figure 3-7: Immumostaining of fixed human glioblastoma cell variants U-87 MG, U-118 MG, and U-373 MG. KBv1 cells served as positive control for pgp-overexpression. Besides the non-specific binding of the secondary antibody, no FITC fluorescence emission was detected in the glioma cells; cm: cytoplasmic membrane; nuc: nucleus; Plan-Apochromat 63x/1.4 oil, Ar 488, HFT 488, LP505.

Compared to the vinblastine-treated KBv1 control cells, the KB wild type cells showed a markedly lower extent of pgp expression (Fig. 3-8). However, KBwt cells were not completely negative for pgp. Since the images represent a single optical section within the z-expansion of the cells, it had to be ensured, that the surrounding cells were imaged too and not excluded from data acquisition due to the confocal image acquisition mode. As becomes obvious from the false color display (Fig. 3-8), the selected z-plane is representative of the surrounding KBwt cells too.

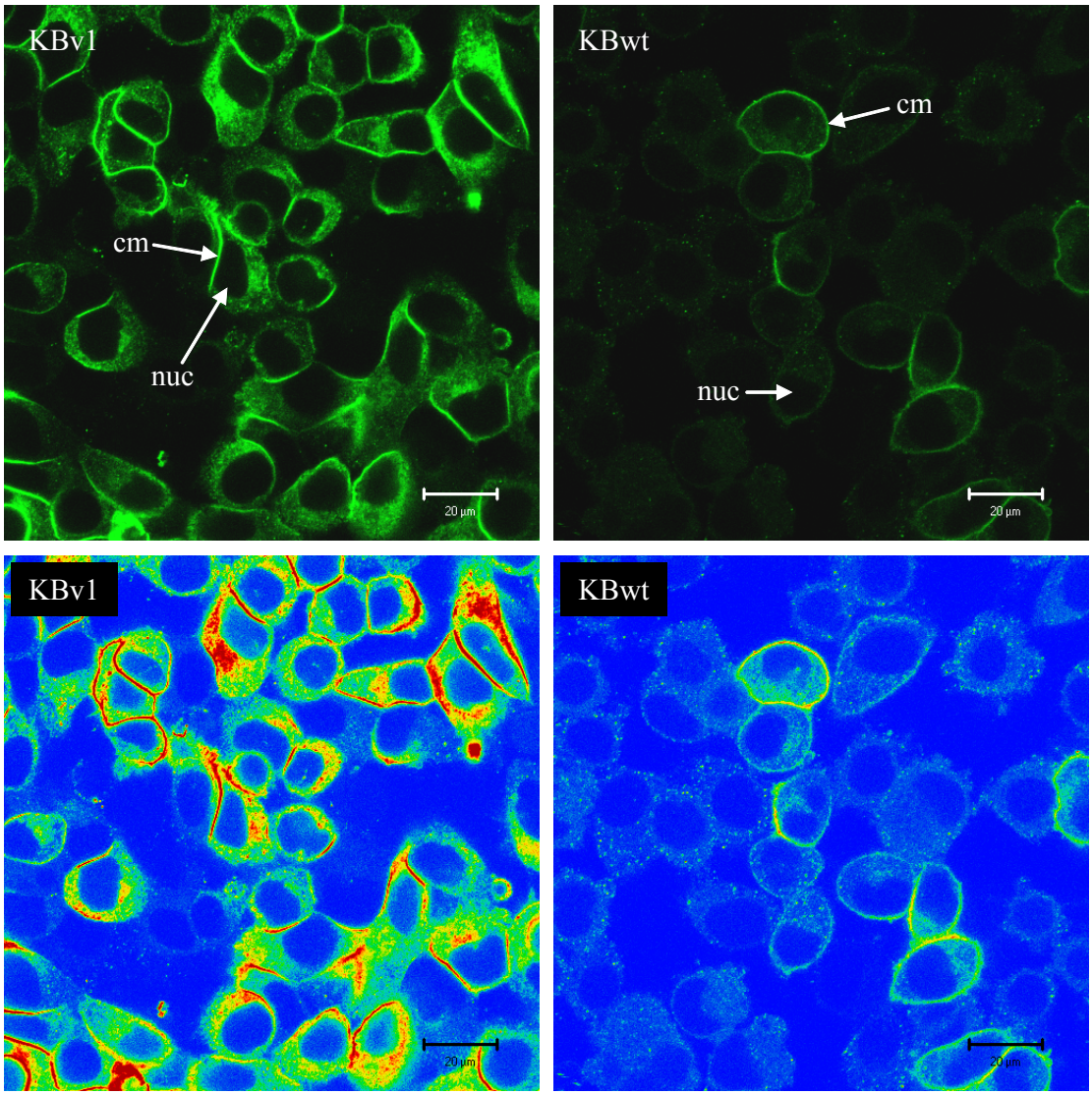

Figure 3-8: Immunofluorescent staining of pgp in KBv1 and KBwt cells. 90 % of the KBv1 cells show high membranous pgp expression compared to ca. 16 % of the wild type cells (upper row). The rainbow false color mode (lower row) displays the fluorescence intensity in each image pixel, whereas warmer colors represent higher intensities. cm: cytoplasmic membrane; nuc: nucleus. Plan-Apochromat 63x/1.4 oil, Ar 488, HFT 488, LP505.

3.4.2 Effect of the mode of doxorubicin application on the proliferation of pgp-overexpressing KBv1 cells

The concentration of the doxorubicin stock solution was determined photometrically (Fig. 3-9). The spectra of two dilutions of the stock solution were acquired (1:100 and 1:200), and the doxorubicin concentration was calculated from the primary absorption maximum value A_{234} and $\varepsilon_{234} = 37120\ M^{-1}\ cm^{-1}$ (European Pharmacopoeia 1997) according to Lambert-Beer's law ($c_{(doxorubicin)} = 2.16$ mM).

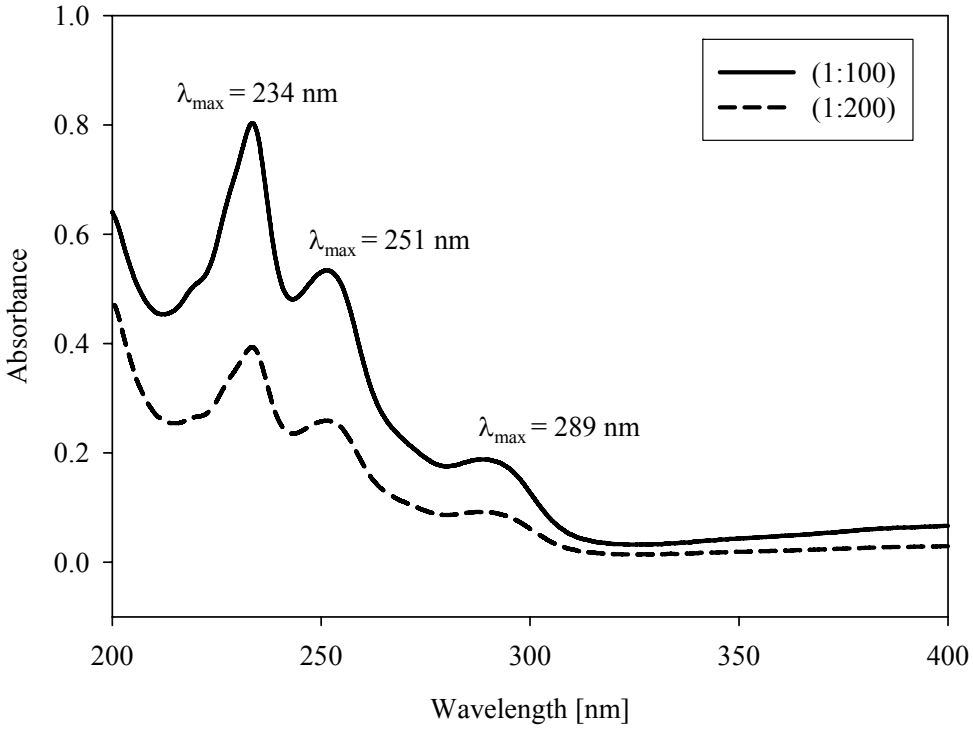

Figure 3-9: Overlay of baseline-corrected UV spectra of doxorubicin stock solutions in 96 % ethanol. The denoted absorption maxima are in accordance with the values of reference spectra in the literature (Ph. Eur. 1997).

According to the results of the UV-measurements, the feed solutions (1000-fold) for the chemosensitivity assays were prepared. The chemosensitivity of pgp-overexpressing KBv1 cells (continuously treated with 300 ng/ml vinblastine in culture) to doxorubicin was determined at concentrations ranging from 100 nM to 2 µM doxorubicin (Fig. 3-10). The highest doxorubicin concentration (2 µM) yielded a moderate cytotoxic effect from which the cells recovered completely. The high resistance of the KBv1 cells is clearly connected to the pgp-overexpression. This becomes obvious from the results of the incubation of KBv1 cells with a combination of doxorubicin to the selective pgp inhibitor valspodar (PSC 833),

demonstrating the dependency of the KBv1 doxorubicin-resistance on pgp functionality (Fig. 3-10). Compared to the sole incubation of the KBv1 with 2 µM doxorubicin, the doxorubicin/valspodar combination resulted in a cytostatic or even cytocidal effect, respectively.

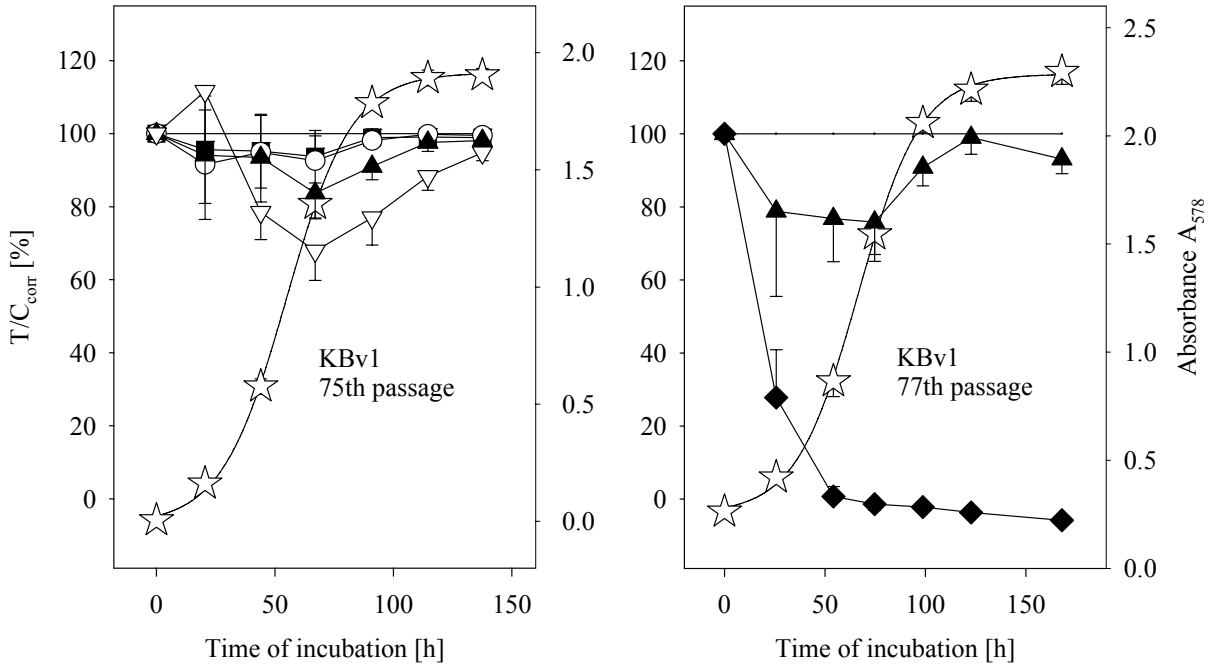

Figure 3-10: Incubation of KBv1 cells with various concentrations of doxorubicin. PBS was used as negative control. ☆ vehicle; doxorubicin concentration: ■ 100 nM, ○ 500 nM, ▲ 1 µM, ▽ 2 µM. ◆ doxorubicin 1 µM + valspodar (PSC 833) 1 µM.

To investigate the effects of different modes of doxorubicin application against pgp-overexpressing cells, KBv1 cells were incubated with DoxoNP and polysorbate 80-caoted DoxoNP up to a concentration corresponding to 3 µM of dissolved doxorubicin (Fig. 3-11). At a doxorubicin concentration of 1 µM all drug formulations exhibited a cytotoxic effect on the KBv1 cells. No significant differences in the antiproliferative activities of doxorubicin in solution, DoxoNP, and doxorubicin combined to polysorbate 80 were observed, even though the latter two modes of application showed a slightly higher cytotoxic effect. Interestingly, incubation of the cells with the polysorbate 80-coated DoxoNP resulted in a stronger inhibition of cell proliferation.. However, the cells recovered from this temporary antiproliferative effect on the same time scale as the cells incubated with the other drug formulations. The same pattern of inhibition of cell growth was found under conditions equivalent to 2 µM doxorubicin, although the incubation of the cells at this concentration led to a generally higher extent of cytotoxicity. The DoxoNP and the mixture of dissolved

doxorubicin with polysorbate 80 exceeded the cytotoxic effect of dissolved doxorubicin alone. Moreover, the coated DoxoNP formulation exceeded the effects of the other formulations, and led to a delay in cell recovery.

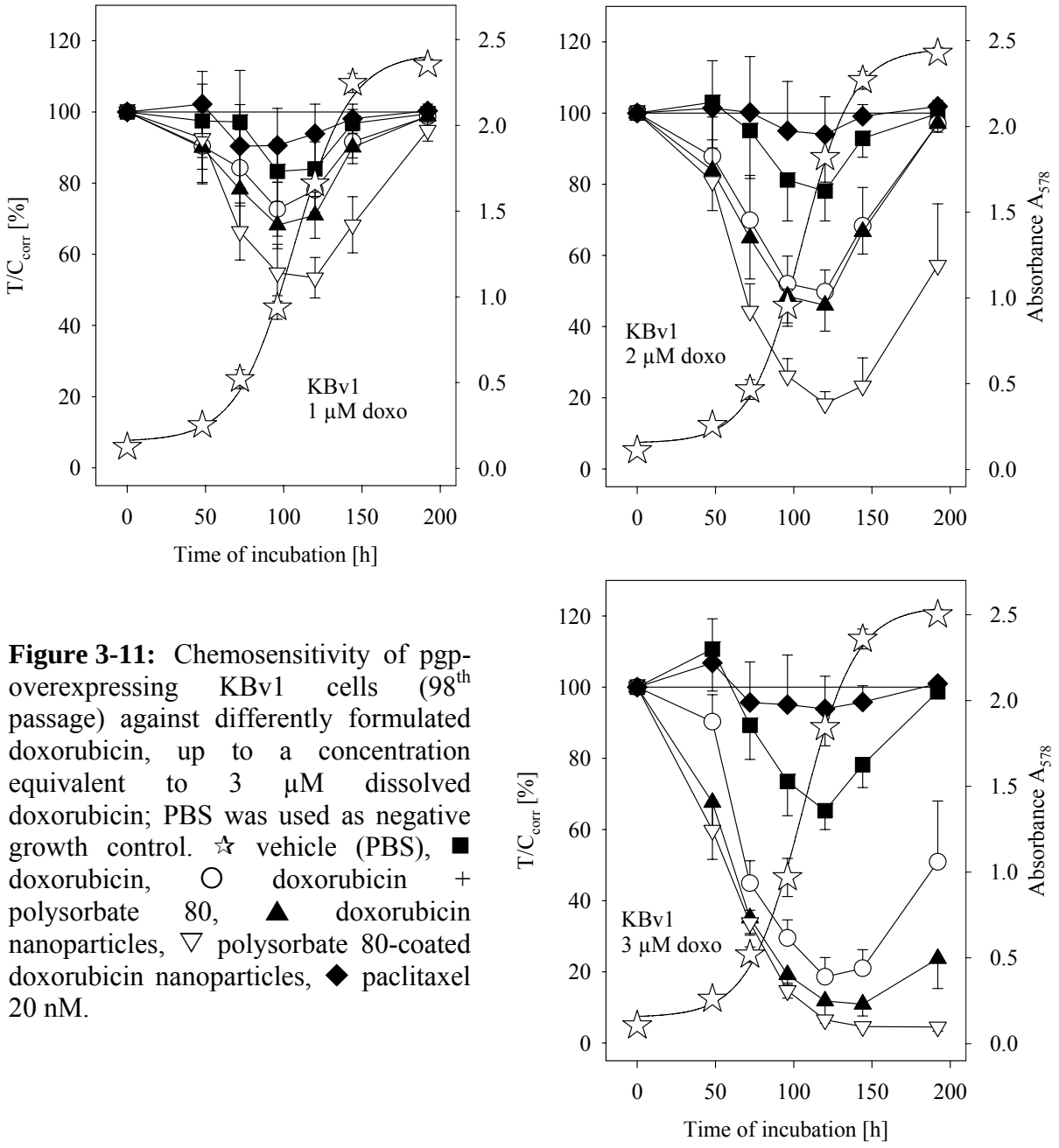

Figure 3-11: Chemosensitivity of pgp-overexpressing KBv1 cells (98th passage) against differently formulated doxorubicin, up to a concentration equivalent to 3 µM dissolved doxorubicin; PBS was used as negative growth control. ☆ vehicle (PBS), ■ doxorubicin, ○ doxorubicin + polysorbate 80, ▲ doxorubicin nanoparticles, ▽ polysorbate 80-coated doxorubicin nanoparticles, ◆ paclitaxel 20 nM.

Finally, under conditions corresponding to 3 µM doxorubicin, differential antiproliferative activities were observed for the different modes of drug application. The incubation with doxorubicin in solution yielded a cytotoxic effect of about 35 % of growth inhibition, compared to the vehicle control. The cells recovered until the end of the incubation period (ca. 200 hours). Doxorubicin + polysorbate 80 produced approximately 80 % inhibition of cell

growth, but the cells started to recover after this nadir. Beginning of cell recovery was also observed after a 90 % growth inhibition by DoxoNP. With the polysorbate 80-coated doxorubicin-loaded PBCA nanoparticles a cytostatic effect occurred. Cell proliferation was inhibited by ca. 95 % of vehicle control, and the cells failed to recover.

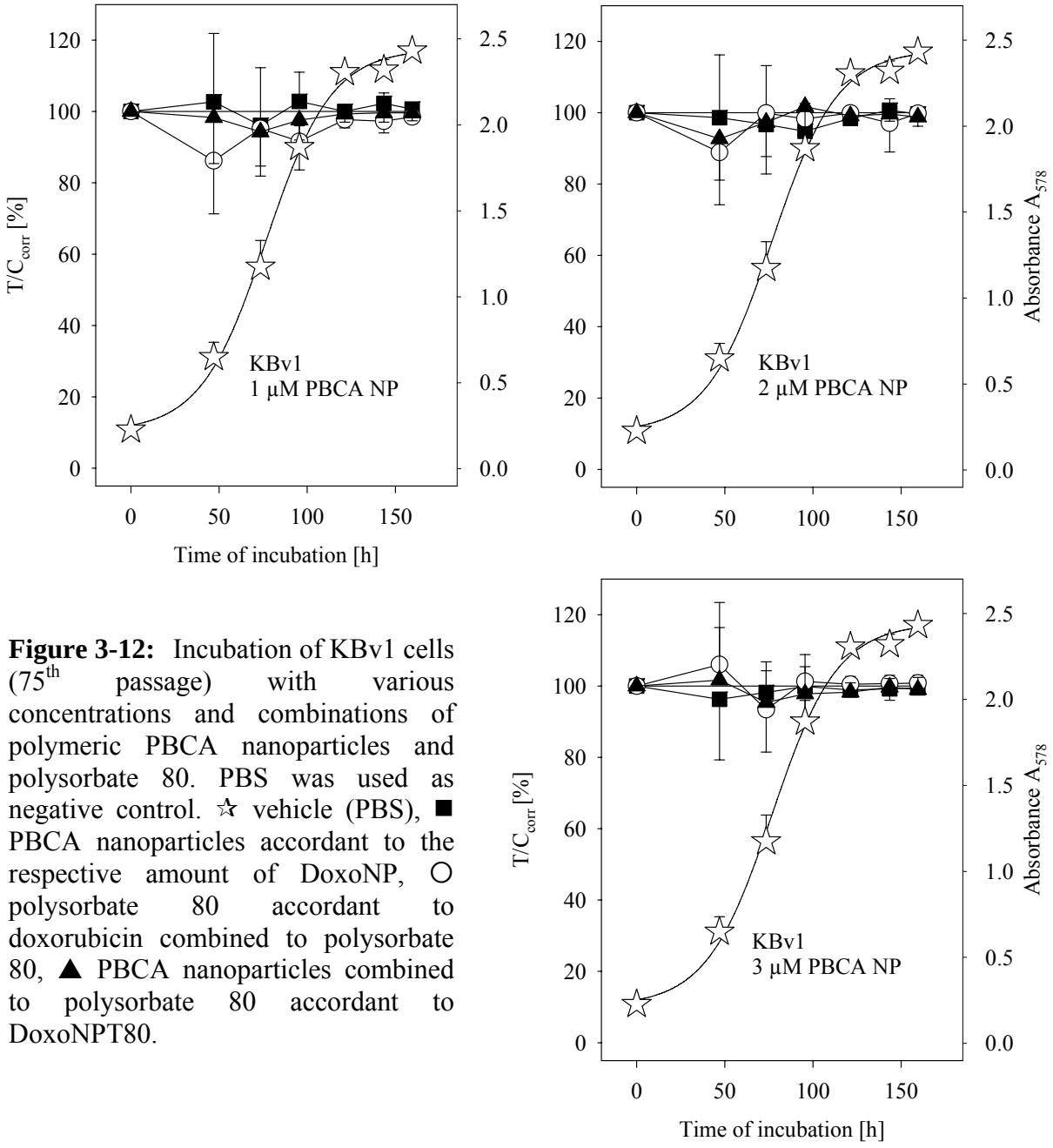

Figure 3-12: Incubation of KBv1 cells (75th passage) with various concentrations and combinations of polymeric PBCA nanoparticles and polysorbate 80. PBS was used as negative control. ☆ vehicle (PBS), ■ PBCA nanoparticles accordant to the respective amount of DoxoNP, ○ polysorbate 80 accordant to doxorubicin combined to polysorbate 80, ▲ PBCA nanoparticles combined to polysorbate 80 accordant to DoxoNPT80.

To ensure that the observed antiproliferative effects did not occur due to non-specific cytotoxicity of the surfactant, the nanoparticle polymer, or a combination of both, KBv1 cells were incubated with the respective amounts of the combination of empty PBCA nanoparticles and polysorbate 80. The results are shown in Fig. 3-12. As becomes obvious from the T/C$_{corr}$

graphs, the proliferation of the KBv1 cells was not inhibited at any concentration of the applied controls. A slight cytotoxic effect seems to occur with polysorbate 80 (according to 1 µM and 2 µM doxorubicin combined to polysorbate 80). However, since the T/C_{corr} values of the vehicle control are found within the experimental errors of the treated cells, this effect is insignificant.

The KBwt cells showed surprisingly low chemosensitivity to doxorubicin, even though expressing low levels of pgp. Concentrations up to 1 µM doxorubicin led to a strong cytotoxic effect. However, the cells recovered, and 2 µM doxorubicin were required to provide a cytocidal effect (Fig. 3-13). These findings may be explained by a fast upregulation of the pgp expression in KB wildtype cells, when incubated with the pgp substrate doxorubicin.

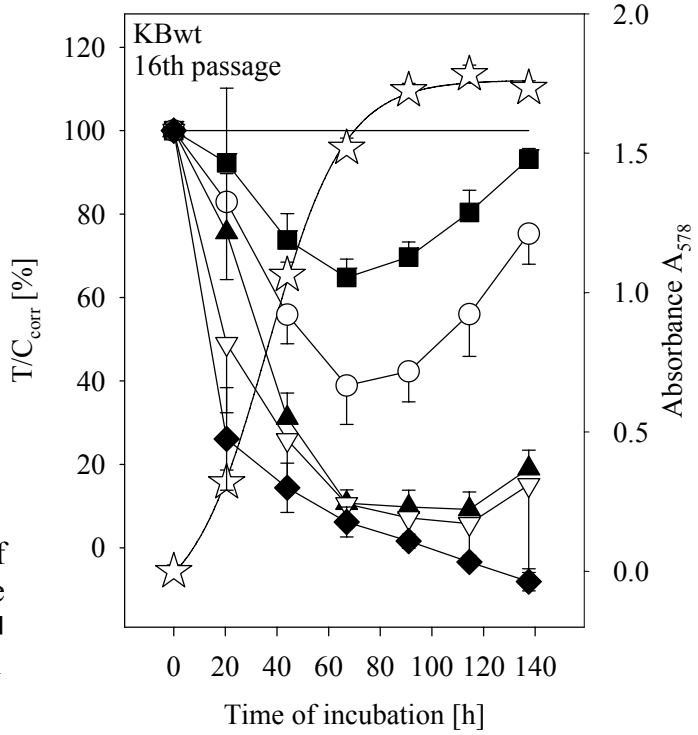

Figure 3-13: Chemosensitivity of KBwt cells to doxorubicin. ☆ vehicle (PBS); doxorubicin concentration: ■ 100 nM, ○ 200 nM, ▲ 500 nM, ▽ 1 µM, ◆ 2 µM.

In order to investigate, if the portion of pgp-overexpressing cells may be raised within a few days of incubation with a pgp substrate, KBwt cells were incubated for 72 hours with 1 µM doxorubicin. Then, after a fixation step, the pgp expression was determined by immunostaining followed by CLSM image acquisition. As shown in Fig. 3-14, the percentage of pgp-overexpressing cells increased from ca. 10 % at 0 hours to almost 100 % at 72 hours of doxorubicin exposure. Fig. 3-14 also depicts a nuclear localization of doxorubicin, which is fluorescent due to its anthracycline partial structure (Fig. 3-5), and thus serves as a nuclear stain in these experiments.

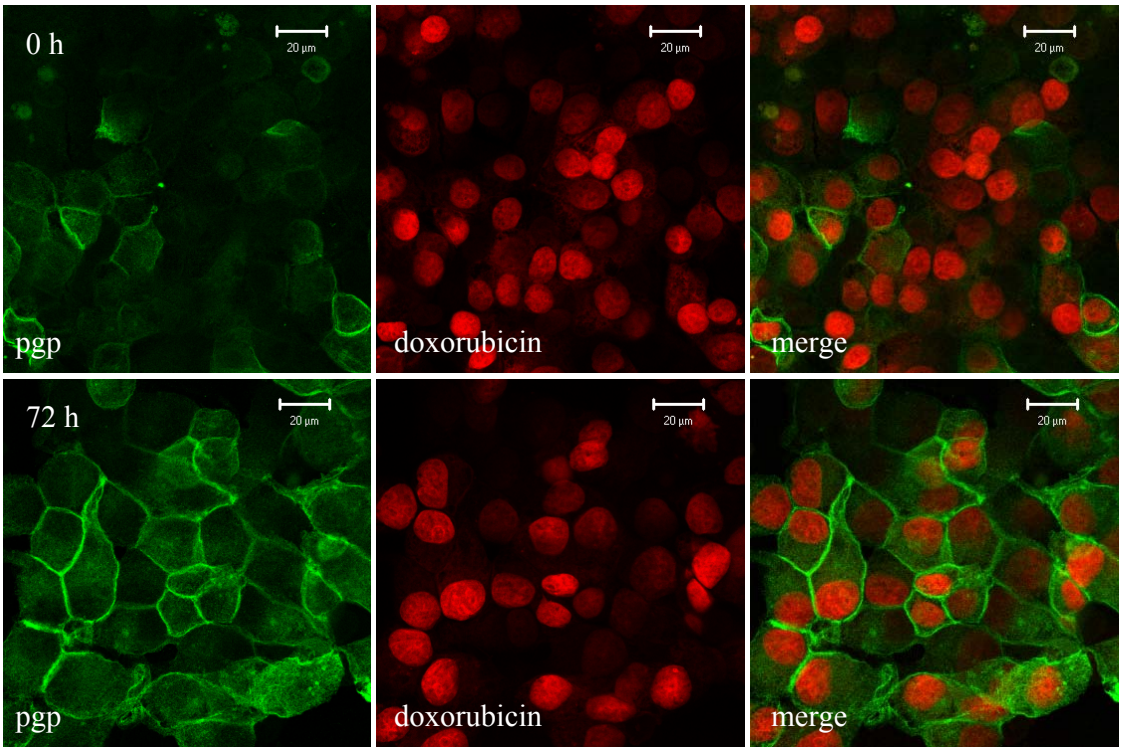

Figure 3-14: Determination of pgp-expression in KBwt cells after 0 hours and 72 hours of incubation with 1 µM doxorubicin. Left: fluorescence emission of Alexa-Fluor® 546-conjugated secondary antibody bound to anti-pgp primary antibody (green false color); middle: fluorescence emission of doxorubicin, localized in the nuclei; right: merged images. Plan-Apochromat 63x/1.4 oil, Ar 488, HFT 488, LP505, HeNe 543, HFT 458/543, BP560-615.

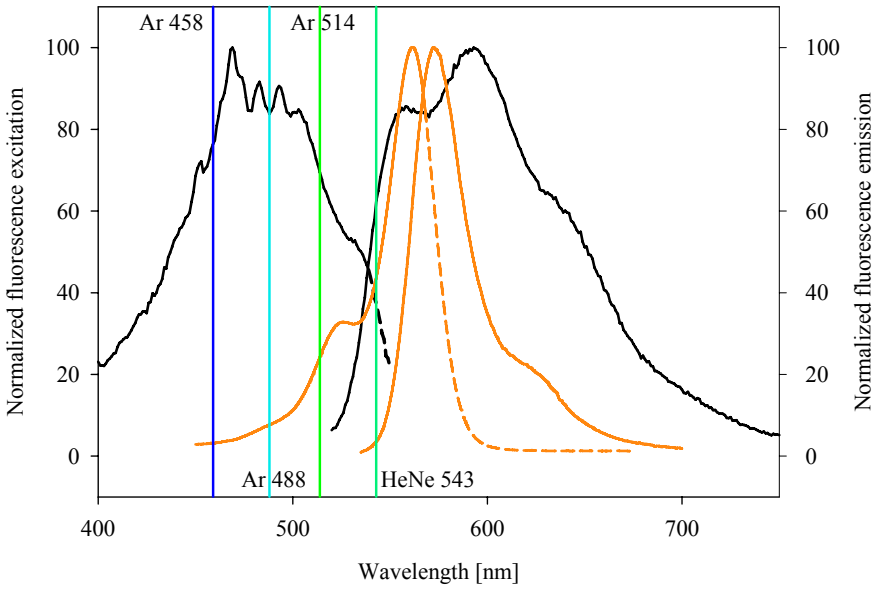

Figure 3-15: Normalized fluorescence excitation and emission spectra of doxorubicin (black, 1 µM in citrate buffered saline, excitation slit: 5, emission slit 10) and Alexa Fluor® 546 (orange, in aqueous buffer, pH 7.2, from http://probes.invitrogen.com). Emission spectra λ_{ex} = 488 nm, excitation spectra λ_{em} = 589 nm. The displayed spectra represent five scans, averaged by the spectrofluorometer. The colored lines parallel to the ordinates represent the laser lines available for doxorubicin excitation.

3.4.3 Flow cytometric quantification of doxorubicin fluorescence associated with glioblastoma cells after incubation with different doxorubicin formulations

The fluorescence properties of doxorubicin allow the flow cytometric quantitation of the cell-associated doxorubicin fluorescence, after cellular uptake or adsorption to the surface of cells. Therefore, the three glioma cell variants were incubated with equivalent doxorubicin concentrations of dissolved drug, DoxoNP, and polysorbate 80-coated DoxoNP, whereas empty PBCA NP and PBCA NP + polysorbate 80 served as controls. The cell-associated doxorubicin fluorescence was determined after incubation periods of 2 hours and 4 hours. Out of the total number of acquired events of each measurement, the intact cell population was gated (Fig. 3-16). From these gated events, the corresponding histogram plot overlays were created, whereas the abscissa scales the relative doxorubicin fluorescence emission and the ordinate depicts the number of events at the respective emission intensity (Fig. 3-17). The geometric means of the histograms were extracted and compared in Fig. 3-18.

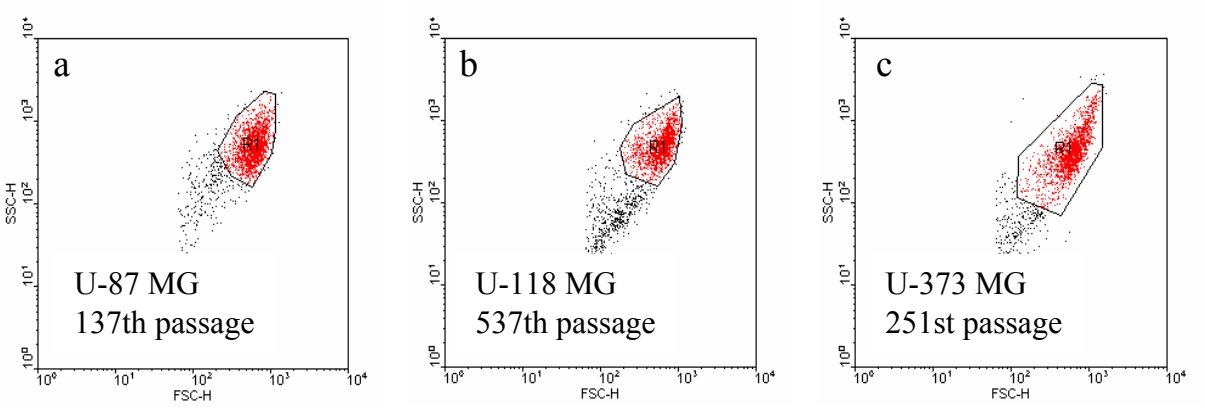

Figure 3-16: Scattergrams of (a) U-87 MG, (b) U-118 MG and (c) U-373 MG cells. The gated (red) events (gate R1) were used for histogram analysis.

Since all of the controls (vehicle, empty nanoparticles with and without polysorbate 80) showed similar results, the histogram and geometric mean data are only shown for the drug containing formulations (Fig. 3-17, 3-18). After an incubation period of 2 hours, cell-associated doxorubicin fluorescence was detected in all of the three glioma cell variants between a 2-fold (U-118 MG) and 4-fold emission intensity (U-87 MG, U-373 MG) compared to the autofluorescence of the cells. Similar fluorescence emission was detected after another two hours of incubation under the same conditions. With U-87 MG cells, after

an incubation period of 2 hours the DoxoNP showed an approximately 2-fold higher increase in fluorescence compared to dissolved doxorubicin. With the latter a further increase in fluorescence was observed after another 2 hours of incubation (2.5-fold of the values of the drug in solution). A similar pattern of cell-associated fluorescence was observed after the incubation of U-118 MG and U-373 MG cells. In the case of U-118 MG cells a 2 hours incubation period with DoxoNP led to a 3-fold higher increase in fluorescence compared to dissolved doxorubicin (4-fold increase after 4 h), whereas a 3-fold and 5-fold raise was measured with U-373 MG after 2 hours and 4 hours, respectively.

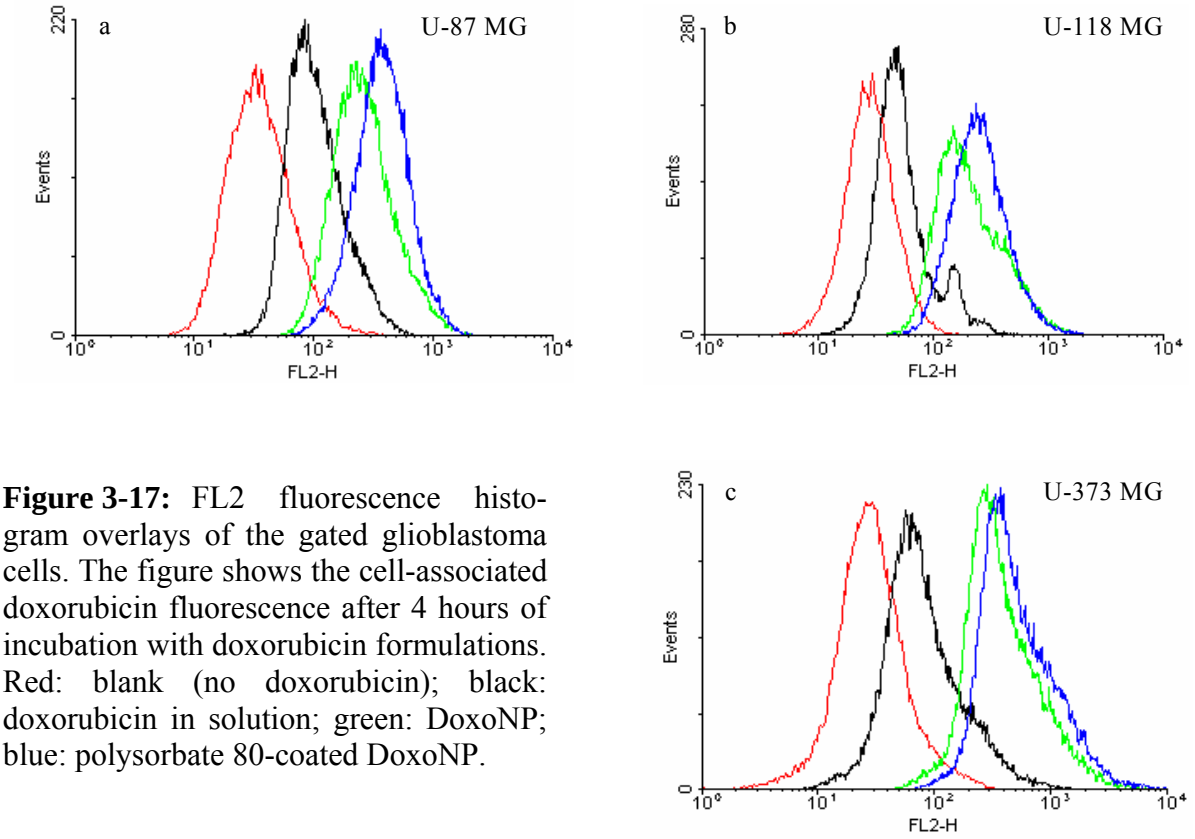

Figure 3-17: FL2 fluorescence histogram overlays of the gated glioblastoma cells. The figure shows the cell-associated doxorubicin fluorescence after 4 hours of incubation with doxorubicin formulations. Red: blank (no doxorubicin); black: doxorubicin in solution; green: DoxoNP; blue: polysorbate 80-coated DoxoNP.

For the first 2 hours of incubation with the Tween80®-coated nanoparticles all three cell variants showed an increase in cell-associated fluorescence slightly higher than observed for the incubation of the glioblastoma cells with the uncoated DoxoNP. After 4 hours, the DoxoNPT80 exceeded the fluorescence of the uncoated DoxoNP formulation. The fluorescence rose to 3.5–7.5-fold, compared to the dissolved drug.

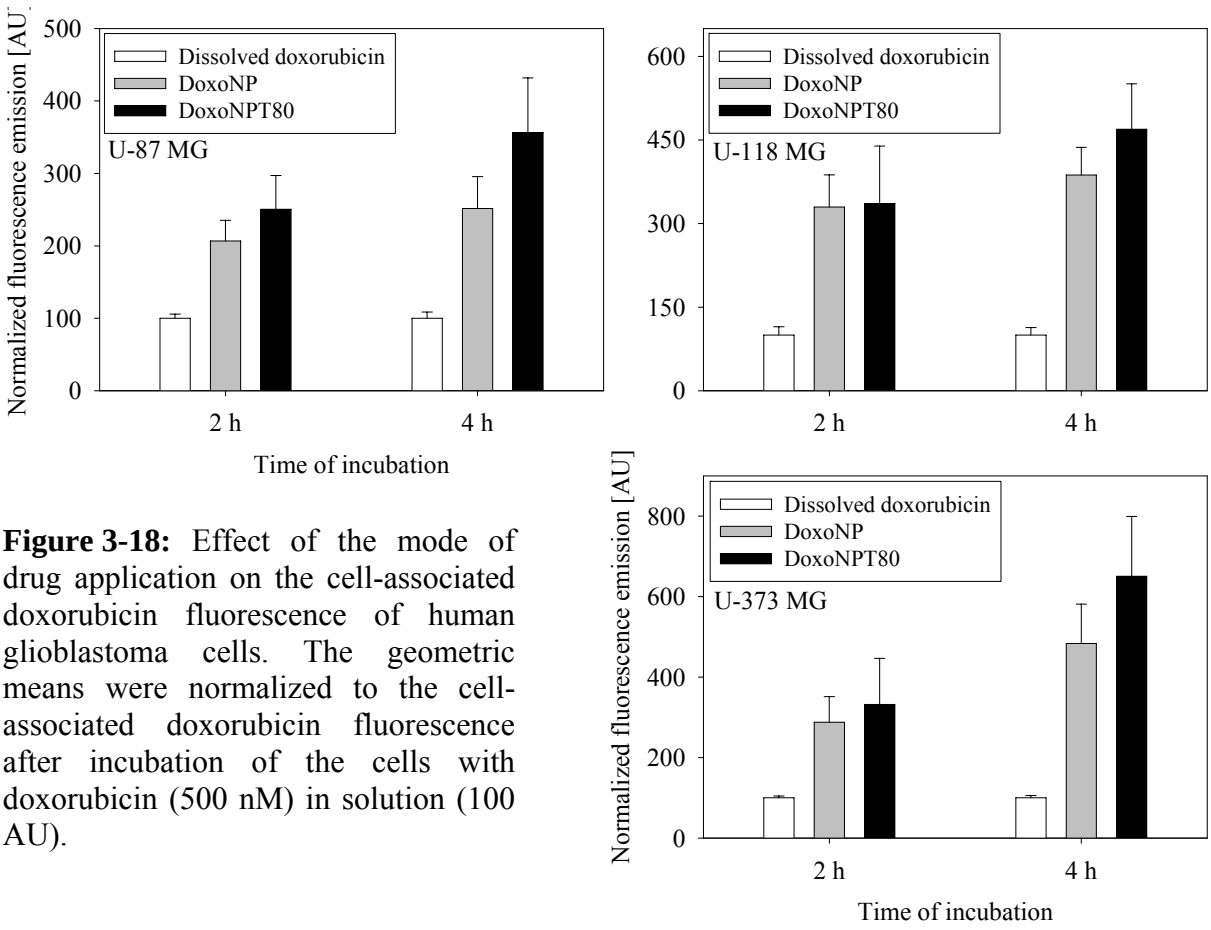

Figure 3-18: Effect of the mode of drug application on the cell-associated doxorubicin fluorescence of human glioblastoma cells. The geometric means were normalized to the cell-associated doxorubicin fluorescence after incubation of the cells with doxorubicin (500 nM) in solution (100 AU).

3.4.4 Flow cytometric determination of cell-associated doxorubicin fluorescence in KB cells

Human KBwt and KBv1 cells were incubated with doxorubicin formulations corresponding to 500 nM of dissolved doxorubicin by analogy to the experiments with the glioblastoma cells. The analysis of the histogram overlay data is shown in Fig. 3-19. Again the geometric means from the histograms were normalized to 100 arbitrary units amounting to the emission intensity of dissolved doxorubicin. After incubation periods of 2 and 4 hours with equivalent doxorubicin concentrations up to 500 nM doxorubicin, the KBwt cells showed a differential increase in the cell-associated doxorubicin fluorescence. The exposure to dissolved doxorubicin yielded an about 1.6-fold increase in the FL2 fluorescence after 4 hours, in the presence of the doxorubicin-loaded PBCA nanoparticles the fluorescence increased 2.5-fold.. The highest increase was observed with the Tween80®-coated nanoparticles. This mode of drug application led to an about 6.6-fold elevation of the cell-associated fluorescence and clearly exceeded the effects of the other drug formulations. Compared to an incubation period

of 2 hours, a further fluorescence increase was observed after 4 hours of incubation, especially for the Tween80®-coated nanoparticles.

The different modes of doxorubicin application show clear differential effects on the increase in the cell-associated fluorescence of the KBwt cells with weak pgp-expression, but not in the cells with pgp-overexpression (KBv1). After 2 hours of incubation a 2-2.5-fold increase in the cell-associated doxorubicin fluorescence was measured. This was followed only by a marginal rise after the 4 hours incubation period. The effect of dissolved doxorubicin on cell-associated fluorescence was not drastically exceeded by the nanoparticle formulations.

As becomes obvious from the results of the chemosensitivity experiments (Fig. 3-10, 3-11), 500 nM doxorubicin is a concentration which does not inhibit the growth of KBv1 cells, presumably due to the overexpression of pgp. A first significant difference in the extent of the cytotoxic effect of different doxorubicin formulations against KBv1 cells was observed with a concentration of 2 µM doxorubicin (Fig. 3-11). Compared to the dissolved drug, an enhanced cytotoxic activity was observed with the DoxoNP and polysorbate 80-coated DoxoNP. This indicates an overcome of the pgp-mediated doxorubicin efflux and an increased cellular accumulation of the compound, respectively, when applied as nanoparticle formulations. Therefore, KBv1 cells were incubated with doxorubicin formulations, equivalent to 2 µM doxorubicin, for 2 and 4 hours. Flow cytometric measurement and data analysis were performed as described for the previously used concentration (500 nM). The results are shown in Fig. 3-20. Both cell types, KBwt and KBv1, show a pattern of doxorubicin-related fluorescence similar to U-87 MG, U-118 MG, and U-373 MG, after incubation with 500 nM doxorubicin. The concentration of 2 µM doxorubicin appears to break through the pgp-mediated multi-drug resistance, leading to high cell-associated doxorubicin fluorescence in pgp-overexpressing KBv1 cells.

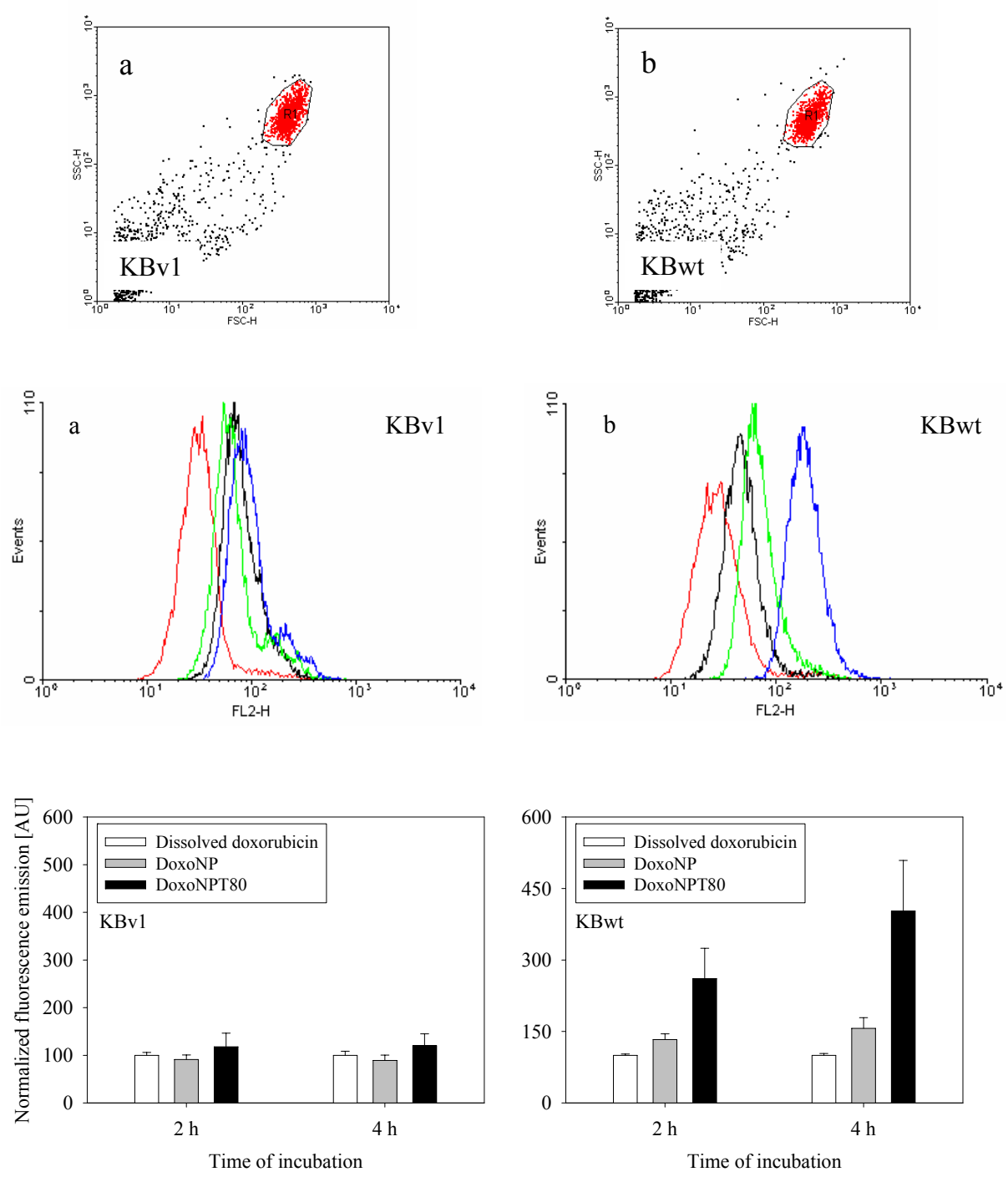

Figure 3-19: Effect of the mode of doxorubicin application on the cell-associated fluorescence of human KB cells. Upper row: dotplots of KBwt and KBv1 cells. Middle row: histogram overlays of gated KB cells after 4 hours of incubation. Red: blank (no doxorubicin); black: doxorubicin in solution; green: DoxoNP; blue: polysorbate 80-coated DoxoNP. Lower row: comparison of normalized doxorubicin-related fluorescence emission associated with pgp low expressing KBwt (right) and pgp high expressing KBv1 cells (left).

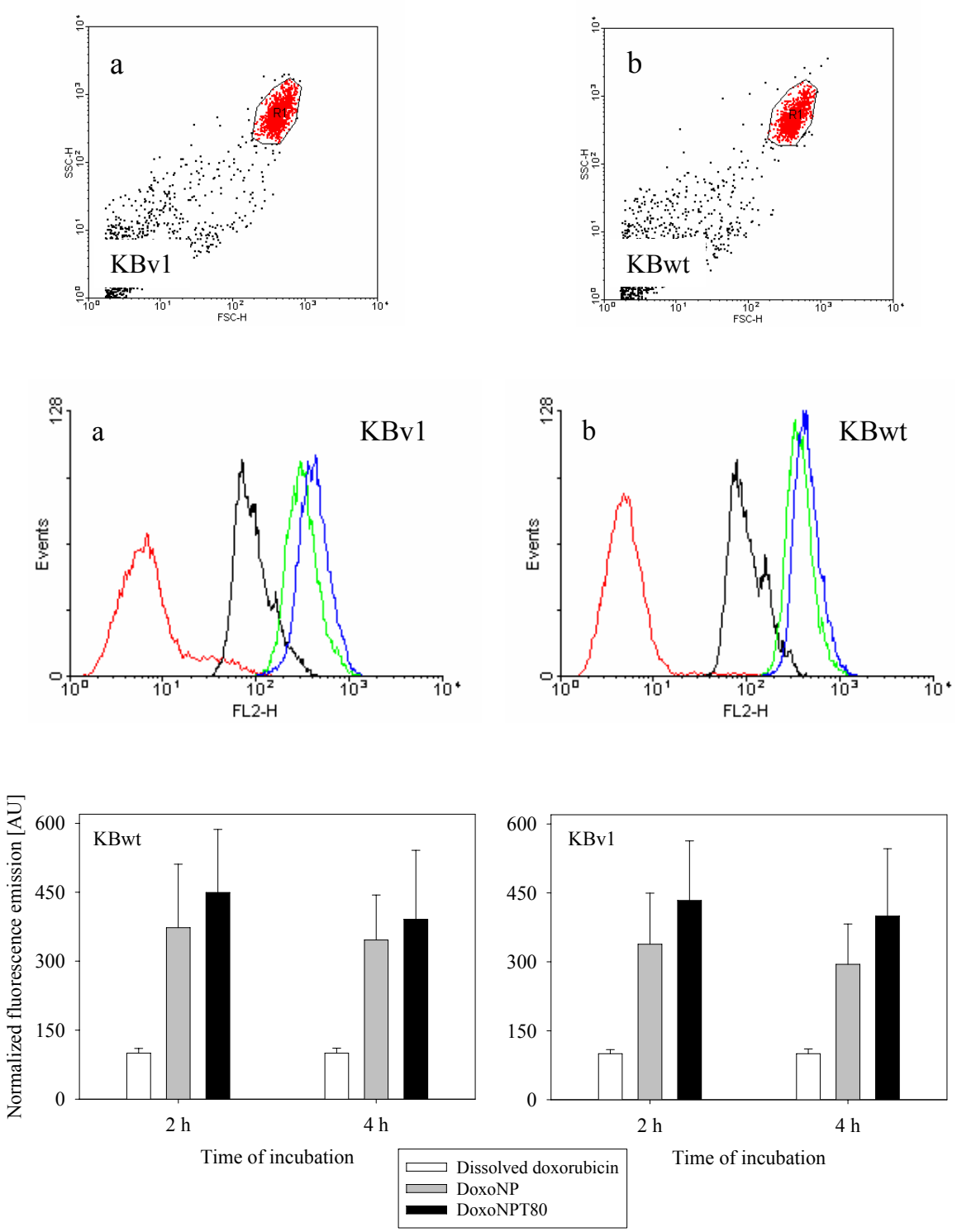

Figure 3-20: Comparison of cell-associated doxorubicin fluorescence in KBwt and KBv1 cells after incubation of the cells with different doxorubicin formulations, amounting to 2 µM doxorubicin. Upper row: forward-sideward scattergrams (dotplots) of KBv1 (a) and KBwt (b) cells. Middle row: FL2 fluorescence histogram overlays of the different samples; red: blank (autofluorescence), black: doxorubicin in solution, green: doxorubicin loaded nanoparticles, blue: polysorbate 80-coated DoxoNP. Lower row: comparison of normalized doxorubicin fluorescence values.

3.4.5 Distribution of doxorubicin fluorescence in human glioblastoma cells

The findings from the flow cytometric experiments indicate a differential cellular doxorubicin accumulation after incubation with various drug formulations. Thus, the cellular distribution of doxorubicin-related fluorescence in living glioblastoma cells was investigated by confocal laser-scanning microscopy. In a preliminary experiment U-87 MG glioblastoma cells were incubated with doxorubicin in solution, at a concentration of 10 µM, for 5 minutes at 37 °C (inside the incubation chamber of the microscope) followed by CLSM image acquisition of the living cells (Fig. 3-21). After this short period of incubation with the dissolved drug, doxorubicin-related fluorescence was detected throughout the cytoplasm with higher intensity in the proximity of the nuclei. Surprisingly, the nuclei remained unstained.

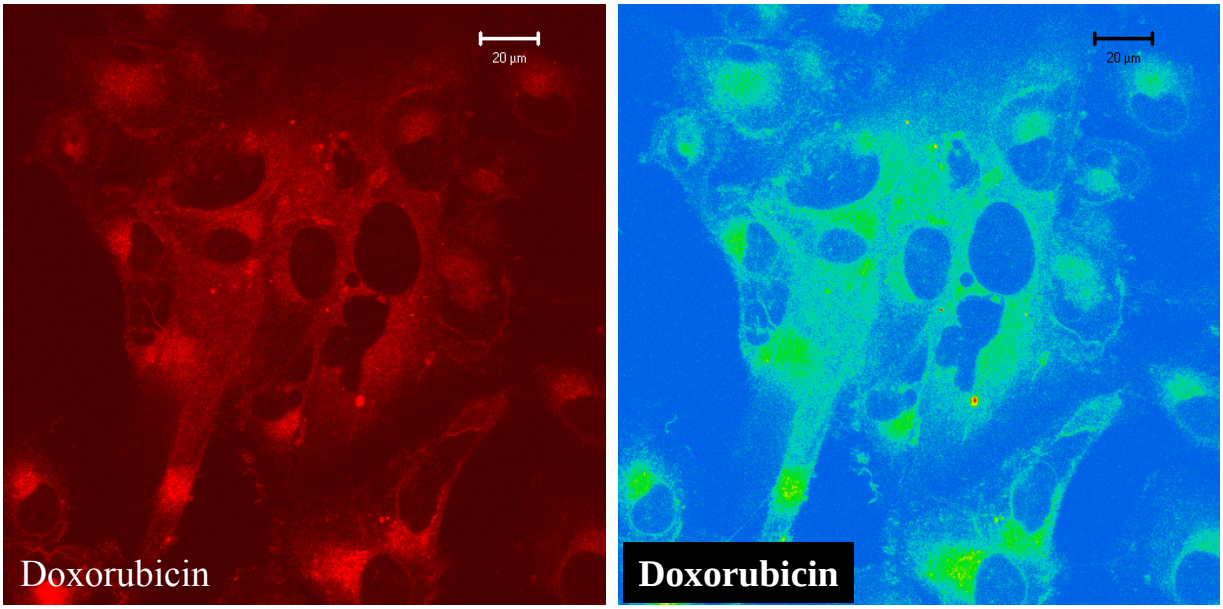

Figure 3-21: Distribution of doxorubicin fluorescence in living U-87 MG cells, incubated with doxorubicin. The rainbow false color mode (right image) displays the fluorescence intensity of each image pixel. Warmer colors represent higher intensities. This display mode illustrates the diffuse fluorescence in the cytosol with accumulation of doxorubicin in the vicinity of the nuclei, which appear unstained. Plan-Apochromat 63x/1.4 oil, HeNe 543, HFT 488/543/633, LP650.

Since doxorubicin exclusively stained cell nuclei in fixed KBwt cells (Fig. 3-14), this major difference in the cellular doxorubicin distribution was further investigated by comparison of living and fixed cells, incubated with doxorubicin under equal conditions. To make sure that lack of nuclear staining did not occur due to the short incubation time of 5 minutes, the incubation time was increased and the doxorubicin concentration was decreased. Doxorubicin

was applied to human U-87 MG glioblastoma cells at a concentration of 2 µM. After 60 minutes of incubation, CLSM images were acquired of the living cells immediately. The cells were fixed with PFA (4 % solution in PBS) for 20 minutes at room temperature and imaged. Images of the living and the fixed cells are shown in Fig. 3-22.

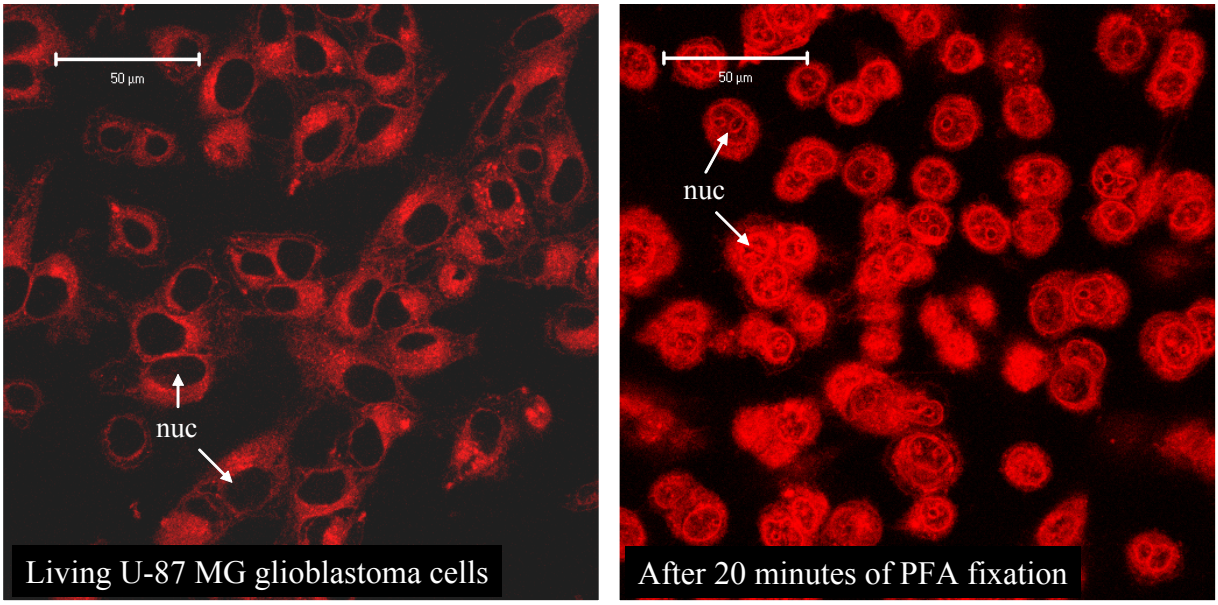

Figure 3-22: Differential distribution pattern of doxorubicin in living and fixed U-87 MG cells after 1 hour of incubation; nuc: nuclei. Plan-Apochromat 63x/1.4 oil, HeNe 543, HFT 488/543/633, BP560-615.

Again, the living cells showed doxorubicin distribution mainly in the cytoplasm but no doxorubicin-related fluorescence was detected in the nuclei of the cells. After PFA fixation this distribution pattern was almost completely inverted, and the doxorubicin fluorescence was localized mainly in the nuclei, as depicted in Fig. 3-14, also representing fixed cells previously incubated with doxorubicin. Since the nuclear DNA is the primary site of action of the intercalating agent doxorubicin, the drug has to enter the nuclei of living cells. The lack of nuclear fluorescence may have occurred due to the interaction of doxorubicin with DNA, leading to altered fluorescence properties of the Doxo-DNA adducts. This hypothesis was investigated by acquisition of doxorubicin/DNA UV-vis difference spectra and fluorescence spectra of doxorubicin/DNA mixtures. For the UV-vis measurements a 20 µM doxorubicin solution was used together with DNA concentrations of 10 µg/ml, 20 µg/ml, and 60 µg/ml, whereas the samples for the acquisition of fluorescence spectra were prepared with 1 µM doxorubicin and DNA concentrations ranging from 0.5 to 50 µg/ml. The high doxorubicin concentration had to be chosen for the UV-vis measurements because of the lower sensitivity of the absorption compared to the sensitivity of fluorescence detection. The acquired

difference spectra and fluorescence excitation and emission spectra are shown in Fig. 3-23 and Fig. 3-24, respectively. The addition of DNA did not reduce doxorubicin absorbance to a remarkable extent (Fig. 3-23). The slight deviations from zero shown in the inset of Fig. 3-23 most probably result from experimental errors during sample preparation. On the contrary, with increasing concentrations of DNA, the relative fluorescence excitation and the fluorescence emission of doxorubicin decreased notably (Fig. 3-24). As becomes obvious from Fig. 3-25, the DNA quenches the doxorubicin fluorescence with decreasing doxorubicin/DNA molar ratio. This explains the observation that doxorubicin fluorescence is hardly found in nuclei of living cells, due to the high excess of DNA in the nucleus. Nuclear staining with doxorubicin after fixation with PFA may occur due to denaturation of the DNA-histon complex, and this may lead to an increase in the nuclear concentration of free, not DNA-bound doxorubicin. As a consequence, further investigations on the subcellular distribution of doxorubicin were performed with living cells.

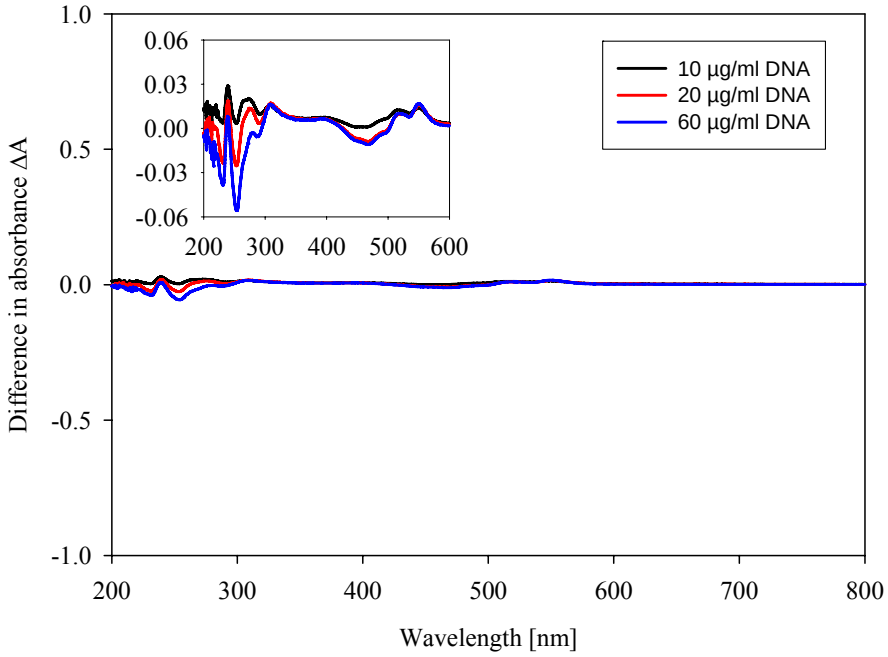

Figure 3-23: UV-vis difference spectra of doxorubicin/DNA. The inset shows the difference spectra with adjusted axes. Only minor differences in absorbance are observed between 200–300 nm and 400–600 nm. The chosen DNA concentrations result in doxorubicin/DNA ratios identical to those of the samples containing the lowest DNA concentration in the spectrofluorometric measurements (see Fig. 3-24).

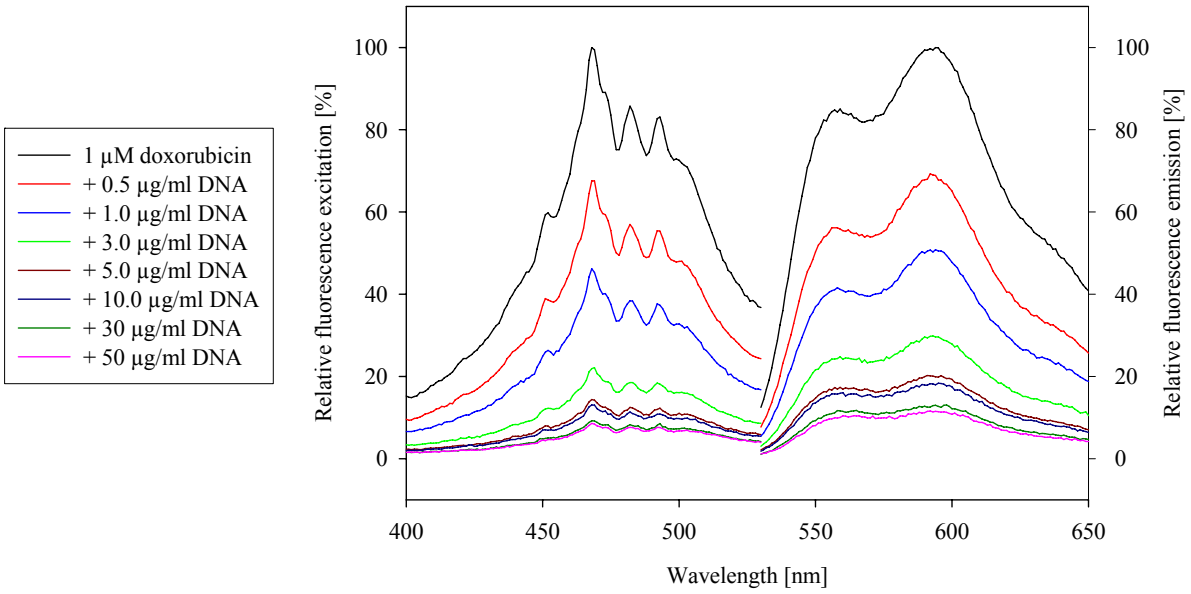

Figure 3-24: Normalized fluorescence spectra of doxorubicin and doxorubicin/DNA mixtures in citrate buffered saline (CS buffer). Excitation spectra λ_{em} = 589 nm; emission spectra λ_{ex} = 488 nm (excitation slit: 5, emission slit: 10).

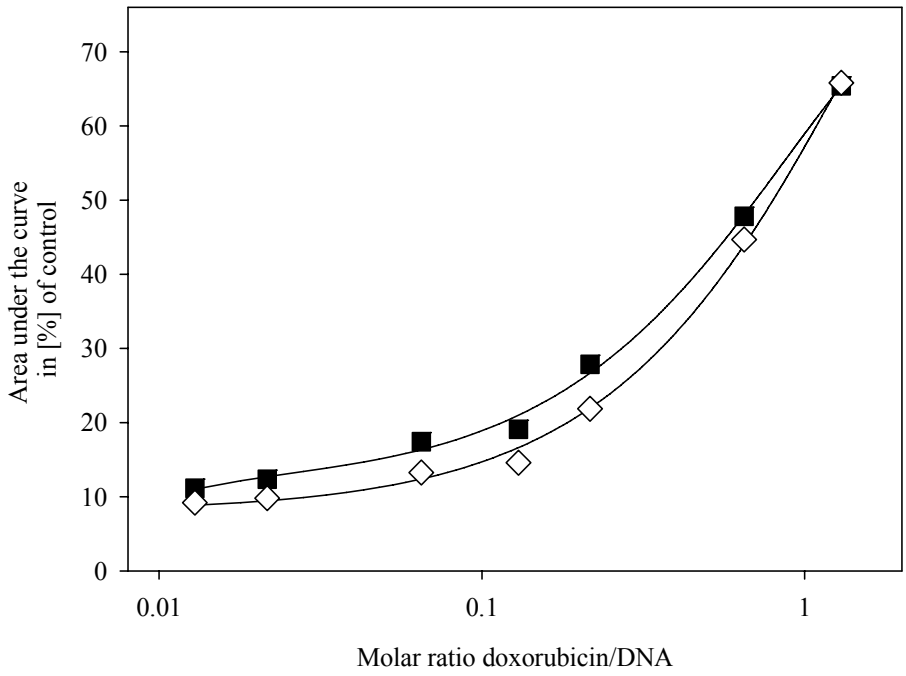

Figure 3-25: Effect of DNA on doxorubicin fluorescence. The abscissa depicts the molar ratio of doxorubicin and DNA. The ordinate scales the fluorescence amount as area under the excitation spectra curve (◇) respectively under the emission spectra curves (■) from Fig. 3-24. All areas under the curves were normalized to the areas of doxorubicin spectra curves without DNA (100 %).

3.4.6 Multifluorescence live-cell imaging and colocalization studies

In order to study the cellular distribution of doxorubicin fluorescence in living cells, selective fluorescent labeling of various cellular compartments was evaluated for multifluorescence imaging, with respect to colocalization with doxorubicin.

3.4.6.1 Fluorescent staining of nuclei in living cells

Several requirements have to be fulfilled by an ideal fluorescent dye as nuclear counterstain for further multifluorescence experiments. Firstly, rapid permeation of the dye into the nuclei of the cells. Secondly, the dye should selectively stain nuclear DNA without causing background fluorescence, neither from the dissolved dye in the culture medium nor by staining of mitochondria or binding to RNA. Furthermore, the staining protocol should not require extensive preincubation periods followed by washing steps, which could lead to changes in the cellular distribution of other fluorescent compounds. All of these prerequisites were fulfilled by the fluorescent nuclear staining dye DRAQ5™ (Fig. 3-26). At a concentration of 5 µM DRAQ5™ selectively stained the nuclei after 1-2 minutes (Fig. 3-27). No washing steps of the cells were necessary and the mitochondria were excluded from staining (Fig. 3-27), even after incubation with DRAQ5™ up to 48 hours.

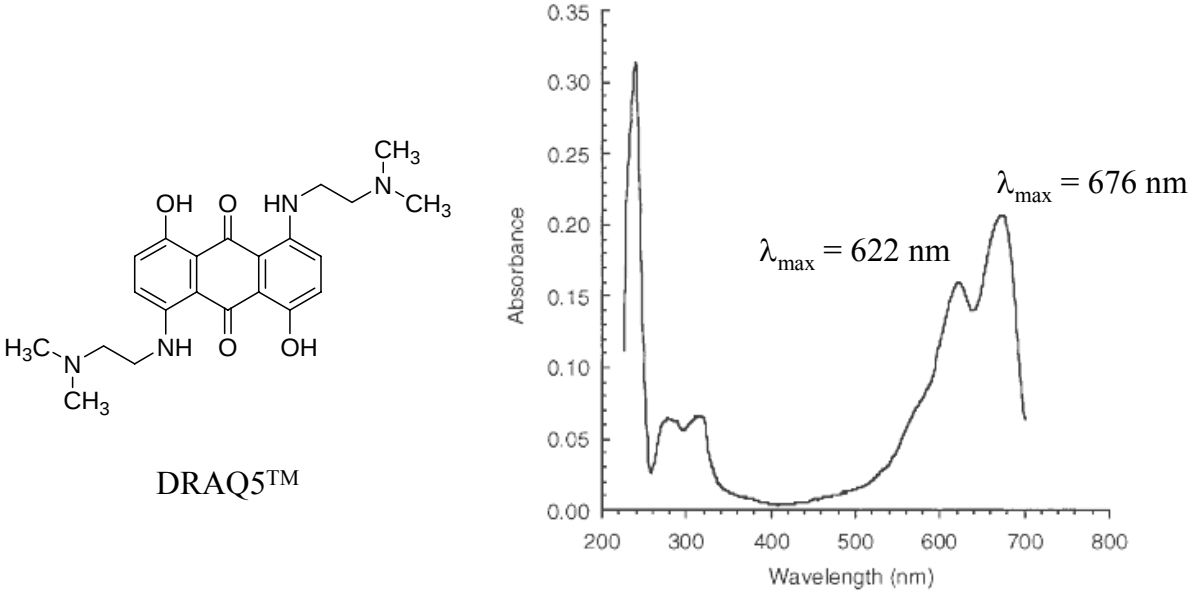

Figure 3-26: Fluorescent cell-permeant anthrachinone derivative DRAQ5™. Left: chemical structure; right: UV-vis absorbance spectrum (Smith et al. 2000).

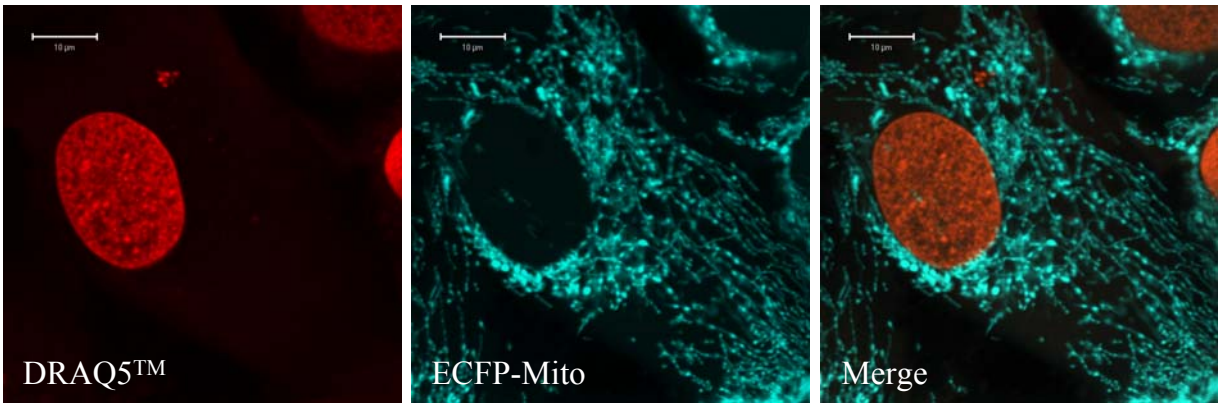

Figure 3-27: DRAQ5™-stained nuclei in living U-87 MG cells, bearing ECFP-labeled mitochondria. The nuclear dye (final concentration 5 µM) was added 1 minute prior to CLSM imaging. DRAQ5™ exclusively stained the nuclei, and no dye was detected in the mitochondria. Moreover, no crosstalk between ECFP and DRAQ5™ was observed. Plan-Apochromat 63x/1.4 oil, Ar 458, HFT 548, LP475; HeNe 633, HFT 488/543/633, LP650.

3.4.6.2 Mitochondrial staining in living cells

Several compounds show high affinity to metabolically active mitochondria due to their high electrical potential at the inner membrane. Up to now a broad variety of fluorescent mitochondrial stains is commercially available, e.g. Rhodamine 123, Tetramethylrosamine, MitoFluor™-, and the MitoTracker®-dyes. Especially the latter compounds stand out by their rapid staining and low cytotoxicity in live cell imaging. Moreover, compared to Rhodamine 123 or Tetramethylrosamine, the MitoTracker® dyes are not washed off the mitochondria when their membrane potential breakes down during fixation.

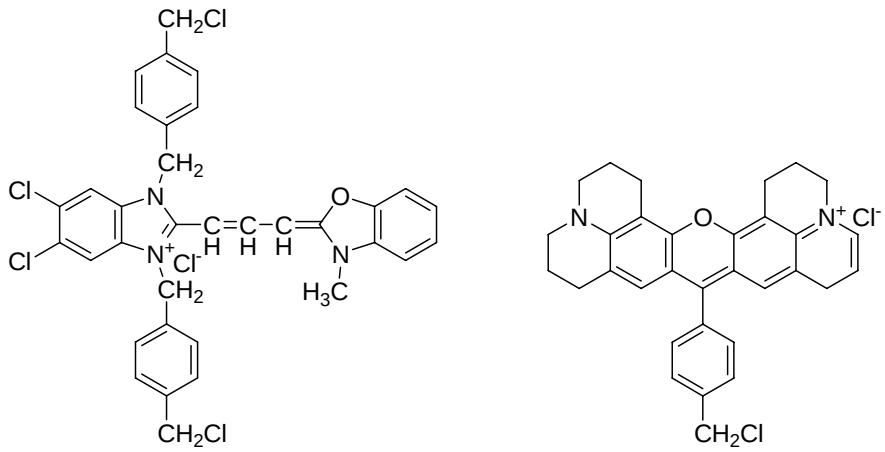

MitoTracker® Green MitoTracker® Red CMXRos

Figure 3-28: Chemical structures of MitoTracker® Green (left) and MitoTracker® Red CMXRos (right). The structures were taken from the Molecular Probes homepage http://probes.invitrogen.com.

Fig. 3-29 shows images of a living U-87 and a U-373 MG cell, stained with MitoTracker® Green and MitoTracker® Red CMXRos, respectively. Due to its fluorescence properties MitoTracker® Green was evaluated for co-labeling of glioblastoma cells, incubated with doxorubicin. An overlay of the fluorescence excitation spectra is given in Fig. 3-30. After co-staining with doxorubicin and MitoTracker® Green, fluorescence images were acquired in the multichannel acquisition mode, using the argon laser (488 nm). Though the excitation spectra of both compounds show a high overlap, the fluorescence signals were separated using proper emission filters (Fig. 3-30).

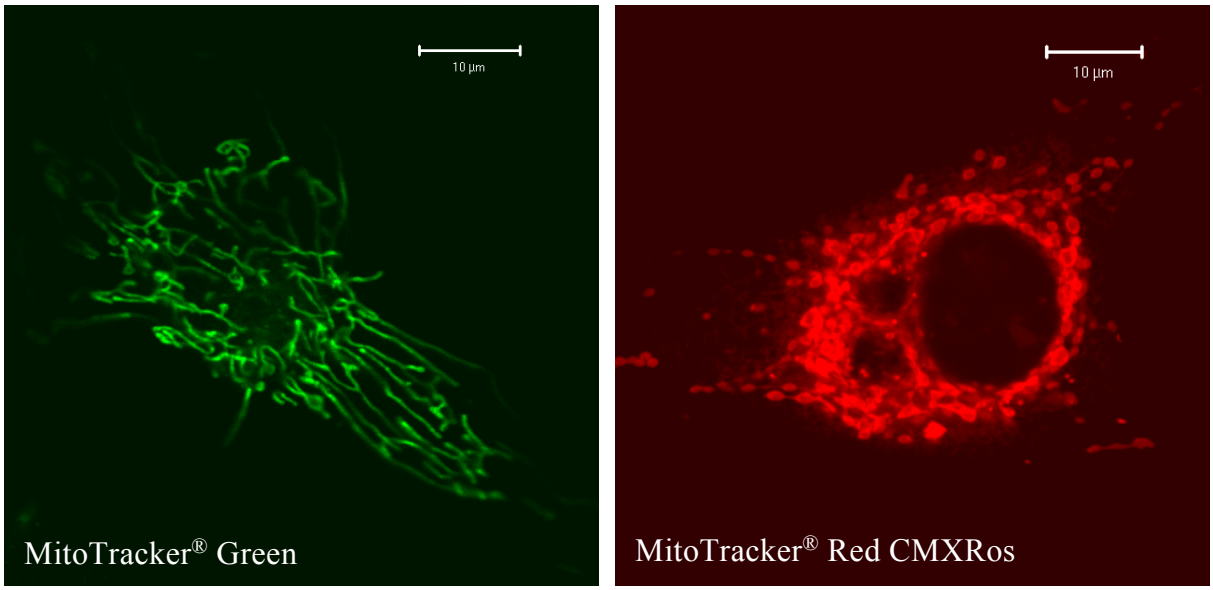

Figure 3-29: Selelctive fluorescent staining of mitochondria in U-373 MG (left) and U-87 MG (right) cells. In U-373 MG the mitochondria appear as twine-like structures, spanning through the whole cell, whereas in U-87 MG they appear as beads. The diameter is about 1 µM with a length of 1-2 µM. Plan-Apochromat 63x/1.4 oil; Ar 488, HFT 488, LP505 (MitoTracker Green); HeNe 543, HFT 488/543/633, LP560 (MitoTracker® Red CMXRos).

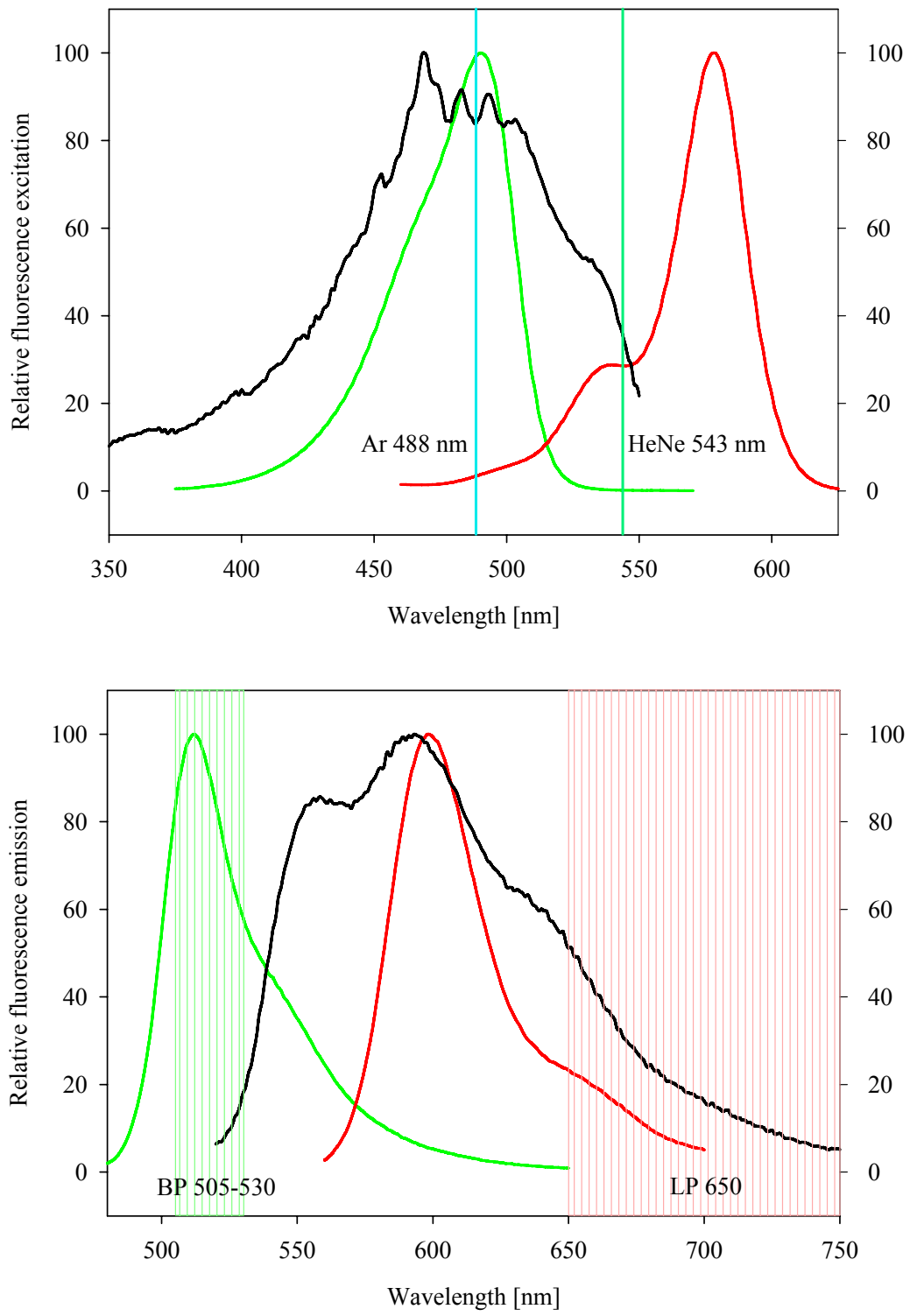

Figure 3-30: Overlay of fluorescence excitation (upper chart) and emission (lower chart) spectra of doxorubicin (black), MitoTracker® Green (light green), and MitoTracker® Red CMXRos (red). Using a 505-530 nm band pass filter and a 650 nm long pass filter, the green MitoTracker® may be considered as a suitable couterstain to doxorubicin. The excitation spectra of MitoTracker® Red CMXRos and doxorubicin overlap at 543 nm (dark green line), which represents the only available excitation wavelength for the mitochondrial stain. Due to the concomitant overlap of fluorescence emission spectra the red MitoTracker® dye is improper for a co-staining with doxorubicin. MitoTracker® reference spectra were taken from the Molecular Probes homepage http://probes.invitrogen.com (with modifications).

After the simultaneous incubation of U-87 MG cells with doxorubicin and MitoTracker® Green, doxorubicin accumulation in an organelle close to the nucleus was observed, whereas the selectively counterstained mitochondria showed a markedly differing distribution pattern (Fig. 3-31). Though anticipating no crosstalk between the two compounds, processing of the original images with the multichannel unmixing module uncloaked a slight bleeding of MitoTracker® emission into the doxorubicin detection channel.

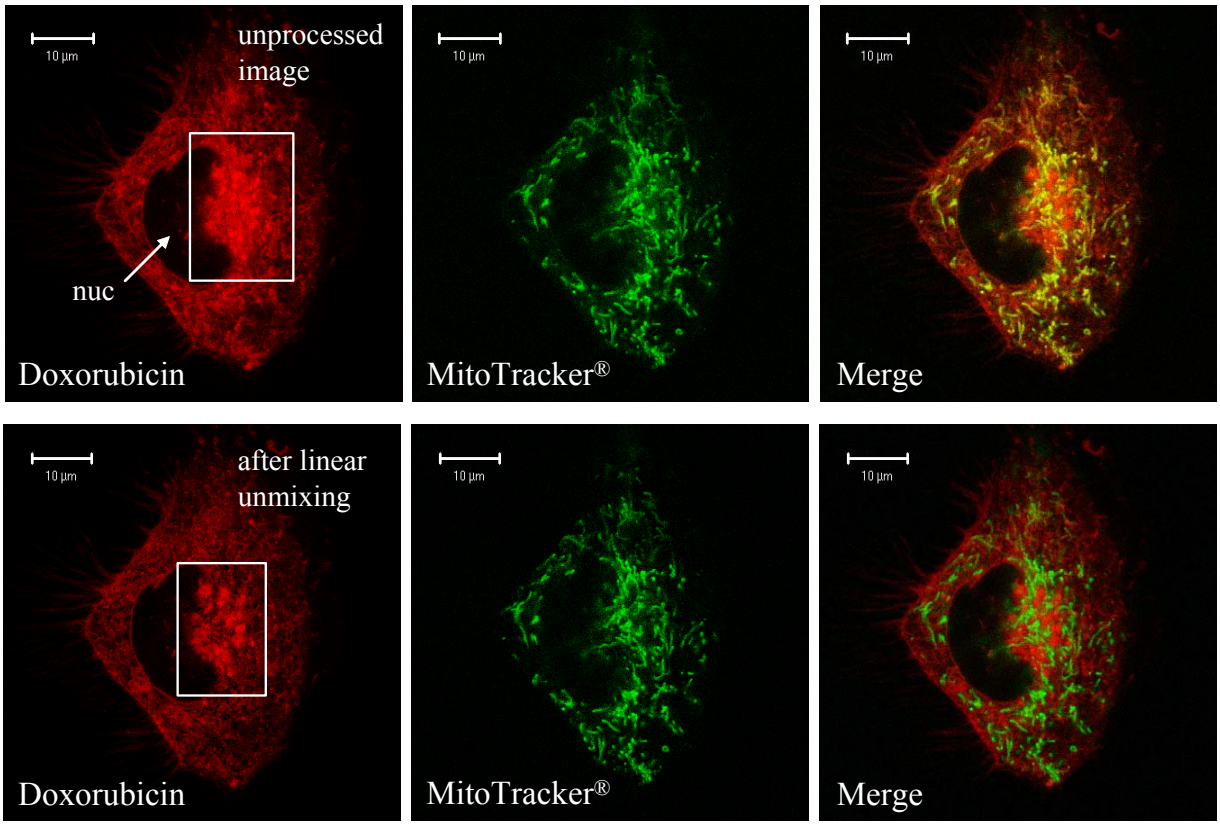

Figure 3-31: U-87 MG cell, labeled with 100 nM of MitoTracker® Green and 1 µM doxorubicin for 30 minutes. Upper row: original images of fluorescence emission channels; lower row: images after linear unmixing. Most of the doxorubicin fluorescence is localized in a compartment near the nucleus. However, the fluorescence channel unmixing revealed slight fluorescence crosstalk between the two stains. Plan-Apochromat 63x/1.4 oil; Ar 488, HFT 488, BP505-530, HeNe 543, HFT 458/543, LP585.

This automatic component extraction (ACE) software module extracts the characteristic fluorescence components of the multifluorescence image and reassigns them to different channels in the processed image. Within certain limitations this method can substitute spectral unmixing procedures, which usually necessitate fluorophor reference spectra and the acquisition of the spectral data of each image pixel. If the fluorescence emission spectra of the used fluorophores do not exceed a certain extent of overlap, the ACE can overcome excitation as well as emission crosstalk. However, the fluorescence of the mitochondrial stain was not

stable under the used imaging conditions. After a few scans, the decreased fluorescence emission had to be compensated by an increased excitation intensity, which led to cytotoxicity, probably caused by phototoxic reactions.

Due to the drawback from the experiments with the MitoTracker® dye, another approach was employed to achieve selective fluorescent labeling of mitochondria in human glioblastoma cells, the transfection with a modified mitochondria localization vector, pECFP-Mito. This vector is specifically designed for the fluorescent labeling of mitochondria. It encodes a modified mitochondrial targeting sequence from the human cytochrome C oxidase precursor fused to the N-terminus of the enhanced cyan fluorescent protein (Rizzuto et al. 1989; Rizzuto et al. 1995) This EGFP variant (Heim et al. 1994; Heim and Tsien 1996; Miyawaki et al. 1997) shows its major fluorescence excitation maximum at 433 nm and its minor excitation maximum at 453 nm, making it suitable for the excitation by the Ar 458 laser plasma line of the CLSM scanning unit. Since the major fluorescence emission maximum is at 475 nm (a minor peak is at 501 nm), the fluorescence emission was detected using either longpass (LP) or bandpass (BP) filters, starting from 475 nm.

Figure 3-32: Agarose gel analysis of pQCXIP/ECFP-Mito. After propagation in *E. coli*, the plasmid was digested the restriction enzymes *Eco*RI and *Bam*HI. Both digests led to bands at 8 kb, representing the linearized vector, whereas the non-digested plasmid showed much slower migration through the gel matrix.

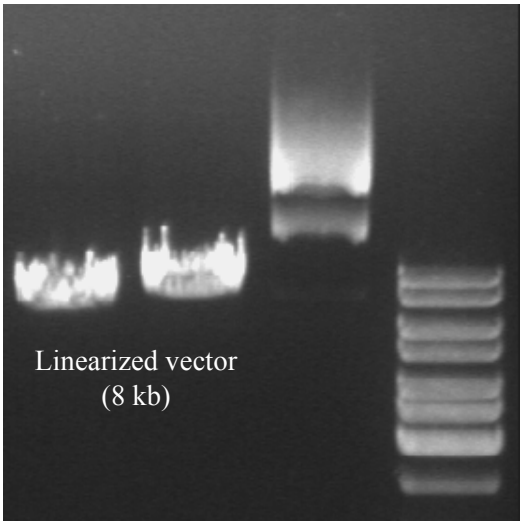

Furthermore, the pECFP-Mito localization vector contains a neomycin resistance (Neor) gene for eukaryotic selection of transfected cells, using geneticin (G418), and a kanamycin resistance sequence for propagation in *E. coli*. The sequence encoding the fluorescent fusion protein was subcloned into the retroviral expression vector pQCXIP, which encodes for puromycin and ampicillin resistance for selection in eukaryotic and procaryotic cells, respectively. After amplification in *E. coli* TOP10, the plasmid was put to a restriction digest as a control of the vector size (Fig. 3-32). The pQCXIP/ECFP-Mito vector was transfected

into U-87 MG, U-118 MG, and U-373 MG cells, and stable cell lines were established with all three glioblastoma cell types by continuous selection with puromycin.

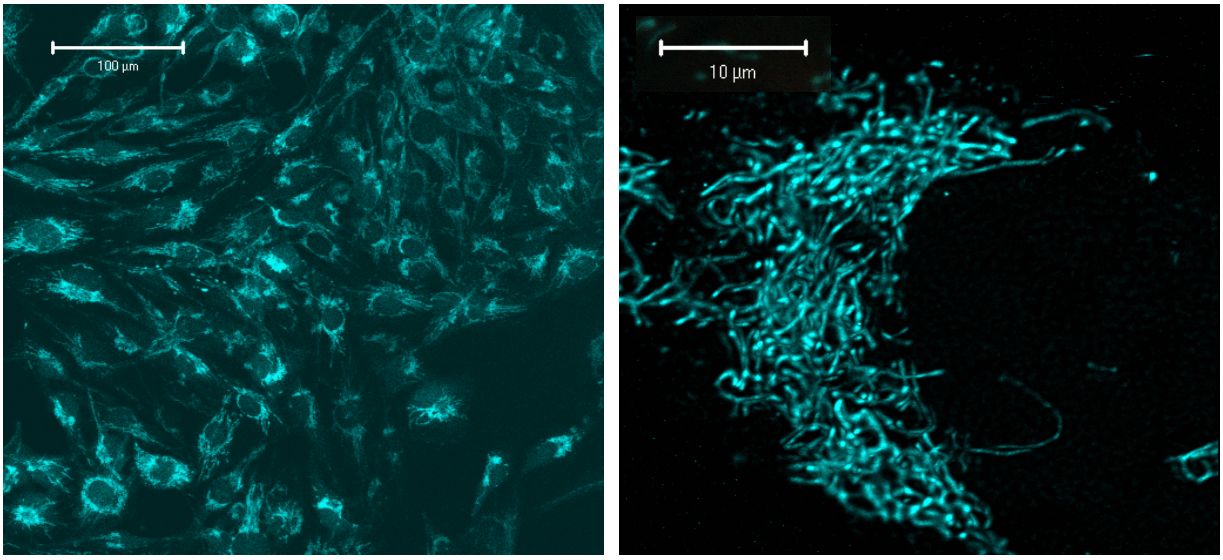

Figure 3-33: U-373 ECFP-Mito cells after continuous selection with G418. Left: overview image. Plan-Neofluar 20x/0.5, Ar 458, HFT 458, BP475-525. Right: single U-373 ECFP-Mito cell. The image represents a 2-d projection of 9 CLSM optical z-sections. The z-stack was processed employing 3-d deconvolution, using an non-blind adaptive point spread function algorithm. Plan-Apochromat 63x/1.4 oil, Ar 477, NT 80/20, LP505.

The expression of mitochondrial expression of ECFP-Mito is exemplarily shown for U-373 ECFP-Mito cells (Fig. 3-33). For colocalization experiments, U-87 ECFP-Mito cells were incubated with 1 µM doxorubicin and 5 µM of the nuclear dye DRAQ5^{TM} for 30 min. Fig. 3-34 shows the successful multifluorescence imaging of doxorubicin and the nuclear counterstain in U-87 ECFP-Mito. As becomes obvious from the merged fluorescence detection channels, doxorubicin is not colocalized with mitochondria. Again, a high accumulation was observed in “vesicular organelles” next to the nucleus.

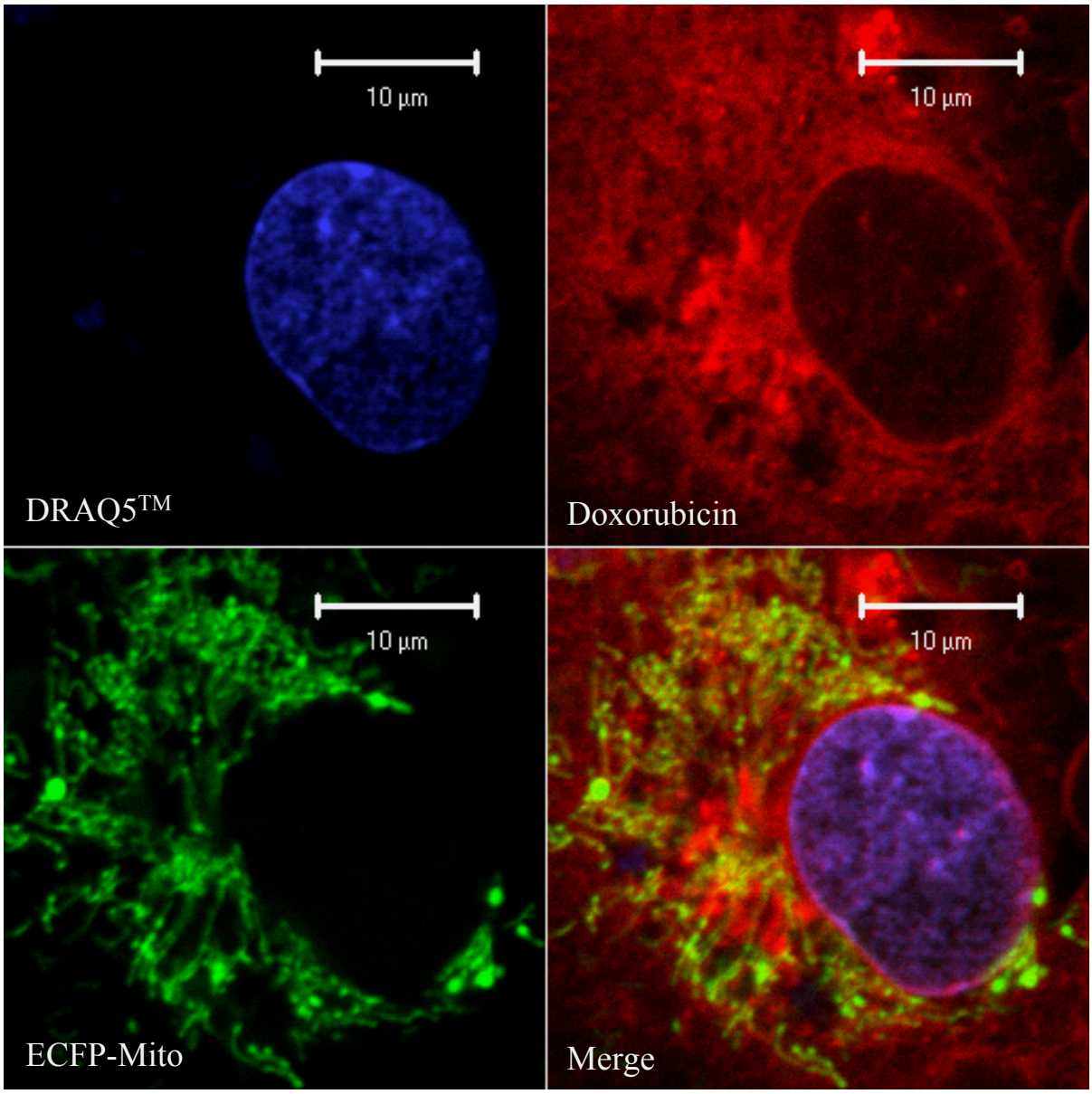

Figure 3-34: Multifluorescence CLSM image (false color display) of a living U-87 ECFP-Mito cell, after incubation with doxorubicin and DRAQ5™. No particular accumulation of doxorubicin in mitochondria was observed, but a rather diffuse distribution in the intracellular room and a vesicular accumulation close to the nucleus. Plan-Apochromat 63x/1.4 oil, Ar 458, HFT 458, BP475-525; HeNe 543, HFT 488/543/633, LP560; HeNe 633, HFT 488/543/633, LP650.

3.4.6.3 CLSM imaging of the plasma membrane

Due to the successful separation of the fluorescence emission of ECFP and doxorubicin, combined to the nuclear counterstain DRAQ5™, other target structures were also fluorescently labeled by transfection with the respective localization vectors. For the fluorescent labeling of the plasma membrane in living cells, U-87 MG and U-373 MG cells were transfected with the localization vector pECFP-Mem, subcloned into the pQCXIP retroviral expression vector, changing the resistance cassettes for prokaryotic and eukaryotic selection from Kan/Neo to Amp/Pur. The vector pECFP-Mem encodes a fusion protein consisting of ECFP and of the N-terminal 20 amino acids of neuromodulin (Skene and Virag 1989). This N-terminal fragment contains a signal for posttranslational palmitoylation of cysteines 3 and 4 within the mature protein, which thereby directs ECFP to cellular membranes.

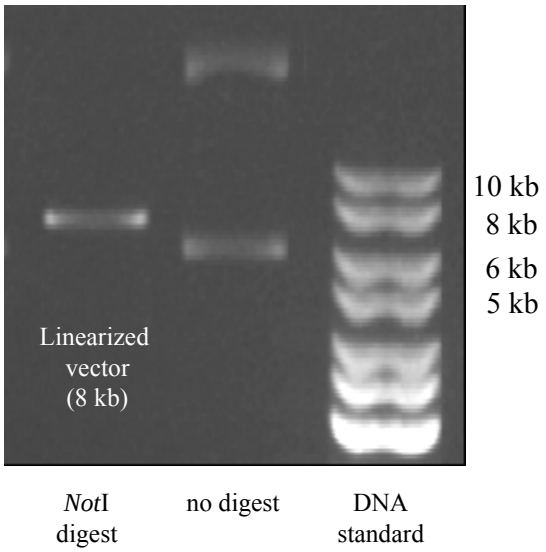

Figure 3-35: Agarose gel electrophoresis of of *Not*I-digested and non-digested pQCXIP/ECFP-Mem. *Not*I digest led to linearization of the localization vector, showing a band at 8 kb. Two bands were detected with the non-digested control from the DNA maxipreparation of the *E. coli* overnight culture. The bands represent the open circular and the supercoiled form of the plasmid, mimicking DNA fragment sizes of far above 10 kb and ca. 7 kb, respectively.

The expression of ECFP-Mem protein after the transfection with pQCXIP/ECFP-Mem is exemplarily shown for U-373 ECFP-Mem cells in Fig. 3-36. However, ECFP-Mem was not only localized in the plasma membrane, but also in intracellular membranes. Fig. 3-37 shows a fixed U-87 ECFP-Mem cell, counterstained with the nuclear stain SYTOXGreen® (Molecular Probes). Due to the fluorescence crosstalk between the two fluorophores, nuclear SYTOXGreen® emission was detected in the detection channel of ECFP, leading to an imaging artefact, which was removed by ACE image processing. ECFP-Mem fluorescence was detected not only in the cytoplasmic membrane but also in an entity indicative for the golgi complex. This may be explained by the posttranslational processing of the ECFP-Mem fusion protein prior to its transport towards the plasma membrane. The multifluorescence

imaging of U-373 ECFP-Mem cells incubated with doxorubicin and DRAQ5™ counterstain showed no accumulation of doxorubicin in the cytoplasmic membrane (Fig. 3-38).

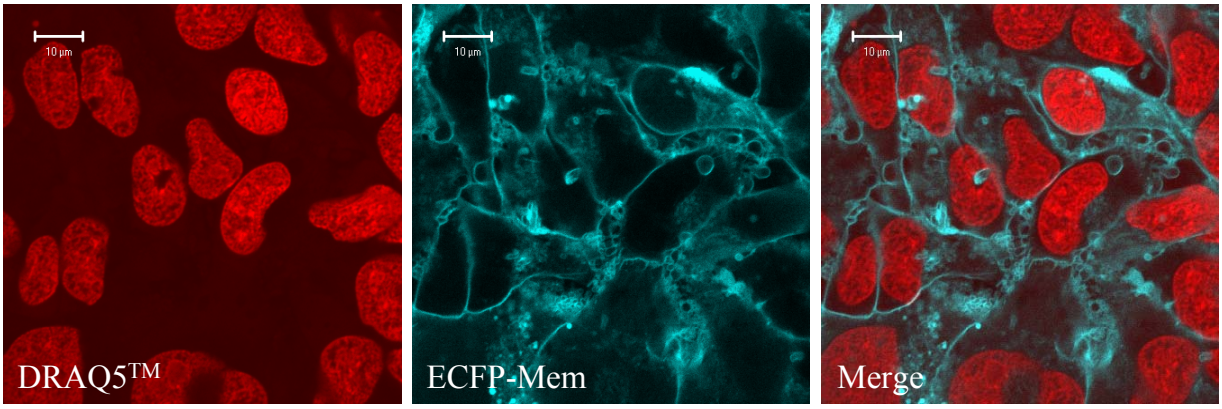

Figure 3-36: CLSM imaging of U-373 ECFP-Mem cells (nuclear counterstain DRAQ5™). Plan-Apochromat 63x/1.4 oil, Ar 458, BP475-525; Ar 514, HFT 514/633, NFT 635/VIS, BP530-600; HeNe 633, HFT 488/543/633, LP650.

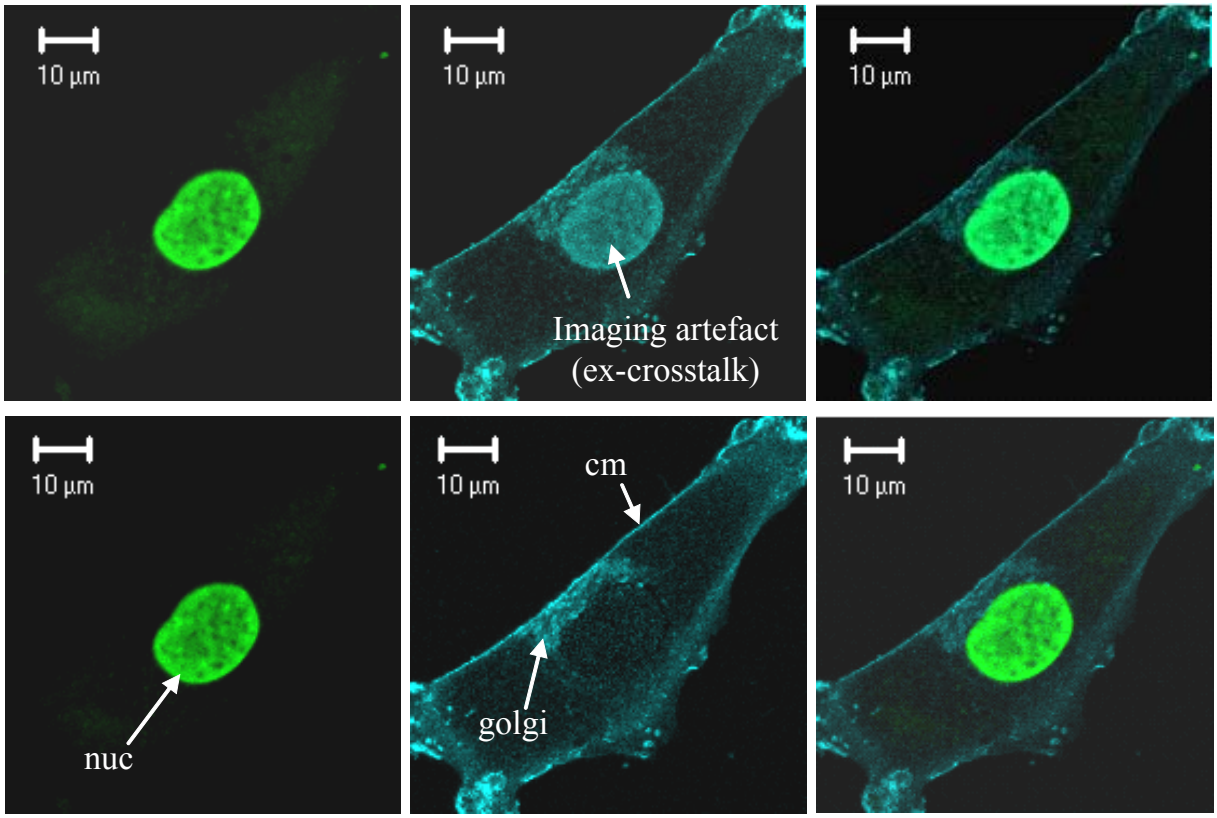

Figure 3-37: U-87 ECFP-Mem cell after PFA fixation, counterstained with SYTOXGreen® nuclear staining dye. Upper row: original images showing excitation crosstalk between SYTOXGreen® and ECFP. Lower row: images after ACE processing. The ECFP-Mem protein is not only found in the cytoplasmic membrane (cm) but also in a vesicular organelle (golgi) next to the nucleus (nuc). Plan-Apochromat 63x/1.4oil, Ar 458 nm/BP475-525 nm; Ar 488 nm/LP505 nm.

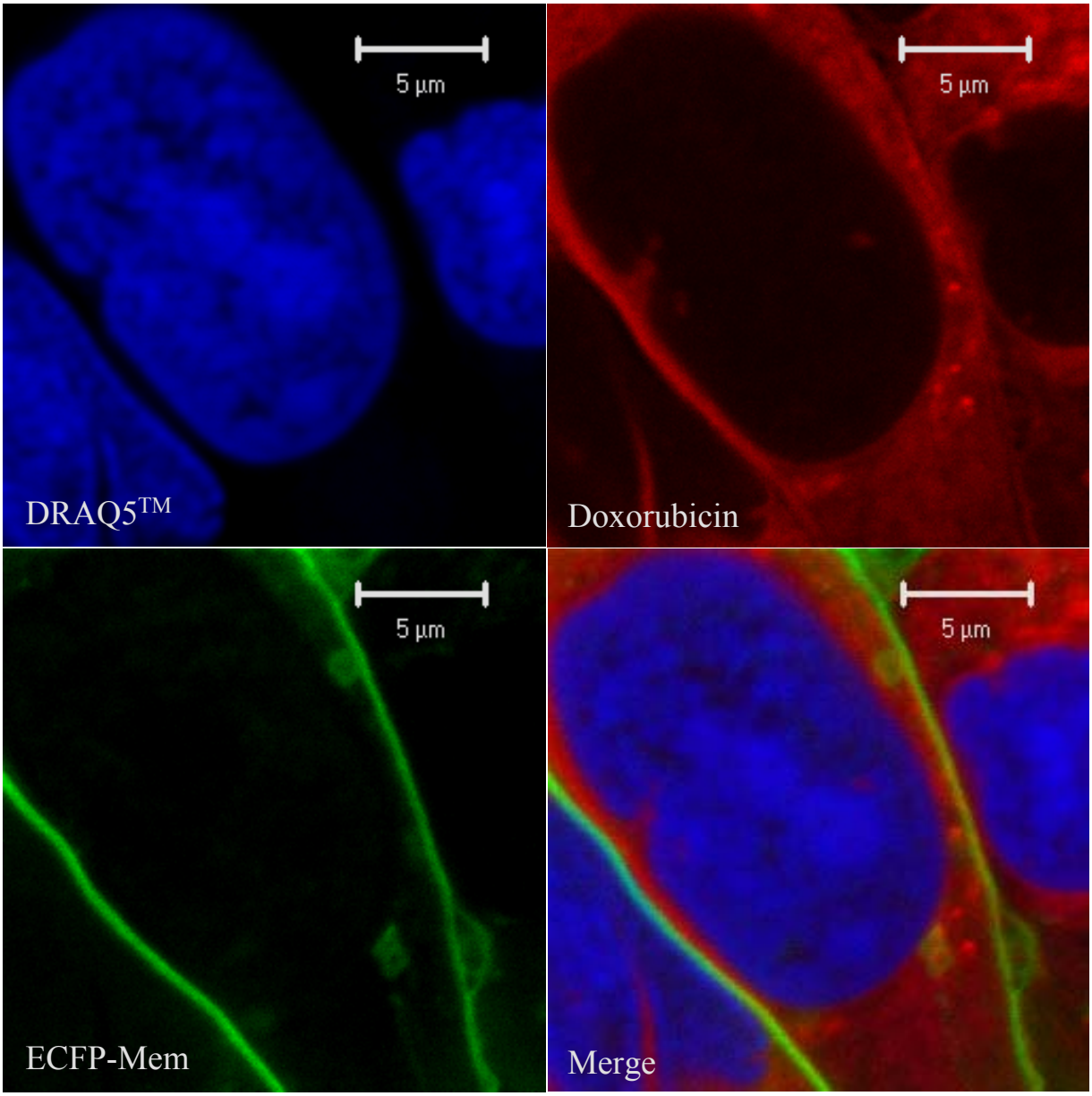

Figure 3-38: False color multifluorescence CLSM image of living U-373 ECFP-Mem cells, after incubation with doxorubicin and DRAQ5™. No distinct colocalization of doxorubicin and the cytoplasmic membrane was observed. Plan-Apochromat 63x/1.4 oil, Ar 458, HFT 458, BP475-525; HeNe 543, HFT 488/543/633, LP560; HeNe 633, HFT 488/543/633, LP650.

3.4.6.4 CLSM imaging of the endoplasmic reticulum in living human glioblastoma cells

For CLSM imaging of the endoplasmatic reticulum (ER), cells were transfected with the pECFP-ER localization vector. This vector contains the DNA sequence for the enhanced cyan fluorescent protein (ECFP) and an endoplasmic reticulum (ER) targeting sequence, encoding for calreticulin (Fliegel et al. 1989), cloned to the 5´-end of the ECFP sequence. To 3´-end is fused to the ER retrieval sequence KDEL (Munro and Pelham 1987; Pelham 1996). When

introduced into mammalian cells, the vector leads to the expression of a soluble protein, localizing in the lumen of the ER (Kendall et al. 1994; Roderick et al. 1997) and bearing ECFP fluorescence emission. Fig. 3-40 shows ECFP-ER transfected U-87 MG cells after continuous selection with G418, counterstained with DRAQ5™. Again, the multifluorescence imaging of U-87 ECFP-ER cells showed no exclusive colocalization of doxorubicin with the ECFP-labeled ER-structures (Fig. 3-41). As observed before in other cell variants, the highest accumulation remains in another, supra-nuclear substructure.

Figure 3-39: Gel analytics of *Nhe*I-digested pECFP-ER and non-digested control. The linearized plasmid is detected close to the 5 kb band of the DNA standard. As observed with the pQCXIP/ECFP-Mem vector, two bands are detected with the non-digested control, representing the open circular and the supercoiled form of the plasmid, mimicking false DNA fragment sizes. (ca. 9 kb and 2.3 kb, respectively).

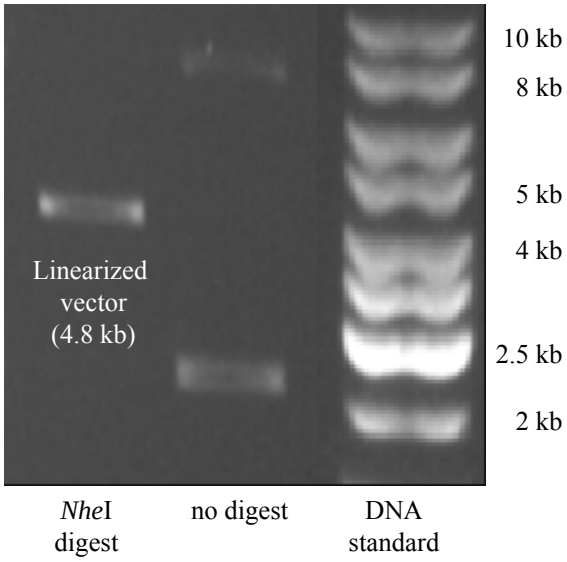

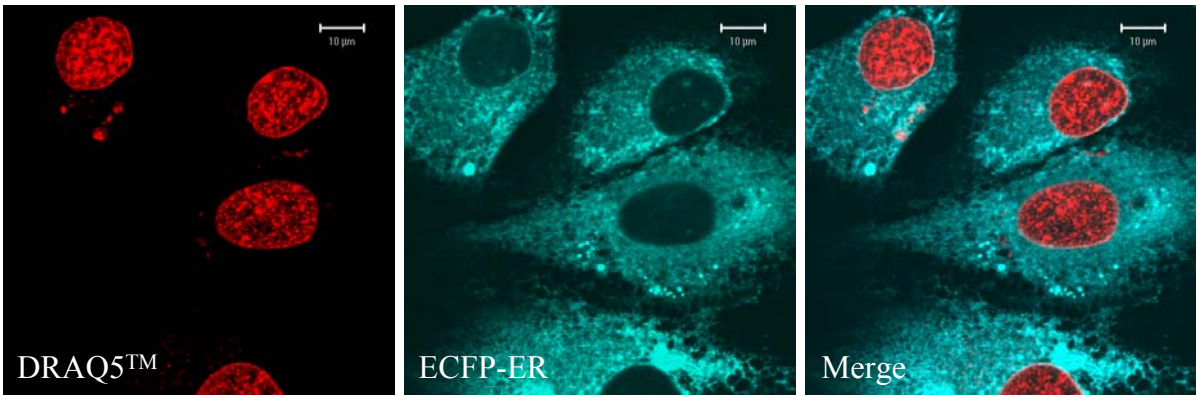

Figure 3-40: ECFP-ER-expressing human U-87 MG glioblastoma cells with nuclear counterstain DRAQ5™. Plan-Apochromat 63x/1.4 oil, Ar 458, BP475-525; Ar 514, HFT 514/633, NFT 635/VIS, BP530-600; HeNe 633, HFT 488/543/633, LP650.

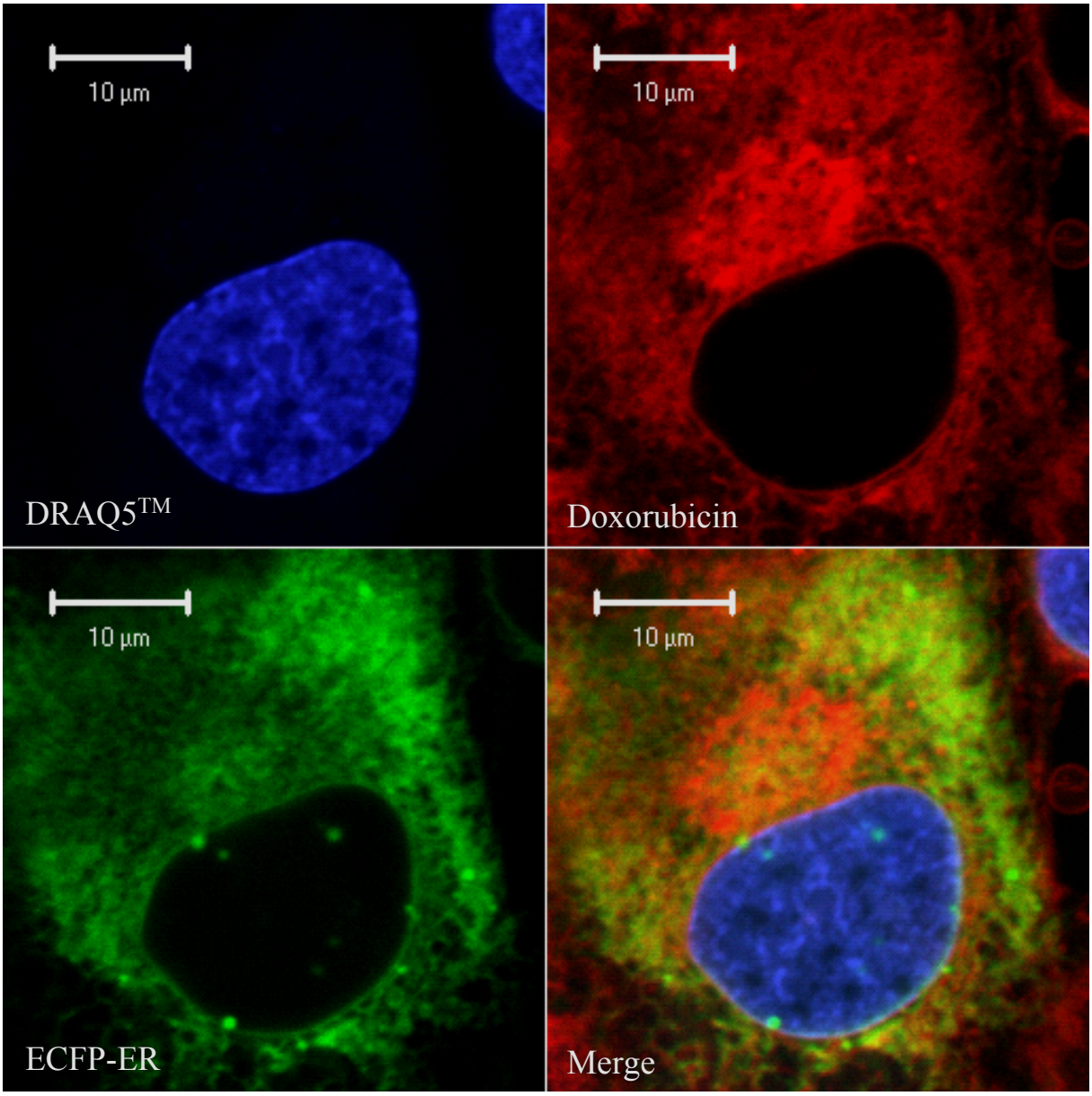

Figure 3-41: Multifluorescence image of a living U-87 ECFP-ER cell, after incubation with doxorubicin and nuclear counterstain. Doxorubicin is partially, but not exclusively colocalized with the ER-structure. Again, the anthracycline accumulates close to the nucleus. Plan-Apochromat 63x/1.4 oil, Ar 458, HFT 458, BP475-525; HeNe 543, HFT 488/543/633, LP560; HeNe 633, HFT 488/543/633, LP650.

3.4.6.5 Fluorescently labeled golgi complex in living human glioblastoma cells

The golgi complex (golgi) consists of smooth membrane-limited cisternae, and is usually localized close to the nucleus. The commercially available localization vector for this organelle, pECFP-Golgi, encodes for a fusion protein consisting of ECFP and the N-terminal 81 amino acid sequence of the human golgi-specific 1,4-galactosyltransferase (Watzele and Berger 1990). The N-terminal sequence contains a membrane-anchoring signal peptide. Thus

the fusion protein is targeted to the trans-medial region of the golgi (Gleeson et al. 1994; Yamaguchi and Fukuda 1995; Llopis et al. 1998). The plasmid further encodes for a resistance cassette, allowing procaryotic and eucaryotic selection, using kanamycin and G418 respectively. Continuously G418-selected U-87 ECFP-Golgi cells are shown in Fig. 3-43. As expected from the preceeding experiments, multifluorescence image acquisition with ECFP-Golgi transfected cells showed partial colocalization of doxorubicin with the ECFP-labeled trans-medial golgi structure (Fig. 3-44).

Figure 3-42: Agarose gel electrophoresis of the pECFP-Golgi restriction digest product. The two bands of the non-digested control, indicative for the open circular and the supercoiled plasmid, disappear after *Not*I digest, and the band for the linearized plasmid is detected ca. 5 kb.

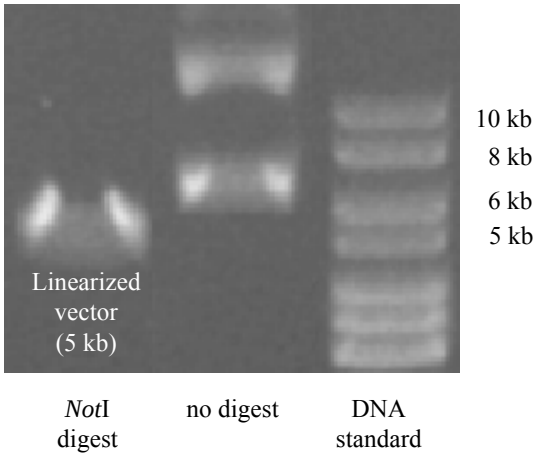

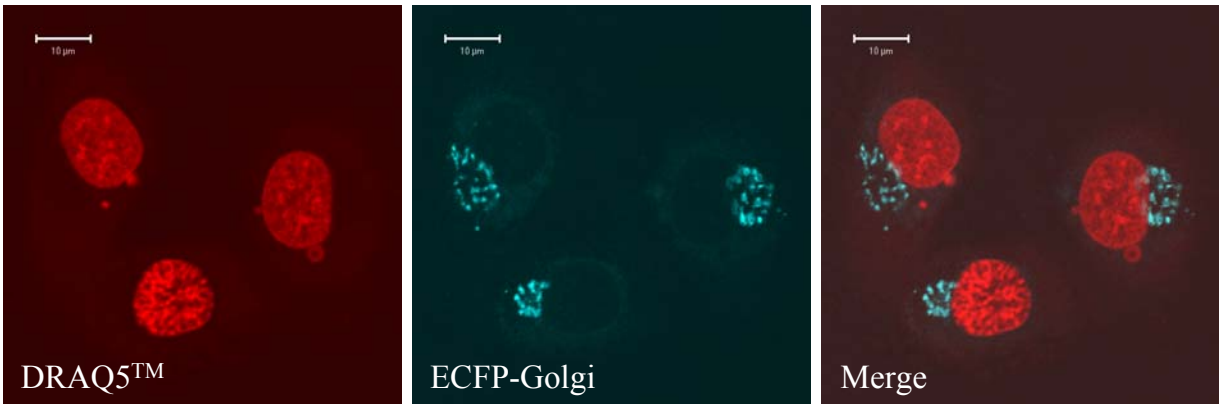

Figure 3-43: Living U-87 MG cells, expressing ECFP-Golgi. The ECFP fluorescence emission is localized next to the nuclei (DRAQ5™ counterstain). Plan-Apochromat 63x/1.4 oil, Ar 458, BP475-525; Ar 514, HFT 514/633, NFT 635/VIS, BP530-600; HeNe 633, HFT 488/543/633, LP650.

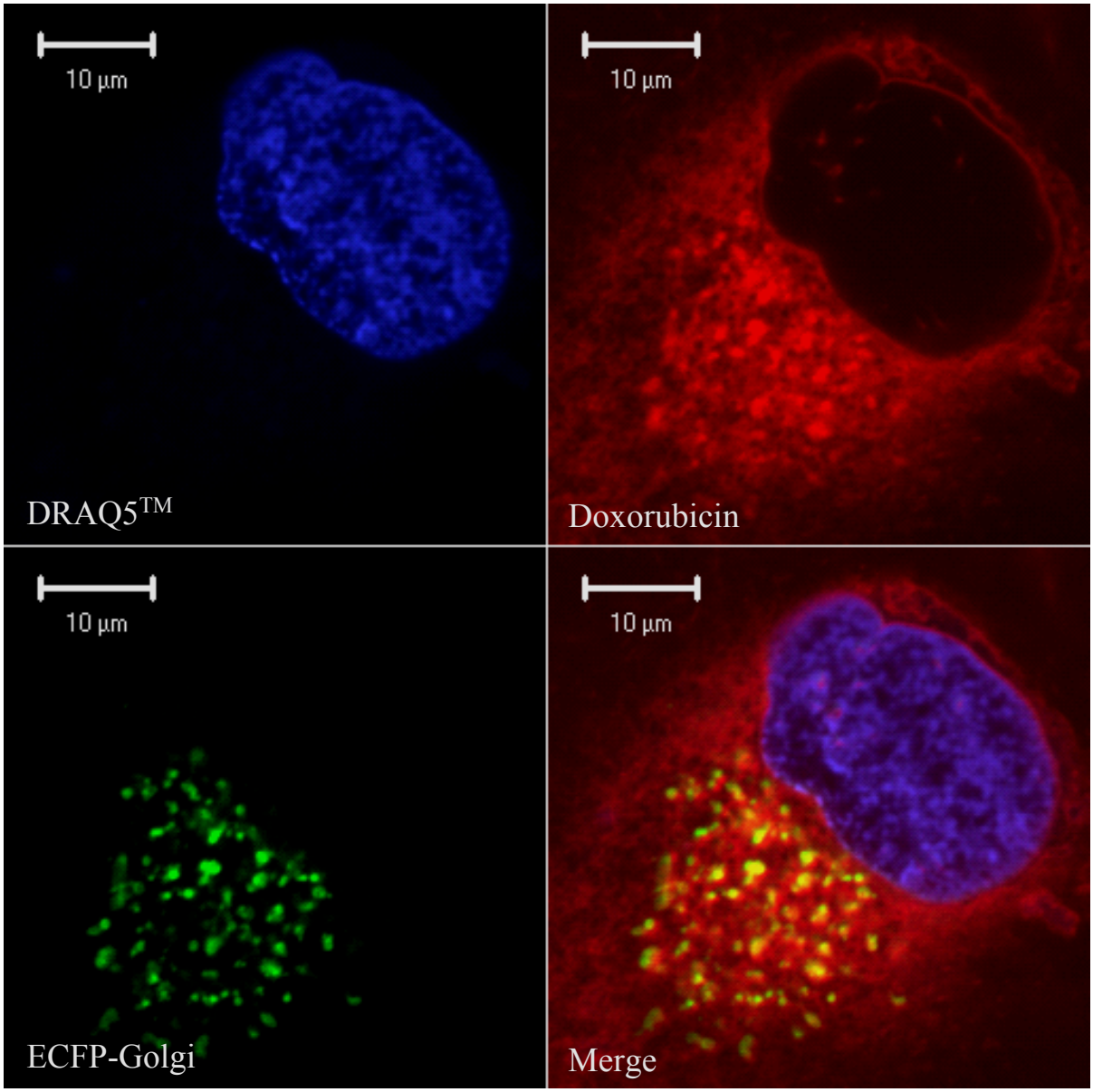

Figure 3-44: Multifluorescence live cell imaging of U-87 ECFP-Golgi. In the displayed optical section, several golgi-cisternae are cut. After incubation with DRAQ5™ and doxorubicin, accumulated doxorubicin fluorescence is colocalized with the fluorescence emission of the ECFP-Golgi fusion protein. Plan-Apochromat 63x/1.4 oil, Ar 458, HFT 458, BP475-525; HeNe 543, HFT 488/543/633, LP560; HeNe 633, HFT 488/543/633, LP650.

3.4.7 Doxorubicin fluorescence in human glioblastoma cells after incubation with different doxorubicin formulations

After the CLSM studies on the distribution of doxorubicin in living cells, further CLSM experiments were performed, according to results from the flow cytometric experiments. Therefore U-87 MG cells were incubated with doxorubicin in solution, doxorubicin

nanoparticles, and polysorbate 80-coated nanoparticles amounting to a doxorubicin concentration of 10 µM, for 5 minutes at 37 °C (in the incubation chamber of the microscope) followed by CLSM image acquisition of the living cells (Fig. 3-45).

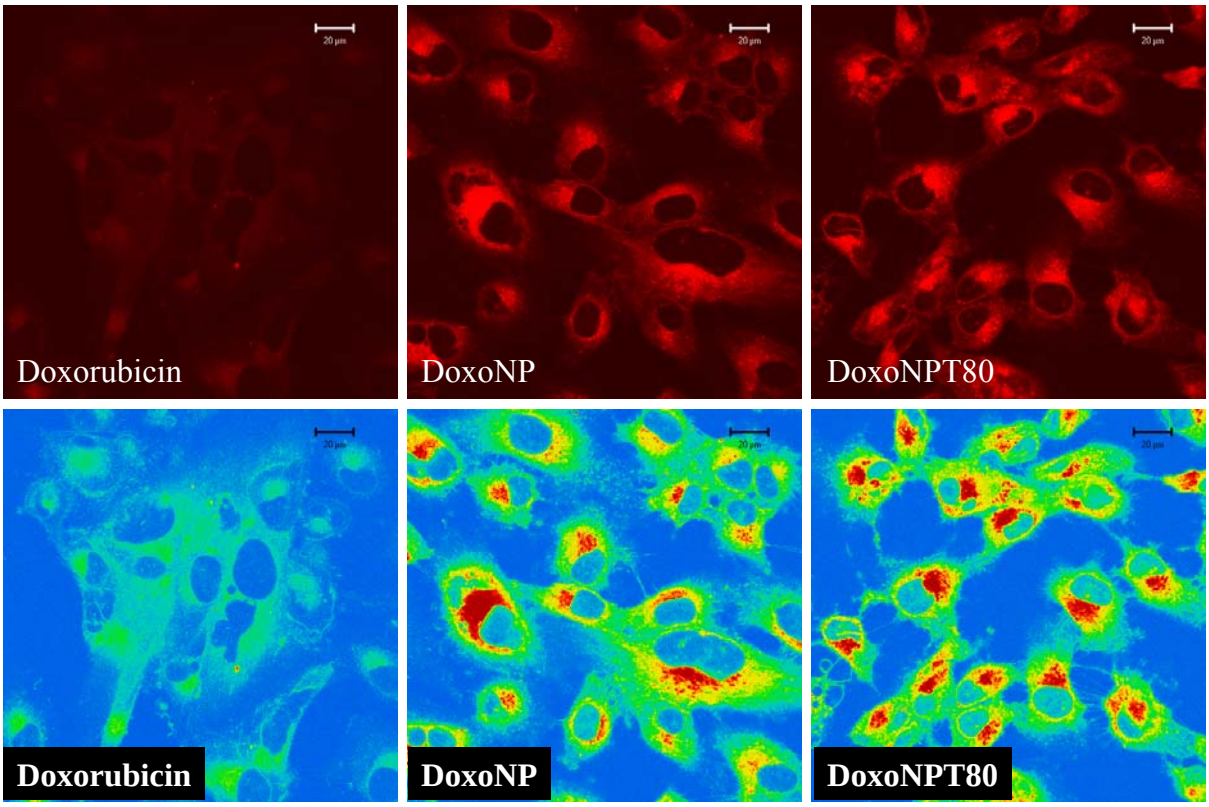

Figure 3-45: Distribution of doxorubicin fluorescence in living U-87 MG cells, incubated with different doxorubicin formulations (upper row). The rainbow false color mode (lower row) displays the fluorescence intensity of each image pixel. The same pattern of fluorescence distribution in the cells was observed for all doxorubicin formulations. Plan-Apochromat 63x/1.4 oil, HeNe 543, HFT 488/543/633, LP650.

After this short period of incubation with dissolved doxorubicin, weak fluorescence was detected throughout the cytoplasm with higher intensity in the proximity of the nuclei. The same pattern of fluorescence distribution was observed after incubation with DoxoNP and coated DoxoNP. Although a cellular uptake of doxorubicin-loaded nanoparticles was not seen, the overall intensity of the doxorubicin-related fluorescence emission was much higher, compared to dissolved doxorubicin. Since no differences in the distribution pattern of doxorubicin fluorescence were found with 10 µM doxorubicin and a short incubaton time (5 minutes), the incubation with doxorubicin in solution, DoxoNP and polysorbate 80-coated DoxoNP was repeated with a decreased doxorubicin concentration (2 µM) and an increased incubation period (1 hour). For this experiment KBwt cells were used, which were demonstrated to express low levels of pgp (Fig. 3-8), and compared to the U-87 MG cells,

they showed similar doxorubicin-related fluorescence in the flow cytometric experiments (Fig. 3-18 and 3-19). As shown in Figure 3-46, the incubation with the different doxorubicin formulations led to a diffuse distribution of doxorubicin fluorescence in the cytoplasm, and again the nuclei were spared out. Compared to the dissolved drug, the doxorubicin related fluorescence was higher in cells incubated with doxorubicin nanoparticle formulations. However, with the DoxoNP and the polysorbate 80-coated DoxoNP, a distinct doxorubicin fluorescence was detected close to the cytoplasmic membrane of the cells. This indicates, that the doxorubicin-loaded nanoparticles adsorb to the cell membrane.

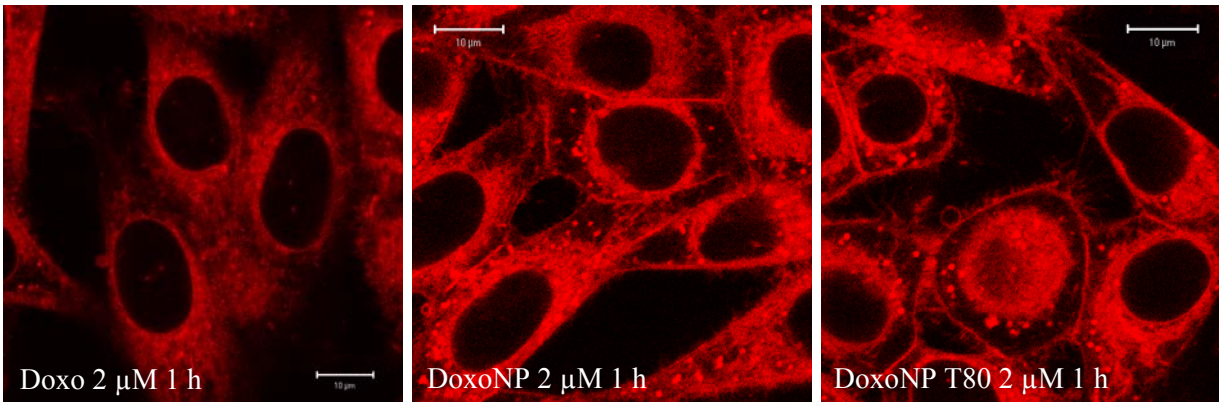

Figure 3-46: Incubation of KBwt cells with doxorubicin and doxorubicin nanoparticle formulations. Dissolved doxorubicin shows distribution all over the cytoplasm (left image), whereas after incubation with the doxorubicin-loaded nanoparticles (middle and right image), the cells are hemmed by doxorubicin-related fluorescence close to their cytoplasmic membrane. Plan-Apochromat 63x/1.4 oil, Ar 514, HFT 514/633, BP530-600.

To investigate whether the nanoparticles permeate into the cells, lyophilized empty PBCA nanoparticles were redispersed in PBS, and diluted to a concentration equivalent 10 µM doxorubicin in DoxoNP. For the dilution to the final concentration PBS was used, containing 0.5 mg/ml lucifer yellow carbohydrazide, dilithium salt (LY-CH, Sigma), a water soluble, and cell impermeant fluorescent dye (see Fig. 3-47). U-373 MG cells were incubated for 1 hour with LY-CH solution (0.5 mg/ml) and with PBCA nanoparticles in PBS 0.5 mg/ml LY-CH. After a washing step with PBS, fluorescence images were acquired by CLSM. Figure 3-48 shows clear differences between the application of LY-CH solution and PBCA nanoparticles + LY-CH. Several brightly fluorescent LY-CH-filled vesicles depicted pinocytosis in U-373 MG cells, whereas the combination of PBCA nanoparticles with LY-CH led to a clearly different pattern of fluorescence distribution. The cell margins appeared as fluorescent hems. Intracellular LY-CH fluorescence was not detected. This indicates that the PBCA nanoparticles do not enter the cytoplasm of the cells.

Figure 3-47: Chemical structure of lucifer yellow carbohydrazide (dilithium salt). Due to its cell impermeant character, this fluorescent dye has been used for visualization of pinocytosis vesicles, and for studies of the three dimensional structure of invertebrate neurons, after direct injection into the studied cells (Stewart 1978).

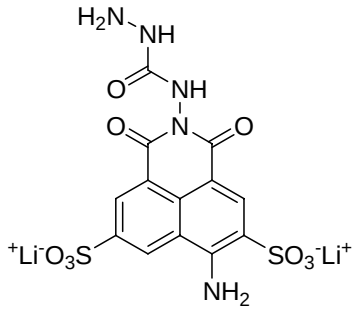

Lucifer yellow carbohydrazide

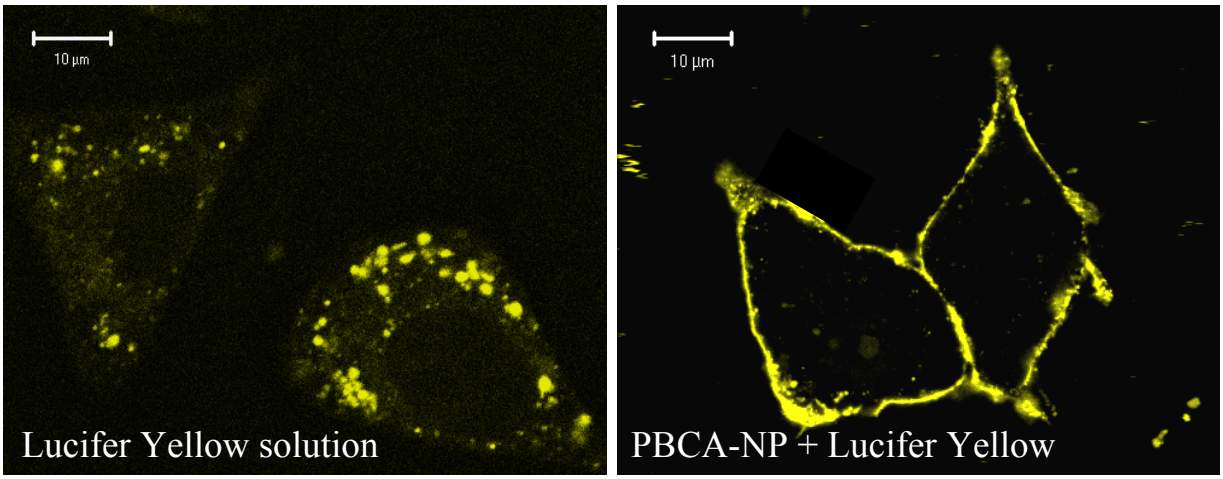

Figure 3-48: Incubation of U-373 MG cells with lucifer yellow solution (left image) and a mixture of PBCA nanoparticles + lucifer yellow (right image). After 1 hour of incubation lucifer yellow solution is found in pinocytosis vesicles inside the cells (left image), whereas the cells incubated with the nanoparticles + lucifer yellow are lined by lucifer yellow fluorescence at their cell membrane, and no fluorescence is found inside the cells. Plan-Apochromat 63x/1.4 oil, Ar 488, HFT 488, LP505.

3.5 Discussion

In the present study polybutylcyanoacrylate-nanoparticles, loaded with doxorubicin, exceeded the antiproliferative effect of dissolved doxorubicin against pgp-overexpressing cells. When the nanoparticles were coated with the surfactant polysorbate 80, the inhibition of cell growth was further increased. This effect was observed at high concentrations equivalent to 2 and 3 µM doxorubicin. Although these amounts of drug are far above clinically applicable concentrations, the nanoparticle formulations indeed overcome the pgp-mediated drug efflux mechanism.

In the flow cytometric experiments with KBwt cells (weak pgp expression) differential effects on the cell-associated fluorescence were observed after incubation with drug formulations equivalent to 500 nM doxorubicin. These results were similar to the effects in pgp-negative U-87 MG, U-118 MG, and U-373 MG glioblastoma cell variants, also incubated with equivalent 500 nM doxorubicin. These differential amounts of cell-associated doxorubicin fluorescence may have occured due to an enhancement of doxorubicin uptake, either by adsorption of doxorubicin-loaded nanoparticles to the cell membrane, or by an uptake of whole nanoparticles into the cells.

However, no differences in the increase in cell-associated fluorescence were observed between the different doxorubicin formulations in the pgp-overexpressing KBv1 cells compared to the wild type cells. This observation can be explained by the assumption that doxorubicin is released from the nanoparticles outside the cells, diffuses into the cytoplasm, and is immediately transported out of the cells by the activity of the pgp efflux transporter. At higher concentrations, equivalent to 2 and 3 μM doxorubicin, the efflux transporter is considered to be saturated, leading to differential doxorubicin accumulation by KBv1 cells as observed in KBwt and the pgp-negative glioblastoma cells.

It is conceivable that adsorption of nanoparticles to the cell surface has enhanced doxorubicin uptake by creating a high doxorubicin concentration gradient around the cells, and consequently has enhanced the diffusion of the drug into the cells. This assumption is supported by the results from the CLSM studies with living cells, indicating, that the nanoparticles are not penetrating into the cells. A cellular uptake of doxorubicin-loaded nanoparticles, e.g. via an endocytotic mechanism, was not observed. It should be pointed out that, when the cells were incubated with the drug-loaded nanoparticles, particle-bound as well as free drug may have contributed to the observed intracellular fluorescence. However, the results from the experiments with LY-CH and empty PBCA nanoparticles indicate retaining of the nanoparticles on the cell surface, even though LY-CH was not covalently linked to the nanoparticle surface, and weakly stained or unstained nanoparticles could have passed the cell membrane due to their differing surface properties.

Although Rejman et al. reported on a size-dependent internalization of fluorescently labeled latex nanoparticles in non-phagocytic B16 cells (Rejman et al. 2004), also a lack of nanoparticle uptake in vitro has been demonstrated for several other nanoparticle types, indicating a major influence of the surface properties and the susceptibility of the used cell type. Bertin et al. synthesized amphiphilic block copolymeric nanoparticles from indomethacin-containing norbornene and tosylated hexaethylene glycol-containing

norbornene, 140–200 nm in size (Bertin et al. 2006). When applied to Her2-expressing human SKBR3 breast cancer cells, an uptake of the nanoparticles was only observed when the nanoparticle surface had been functionalized with an anti-Her2 antibody. The nanoparticles without antibody conjugation did not enter the cells. Moreover, also smaller nanoparticles have been reported not to enter into cells in vitro. Tkachenko et al. studied the influence of peptidic surface modifications of gold nanoparticles, ca. 20 nm in size (Tkachenko et al. 2004). In NIH/3T3 cells, a lack of nanoparticle uptake was observed despite a modification of the nanoparticle surface with HIV-1 Tat transduction domain protein, which was assumed to enhance nanoparticle uptake. However, when applied to HepG2 hepatocyte cells, the same type of nanoparticles entered the cells. Furthermore, KB cells, expressing folic acid receptors, were able to internalize fluorescein isothiocyanate-labeled polyamidoamine dendrimers (1-10 nm in size), conjugated with folic acid (Quintana et al. 2002). The dendrimers without folic acid conjugation were excluded by the KB cells, and folic acid receptor-negative NIH/3T3 cells also showed no uptake of the nanodevices. These results indicate, that the particle surface modality rather than the particle size determines the cellular uptake in vitro. Since the PBCA nanoparticles used in the presented study were not further functionalized, except for the Tween80® coating, the abovementioned enhancement mechanism of doxorubicin delivery to the pgp-overexpressing cells is conceivable.

This hypothesis is further supported by a study from de Verdiere et al., who reported on the enhanced antiproliferative activity of doxorubicin, bound to polyisohexylcyanoacrylate nanoparticles, against pgp-overexpressing P388 cells (de Verdiere et al. 1997). The experiments were also performed in two-compartment wells, where direct interaction of the nanoparticles with the cells during the incubation period was prevented by a polycarbonate membrane. Under these conditions the drug-loaded nanoparticles did not exceed the effect of the dissolved doxorubicin, suggesting that the direct interaction of the particulate form with the cell membrane is important for the observed enhanced antiproliferative effects. Moreover, concluding from drug accumulation studies, the authors postulated an enhanced uptake of doxorubicin by ion pair formation of doxorubicin and polycyanoacrylic acid, both released by nanoparticle degradation.

However, the role of Tween80® in the further enhancement of cytotoxicity of doxorubicin-loaded nanoparticles remains unclear, since Twen80® itself had no antiproliferative effect. It may be speculated that the surfactant could influence nanoparticle adsorption on the cell surface, or might enhance membrane permeability of the drug by solubilization of the water-dissolved portion of the drug, while a concentration gradient is

created by the nanoparticles. Another effect could be the modulation of the pgp-mediated drug efflux by polysorbate 80, which has been described to enhance daunorubicin cytotoxicity in P388 cells (Woodcock et al. 1992). This effect also may contribute to the suggested mechanism of the purported overcome of the blood-brain barrier by polysorbate 80-coated doxorubicin nanoparticles (Gulyaev et al. 1999), which however remains controversial.

In vivo, the mode of application of the nanoparticle could produce an enhanced uptake of doxorubicin through the blood brain barrier via different mechanisms. Kreuter et al. investigated the influence of various apolipoproteins (Apo) on the delivery of nanoparticle-bound dalargin and loperamide (Kreuter et al. 2002). For this purpose both drugs were bound to PBCA nanoparticles and coated with various apolipoproteins. The achieved antinociceptive effect of both nanoparticle-bound drugs was determined in the tail flick test after intravenous injection to mice. The effect was significantly increased when the Apo B- or Apo E-coated nanoparticles were precoated with Tween 80®. Moreover, when polysorbate 80-coated nanoparticles were administered to Apo E-deficient ApoEtm1Unc mice, the antinociceptive effect of the drug formulations was markedly reduced compared to normal mice. ApoB and ApoE are known low density lipoprotein (LDL) receptor ligands. Binding to LDL receptors initiates endocytosis of the ligand-receptor complex (Goldstein et al. 1985). Therefore, the adsorption of the ApoB and/or ApoE from blood after i.v. administration might target the Tween 80®-coated nanoparticles to LDL receptor-expressing cells, such as brain capillary endothelial cells. Consequently, the enhancement of drug delivery to the brain, using the coated PBCA nanoparticle carrier system, could be explained by this LDL receptor-mediated endocytotic mechanism, followed by the intracellular degradation of the nanoparticles and drug release. Then the drug may be distributed within the brain by diffusion.

Olivier et al. reported on a completely different effect of drug delivery enhancement with coated nanoparticles (Olivier et al. 1999), contradictory to the results of Kreuter et al. (Kreuter et al. 2002). The coating of dalargin-loaded PBCA NP with Tween 80® led to a complete desorption of the drug from the nanoparticles. Despite of that, and compared to non-biodegradable polystyrene nanoparticles, the coated PBCA NP formulation still exhibited a potent and prolonged analgetic effect in mice (tail flick test). Moreover, Olivier et al. performed in vitro experiments on BBB permeabilization effects using a co-culture of bovine brain capillary endothelial cells and rat astrocytes as a BBB model. A concentration of 10 µg/ml PBCA NP induced a permeabilization of the artificial BBB. Again, Olivier et al. proposed a non-specific permeabilization, respectively disruption of the BBB due to the toxicity of the carrier as the major account for the enhanced dalargin penetration into the

CNS, when associated with PBCA NP and polysorbate 80. However, further studies on the interaction of PBCA NP with the BBB in vitro and in vivo did not confirm a generalized toxic effect as a primary mechanism for drug delivery to the brain (Alyautdin et al. 2001; Kreuter et al. 2003). Nevertheless, an additional, undirected route may contribute to the enhanced drug delivery to the brain too. As a result of tumor growth and progression, the BBB can be partially disrupted. Thus, the administration of drug-loaded nanoparticle formulations at certain, especially late stages of the tumor development may enable drug transport or carriage through the leaking endothelium to the site of the tumor. Since Tween 80®-coated PBCA NP can deliver doxorubicin across an intact BBB too (Gulyaev et al. 1999), this drug formulation is considered to be also effective in earlier stages of brain tumor development.

Further investigations have to be performed, to determine whether PBCA nanoparticles, with or without Tween80®-coating, indeed penetrate into cells or not. A stable fluorescent labeling of the PBCA nanoparticles would provide a major advantage for monitoring a potential cellular uptake in vitro, and consequently further elucidate the in vivo mechanism of nanoparticle drug delivery. Regardless of the drug delivery mechanism, PBCA nanoparticle-mediated drug delivery to the brain may be considered as an attractive delivery pathway for pharmacologically active compounds, which otherwise would be excluded from the brain by physiological efflux mechanisms at the BBB, such as the pgp.

3.6 Summary

The chemosensitivity of KBwt and pgp-overexpressing KBv1 cells against doxorubicin was determined with the crystal violet based cytotoxicity assay. As expected, the KBv1 cells were highly resistant to doxorubicin, and a cytotoxic effect was observed at a drug concentrations of 1 µM and above. The KBwt cells were less sensitive to doxorubicin than expected from their pgp expression status. This can be well explained by an upregulation of the pgp-expression in these cells during the time of incubation with the pgp-substrate doxorubicin. When the KBv1 cells were incubated with different doxorubicin formulations, the doxorubicin nanoparticle formulations exceeded the antiproliferative effect of the dissolved drug at doxorubicin concentrations equivalent to 2 and 3 µM dissolved drug. The coating of the nanoparticles with the surfactant polysorbate 80 led to a further increase of the antiproliferative effect.

The flow cytometric experiments showed formulation-dependent effects on the cell-associated doxorubicin fluorescence in pgp-negative human glioblastoma cells as well as in KBwt cells. In pgp-overexpressing KBv1 cells these differential effects were not observed at a drug concentration equivalent to 500 nM doxorubicin. However, at a concentration of 2 µM doxorubicin similar effects were observed with KBv1 cells as observed for the pgp-negative glioblastoma cells and the KBwt cells.

The confocal laser-scanning microscopic (CLSM) studies with living cells showed that the doxorubicin-related fluorescence originates from drug, distributed in the cytoplasm, but not localized in the nucleus, where doxorubicin fluorescence is quenched by the nuclear DNA. Within the cytoplasm the drug slightly accumulated in the vicinity of the nuclei, whereas a distinct colocalization of doxorubicin with the cell membrane and cellular organelles, such as the golgi, the endoplasmic reticulum, and the mitochondria was not observed. Similar cytoplasmic doxorubicin distribution was observed after incubation of KBwt cells with dissolved and nanoparticle-bound doxorubicin, whereas a higher overall doxorubicin–related fluorescence was observed in case of the nanoparticle formulations. Moreover, cells were hemmed by doxorubicin fluorescence when incubated with the nanoparticles, indicating that the particles do not enter the cytoplasm. With a mixture of "empty" PBCA nanoparticles and lucifer yellow, pgp-negative U-373 MG were hemmed by lucifer yellow derived fluorescence, supporting the hypothesis that the nanoparticles do not enter the cells.

Based on these results, the enhanced antiproliferative efficacy of the doxorubicin nanoparticle formulations against pgp-overexpressing cells can be ascribed to drug release from nanoparticles after adsorption to the cell surface. The resulting concentration gradient of dissolved drug around the cells and the cytoplasm leads to a fast and high increase in the intracellular doxorubicin concentration, exceeding the pgp efflux capacity.

Bibliography

Alyautdin R N, Petrov V E, Langer K, Berthold A, Kharkevich D A and Kreuter J (1997). Delivery of loperamide across the blood-brain barrier with polysorbate 80-coated polybutylcyanoacrylate nanoparticles. *Pharm Res* **14**: 325-8.

Alyautdin R N, Reichel A, Lobenberg R, Ramge P, Kreuter J and Begley D J (2001). Interaction of poly(butylcyanoacrylate) nanoparticles with the blood-brain barrier in vivo and in vitro. *J Drug Target* **9**: 209-21.

Alyautdin R N, Tezikov E B, Ramge P, Kharkevich D A, Begley D J and Kreuter J (1998). Significant entry of tubocurarine into the brain of rats by adsorption to polysorbate 80-coated polybutylcyanoacrylate nanoparticles: an in situ brain perfusion study. *J Microencapsul* **15**: 67-74.

Beckman G, Beckman L, Ponten J and Westermark B (1971). G-6-PD and PGM phenotypes of 16 continuous human tumor cell lines. Evidence against cross-contamination and contamination by HeLa cells. *Hum Hered* **21**: 238-41.

Begley D J (2003). Understanding and circumventing the blood-brain barrier. *Acta Paediatr Suppl* **92**: 83-91.

Begley D J (2004). Delivery of therapeutic agents to the central nervous system: the problems and the possibilities. *Pharmacol Ther* **104**: 29-45.

Bernhardt G, Reile H, Birnbock H, Spruss T and Schonenberger H (1992). Standardized kinetic microassay to quantify differential chemosensitivity on the basis of proliferative activity. *J Cancer Res Clin Oncol* **118**: 35-43.

Bertin P A, Gibbs J M, Shen C K, Thaxton C S, Russin W A, Mirkin C A and Nguyen S T (2006). Multifunctional polymeric nanoparticles from diverse bioactive agents. *J Am Chem Soc* **128**: 4168-9.

Bickel U, Kang Y S, Yoshikawa T and Pardridge W M (1994). In vivo demonstration of subcellular localization of anti-transferrin receptor monoclonal antibody-colloidal gold conjugate in brain capillary endothelium. *J Histochem Cytochem* **42**: 1493-7.

Bodor N and Buchwald P (1999). Recent advances in the brain targeting of neuropharmaceuticals by chemical delivery systems. *Adv Drug Deliv Rev* **36**: 229-254.

Bodor N and Buchwald P (2002). Barriers to remember: brain-targeting chemical delivery systems and Alzheimer's disease. *Drug Discov Today* **7**: 766-74.

Boiardi A, Pozzi A, Salmaggi A, Eoli M, Zucchetti M and Silvani A (1999). Safety and potential effectiveness of daunorubicin-containing liposomes in patients with advanced recurrent malignant CNS tumors. *Cancer Chemother Pharmacol* **43**: 178-9.

Bootz A, Vogel V, Schubert D and Kreuter J (2004). Comparison of scanning electron microscopy, dynamic light scattering and analytical ultracentrifugation for the sizing of poly(butyl cyanoacrylate) nanoparticles. *Eur J Pharm Biopharm* **57**: 369-75.

Brewster M E, Anderson W and Bodor N (1991). Brain, blood, and cerebrospinal fluid distribution of a zidovudine chemical delivery system in rabbits. *J Pharm Sci* **80**: 843-6.

Cordon-Cardo C, O'Brien J P, Casals D, Rittman-Grauer L, Biedler J L, Melamed M R and Bertino J R (1989). Multidrug-resistance gene (P-glycoprotein) is expressed by endothelial cells at blood-brain barrier sites. *Proc Natl Acad Sci U S A* **86**: 695-8.

Couvreur P, Kante B, Grislain L, Roland M and Speiser P (1982). Toxicity of polyalkylcyanoacrylate nanoparticles II: Doxorubicin-loaded nanoparticles. *J Pharm Sci* **71**: 790-2.

de Verdiere A C, Dubernet C, Nemati F, Soma E, Appel M, Ferte J, Bernard S, Puisieux F and Couvreur P (1997). Reversion of multidrug resistance with

polyalkylcyanoacrylate nanoparticles: towards a mechanism of action. *Br J Cancer* **76**: 198-205.

Dore-Duffy P (2003). Isolation and characterization of cerebral microvascular pericytes. *Methods Mol Med* **89**: 375-82.

Drion N, Lemaire M, Lefauconnier J M and Scherrmann J M (1996). Role of P-glycoprotein in the blood-brain transport of colchicine and vinblastine. *J Neurochem* **67**: 1688-93.

Farrugia C A and Groves M J (1999). Gelatin behaviour in dilute aqueous solution: designing a nanoparticulate formulation. *J Pharm Pharmacol* **51**: 643-9.

Fernandez-Urrusuno R, Calvo P, Remunan-Lopez C, Vila-Jato J L and Alonso M J (1999). Enhancement of nasal absorption of insulin using chitosan nanoparticles. *Pharm Res* **16**: 1576-81.

Fliegel L, Burns K, MacLennan D H, Reithmeier R A and Michalak M (1989). Molecular cloning of the high affinity calcium-binding protein (calreticulin) of skeletal muscle sarcoplasmic reticulum. *J Biol Chem* **264**: 21522-8.

Friese A, Seiller E, Quack G, Lorenz B and Kreuter J (2000). Increase of the duration of the anticonvulsive activity of a novel NMDA receptor antagonist using poly(butylcyanoacrylate) nanoparticles as a parenteral controlled release system. *Eur J Pharm Biopharm* **49**: 103-9.

Gelperina S E, Khalansky A S, Skidan I N, Smirnova Z S, Bobruskin A I, Severin S E, Turowski B, Zanella F E and Kreuter J (2002). Toxicological studies of doxorubicin bound to polysorbate 80-coated poly(butyl cyanoacrylate) nanoparticles in healthy rats and rats with intracranial glioblastoma. *Toxicol Lett* **126**: 131-41.

Ghersi-Egea J F, Leninger-Muller B, Suleman G, Siest G and Minn A (1994). Localization of drug-metabolizing enzyme activities to blood-brain interfaces and circumventricular organs. *J Neurochem* **62**: 1089-96.

Gleeson P A, Teasdale R D and Burke J (1994). Targeting of proteins to the Golgi apparatus. *Glycoconj J* **11**: 381-94.

Goldstein J L, Brown M S, Anderson R G, Russell D W and Schneider W J (1985). Receptor-mediated endocytosis: concepts emerging from the LDL receptor system. *Annu Rev Cell Biol* **1**: 1-39.

Gulyaev A E, Gelperina S E, Skidan I N, Antropov A S, Kivman G Y and Kreuter J (1999). Significant transport of doxorubicin into the brain with polysorbate 80-coated nanoparticles. *Pharm Res* **16**: 1564-9.

Hay R J (1988). The seed stock concept and quality control for cell lines. *Anal Biochem* **171**: 225-37.

Heim R, Prasher D C and Tsien R Y (1994). Wavelength mutations and posttranslational autoxidation of green fluorescent protein. *Proc Natl Acad Sci U S A* **91**: 12501-4.

Heim R and Tsien R Y (1996). Engineering green fluorescent protein for improved brightness, longer wavelengths and fluorescence resonance energy transfer. *Curr Biol* **6**: 178-82.

Huwyler J, Cerletti A, Fricker G, Eberle A N and Drewe J (2002). By-passing of P-glycoprotein using immunoliposomes. *J Drug Target* **10**: 73-9.

Illum L, Davis S S, Muller R H, Mak E and West P (1987). The organ distribution and circulation time of intravenously injected colloidal carriers sterically stabilized with a block copolymer--poloxamine 908. *Life Sci* **40**: 367-74.

Illum S L and Davis S S (1983). Effect of the nonionic surfactant poloxamer 338 on the fate and deposition of polystyrene microspheres following intravenous administration. *J Pharm Sci* **72**: 1086-9.

Janes K A, Fresneau M P, Marazuela A, Fabra A and Alonso M J (2001). Chitosan nanoparticles as delivery systems for doxorubicin. *J Control Release* **73**: 255-67.

Kacem K, Lacombe P, Seylaz J and Bonvento G (1998). Structural organization of the perivascular astrocyte endfeet and their relationship with the endothelial glucose transporter: a confocal microscopy study. *Glia* **23**: 1-10.

Kendall J M, Badminton M N, Dormer R L and Campbell A K (1994). Changes in free calcium in the endoplasmic reticulum of living cells detected using targeted aequorin. *Anal Biochem* **221**: 173-81.

Kniesel U and Wolburg H (2000). Tight junctions of the blood-brain barrier. *Cell Mol Neurobiol* **20**: 57-76.

Koukourakis M I, Koukouraki S, Fezoulidis I, Kelekis N, Kyrias G, Archimandritis S and Karkavitsas N (2000). High intratumoural accumulation of stealth liposomal doxorubicin (Caelyx) in glioblastomas and in metastatic brain tumours. *Br J Cancer* **83**: 1281-6.

Kreuter J (1994). Drug targeting with nanoparticles. *Eur J Drug Metab Pharmacokinet* **19**: 253-6.

Kreuter J (2001). Nanoparticulate systems for brain delivery of drugs. *Adv Drug Deliv Rev* **47**: 65-81.

Kreuter J, Alyautdin R N, Kharkevich D A and Ivanov A A (1995). Passage of peptides through the blood-brain barrier with colloidal polymer particles (nanoparticles). *Brain Res* **674**: 171-4.

Kreuter J, Petrov V E, Kharkevich D A and Alyautdin R N (1997). Influence of the type of surfactant on the analgesic effects induced by the peptide dalargin after its delivery across the blood-brain barrier using surfactant-coated nanoparticles. *J Control Release* **49**: 81-87.

Kreuter J, Ramge P, Petrov V, Hamm S, Gelperina S E, Engelhardt B, Alyautdin R, von Briesen H and Begley D J (2003). Direct evidence that polysorbate-80-coated poly(butylcyanoacrylate) nanoparticles deliver drugs to the CNS via specific mechanisms requiring prior binding of drug to the nanoparticles. *Pharm Res* **20**: 409-16.

Kreuter J, Shamenkov D, Petrov V, Ramge P, Cychutek K, Koch-Brandt C and Alyautdin R (2002). Apolipoprotein-mediated transport of nanoparticle-bound drugs across the blood-brain barrier. *J Drug Target* **10**: 317-25.

Langer R (2000). Biomaterials in drug delivery and tissue engineering: one laboratory's experience. *Acc Chem Res* **33**: 94-101.

Lescure F, Seguin C, Breton P, Bourrinet P, Roy D and Couvreur P (1994). Preparation and characterization of novel poly(methylidene malonate 2.1.2.)-made nanoparticles. *Pharm Res* **11**: 1270-7.

Levin V A (1980). Relationship of octanol/water partition coefficient and molecular weight to rat brain capillary permeability. *J Med Chem* **23**: 682-4.

Lippens R J (1999). Liposomal daunorubicin (DaunoXome) in children with recurrent or progressive brain tumors. *Pediatr Hematol Oncol* **16**: 131-9.

Llopis J, McCaffery J M, Miyawaki A, Farquhar M G and Tsien R Y (1998). Measurement of cytosolic, mitochondrial, and Golgi pH in single living cells with green fluorescent proteins. *Proc Natl Acad Sci U S A* **95**: 6803-8.

Madrid Y, Langer L F, Brem H and Langer R (1991). New directions in the delivery of drugs and other substances to the central nervous system. *Adv Pharmacol* **22**: 299-324.

Miyawaki A, Llopis J, Heim R, McCaffery J M, Adams J A, Ikura M and Tsien R Y (1997). Fluorescent indicators for Ca2+ based on green fluorescent proteins and calmodulin. *Nature* **388**: 882-7.

Müller M, Voros J, Csucs G, Walter E, Danuser G, Merkle H P, Spencer N D and Textor M (2003). Surface modification of PLGA microspheres. *J Biomed Mater Res A* **66**: 55-61.

Munro S and Pelham H R (1987). A C-terminal signal prevents secretion of luminal ER proteins. *Cell* **48**: 899-907.

Neuwelt E A, Pagel M, Barnett P, Glassberg M and Frenkel E P (1981). Pharmacology and toxicity of intracarotid adriamycin administration following osmotic blood-brain barrier modification. *Cancer Res* **41**: 4466-70.

Olivier J C, Fenart L, Chauvet R, Pariat C, Cecchelli R and Couet W (1999). Indirect evidence that drug brain targeting using polysorbate 80-coated polybutylcyanoacrylate nanoparticles is related to toxicity. *Pharm Res* **16**: 1836-42.

Panchuk-Voloshina N, Haugland R P, Bishop-Stewart J, Bhalgat M K, Millard P J, Mao F, Leung W Y and Haugland R P (1999). Alexa dyes, a series of new fluorescent dyes that yield exceptionally bright, photostable conjugates. *J Histochem Cytochem* **47**: 1179-88.

Pardridge W M (1999). Vector-mediated drug delivery to the brain. *Adv Drug Deliv Rev* **36**: 299-321.

Pardridge W M, Triguero D, Buciak J and Yang J (1990). Evaluation of cationized rat albumin as a potential blood-brain barrier drug transport vector. *J Pharmacol Exp Ther* **255**: 893-9.

Pelham H R (1996). The dynamic organisation of the secretory pathway. *Cell Struct Funct* **21**: 413-9.

Quintana A, Raczka E, Piehler L, Lee I, Myc A, Majoros I, Patri A K, Thomas T, Mule J and Baker J R, Jr. (2002). Design and function of a dendrimer-based therapeutic nanodevice targeted to tumor cells through the folate receptor. *Pharm Res* **19**: 1310-6.

Rautioa J and Chikhale P J (2004). Drug delivery systems for brain tumor therapy. *Curr Pharm Des* **10**: 1341-53.

Rejman J, Oberle V, Zuhorn I S and Hoekstra D (2004). Size-dependent internalization of particles via the pathways of clathrin- and caveolae-mediated endocytosis. *Biochem J* **377**: 159-69.

Rizzuto R, Brini M, Pizzo P, Murgia M and Pozzan T (1995). Chimeric green fluorescent protein as a tool for visualizing subcellular organelles in living cells. *Curr Biol* **5**: 635-42.

Rizzuto R, Nakase H, Darras B, Francke U, Fabrizi G M, Mengel T, Walsh F, Kadenbach B, DiMauro S and Schon E A (1989). A gene specifying subunit VIII of human cytochrome c oxidase is localized to chromosome 11 and is expressed in both muscle and non-muscle tissues. *J Biol Chem* **264**: 10595-600.

Roderick H L, Campbell A K and Llewellyn D H (1997). Nuclear localisation of calreticulin in vivo is enhanced by its interaction with glucocorticoid receptors. *FEBS Lett* **405**: 181-5.

Scherrmann J M (2002). Drug delivery to brain via the blood-brain barrier. *Vascul Pharmacol* **38**: 349-54.

Schroeder U, Sommerfeld P, Ulrich S and Sabel B A (1998). Nanoparticle technology for delivery of drugs across the blood-brain barrier. *J Pharm Sci* **87**: 1305-7.

Skene J H and Virag I (1989). Posttranslational membrane attachment and dynamic fatty acylation of a neuronal growth cone protein, GAP-43. *J Cell Biol* **108**: 613-24.

Smith P J, Blunt N, Wiltshire M, Hoy T, Teesdale-Spittle P, Craven M R, Watson J V, Amos W B, Errington R J and Patterson L H (2000). Characteristics of a novel deep red/infrared fluorescent cell-permeant DNA probe, DRAQ5, in intact human cells analyzed by flow cytometry, confocal and multiphoton microscopy. *Cytometry* **40**: 280-91.

Soppimath K S, Aminabhavi T M, Kulkarni A R and Rudzinski W E (2001). Biodegradable polymeric nanoparticles as drug delivery devices. *J Control Release* **70**: 1-20.

Steiniger S C, Kreuter J, Khalansky A S, Skidan I N, Bobruskin A I, Smirnova Z S, Severin S E, Uhl R, Kock M, Geiger K D and Gelperina S E (2004). Chemotherapy of glioblastoma in rats using doxorubicin-loaded nanoparticles. *Int J Cancer* **109**: 759-67.

Stewart W W (1978). Functional connections between cells as revealed by dye-coupling with a highly fluorescent naphthalimide tracer. *Cell* **14**: 741-59.

Tkachenko A G, Xie H, Liu Y, Coleman D, Ryan J, Glomm W R, Shipton M K, Franzen S and Feldheim D L (2004). Cellular trajectories of peptide-modified gold particle complexes: comparison of nuclear localization signals and peptide transduction domains. *Bioconjug Chem* **15**: 482-90.

van Oss C J (1978). Phagocytosis as a surface phenomenon. *Annu Rev Microbiol* **32**: 19-39.

Watzele G and Berger E G (1990). Near identity of HeLa cell galactosyltransferase with the human placental enzyme. *Nucleic Acids Res* **18**: 7174.

Woodcock D M, Linsenmeyer M E, Chojnowski G, Kriegler A B, Nink V, Webster L K and Sawyer W H (1992). Reversal of multidrug resistance by surfactants. *Br J Cancer* **66**: 62-8.

Yamaguchi N and Fukuda M N (1995). Golgi retention mechanism of beta-1,4-galactosyltransferase. Membrane-spanning domain-dependent homodimerization and association with alpha- and beta-tubulins. *J Biol Chem* **270**: 12170-6.

Chapter 4

Investigations on the platelet-derived growth factor receptor as a target for the treatment of malignant brain tumors

4.1 Introduction

4.1.1 Platelet-derived growth factor (PDGF)

Since the 1970s PDGF, a major mitogen of fibroblasts, smooth muscle and other cells (Heldin and Westermark 1999) has been subject of extensive studies, focusing on the two isoforms designated PDGF-A and –B. The other two members of the PDGF family PDGF-C and -D were discovered more recently (Reigstad et al. 2005). PDGF was identified as a constituent of whole blood serum that was absent in cell-free serum (Kohler and Lipton 1974; Ross et al. 1974; Westermark and Wasteson 1976). Subsequently it was purified from human platelets where the α-granules are the major storage sites of PDGF (Antoniades et al. 1979; Heldin et al. 1979; Deuel et al. 1981; Raines and Ross 1982). However, as shown in Table 4-1, PDGF-A and PDGF-B can be synthesized by a number of different cell types (Heldin and Westermark 1999). Moreover, PDGF-C and –D are expressed in various embryonic and adult tissues (Reigstad et al. 2005). In embryonic mice, PDGF-C is expressed in the kidney, lung, brain, heart, spinal cord, and other tissues. It also is expressed in human adult tissues, such as kidney, testis, liver brain, and heart.

Table 4-1: PDGF expression in normal cells (from Heldin and Westermark 1999).

Cell Type	PDGF-A	PDGF-B
Fibroblasts	+	+
Keratinocytes	+	+
Placental cytotrophoblasts	+	+
Leydig cells	+	+
Glomerular mesangial cells	+	+
Skeletal myoblasts	+	
Vascular smooth muscle cells	+	+
Vascular endothelial cells	+	+
Astrocytes	+	
Neurons	+	+
Schwann cells	+	+
Oocyte	+	
Uterine endometrial/myometrial cells	+	+
Mammary epithelial cells	+	+
Retinal pigment epithelial cells	+	+
Macrophages	+	+
Platelets/Megakaryocytes	+	+

4.1.2 Gene location, biosynthesis and structure of PDGF

The genes for PDGF-A and PDGF-B are located on chromosomes 7 and 22 (Dalla-Favera et al. 1982; Swan et al. 1982; Betsholtz et al. 1986), whereas those for PDGF-C and PDGF-D are located on chromosomes 4 and 11 (Uutela et al. 2001). The A and B chain, consisting of ~ 100 amino acid residues, show 60 % amino acid sequence identity. PDGF-C and -D share an overall sequence identity of 42 %, with a high similarity in the CUB region (complement subcomponents C1r/C1s, Uegf, and Bmp1), which is an innate domain of the C- and D-type (Bergsten et al. 2001; LaRochelle et al. 2001).

The mature forms of PDGF-A and PDGF-B originate from their respective precursor proteins, after proteolytic processing (Ostman et al. 1991), whereas the subtypes PDGF-C and PDGF-D (mature forms) carry an innate CUB domain, consisting of 110 amino acid residues, which has to be cleaved extracellularly to make the C-terminal growth factor domains active (Li et al. 2000; Bergsten et al. 2001; LaRochelle et al. 2001). Though the biosynthesis of PDGF-A and PDGF-B is strictly regulated, the assembly to the different dimeric subtypes is suggested to be a random process (Hammacher et al. 1988; Hart et al. 1990).

The platelet-derived growth factors are either cationic homodimers consisting of the polypeptide subtypes A, B, C, and D, or heterodimers of the A and B subunits, all connected by two interchenar disulfide bonds. All PDGF monomer subtypes bear eight highly conserved cysteine residues. The X-ray structure of the platelet-derived growth factor-BB isoform with a resolution of 3.0 Å, published by Oefner et al. 1992, has revealed that two of those cysteine residues (cysteines 43 and 52 in PDGF-B) form disulfide bridges between the two PDGF chains within the PDGF dimer. The second cysteine residue from the N-terminal in the first PDGF chain forms a disulfide bridge with the fourth cysteine residue of the second chain and vice versa. All other cysteine residues form intramolecular disulfide bonds. Both chains are folded into twisted antiparallel pairs of β-strands, and the two monomers are arranged in an antiparallel manner referring to the two β-strands containing the connecting cysteine residues (Oefner et al. 1992; Haniu et al. 1993; Haniu et al. 1994). Fig. 4-1 shows the structure of the PDGF-B dimer with its cysteine linkage (Borkham-Kamphorst et al. 2005), also described as cystine knot.

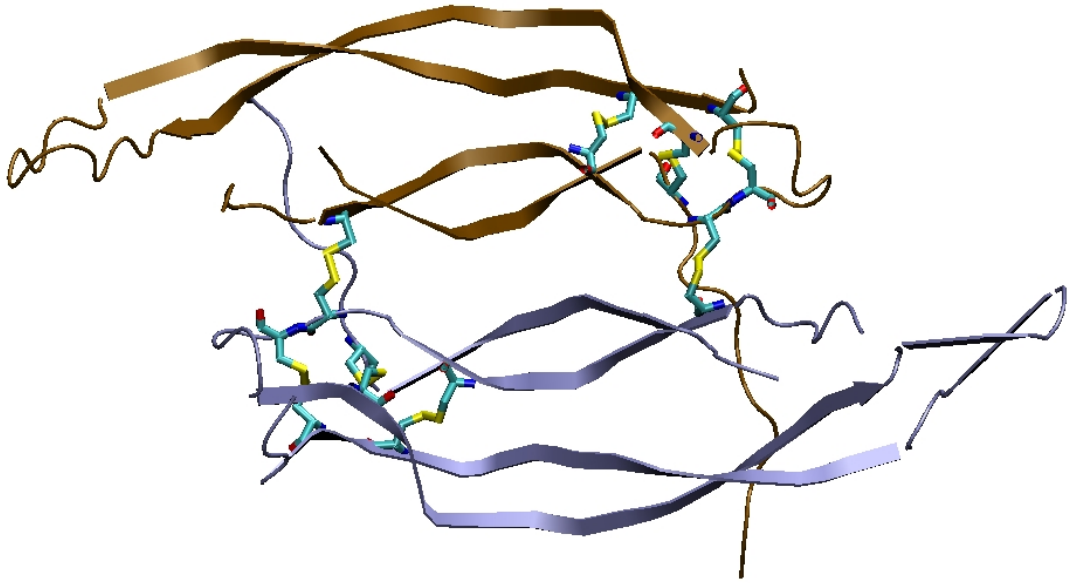

Figure 4-1: Structure of PDGF-B dimer. The structures of the two subunits are shown in brown and metallic blue, respectively. The disulfide bridges are shown as stick models.

Other growth factors showing similarities to the three dimensional structure of PDGF-BB are NGF, TGF-β, (Murray-Rust et al. 1993) and VEGF, despite a low sequence homology of 19 % (Muller et al. 1997). All these growth factors are dimers and show the characteristic cystine knot structure (Sun and Davies 1995). Though the quarternary structure seems to be crucial for the biological activity of PDGF (Prestrelski et al. 1994) the formation of the

biologically active PDGF-B dimer does not require interchain disulfide bonds (Kenney et al. 1994).

4.1.3 Expression of PDGF receptors

The biological effects of all dimeric PDGF variants are mediated by transmembrane protein tyrosine kinase receptors, the PDGF receptors (PDGFR). The two subtypes PDGFRα and PDGFRβ (Yarden et al. 1986; Matsui et al. 1989) are differentially expressed in various cell types (Tab. 4-2) according to Heldin and Westermark (Heldin and Westermark 1999).

Table 4-2: Expression of PDGF receptor subtypes in normal cell types (from Heldin and Westermark 1999, modified).

Cell Type	α-Receptor	β-Receptor
Fibroblasts	+	+
Kidney mesangial cells	+	+
Leydig cells	+	+
Itoh cells of the liver		+
Liver sinusoidal endothelial cells	+	
Myoblasts		+
Vascular smooth muscle cells	+	+
Capillary endothelial cells		+
Pericytes		+
Astrocytes	+	
Neurons	+	+
Schwann cells	+	+
Mammary epithelial cells		+
Retinal pigment epithelial cells	+	+
Platelets/Megakaryocytes	+	
T cells		+
Myeloid hematopoietic cells		+
Macrophages		+

4.1.4 Gene locations and structure of PDGFRs

The gene encoding for PDGFRα is situated on chromosome 4q12, which is close to two other gene loci, the gene for the SCF receptor *c-kit* and the VEGF receptor-2 (Spritz et al. 1994), both protein tyrosine kinase receptors. The PDGFRβ gene is localized on chromosome 5, also close to another tyrosine kinase receptor gene, *c-fms*, encoding for the macrophage colony stimulating factor-1 (CSF-1) receptor (Roberts et al. 1988). Moreover, the PDGFR proteins show structural similarity with CSF-1 and SCF receptor proteins (Coussens et al. 1986; Yarden et al. 1987). The molecular weight of the PDGFR subtypes is ~ 170 kDa (PDGFRα) and 180 kDa, respectively (PDGFRβ). The transmembrane part connects five extracellular immuno-globulin-like domains to an intracellular tyrosine kinase domain, containing a characteristic sequence, which is unique for PDGF receptor kinase (Claesson-Welsh et al. 1989).

4.1.5 Interaction of PDGF with PDGFR, and PDGF receptor cycle

The PDGF receptors form homo- and heterodimeric receptor complexes, whereas dimerization takes place upon binding of the dimeric PDGF ligand only (Bishayee et al. 1989; Heldin et al. 1989; Seifert et al. 1989). As illustrated in Figure 4-2, the A- and B-chain of PDGF show similar affinity to PDGFRα, but only the B-chain is also able to bind the PDGFRβ subtype. Consequently, PDGF-AA leads to the formation of PDGFRαα complexes, PDGF-AB to PDGFRαα and -αβ dimers, and PDGF-BB to the dimerization of all three possible combinations of α- and β-receptors (Hart et al. 1988; Hammacher et al. 1989; Seifert et al. 1989; Kanakaraj et al. 1991). PDGF-CC behaves similarly to PDGF-AB. It specifically leads to PDGFRαα and PDGFRαβ, but not to PDGFRββ dimer formation (Li et al. 2000; Gilbertson et al. 2001). PDGF-DD is regarded as PDGFRββ selective, due to its high binding affinity to the β-homodimer and its much lower affinity to PDGFRαβ (Bergsten et al. 2001; LaRochelle et al. 2001).

After receptor binding the ligand-receptor complex is internalized via an endocytotic mechanism into endosomes, where the ligand dissociates from the receptor molecules. Later on the receptor proteins are recycled and transported to the plasma membrane again or are degraded after fusion of the endosomes with lysosomes (Sorkin et al. 1991; Liu et al. 1996).

As an alternative route, PDGF receptor proteins can undergo cytosolic degradation in proteasomes (Mori et al. 1995).

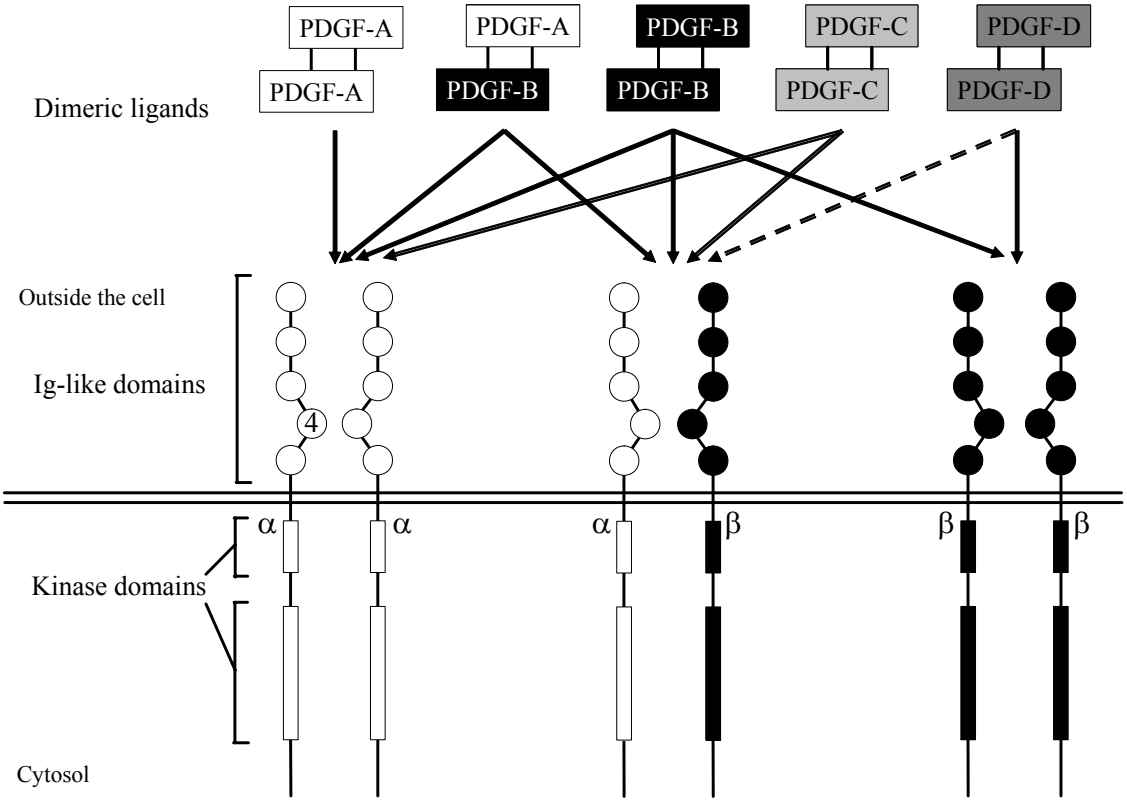

Figure 4-2: Binding affinities of PDGF isoforms to PDGF receptor subtypes. α- and β-receptors are bound and dimerized with different specificities of the PDGF isoforms. The illustration schematically shows the three possible combinations of PDGFR subtypes. The dimeric ligands bind to the three outer Ig-like domains, whereas the Ig-like domain 4 is interacting with the corresponding domain of a second receptor monomer (based on Heldin and Westermark 1999).

4.1.6 PDGFR-mediated effects

The homo- and heterodimeric receptor complexes PDGFRαα, -ββ, and –αβ mediate qualitatively different effects on PDGF responsive cells (Table 4-3). Consequently, due to the different binding affinities of the PDGF isoforms to the PDGFR subtypes, the reaction of a cell upon stimulation with PDGF is determined by the qualitative and quantitative expression of the PDGFR monomers. Compared to the other isoforms, PDGF-AB has a stronger mitogenic and chemotactic effect on cells expressing both PDGFRα and -β subtypes (Heidaran et al. 1991; Ekman et al. 1999). As an explanation for the cellular effects preferentially mediated by the different PDGF dimers, it has been suggested, that binding of

different isoforms leads to a particular phosphorylation pattern of the dimerized PDGF receptors (Rupp et al. 1994; Ekman et al. 1999).

Table 4-3: PDGFR homodimers-mediated cellular effects (from Heldin and Westermark 1999, modified).

Effect	PDGFRα	PDGFRβ
Cell growth	Stimulation	Stimulation
Actin reorganization	Stimulation of edge ruffling and loss of stress fibers	Stimulation of edge ruffling, loss of stress fibers, circular ruffles
Chemotaxis	Stimulation or inhibition depending on cell type	Stimulation
Ca^{2+} mobilization	Weak stimulation	Stimulation
GAP* junctional communication		Inhibition
Apoptosis		Inhibition

*GAP: GTPase activating protein

4.1.7 PDGFR signal transduction

For the start of any PDGFR signal transduction the dimerization of two PDGFR monomers is necessary. This approximates the intracellular kinase domains of both monomers and causes autophosphorylation of conserved tyrosine residues within the kinase domains, Tyr-849 in PDGFRα (Heldin and Westermark 1999) and Tyr-857 in PDGFRβ (Kazlauskas and Cooper 1989). Activation of the kinase domains increases their catalytic efficiency and entails autophosphorylation of several tyrosine residues outside the kinase domains, creating docking sites for various adapter proteins, listed in Table 4-4 (Heldin and Westermark 1999).

The PDGFR signal transduction is intracellularly regulated by several effects, e.g. in human arterial smooth muscle cells PDGF increases cAMP formation and protein kinase A activity through a mitogen activated protein (MAP) kinase-mediated activation of cytosolic phospholipase A2, arachidonic acid release, and prostaglandin E2 synthesis (Graves et al. 1996). Furthermore, the PDGF receptor signalling is modulated by tyrosine phosphatases, which are balancing the phosphorylation state of several tyrosine residues after PDGF receptor activation. A prominent member of these tyrosine phosphatases is SHP-2, which is

capable of dephosphorylation of autophosphorylated PDGF receptors and of substrates of the PDGF receptor kinase (Klinghoffer and Kazlauskas 1995).

Table 4-4: Signal transduction molecules interacting with intracellularly phosphorylated PDGF receptor domains (Heldin and Westermark 1999).

Adapter protein	Downstream signal transduction
PI 3-kinase	Activates members of serine/threonine, PKC, and RHO kinase families; activates Akt/PKB and JNK/SAPK kinases
PLCγ	Increase in intracellular calcium and diacyl-glycerol concentration (subsequently certain members of the PKC members)
Src	
SHP-2	Dephosphorylates autophosphorylated receptors and binds Grb2/SOS
GAP	Deactivates RAS
Stat5	Binds to promotor regions of specific genes
Shc	Binds Grb2/SOS
Grb2	
Grb7	
Nck	Activates the serin/threonin kinases PAK and NIK
Crk	Activates the nucleotide exchange factor C3G

Furthermore, PDGFR signal transduction forms a complex regulative system of interactions with integrin signalling (Assoian 1997; Frisch and Ruoslahti 1997). The growth of several PDGF-responsive cell types is dependent on contacts with extracellular matrix molecules. These contacts are mediated and controlled by integrins, transmembrane receptors for matrix molecules. Growth factor-mediated effects like cell proliferation and cell migration can be enhanced by integrin signalling (Assoian 1997; Frisch et al. 1997). PDGF β-receptors can interact with certain integrins by formation of PDGFR/integrin complexes after PDGFR autophosphorylation, as shown for NIH 3T3 cells (Sundberg and Rubin 1996; Schneller et al. 1997). Transient, PDGF-independent tyrosine phosphorylation of PDGF receptors was observed after binding of collagen and fibronectin to β_1-integrin to PDGF receptors in human fibroblasts (Sundberg et al. 1996). Moreover, the binding of PDGF to PDGF receptors stimulated the synthesis of collagen binding β_1 integrin subunit α_2 in human fibroblasts too (Ahlen and Rubin 1994).

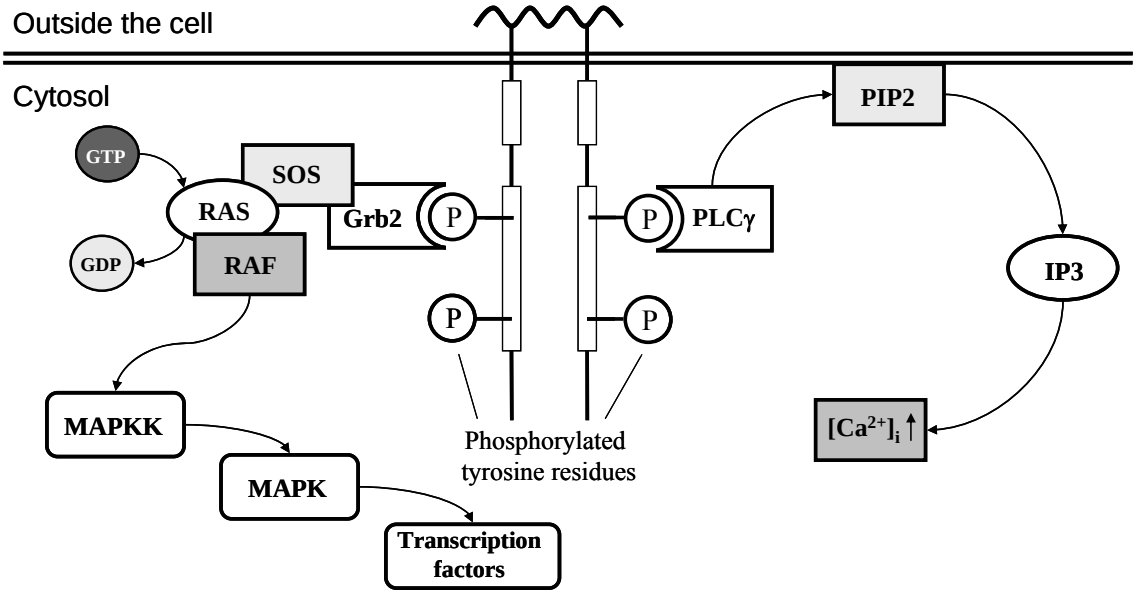

Figure 4-3: Binding of various adapter proteins to phosphorylated PDGF receptor tyrosine kinase domains after dimerization of two receptor monomers. The drawing exemplarily illustrates the MAP kinase and the PLCγ signal transduction pathway. PLC: Phospholipase C; PIP2: Phosphatidylinositol-4,5-bisphosphate; IP3: Inositol-1,4,5-trisphosphate; Grb2: adapter protein with SH2 and SOS domain; SOS: son of sevenless nucleotide exchange factor (drosophila related protein); RAS: RAS protein kinase; RAF: RAF protein kinase; MAPK: mitogen activated protein kinase.

4.1.8 Oncogenic potential of PDGF

PDGF and PDGF receptors are expressed in many different embryonic and adult tissues, where they serve a broad variety of physiological functions. As reviewed in detail by Heldin and Westermark (Heldin and Westermark 1999) and Reigstad et al. (Reigstad et al. 2005), PDGF/PDGFR are crucial in embryonic development and contribute to wound healing processes. Furthermore they are suggested to contribute to tissue homeostasis and to exert neurotrophic effects in the CNS.

However, PDGF has also been suggested to be involved in tumorigenesis, due to the finding of genetic aberrations in PDGF/PDGFR genes. The amplification of the PDGFRα gene has been shown to lead to an overexpression of an aberrant receptor protein (Fleming et al. 1992; Kumabe et al. 1992; Hermanson et al. 1996). Some dermatofibrosarcoma and giant-cell sarcoma exhibit an abnormal PDGF-B gene resulting from a fusion of the PDGF-B gene to the collagen gene COL1A1 (Simon et al. 1997). A constitutively active PDGF β-receptor

has been described in chronic myelomonocytic leukemia, where the PDGFRβ gene is fused to the *TEL* gene by a chromosome translocation (Golub et al. 1994; Carroll et al. 1996).

Besides the described genetic aberrations, it has been suggested that PDGF may exert a transforming potential by an autocrine PDGF receptor activation, when PDGF and PDGFR are coexpressed. The *v-sis* oncogene product, respectively its cellular counterpart, the *c-sis* oncogene product, is identical to the PDGF-B precursor protein. Moreover, it is identically synthesized, assembled, processed, and secreted (Doolittle et al. 1983; Robbins et al. 1983; Ostman et al. 1991). The transduction of cells with the acutely transforming retrovirus simian sarcoma virus (SSV, Devare et al. 1983) or the Parodi-Irgens feline sarcoma virus (Besmer et al. 1983) carrying the *v-sis* oncogene, leads to *v-sis* expression and to transformation of the transduced cells, if the target cells express either PDGF α- or β-receptors (Leal et al. 1985; Beckmann et al. 1988). According to the binding affinity of PDGF-A, the transfection of cells with the PDGF-A gene leads to transformation only in α-receptor positive cells (Matsui et al. 1989; Matsui et al. 1989). In *sis*-transformed cells the newly synthesized PDGF-B is not only able to bind membranous PDGF receptors, but it also binds to immature PDGF receptors, which haven´t been transported to the cellular membrane yet. However, the transforming signal is suggested to be a result of the interaction of PDGF-B with the membranous receptors (Johnsson et al. 1985).

Apart from its transforming effect in vitro, the *sis*-gene furthermore causes development of fibrosarcoma (Pech et al. 1989) and glioblastoma in mice (Uhrbom et al. 1998). Heldin and Westermark pointed out as unlikely that an autocrine growth stimulation is sufficient to cause a fully malignant phenotype in the virally induced tumors (Heldin and Westermark 1999) and that additional, yet unknown aberrations might contribute to the transformation of the cells.

More recent studies have also involved the more recently discovered members of the PDGF subtype family, PDGF-C and PDGF-D. An autocrine activation loop, consisting of PDGF α-receptors and PDGF-CC has been suggested to be important for the malignancy of Ewing family sarcoma (Zwerner and May 2002). When PDGF-C was co-expressed with a dominant negative PDGF-C mutant in a fibroblast transformation model, anchorage dependent cell growth was reduced. Other authors have provided contradicting results, by showing the expression of only PDGFR β-receptors in ewing family sarcoma cell lines and tissues (Uren et al. 2003). Since PDGF-C does not bind homodimeric PDGFRβ receptors, an increasing effect of PDGF-C on the proliferation of Ewing family sarcoma seems rather unlikely. PDGF-C mRNA was detected in several glioblastoma and medulloblastoma cell lines and in five glioblastoma multiforme tissues, whereas little expression was found in

normal foetal and adult brain tissue (Andrae et al. 2002; Lokker et al. 2002), indicating PDGF-C to play a role in the development and/or the maintenance of those tumors mentioned. In glioblastoma and medulloblastoma PDGF-D has been suggested to mimic PDGF-B, which was not detected in a majority of the cases investigated by Lokker et al. (Lokker et al. 2002). Moreover, PDGF-D has been shown to accelerate migration of prostate fibroblast cells and accelerate progression and metastasis of prostate cancer in immunodeficient mice (Ustach et al. 2004). It is coexpressed with PDGF β-eceptor in human prostate cancer tissue and has been linked to prostate cancer progression by colocalization with its activator urokinase plasminogen activator in prostate cancer cells (Ustach and Kim 2005). Finally, compared to normal tissues, PDGF-D is upregulated in human lung and ovarian cancers, and in sera of lung and ovarian cancer patients increased PDGF-D levels were detected (LaRochelle et al. 2002).

As becomes obvious from Table 4-5, several tumors coexpress at least one PDGFR subtype and one PDGFR ligand subtype, capable of binding the coexpressed receptor (Heldin and Westermark 1999).

Table 4-5: Expression of PDGF and PDGF receptors in human malignancies (from Heldin and Westermark 1999).

Cell Type	PDGF-A	PDGF-B	PDGFRα	PDGFRβ
Medullablastoma			+	+
Meningioma	+	+	+	+
Soft tissue sarcoma		+		
Kaposi sarcoma		+		
Capillary hemangioblastoma			+	+
Mesothelioma	+	+	+	+
Choriocarcinoma		+		+
Ovarian carcinoma		+	+	
Midget carcinoid		+	+	
Breast cancer		+		+*
Prostate cancer	+		+	+
Pancreatic carcinoma			+	+
Colorectal carcinoma		+		
Gastric carcinoma		+		+
Acute megaloblastic leukemia	+	+		

* cytosolic protein

However, the question whether autocrine PDGFR stimulation is responsible either for the development or for the maintenance of spontaneous tumors in humans is not sufficiently answered yet. Many of the PDGF/PDGFR expression studies referred to the mRNA detection, but not to the detection of the ligand or the receptor protein. Moreover, in most of the studied tumors the expression of PDGF and PDGF receptors was unknown in the normal tissues from which the tumor had developed. It also has to be highlighted, that except for the analysis of PDGF/PDGFR expression no further investigations have been done to determine the receptor activation in terms of autophosphorylation or binding of substrates to the PDGFR kinase domain. Heldin and Westermark mention, that even if an autocrine activation loop between PDGF and PDGF receptors of the tumor cells should occur, it is unknown if this plays a crucial role in the development of the tumor or even contributes to it (Heldin and Westermark 1999).

In summary, PDGF has been linked to oncogenic effects, but a generally accepted assertion about its contribution to tumorigenesis, maintenance, and progression of certain tumor types remains controversial.

4.1.9 PDGF and PDGFR antagonists and PDGFR inhibitors

As mentioned above, PDGF is implicated in autocrine and paracrine stimulation processes, possibly leading to several pathological conditions. This poses the question for the clinical use of the PDGF inhibition and the inhibition of PDGF receptors, respectively. PDGF antiserum has been shown to inhibit neointimal smooth muscle cell accumulation in a restinosis model in the rat (Ferns et al. 1991). Several other approaches have been carried out to bind PDGF in order to prevent it from binding to its receptor, including soluble extracellular PDGF receptor domains (Duan et al. 1991), PDGF binding DNA aptamers (Green et al. 1996), and low molecular weight compounds capable of binding PDGF (Mullins et al. 1994). Moreover monoclonal antibodies against PDGF receptors can be used as virtual PDGFR antagonists, functioning as a block for ligand binding and consequently for PDGF receptor activation (LaRochelle et al. 1993; Ramakrishnan et al. 1993; Lokker et al. 1997).

The selective inhibition of the PDGF tyrosine receptor kinase by low molecular weight compounds is currently evaluated for clinical purposes, e.g. for the treatment of human glioblastoma (National cancer institute 2005; U.S. National institutes of health 2005; U.S. National institutes of health 2005). Presuming that maintenance and progression of various

malignancies in humans essentially depend on the autocrine and paracrine stimulation, this is a promising approach. Up to now several classes of selective PDGF receptor inhibitors have been described. A series of 3-indoleacrylonitrile tyrphostins, 2-chloro-3-phenylquinolines, and 3-arylquinoxalines have been examined for their potency of inhibition of platelet-derived growth factor receptor tyrosine kinase, whereas the potency decreased in the order from quinoxalines > quinolines > indoles (Gazit et al. 1996). Lipophilic groups (methyl, methoxy) in the 6 and 7 positions and phenyl at the 3 position of quinoxalines and quinolines were essential for potency. Compared to their affinities to EGF-, HER-2/c-ErB-2 receptors, the compounds showed selectivity for the inhibition of autophosphorylation of PDGF receptors in experiments with isolated membranes of Swiss 3T3 mouse fibroblasts. However, only a few compounds were selective for PDGFR inhibition and showed IC_{50} values in the low micromolar range (1-1.5 μM). A commercially available tyrphostin is the compound AG-1296, which selectively inhibits autophosphorylation of the PDGFR kinase and the PDGF-dependent DNA synthesis in Swiss 3T3 cells and in porcine aorta endothelial cells with a 50 % inhibitory concentration of 1 μM (Kovalenko et al. 1994; Kovalenko et al. 1997). Furthermore, certain compounds from the classes of bisindolylmethanones as well as of 3-arylquinolines showed higher potency of inhibition of PDGFR autophosphorylation with IC_{50} values in the high nanomolar range (Dolle et al. 1994; Maguire et al. 1994; Bohmer et al. 2003). 1-Phenylbenzimidazoles (Palmer et al. 1998) including the recently described compound CP-673451 (Roberts et al. 2005) consist the most potent class of PDGF receptor kinase inhibitors by now. Moreover, leflunomide, a registered drug against rheumatoid arthritis (Arava®), and its active metabolite A771726 also have been shown to inhibit PDGFR autophosphorylation, but at concentrations of 65 μM and 75 μM respectively (Shawver et al. 1997; Eckhardt et al. 1999; Xu et al. 1999). Finally, the phenylaminopyrimidine imatinib (Gleevec®), which is registered for the treatment of chronic myelogenous leukemia (CML) and for the treatment of gastrointestinal stromal tumors (GIST), selectively inhibits autophosphorylation of the PDGFR kinase with an IC_{50} value of 100 nM (Kilic et al. 2000). Fig. 4-4 shows the chemical structures of representative examples of different compound classes with their IC_{50} values for the inhibition of PDGFR autophosphorylation.

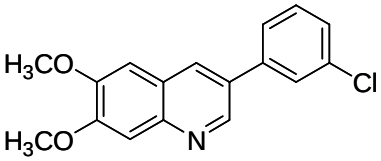

Tyrphostin CP17, IC_{50} = 1.5 µM
Gazit et al. 1996

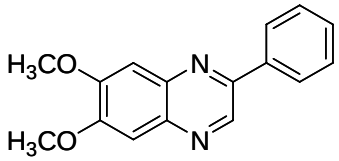

Tyrphostin AG-1296, IC_{50} = 300 nM
Kovalenko et al. 1994

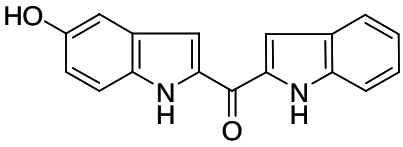

CP39, IC_{50} = 200 nM
Mahboobi et al. 2002

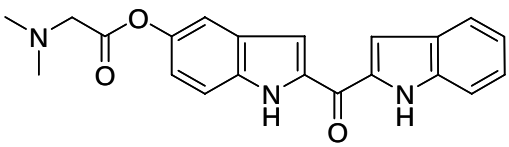

CP53, IC_{50} = 100 nM
Mahboobi et al. 2002

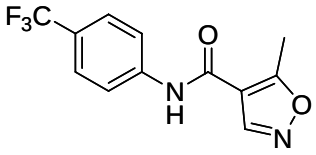

Leflunomide (SU101), IC_{50} = 65 µM
Shawver et al. 1997

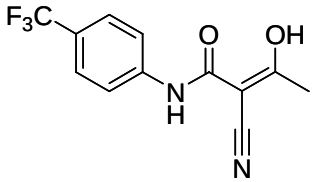

SU0020 (A771726), IC_{50} = 75 µM
Xu et al. 1999

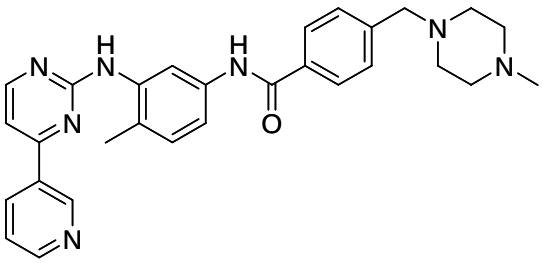

Imatinib (STI-571), IC_{50} = 100 nM
Buchdunger et al. 2000

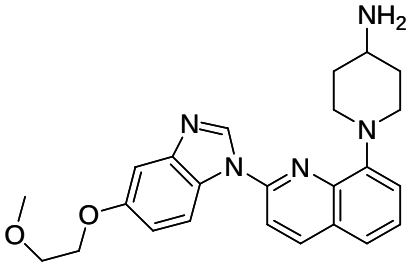

CP-673451, IC_{50} = 1 nM
Roberts et al. 2005

Figure 4-4: Chemical structures of various PDGF receptor tyrosine kinase inhibitors with their IC_{50} value referring to inhibition of PDGFR autophosphorylation.

4.2 Objective

Glioblastoma multiforme, the most common form of malignant brain tumors in adults, is resistant to all forms of therapy, causing the death of most patients within 9–12 months after diagnosis. Glioblastoma are known to exhibit numerous genetic and physiological peculiarities such as the coexpression of platelet derived growth factors (PDGF) and their receptors (PDGFR) (Nister et al. 1991), an observation, which has been suggested to result in an increase in cell proliferation due to an autocrine loop (Hermanson et al. 1992; Guha et al. 1995; Yu et al. 1998; Lokker et al. 2002). The expression of different PDGFR ligands (PDGF-A, PDGF-B, PDGF-C, and PDGF-D) and PDGFR subtypes (PDGFRα and PDGFRβ) has been reported in various glioblastoma cell lines (Nister et al. 1991), including U-87 MG, U-118 MG, and U-373 MG cells.

Recently, the inhibition of the growth of U-343 MG and U-87 MG human glioblastoma cells by disruption of the PDGF/PDRFR autocrine loops with the selective tyrosine kinase inhibitor imatinib was reported as well as the growth inhibition of subcutaneous and intracranial tumors in nude mice, established by the injection of human U-343 and U-87 MG cells, suggesting that PDGF receptors might be a therapeutic target for glioblastoma (Kilic et al. 2000). Furthermore, imatinib was reported to act as a radiosensitizer in human glioblastoma cells through the inhibition of PDGFR (Holdhoff et al. 2005). Currently the efficacy of imatinib in the treatment of human adult glioma is evaluated in clinical trials (Raymond E 2004; National cancer institute 2005; U.S. National institutes of health 2005), as well as in combination with hydroxyurea (Dresemann 2003; Dresemann 2004) and with or without radiation therapy in childhood glioma (U.S. National institutes of health 2005).

The aim of this work was to corroborate the expression and the functionality of PDGFR and PDGF subtypes in human U-87 MG, U-118 MG, and U-373 MG glioblastoma cells as a prerequisite for an autocrine loop, to study the effect of exogenous PDGF-BB on the proliferation of human glioblastoma, and to investigate the purported antiproliferative activity of selective PDGF receptor tyrosine kinase inhibitors against human glioblastoma cells.

4.3 Materials and methods

4.3.1 Drugs and chemicals

Imatinib (STI-571) was a gift from Novartis (Basel, Switzerland); a 10 mM stock solution was prepared in DMSO. Paclitaxel was from Bristol-Myers Squibb (Munich, Germany) and was used as a 100 µM stock solution in 70 % ethanol. Doxorubicin was purchased from Sigma (Munich, Germany), a 1 mM stock solution in DMSO was made. Topotecan (GlaxoSmithKline, Munich, Germany) was kept as a 1 mM stock solution in 70 % ethanol. Mitoxantrone (Sigma, Munich, Germany) was stored as a 3 mM stock solution in 70 % ethanol. Leflunomide was kindly provided by Aventis (Bad Soden, Germany), whereas AG-1296 was obtained from Calbiochem-Novabiochem (Bad Soden, Germany). The latter compounds were dissolved in DMSO yielding concentrations of 100 mM and 10 mM, respectively. All stock solutions were stored at -20 °C.

4.3.2 Cell lines and culture conditions

The human U-87 MG (ATCC HTB 14, passage 126), the U-118 MG (ATCC HTB 15, passage 448) and the U-373 MG (ATCC HTB-17, passage 182) glioblastoma/ astrocytoma cell lines (Beckman et al. 1971) were obtained from the American Type Culture Collection (ATCC). Cell banking and quality control were performed according to the "seed stock concept" (Hay 1988). U-87 MG and U-373 MG cells were grown in Eagle´s minimum essential medium (EMEM, Sigma, Munich, Germany) containing L-glutamine, 2.2 g/l $NaHCO_3$, 110 mg/l sodium pyruvate, and 5 % fetal calf serum (FCS, Biochrom, Berlin, Germany), whereas the U-118 MG cells were maintained in Dulbecco´s minimum essential medium (DMEM, Sigma, Munich, Germany) which was also supplemented with 5 % FCS. Human CCD-11Lu fibroblasts (ATCC CCL-202, passage 10) and human A431 epidermoid carcinoma cells (ATCC CRL-1555) (Giard et al. 1973) were cultured in DMEM supplemented with 10 % FCS. All cells were cultured in a water-saturated atmosphere of 95 % air and 5 % carbon dioxide at 37 °C in 75-cm² culture flasks (Nunc, Wiesbaden, Germany) and were serially passaged following trypsinization using trypsin (0.05 %)/EDTA(0.02 %) (Roche Diagnostics, Mannheim, Germany). Human K-562 chronic myelogenous leukemia

(CML) cells, German collection of microorganisms and cell cultures (DSMZ, Braunschweig, Germany; ACC 10, passage 21) (Koeffler and Golde 1980) were kindly provided by Dr. Robert Gastpar, department of hematology and internist oncology, University of Regensburg. Cells were cultured in RPMI-1640 (Sigma, Munich, Germany) medium, supplemented with 5 % FCS. Cells were passaged every 4-5 days. Swiss 3T3 mouse fibroblasts (ATCC CCL-92) (Todaro and Green 1963) were kindly provided by Prof. Dr. Frank Böhmer, research unit of molecular cell biology, University of Jena. Cells were maintained in DMEM containing 10 % FCS and were passaged once a week. HeLa cell derived human KB cells (ATCC CCL-17) (Eagle 1955) were cultured in DMEM 10 %, supplemented with 300 ng/ml vninblastine and passaged every 4-5 days. MCF7 breast adenocarcinoma cells (ATCC HTB-22) (Sugarman et al. 1985; Bacus et al. 1990) were maintained in EMEM 5 % with weekly passaging. MCF7/Topo cells were additionally cultured with 500 ng/ml topotecan.

4.3.3 Isolation of total RNA

For the RNA isolation procedure all cells types were cultured in 75 cm^2 culture flasks and the total RNA was isolated by the guanidinium thiocyanate method (Chomczynski and Sacchi 1987). To prevent a loss and destruction of RNA by RNAses during isolation and storage, all surfaces that may come into contact with the RNA preparation were treated with a 0.1 % solution of DEPC (diethyl pyrocarbonate, Fluka, Steinheim, Germany) in millipore water. Solution D was prepared by dissolving 250 g of guanidinium thiocyanate (Merck, Darmstadt, Germany) in 293 ml of DEPC treated water and addition of 17.6 ml of a 0.1 M sodium citrate solution (Merck) pH 7.0 and 26.4 ml of a 0.5 % sarcosyl (N-lauryl sarcosine sodium salt; Merck) solution. 360 µl of β-mercaptoethanol (Serva, Heidelberg, Germany) were added to solution D before use. Almost confluent (90 %) cultures of U-87 MG, U-118 MG, U-373 MG, and CCD-11Lu cells, were used for the isolation prodecure whereas the RNA of K-562 CML suspension cells was isolated when the cells had reached a density of 10 million per flask. After the culture medium was removed, cells were lysed by the addition of 5 ml of solution D. The lysate was mixed with 0.5 ml of sodium acetate (pH 4, 2 M), 5 ml of water-saturated phenol, and 1 ml of chloroform, followed by vortexing. After incubation on ice for 15 minutes and centrifugation at 10,000 g (Sorvall RC-5B, DuPont, Wilmington, Delaware, USA) for 15 minutes at 4 °C, the aqueous phase of the mixture was transferred into a new reaction vessel. An equal volume of isopropyl alcohol p.a. (Merck, Darmstadt, Germany) was added for RNA

precipitation, and after an incubation period of 1 hour at -20 °C the RNA was pelleted by centrifugation at 15,000 g for 15 minutes at 4 °C. The supernatant was discarded and the RNA pellet was resuspended in 1 ml of solution D. As a further purification step the RNA was precipitated again by addition of 1 ml of isopropyl alcohol p.a., incubation for 1 hour at -20 °C, and centrifugation at 13,000 g for 30 minutes at 4 °C. The supernatant was removed and the pellet was washed with 70 % ethanol. After centrifugation at 15,000 g for 15 minutes at 4 °C the pellet was dried at room temperature under sterile conditions, and afterwards it was redissolved in DEPC treated water (DEPC water) and stored at -80 °C. The concentration and purity of the isolated RNA samples were measured using a Cary 100 UV-Vis spectrophotometer, confirming $A_{260/280}$ ratio values between 1.4 and 1.9.

4.3.4 RT-PCR

For RT-PCR M-MLV reverse transcriptase (Invitrogen, Karlsruhe, Germany) and Taq-polymerase (Promega, Mannheim, Germany) were used. The PCR primer sequences (Tab. 4-6) for PDGFR were taken from the literature (Denk and Knorr 2002). All other primer sequences (Tab. 4-6) were computed with the Web-Primer program, (http://genome-www2.stanford.edu /cgi-bin/SGD/web-primer) whereas the template nucleotide sequences for primer design were obtained from the NCBI database.

Table 4-6: Primer sequences for RT-PCR (5′-3′). All primers were synthesized by MWG Biotech AG.

mRNA	Sense-Primer	Antisense-Primer
β-actin	5'-CGGGATCCCCAACTGGGAC-3'	5'-GGAATTCTGGCGTGAGGGA-3′
PDGFRα	5′-TCAAAGTCCCATCCATCAAAT-3′	5′-GCTTCAGCTCTCGGTTCTCAG-3′
PDGFRβ	5′-ACGTGGCTTTTCTGGTATCTT-3′	5′-TTTCTTTGCGGGGGTATGTCC-3′
PDGF-A	5′-ATACCTCGCCCATGTTCTG-3′	5′-TGACTCCGAGGAATCTCGTAA-3′
PDGF-B	5′-AGGAGGGAGACTGTGGTAGGG-3′	5′-GAGGACTTTGGGAAATGGAGG-3′
PDGF-C	5′-GGAGTCGCTGCT TCCAAAGT-3′	5′-GCCAGAAAATGGTATCGGTT-3′
PDGF-D	5′-GGGTAGAGCTAAGACCATGGC-3′	5′-TCAGCAACCACTTGTGTTCA-3′
Bcr-Abl	5′-TCCGGGGCTCTATGGGTTT-3′	5′-AAGGTTTGGCTCAGCTGTGT-3′
MDR1	5′-TCCAAGCTCAAAGAAGCAGA-3′	5′-TTGCCATTGACTGAAAGAACA-3′
BCRP	5′-GCCTTGGGATACTTTGAATCA-3′	5′-AACCCCAGCTCTGTTCTGGAT-3′
MRP	5′-ATGTTGTATCCCCTCTTCCCT-3′	5′-TTCGCATCTCTGTCTCTCCTG-3′

Primers were synthesized by MWG Biotech AG (Ebersberg, Germany). RT-PCR was carried out with a Mastercycler (Eppendorf, Wesseling-Berzdorf, Germany) gradient. PCR was performed with an initial step at 95 °C for 30 seconds, then 32 cycles at 60 °C for 1 minute and 72 °C for 30 seconds, followed by a final elongation step at 72 °C for 2 minutes. The PCR products were detected by agarose gel electrophoresis (1.5 % agarose [peqGOLD, Peqlab, Erlangen, Germany] in tris-borate-EDTA buffer, 0.4 µg/ml ethidium bromide [Sigma, Munich, Germany]).

4.3.5 Immunostaining

The expression of the PDGF receptor protein by human glioblastoma cells was visualized by immunofluorescence. CCD-11Lu fibroblasts were used as positive control. The cells were seeded into chamberslides (Nunc, Wiesbaden, Germany). At 90 % confluence of the cells the medium was removed and the cells were washed with phosphate buffered saline (PBS, 8.0 g/l NaCl, 1.0 g/l $Na_2HPO_4 \cdot 2H_2O$, 0.2 g/l KCl, 0.2 g/l KH_2PO_4 and 0.15 g/l $NaH_2PO_4 \cdot H_2O$) containing 0.1 % NaN_3 and 2 % FCS. 50 µl (1:100 dilution in PBS) of the primary anti PDGFRα and PDGFRβ antibody solution (monoclonal anti-human PDGFRαMAB1264, monoclonal anti-human PDGFRβMAB1263, R&D Systems, Wiesbaden-Nordenstadt, Germany) were added, and the cells were incubated at room temperature for 1 hour. The supernatant was removed and the cells were washed 3 times with PBS. 50 µl (1:100 dilution in PBS) of the secondary antibody solution (polyclonal rabbit anti-mouse IgG fluorescein isothiocyanate (FITC) conjugated, F0261, DAKO, Hamburg, Germany) were added and the cells were incubated for 1 hour at 4 °C, protected from light. After removal of the supernatant and washing (3 times with PBS) the cells were inspected under a fluorescence microscope (DMI-RB, Leica, Wetzlar, Germany). For non-specific binding cells were processed without primary antibody.

For the determination of the expression of the p-glycoprotein 170 (pgp) and of the breast cancer resistance protein (bcrp) the glioblastoma cell variants were seeded into chamberslides (Nunc, Wiesbaden, Germany). KBv1 cells served as positive control for pgp while MCF7 wild type cells were used as positive control for bcrp. After 48 hours of attachment period the cells were fixed with 4 % PFA solution in PBS for 20 minutes at room temperature. After discarding the fixative the cells were washed 3 times with 300 µl PBS 0.5 % bovine serum albumin (BSA, Serva, Heidelberg, Germany) and permeabilized by incubation with 0.1 %

Triton X-100 solution in PBS 0.5 % BSA, 150 µl per well, for 10 minutes at room temperature. The cells were washed again 3 times with 300 µl PBS 0.5 % BSA and then were incubated with 125 µl of a 1:200 dilution of monoclonal mouse anti-human pgp Ab2 primary antibody Clone F4 (Dianova, Hamburg, Germany) and monoclonal mouse anti-human bcrp BXP-21 primary antibody (Calbiochem, Bad Soden, Germany), respectively, for 1 hour at room temperature. After removing the excess primary antibody and washing 3 times with PBS 0.5 % BSA, the cells were incubated with 125 µl of 1:200 diluted Cy5-conjugated rabbit anti-mouse IgG secondary antibody (Dianova, Hamburg, Germany) for 1 hour at room temperature. The incubation of the cells with the anti-bcrp antibody was followed by a 10 minutes incubation period with the nucleic acid stain SYTOXGreen® (500 nM in PBS 0.5 % BSA, 125 µl per well, Molecular probes, Eugene, Oregon, USA). The cells were washed 3 times with PBS 0.5 % BSA and with millipore water. After air drying and mounting using fluoromount mounting medium (Serva, Heidelberg, Germany), the cells were inspected with a Carl Zeiss Axiovert 200M confocal laser-scanning microscope, equipped with a LSM510 scanning unit.

4.3.6 Flow cytometric determination of PDGFR expression

The human glioblastoma cells were trypsinized and suspended in medium to 1 million cells/ml. The cells were washed with PBS and stained in the same way as for fluorescence microscopy (immunostaining of PDGFR). For flow cytometric analysis with a FACSCalibur (BD Biosciences, Heidelberg, Germany) the cells were centrifuged after the last washing step, the supernatant was discarded, and the pellet was suspended in 0.5 ml of PBS. For each measurement 100,000 events were acquired, and fluorescence was measured in the FL1 channel.

4.3.7 Fluorimetric quantification of intracellular Ca^{2+} mobilization

The PDGF receptor-mediated effect of PDGF-BB on $[Ca^{2+}]_i$ mobilization (Berridge et al. 1984; Moolenaar et al. 1984; Diliberto et al. 1992) in human glioblastoma cells was determined by the ratiometric Fura-2 method, which is based on a shift of the excitation spectra of the Ca^{2+} indicator dye Fura-2 (Takahashi et al. 1999) and the Ca^{2+}-dye chelate. In brief: after 12 hours under serum-free culture conditions, cells were trypsinized and

suspended in loading buffer (120 mM NaCl, 5 mM KCl, 2 mM $MgCl_2 \cdot 6\ H_2O$, 1.5 mM $CaCl_2 \cdot 2\ H_2O$, 25 mM HEPES, 10 mM Glucose, pH 7.4) containing 1 % BSA at a concentration of 10^6 cells/ml, and loaded with 1.0 µM of Fura-2. The cells were immediately used for the assay after a postincubation step (30 minutes). After addition of 20 ng/ml of rhPDGF-BB fluorescence ratio (R, 340/380 nm excitation) was measured at 510 nm with a Perkin-Elmer LS 50 B fluorimeter (Rodgau-Jügesheim, Germany). During the assay the dye-loaded cells were maintained at 25 °C. The fluorescence values were converted into $[Ca^{2+}]_i$ concentrations using the Grynkiewicz equation (Grynkiewicz et al. 1985; Takahashi et al. 1999).

4.3.8 Chemosensitivity assay

The assays were performed as described previously (Bernhardt et al. 1992). In brief: tumor cell suspensions (100 µl/well) were seeded into 96-well flat bottomed microtitration plates (Greiner, Frickenhausen, Germany) at a density of ca. 15 cells/microscopic field (magnification 320x). After 2-3 days the culture medium was removed by suction and replaced by fresh culture medium (200 µl/well) containing varying drug concentrations or vehicle. Drugs were added as 1000-fold concentrated feed solutions. On every plate 16 wells served as controls and 16 wells were used per drug concentration. After various times of incubation the cells were fixed with glutardialdehyde (Merck, Darmstadt, Germany) and stored in a refrigerator. At the end of the experiment all plates were stained with crystal violet (Serva, Heidelberg, Germany) simultaneously. Absorbance was measured at 578 nm using a Biotek 309 Autoreader (Tecnomara, Fernwald, Germany).

4.3.9 Incubation of the cells with exogenous PDGF-BB

Incubation of the cells with PDGF was performed by analogy with the chemosensitivity assays. Cells were seeded in medium supplemented with FCS. Instead of drug 3 concentrations (0.1, 1.0, and 10 ng/ml) of recombinant human PDGF-BB (BIOCHROM AG) were used in different serum-free media (EMEM, DMEM, HAMs F12, and MCDB 105 (Sigma, Munich, Germany). Growth curves were quantified by the crystal violet method.

4.3.10 MTT assay

(Gupta et al. 2002; Sargent 2003) Human K-562 CML cells were seeded into 96 well plates, 100 µl of cell suspension per well. After 24 hours the medium was removed after centrifugation and 200 µl of medium, containing different concentrations of imatinib (0.1, 1.0, 2.5, 5.0, and 10 µM), were added. After varying times of incubation the medium was removed, 100 µl of a MTT (Sigma, Munich, Germany) solution (5 mg/ml) in PBS were added, and the cells were left in the incubator for 2.5 hours. The microplates were centrifuged and the supernatant was removed. The formed formazan was dissolved with 100 µl of DMSO per well, and the absorbance was measured at 540 nm using a Biotek EL 309 plate reader.

4.3.11 Flow cytometric calcein-AM efflux assay (pgp/ABCB1 assay)

The assay was performed with minor modifications according to the cited literature (Homolya et al. 1993; Hollo et al. 1994; Homolya et al. 1996). Calcein-AM was obtained from Molecular Probes (Molecular Probes, Eugene, Oregon, USA). Calcein-AM was stored as a aliquoted 1 mM stock solution in DMSO (Merck, Darmstadt, Germany) at -20 °C. The loading buffer consisted of 120 mM NaCl, 5 mM KCl, 2 mM $MgCl_2 \cdot 6H_2O$, 1.5 mM $CaCl_2 \cdot 2H_2O$, 25 mM HEPES and 10 mM glucose, and was adjusted to pH 7.4. The loading suspension contained loading buffer supplemented with 20 mg/ml of BSA (Serva, Heidelberg, Germany) and 5 µl/ml of Pluronic F127 (20 % in DMSO, Molecular Probes, Eugene, Oregon, USA). KBv1 cells were trypsinized 3-4 days after the last passaging and washed with PBS at 25 °C. To 0.75 ml cell suspension containing $1 \cdot 10^6$ cells in loading buffer 0.25 ml loading suspension was added. The samples were mixed with different concentrations of imatinib and vortexed. After 15 minutes calcein-AM solution (1 mM in DMSO) was added to achieve a concentration of 1 µM. After an incubation for 10 minutes at 37 °C/5 % CO_2 and centrifugation for 7 minutes at 4 °C at 1100 rpm the supernatant was discarded. The cell pellet was rinsed once with ice cold PBS and resuspended in 0.5 ml of loading buffer per $1 \cdot 10^6$ cells. The calcein fluorescence was measured by a FACSCalibur™ (Becton Dickinson, Heidelberg, Germany) flow cytometer using the FL1 detection channel. Each measurement included data acquisition of 30,000 events, gated from a FSC/SSC dotplot. The following photomultiplier settings were used: E^{-1} for FSC, 270 for SSC and 300 for FL1. Data were analyzed by the WinMDI 2.8 FACS analysis software.

4.3.12 Flow cytometric mitoxantrone efflux assay (bcrp/ABCG2 assay)

The assay was performed according to the cited literature (Spritz et al. 1994; de Bruin et al. 1999; Maliepaard et al. 1999; Robey et al. 2001) with modified assay conditions. ABCG2-expressing MCF-7/Topo cells were passaged 3 or 4 days before the assay was carried out, trypsinized, washed with PBS at 25 °C, and adjusted to number of 1of $1 \cdot 10^6$ cells per ml with culture medium. Mitoxantrone was added to the cell suspensions to achieve a concentration of 20 µM (6.67 µl of 3 mM stock solution in 70 % ethanol). Different concentrations of imatinib were added after a short vortexing step. Again the cell suspensions were vortexed followed by 30 minutes of incubation at 37 °C/5 % CO_2, which is a sufficient incubation period for mitoxantrone uptake into the cells, according to the literature. The cells were washed with ice-cold PBS and resuspended in culture medium. After an incubation period of 1 hour at 37 °C/5 % CO_2 an equilibrium of mitoxantrone had developed between the cytoplasm of the cells and the surrounding medium. After the medium was removed by centrifugation, the cell pellet was rinsed once with ice-cold PBS, and resuspended in 0.5 ml of PBS ($2 \cdot 10^6$ cells/ml). Data acquisition for all samples was performed using a FACSCalibur™ (Becton Dickinson, Heidelberg, Germany), collecting data of 20,000 events, gated from a FSC/SSC dotplot. The following photomultiplier settings were used: E^{-1} for FSC, 200 for SSC, 450 for FL1 and 700 for FL4. FL4 histograms were analyzed by the WinMDI FACS 2.8 data analysis software.

4.4 Results

4.4.1 Detection of PDGFR and PDGF mRNAs by RT-PCR

To investigate, if the requirements for an autocrine PDGF/PDGFR loop are fulfilled in human glioblastoma cells, the total RNAs of U-87 MG, U-118 MG, and U-373 MG cells were isolated, and the PDGF/PDGFR mRNAs were detected by RT-PCR. All of the three human glioblastoma cell lines showed positive results for different PDGFR subtypes (Fig. 4-5 and 4-6). The PCR products of all PDGF variants were detected in U-87 MG and U-373 MG cells, whereas PDGF-D mRNA was not detected in U-118 MG glioblastoma cells (Fig. 4-7). All PDGF and PDGFR subtypes were additionally detected in non-malignant human CCD-11Lu fibroblasts. The RT-PCR results are summarized in Table 4-7.

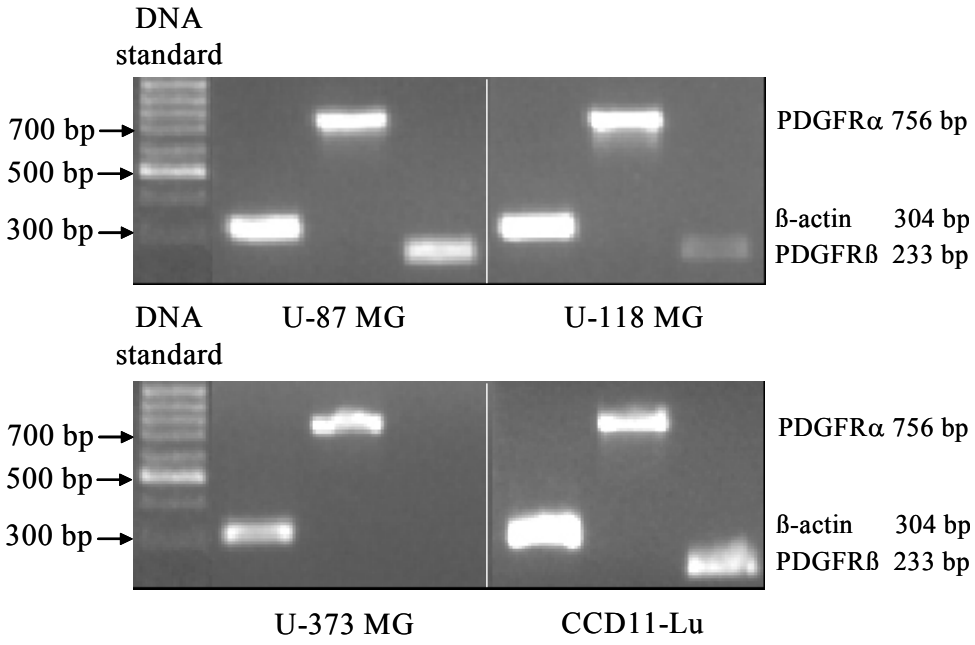

Figure 4-5: Detection of the PCR products of PDGFR mRNAs by agarose gel electrophoresis. Except U-373 MG, which shows only one band (756 bp) for the PDGFRα mRNA, the other glioblastoma cell variants U-87 MG and U-118 MG as well as the CCD-11Lu fibroblasts show bands for both PDGFR mRNA subtypes (PDGFRα 756 bp, PDGFRβ 233 bp). PCR products of β-actin (304 bp) were used as control. CCD-11Lu fibroblast cDNA was used as a positive control for the detection of PDGFR cDNA subtypes.

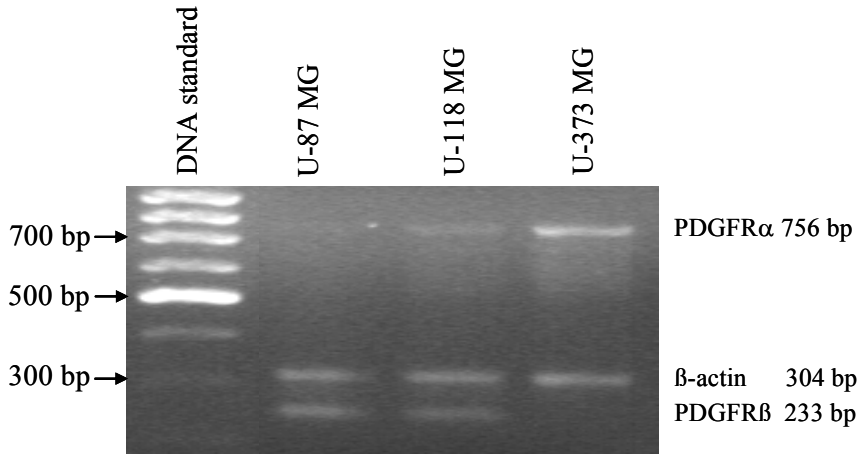

Figure 4-6: Detection of the competitively amplified PCR templates of PDGFR mRNAs by agarose gel electrophoresis. The U-373 MG cells show only one band indicative of PDGFRα mRNA (756 bp), whereas in U-118 MG cells two bands show the presence of mRNA of both PDGFR subtypes. On the contrary, only the one PCR product, indicating the PDGFRβ mRNA (233 bp), was detected in U-87 MG cells. PCR products of β-actin (304 bp) were used as control.

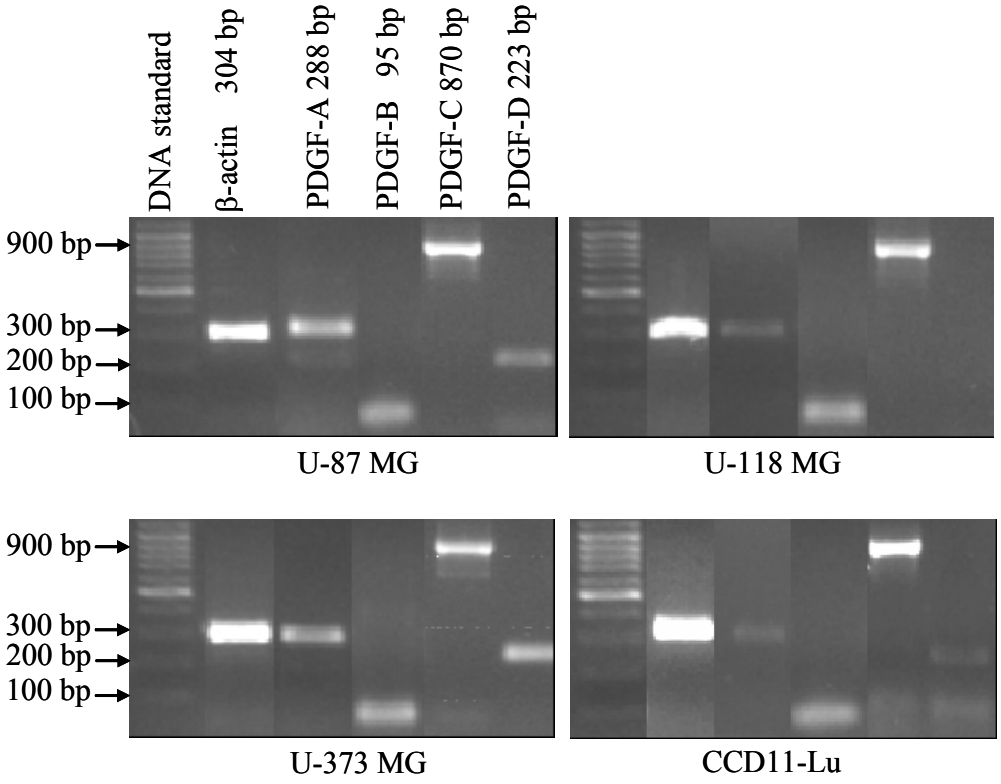

Figure 4-7: Agarose gel electrophoresis of PCR products of PDGF mRNA subtypes. U-87 MG, U-373 MG, and CCD-11Lu show bands for all of the four subtypes PDGF-A, -B, -C and –D whereas U-118 MG lacks the band for PDGF-D. Primers for β-actin (product band at 304 bp) were used as control.

Table 4-7: Relative amounts of PDGF and PDGFR mRNA detected by RT-PCR. The RT-PCR results indicate a differential expression of PDGFR subtypes in human glioblastoma cells. Each of the three cell lines shows high levels of at least one PDGFR subtype (++) and all cells are positive for every PDGF subtype, only U-118 lacks mRNA for PDGF-D (-).

PCR product	U-87 MG	U-118 MG	U-373 MG	CCD11-Lu
PDGFRα	+ *	++ †	++	+
PDGFRβ	++	+	- ‡	+
PDGF-A	++	+	+	+
PDGF-B	+	+	+	+
PDGF-C	++	++	++	++
PDGF-D	+	-	+	+

* positive for mRNA,† positive, broad band, ‡ negative, i.e. no PCR product.

4.4.2 Expression of PDGFR protein

The detection of mRNA for PDGFR subtypes in human glioblastoma cells suggests a differential expression of PDGFR protein. This hypothesis was investigated by fluorescence microscopy after immunostaining of the different PDGFR proteins. The results of the immunostaining (Fig. 4-8) confirmed the RT-PCR data by demonstrating the PDGFR phenotype in the human glioblastoma cells as well as in the fibroblast cells. The flow cytometric data (Fig. 4-9 and 4-10) is in agreement with the microscopic results. U-87 MG cells mainly express PDGFRβ, the expression of the PDGFRα subtype is weak. U-118 MG cells bear both PDGFR subtypes at similar levels, whereas mainly the PDGFRα subtype was detected in the U-373 MG cells.

In summary, all of the human glioblastoma cell lines express at least one subtype of the PDGFR protein. In view of the positive RT-PCR results for PDGF-A and PDGF-B, which were detected in all three glioblastoma cell lines, a PDGFR/PDGF autocrine loop is conceivable.

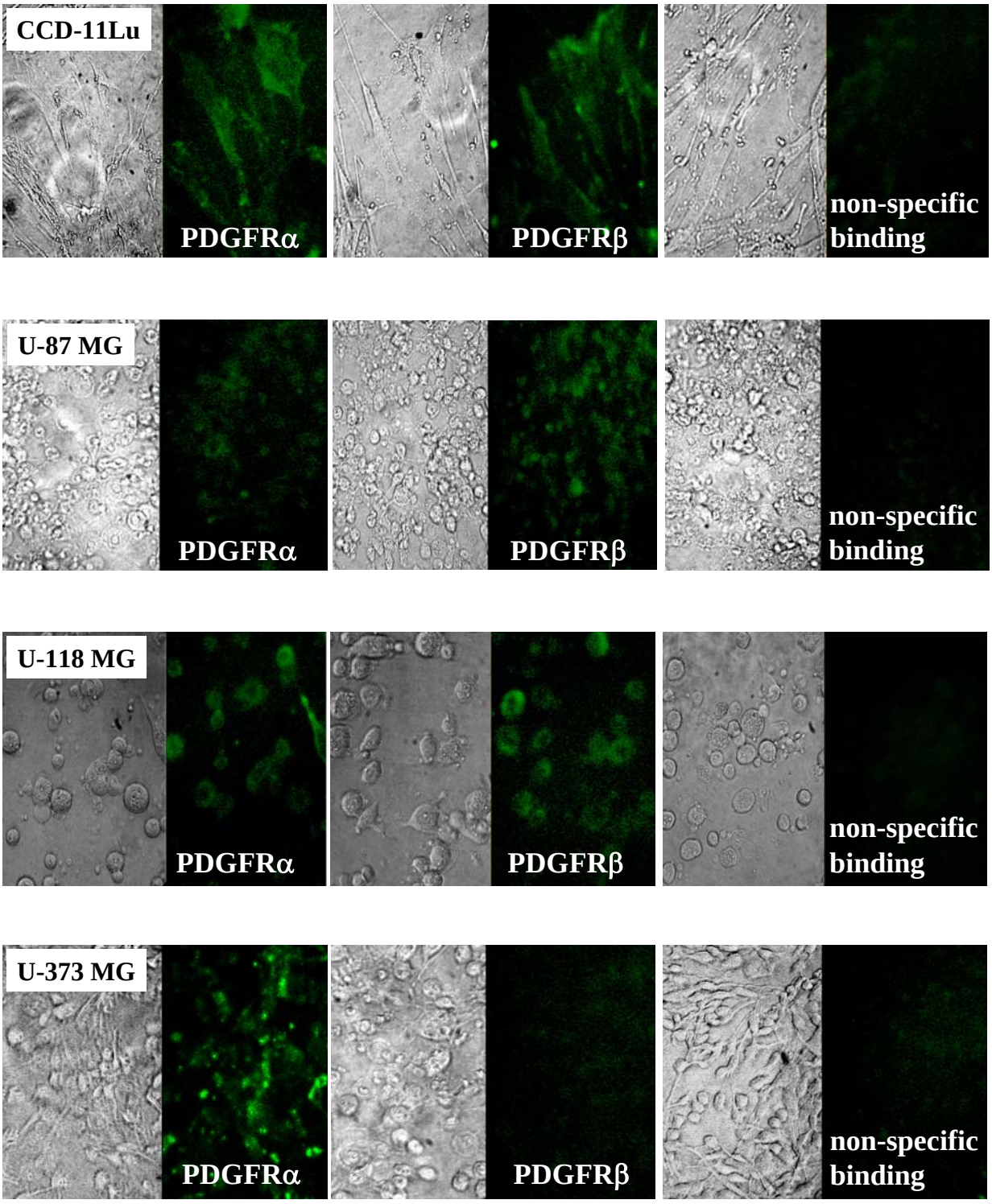

Figure 4-8: Immunochemical determination of PDGFR expression. Micrographs of human CCD-11Lu fibroblasts, human U-87 MG, U-118 MG, and U-373 MG glioblastoma cells, immunostained with anti-human PDGFR antibodies; phase contrast image (left) and fluorescence image (right). Control: non-specific binding of the FITC-labeled secondary antibody.

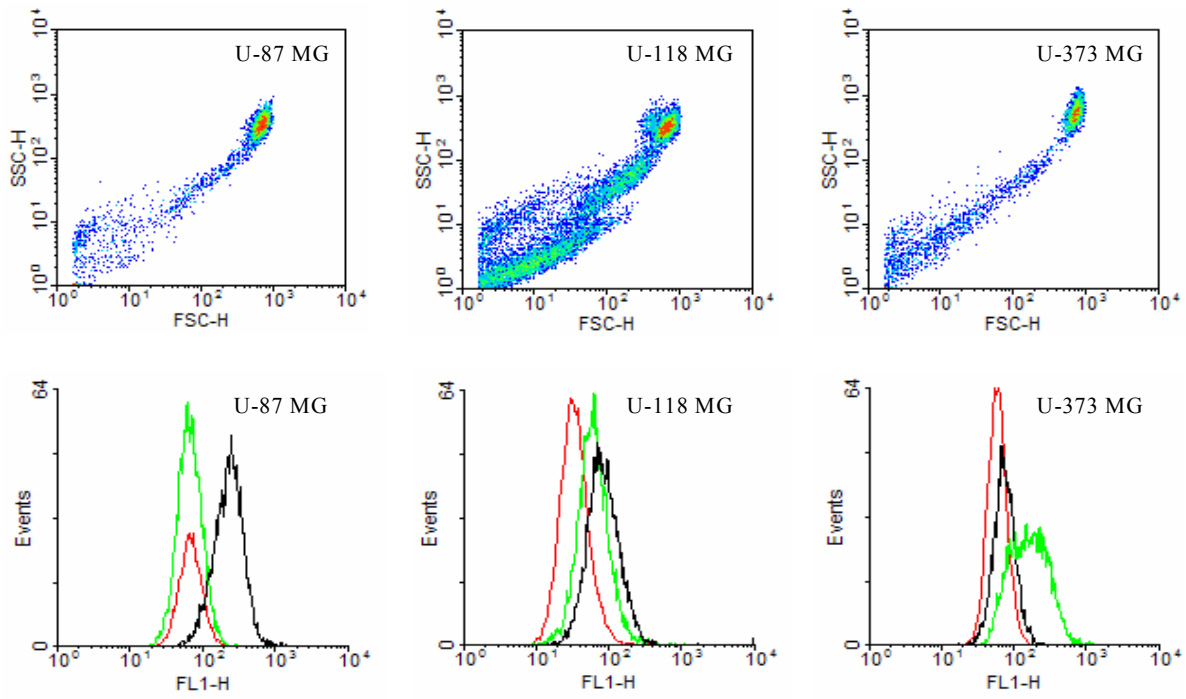

Figure 4-9: Flow cytometric determination of PDGFR phenotype: density dotplot and corresponding overlay histograms of the PDGFR staining data of human glioblastoma cell variants. The density plots show all events occurred during the measurement, including cell debris (upper row). Intact cells were gated and used for histogram analysis (lower row). The non-specific binding of the FITC-labeled secondary antibody is shown in red, binding of anti PDGFRα in green and binding of anti PDGFRβ in black.

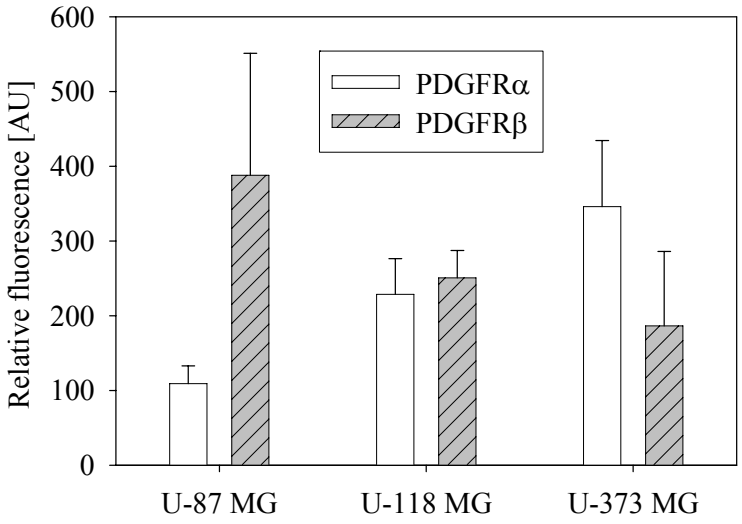

Figure 4-10: Relative fluorescence of human glioblastoma cells after immunostaining of PDGFRs compared to non-specific binding of the FITC-conjugated secondary antibody (100 AU). The comparison of the geometric means shows various degrees of PDGFR subtype expression by the different glioblastoma cell variants.

4.4.3 Ratiometric determination of intracellular Ca^{2+} concentration after activation of receptor tyrosine kinases EGFR and PDGFR

4.4.3.1 Fura-2 assay

The ratiometric Ca^{2+} indicator dye Fura-2 is a commonly used compound for the fluorimetric determination of changes in the intracellular Ca^{2+} concentration. The cells of interest are incubated and thereby loaded with the lipophilic Fura-2 acetoxymethylester (Fura2/AM, Fig. 4-11), which is capable of permeating through the plasma membrane into the cytosol. After cleavage by cytoplasmic esterases the now highly hydrophilic and membrane impermeable compound accumulates inside the cells.

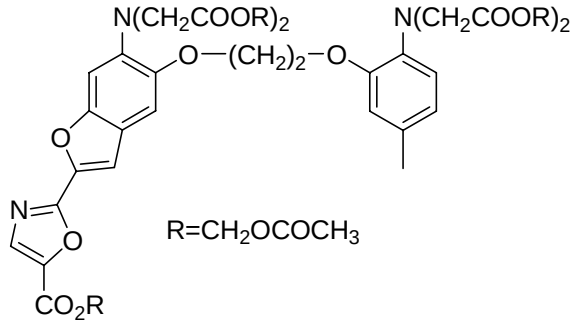

Figure 4-11: Chemical structure of the calcium indicator dye Fura-2/AM.

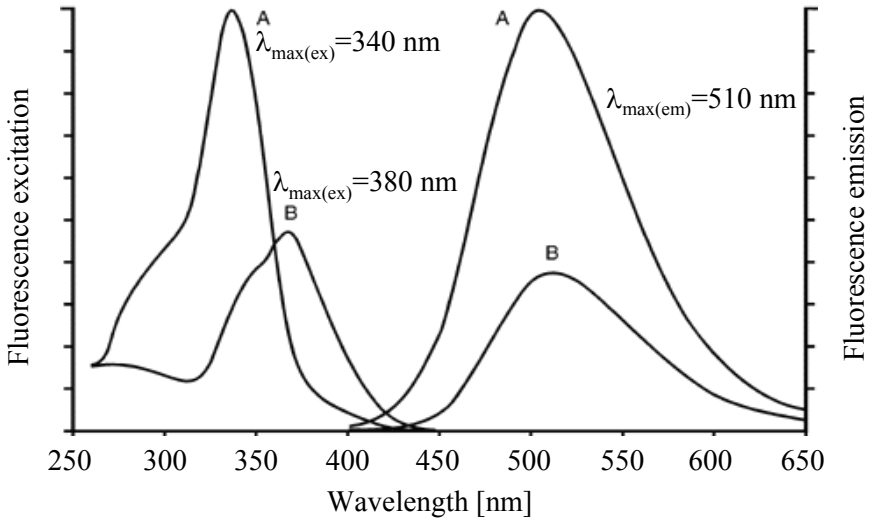

Figure 4-12: Fluorescence excitation and emission spectra of the Fura-2/Ca^{2+} complex (A) and the free Fura-2 (B).

After enzymatic ester hydrolysis in the cytosol an equilibrium is formed between free and Ca^{2+}-bound Fura-2, whereby both Fura-2 forms show different excitation, but similar fluorescence emission spectra (Fig. 4-12). The fluorimetric readout of a given Ca^{2+} concentration is the ratio R of the fluorescence emission F at 510 nm of the Ca^{2+}-bound form (λ_{ex} = 340 nm, $F_{340\,nm}$) and the free form of Fura-2 (λ_{ex} = 380 nm, $F_{380\,nm}$):

$$(1) \qquad R = \frac{F_{340nm}}{F_{380nm}}$$

Changes in the intracellular Ca^{2+} concentration shift the equilibrium either towards the free or the Ca^{2+}-bound form of Fura-2, and thus the measured fluorescence ratio is accordingly decreased or increased. The actual intracellular Ca^{2+} concentration $[Ca^{2+}]_i$ can be calculated from the fluorescence ratio R using the equation after Grynkiewicz (equation 2) (Grynkiewicz et al. 1985):

$$(2) \qquad [Ca^{2+}]_i = K_d * \frac{(R - R_{\min})}{(R_{\max} - R)} * S_{fb}$$

The Grynkiewicz equation also considers the dissociation constant K_d of the Fura-2/Ca^{2+} complex and the relative fluorescence contribution S_{fb} of Ca^{2+}-free and Ca^{2+}-bound Fura-2 at an excitation wavelength of 380 nm. R_{max} constitutes the fluorescence ratio of all the Fura-2 from the loaded cells, quatitatively bound to Ca^{2+}. Therefore the cells are permeabilized with the steroidal saponin digitonin, so the dye leaks into the surrounding sample buffer and is completely bound to Ca^{2+}. After measurement of R_{max} the potent Ca^{2+} complexing agent EGTA is added to the sample, all Fura-2 is set free from its Ca^{2+} complex, and R_{min}, representing the fluorescence ratio of quantitatively free Fura-2, can be determined.

4.4.3.2 Mobilization of intracellular Ca^{2+} upon stimulation of epidermal growth factor (EGF) receptors in A431 cells

An increase in intracellular Ca^{2+} concentration upon activation of receptor tyrosine kinases has been reported in literature (Diliberto et al. 1992). A prerequisite for the intracellular Ca^{2+} mobilization is the coupling of a PLCγ pathway to the initial activation of the receptor tyrosine kinase of interest (Berridge et al. 1984; Carpenter and Ji 1999). In this study human

A431 epidermoid carcinoma cells (Giard et al. 1973) and Swiss 3T3 mouse fibroblast cells were used as models for transferring the Fura-2 method to tyrosine kinase receptors and to confirm its functionality for the determination of RTK activity. After loading of the cells with the Ca^{2+} indicator dye, according to the materials and methods section, various concentrations of recombinant human epidermal growth factor (rhEGF) were added to the samples. The Ca^{2+} response was monitored over a time period of 300 seconds The acquired calcium signals are shown in Fig. 4-13.

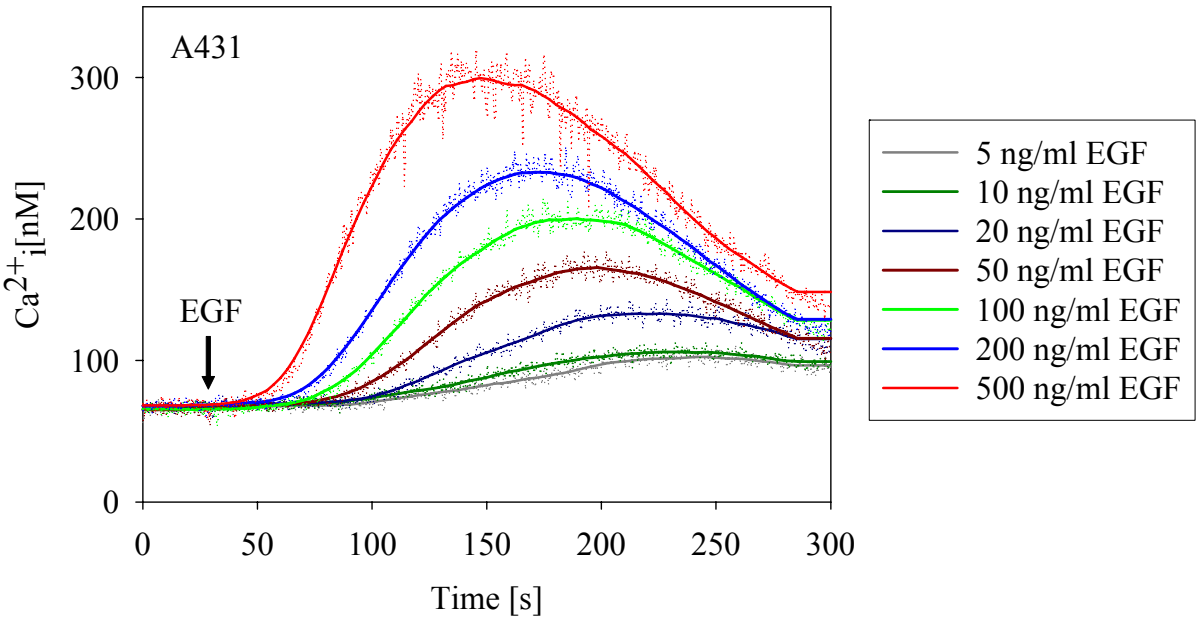

Figure 4-13: Mobilization of intracellular Ca^{2+} in human A431 cells after stimulation with various concentrations of rhEGF. A concentration-dependent increase in the maximal $[Ca^{2+}]_i$ can be observed as well as a delay of the Ca^{2+} response towards lower rhEGF concentrations. Compared to the commonly observed immediate response of G-protein coupled receptors a few seconds after addition of an agonist, the beginning of the Ca^{2+} mobilization in A431 cells is delayed by at least 30 seconds at the highest used rhEGF concentration.

4.4.3.3 Mobilization of intracellular Ca^{2+} upon stimulation of PDGF receptors in Swiss 3T3 cells

Since the PLCγ pathway is known to be connected to the PDGF receptor autophosphorylation (Ronnstrand et al. 1992; Larose et al. 1993; Valius et al. 1993), Swiss 3T3 mouse embryo fibroblast cells were used as a model for monitoring the PDGF receptor-mediated Ca^{2+} release. In Swiss 3T3 mouse embryo fibroblasts a strong $[Ca^{2+}]_i$ mobilization was observed upon PDGF-BB stimulation (Fig. 4-14), which was suppressed by imatinib in a concentration-dependent manner (Fig. 4-15, 4-16). Imatinib was added 5 seconds prior to the PDGF-BB

stimulus. The experiment was performed in triplicate, and an IC_{50} value of 4.2 µM was calculated for imatinib.

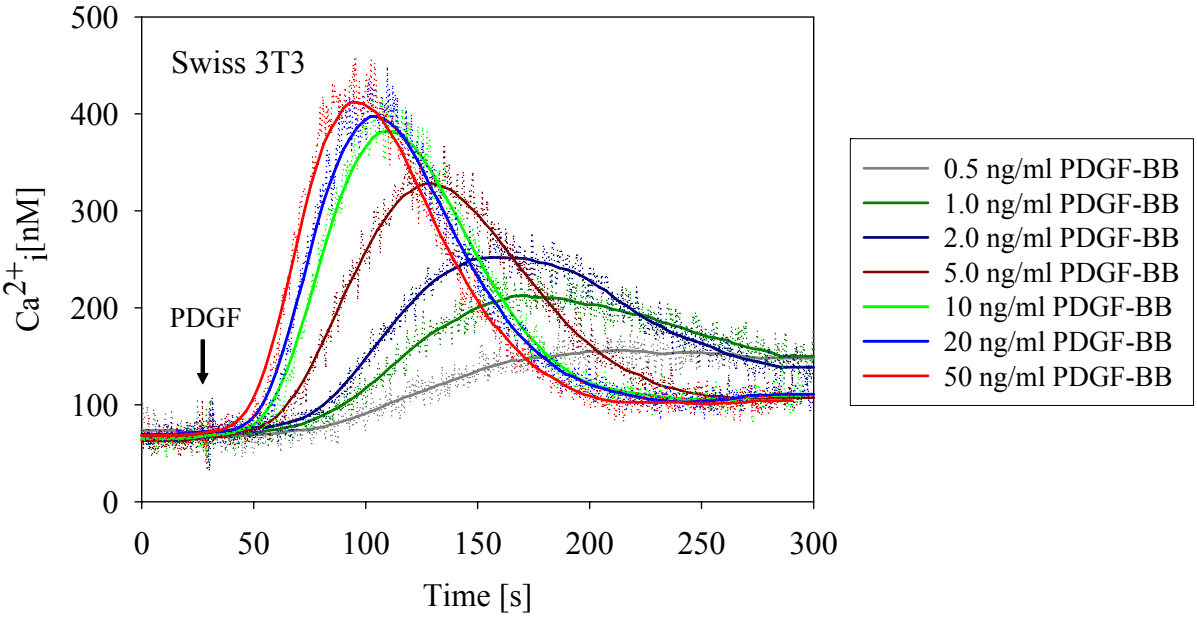

Figure 4-14: Mobilization of intracellular Ca^{2+} in Swiss 3T3 embryo cells after stimulation with various concentrations of rhPDGF-BB. As shown before for the stimulation of the EGF receptors in A431 cells, PDGF triggered a concentration-dependent increase in the maximum $[Ca^{2+}]_i$ in the mouse fibroblast cells. Also a delay of the Ca^{2+} response towards lower rhPDGF-BB concentrations was observed.

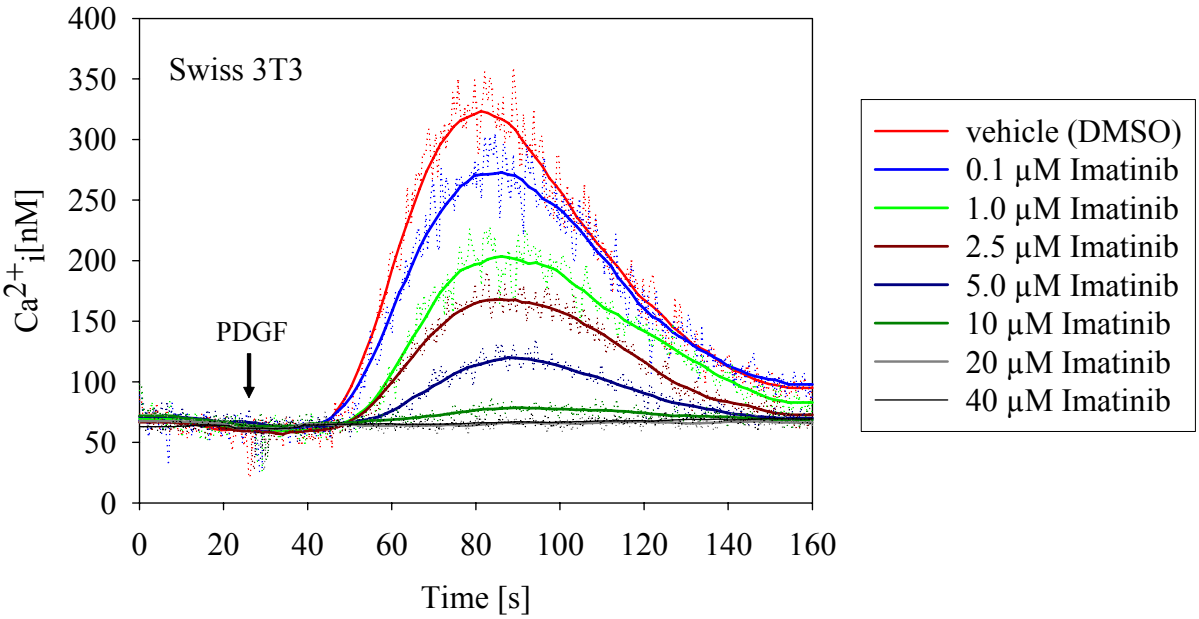

Figure 4-15: Effect of imatinib on the mobilization of intracellular Ca^{2+} upon stimulation of Swiss 3T3 mouse fibroblasts with 20 ng/ml of rhPDGF-BB. Calcium transients in the absence and presence of different imatinib concentrations.

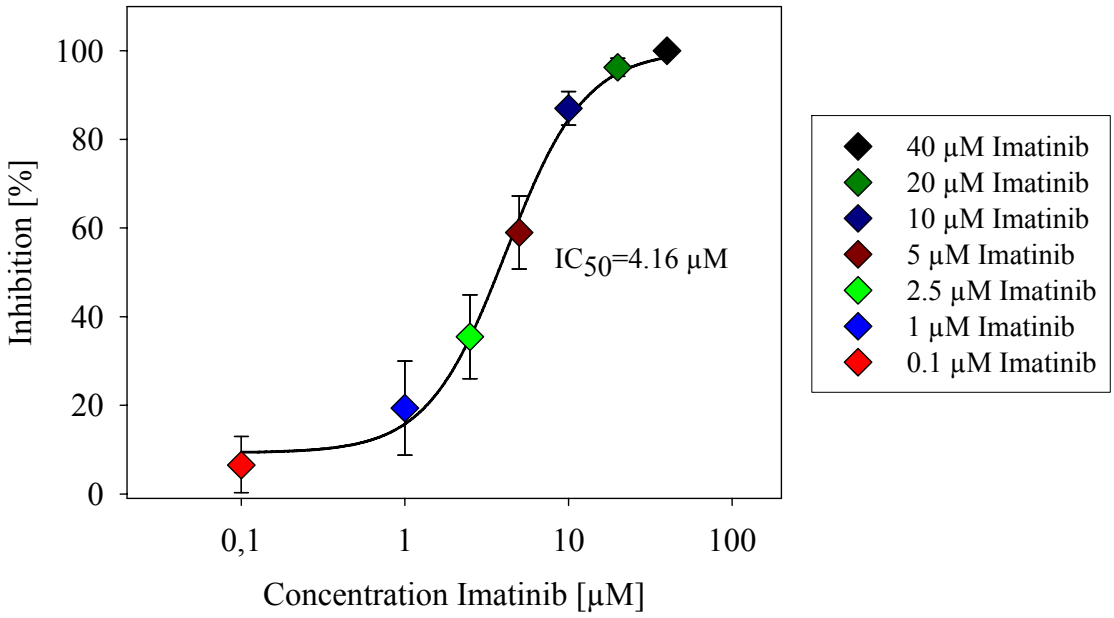

Figure 4-16: Concentration-dependent inhibition of PDGFR-mediated Ca^{2+} mobilization in Swiss 3T3 mouse fibroblasts by imatinib.

4.4.3.4 Effect of PDGF-BB on the mobilization of intracellular Ca^{2+} in human glioblastoma cells

Due to the constitutive expression of histamine H_1 receptors by U-87 MG and U-373 MG cells, histamine was used at a concentration of 100 µM to trigger a $[Ca^{2+}]_i$ signal as a control. FCS was used as a positive control in U-118 MG cells, which lack H_1 receptors.

Upon stimulation with 20 ng/ml of rhPDGF-BB, U-87 MG cells showed slow and moderate $[Ca^{2+}]_i$ mobilization, compared to the control (Fig. 4-17), whereas in U-118 MG cells only a marginal $[Ca^{2+}]_i$ increase was observed. In U-373 MG cells no mobilization of $[Ca^{2+}]_i$ was detected. Considering the flow cytometric data shown above, the U-87 MG glioblastoma variant with a relatively high expression of the PDGFRβ protein showed the highest sensitivity with respect to $[Ca^{2+}]_i$ mobilization upon PDGF-BB stimulation. In U-118 MG cells, expressing almost equal amounts of the PDGFRα and PDGFRβ subtypes, only a slight sensitivity was detected, whereas U-373 MG cells, which mainly express the PDGFRα subtype, did not respond to the PDGF-BB stimulus. These results confirm the previously reported PDGFRβ-associated $[Ca^{2+}]_i$ mobilization upon PDGF stimulation (Diliberto et al. 1992) and the functionality of the PDGF receptors in the U-87 MG and U-118 MG glioblastoma variants.

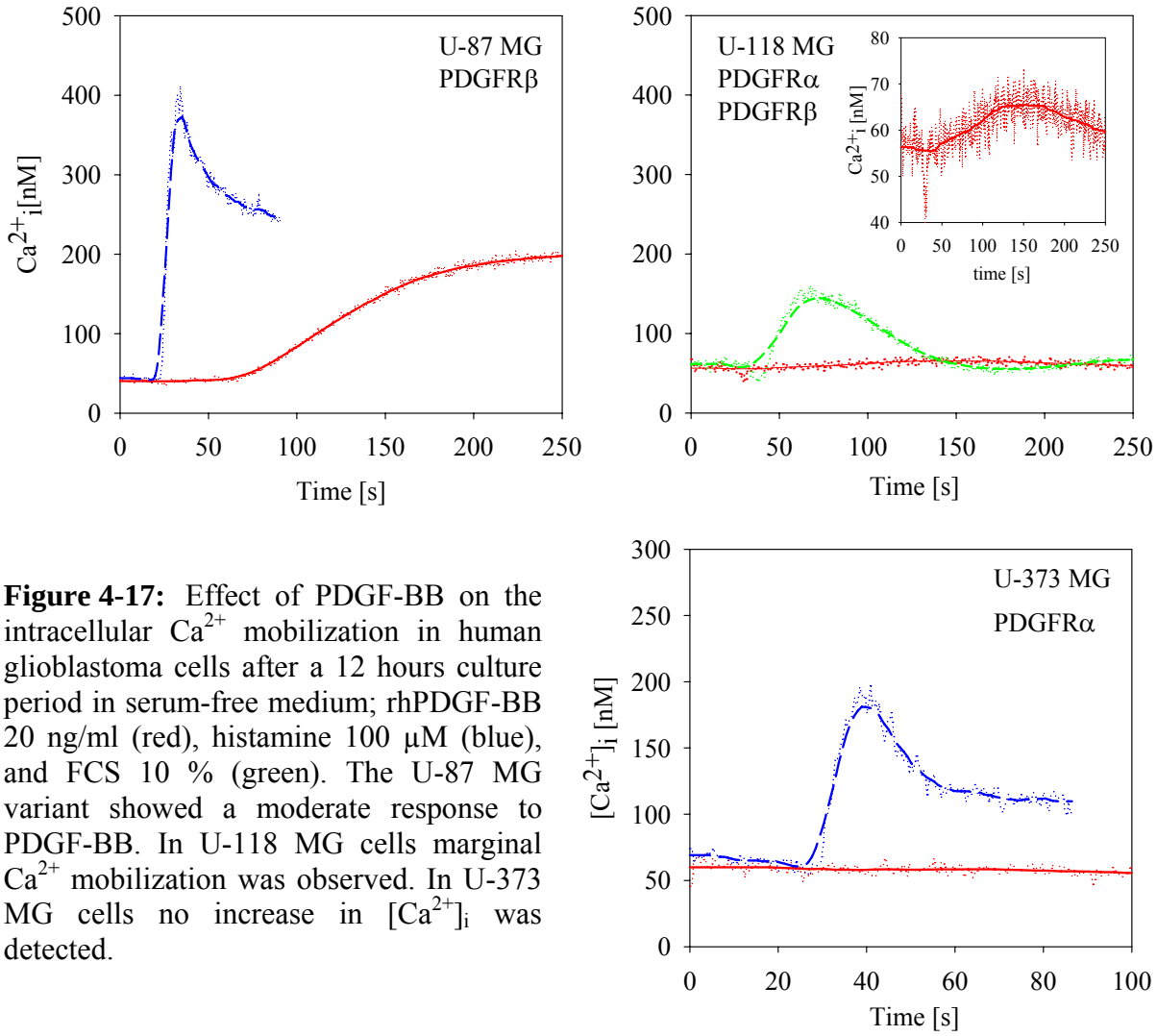

Figure 4-17: Effect of PDGF-BB on the intracellular Ca^{2+} mobilization in human glioblastoma cells after a 12 hours culture period in serum-free medium; rhPDGF-BB 20 ng/ml (red), histamine 100 µM (blue), and FCS 10 % (green). The U-87 MG variant showed a moderate response to PDGF-BB. In U-118 MG cells marginal Ca^{2+} mobilization was observed. In U-373 MG cells no increase in $[Ca^{2+}]_i$ was detected.

4.4.4 Effect of selective PDGFR tyrosine kinase inhibitors on the proliferation of human glioblastoma cells

To investigate, whether the proliferation of human glioblastoma cells can be mainly ascribed to PDGFR-mediated processes, the cells were incubated with the selective PDGFR tyrosine kinase inhibitor imatinib. Doxorubicin was used as positive control for the inhibition of cell growth. Imatinib showed no inhibition of cell growth up to a concentration of 10 µM (Fig. 4-18). The assays were also performed with an extended incubation period of 264 hours with similar results (Fig. 4-19), which are opposite to a report in the literature (Kilic et al. 2000).

To investigate if the inhibition of PDGFR-mediated pathways does affect the proliferation of glioblastoma cells, U-87 MG and U-373 MG cells were additionally incubated with the selective PDGFR inhibitors tyrphostin AG-1296 (Kovalenko et al. 1994), leflunomide

(Eckhardt et al. 1999), and two indolylmethanone compounds, CP39 and CP53 (Bohmer et al. 2003). U-118 MG cells were incubated with all tyrosine inhibitors but leflunomide. For chemical structures of all used tyrosine kinase inhibitors see Fig. 4-4. The incubation of the human glioblastoma cells with AG-1296 (Fig. 4-20) and leflunomide (Fig. 4-21) up to a concentration of 10 µM also did not inhibit cell growth. Leflunomide showed a cytotoxic and cytostatic effect on U-373 MG and U-87 MG cells, respectively, at a concentration of 100 µM. Both of the bisindolylmethanone compounds CP39 and CP53 exhibited a cytotoxic effect on U-87 MG and on U-373 MG cells at a concentration of 10 µM and a cytostatic effect at 100 µM (Fig. 4-22, 4-24). U-118 MG showed chemosensitivity to both compounds at 1 µM (cytotoxic effect). At higher concentrations of 10 µM and 100 µM a cytostatic effect was observed (Fig. 4-23).

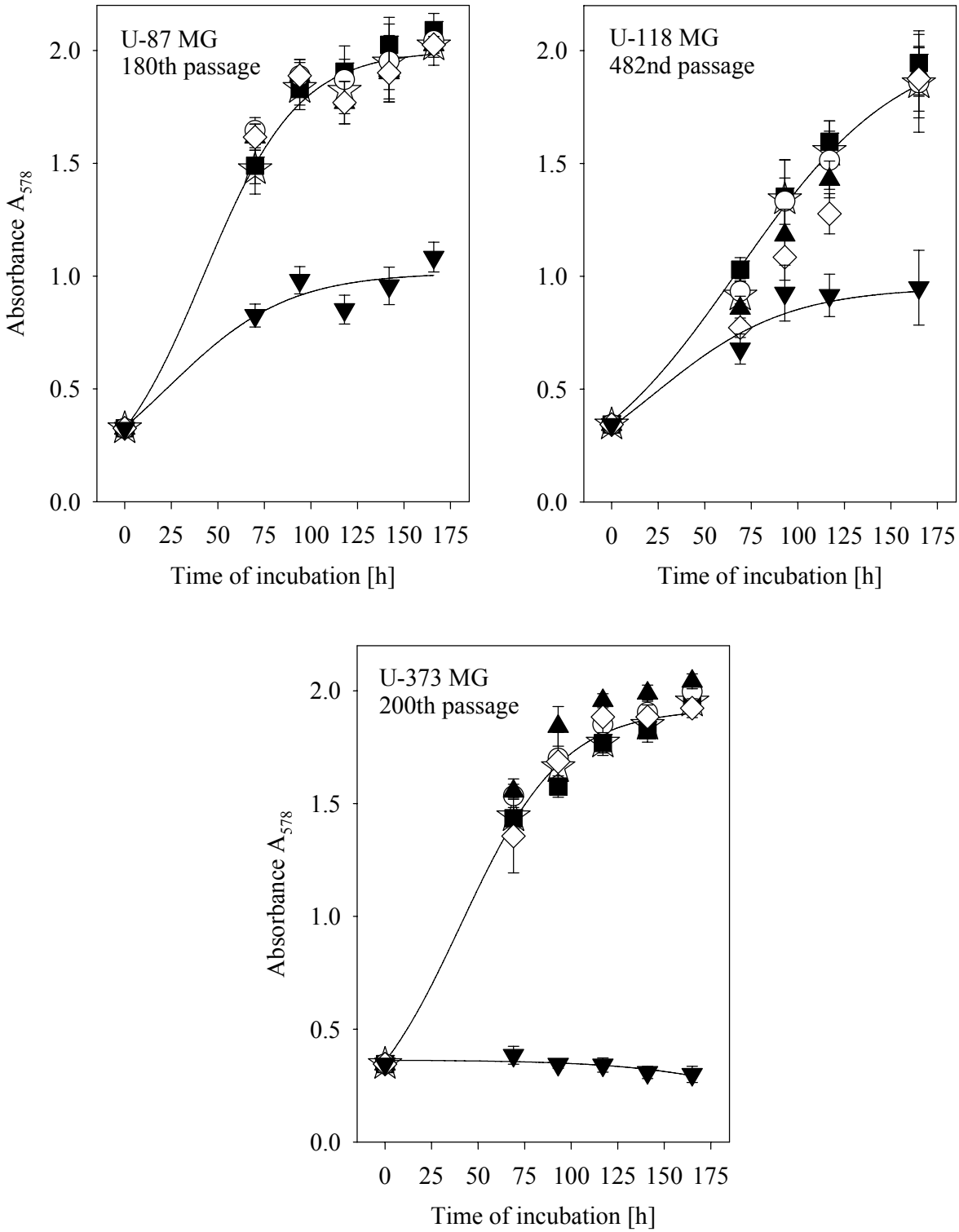

Figure 4-18: Effect of the tyrosine kinase inhibitor imatinib on the proliferation of human glioblastoma cells. Imatinib lacks inhibitory activity against the human U-87 MG, U-118 MG, and U-373 MG glioblastoma cells. After 160 hours no difference between incubation with imatinib and the vehicle control is observed. ☆ vehicle, imatinib concentration: ■ 0.1 µM, ○ 1 µM, ▲ 2.5 µM, and ◇ 10 µM; ▼ doxorubicin (50 nM).

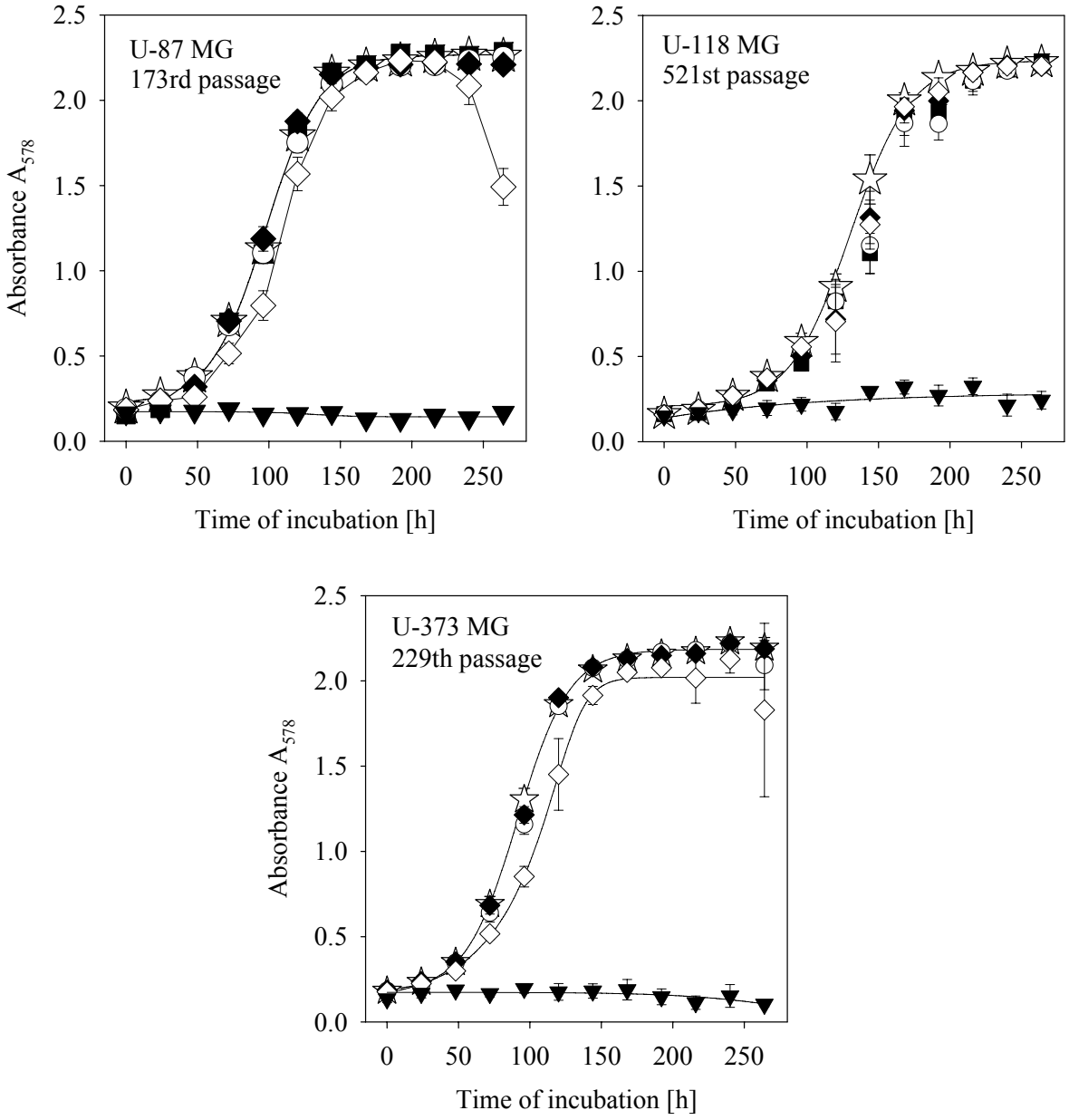

Figure 4-19: Incubation of human glioblastoma cells with imatinib over 264 hours. At a concentration of 10 µM, imatinib slightly affected cell proliferation of U-87 MG and U-373 MG in the exponential growth phase. Both cell variants recovered and reached absorbance values of the vehicle control. In U-87 MG cells the drug exhibited cytotoxic respectively cytocidal effects at the end of the incubation period (days 10 and 11). No inhibition of cell proliferation was observed in U-118 MG. ☆ vehicle, imatinib concentration: ○ 1 µM, ◆ 5 µM, and ◇ 10 µM; ▼ paclitaxel 8 nM.

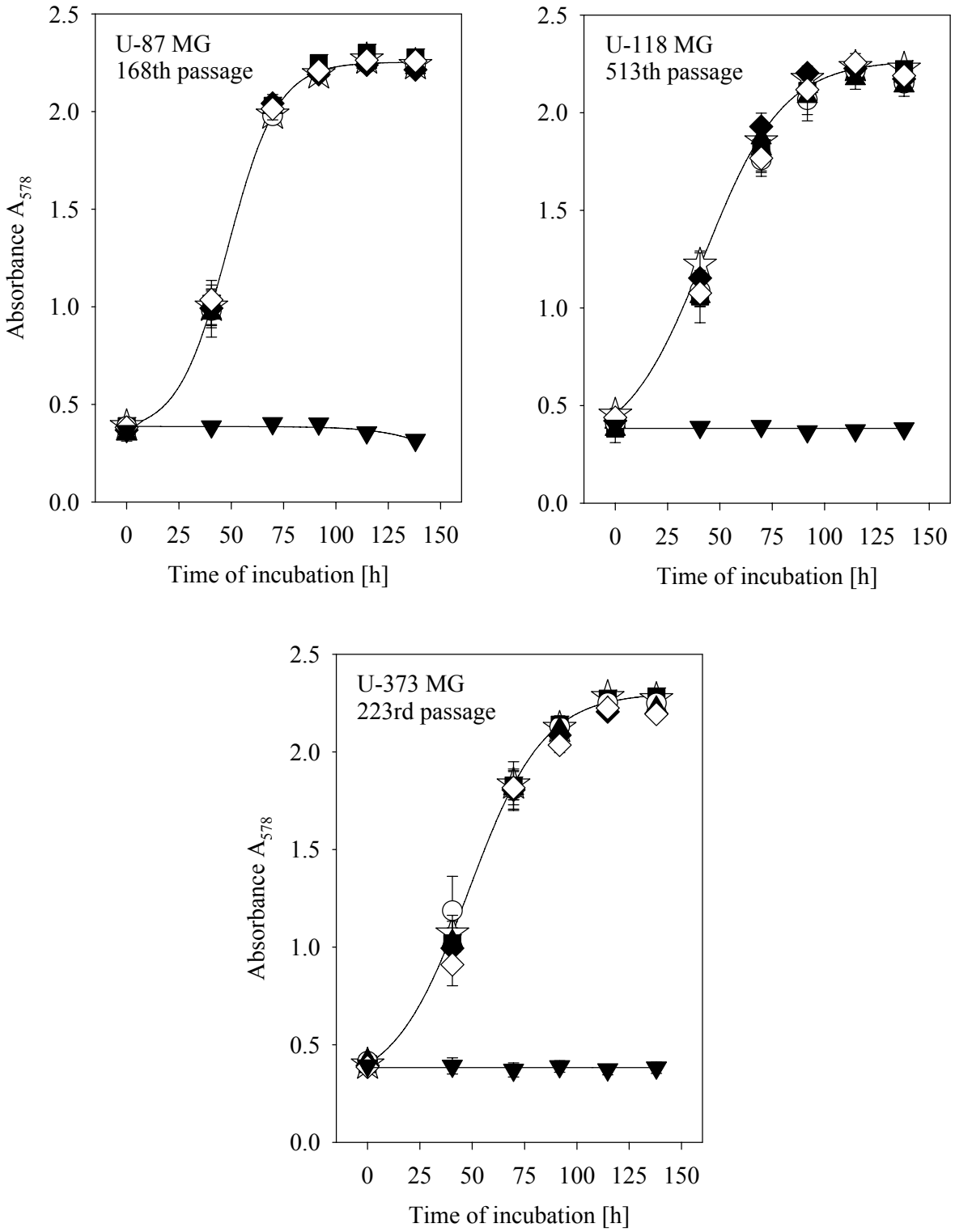

Figure 4-20: Incubation of human glioblastoma cells with tyrphostin (AG-1296). No inhibition of cell proliferation was observed in any of the three cell variants up to a concentration of 10 µM AG-1296. ☆ vehicle, AG-1296 concentration: ■ 0.1 µM, ○ 1 µM, ▲ 2.5 µM, ◆ 5 µM and ◇ 10 µM; ▼ paclitaxel 8 nM.

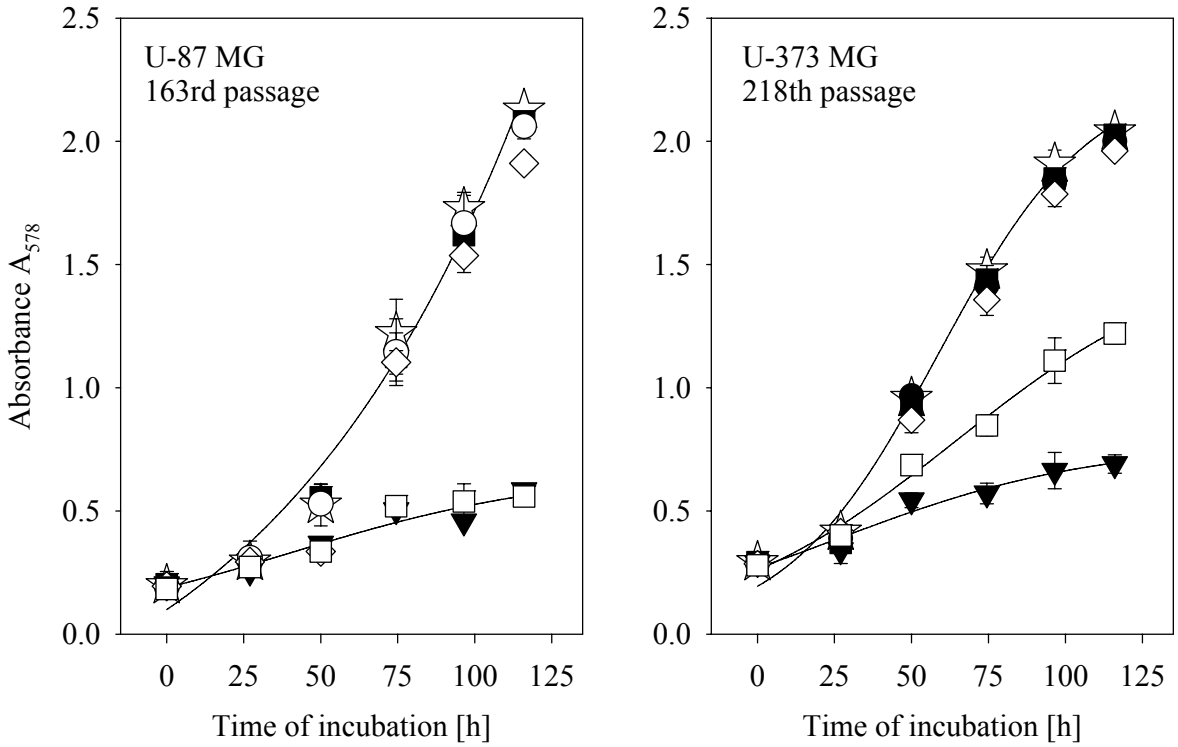

Figure 4-21: Effect of leflunomide on the proliferation of U-87 MG and U-373 MG glioblastoma cells. Incubation with leflunomide did not affect cell proliferation of U-373 MG cells, whereas in U-87 MG a very weak inhibition of cell growth was observed at a concentration of 10 µM. At a concentration of 100 µM leflunomide exhibited a cytostatic effect on U-87 MG and a cytotoxic effect on U-373 MG cells. ☆ vehicle, Leflunomide concentration: ■ 0.1 µM, ○ 1 µM, ◇ 10 µM, and □ 100 µM; ▼ paclitaxel 8 nM.

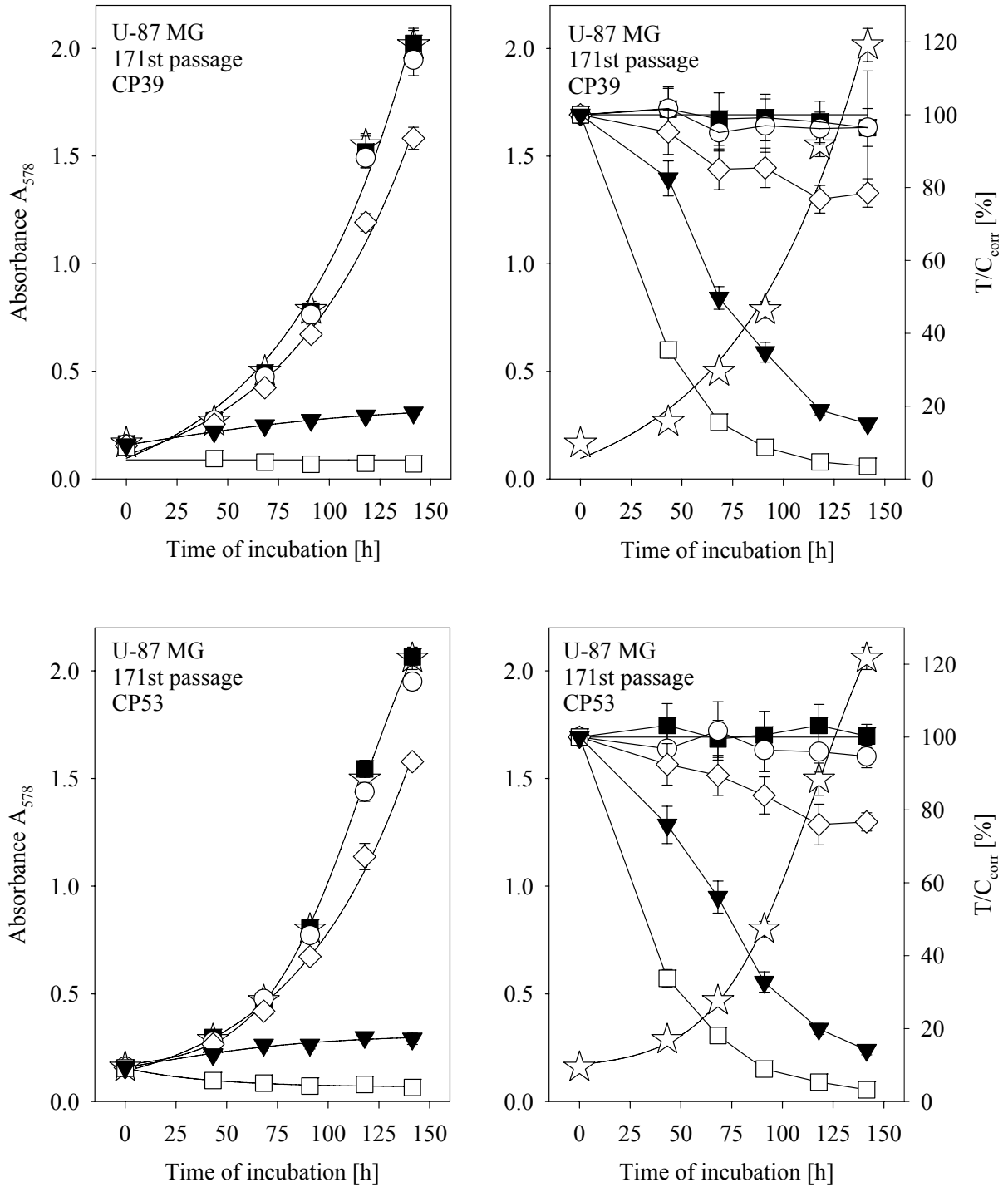

Figure 4-22: Effect of the bisindolylcompounds CP39 and CP53 (see also Fig. 4-4) on the proliferation of U-87 glioblastoma cells. Incubation did affect cell proliferation at concentrations of 10 µM and 100 µM respectively, showing a cytostatic effect on cell growth. ☆ vehicle, CP39/CP53 concentration: ■ 0.1 µM, ○ 1 µM, ◇ 10 µM, and □ 100 µM; ▼ paclitaxel 8 nM.

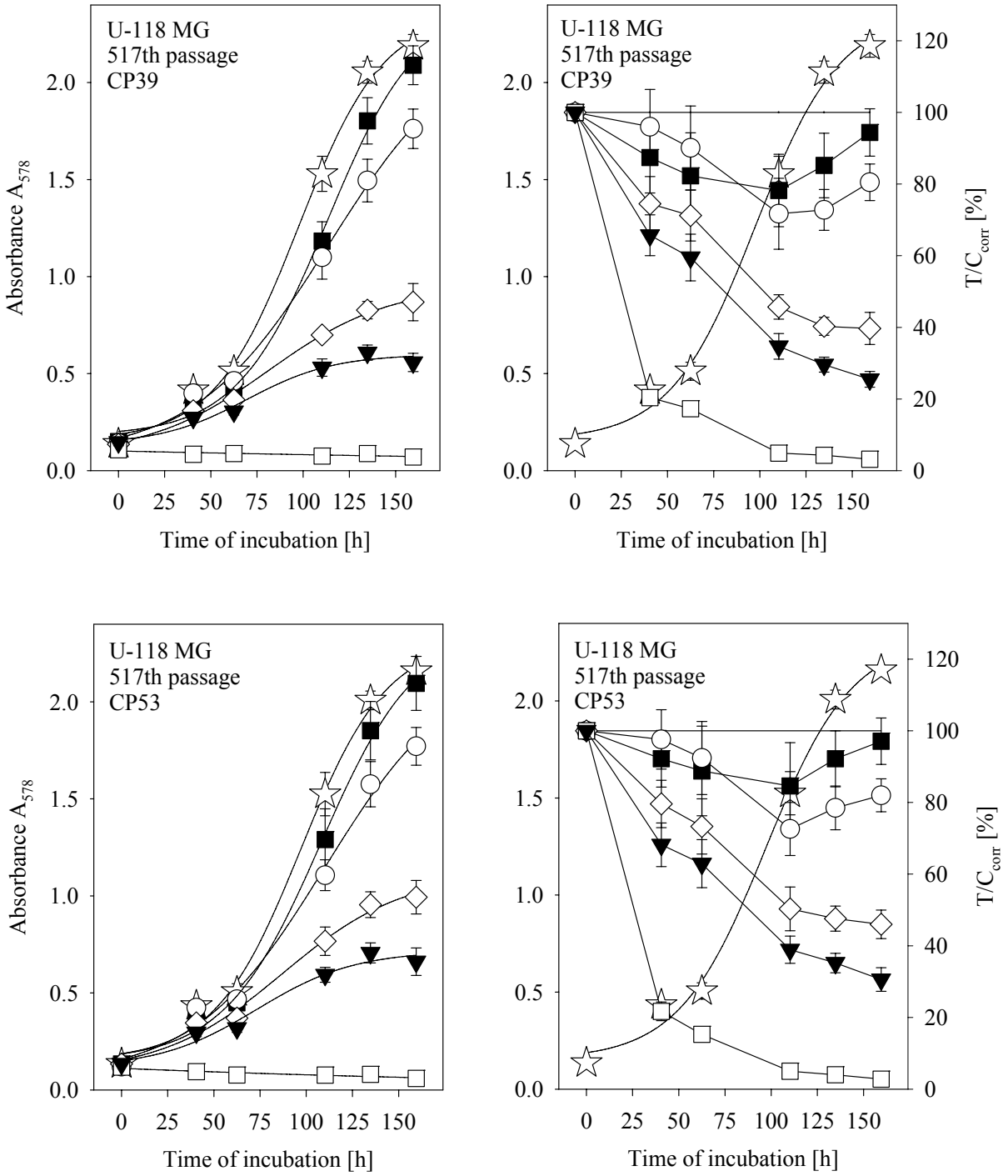

Figure 4-23: Incubation of U-118 MG glioblastoma cells with CP39 and CP53 (see also Fig. 4-4). At concentrations of 0.1 µM and 1.0 µM the cell proliferation was slightly inhibited by both compounds, but the cells started to recover after 120 hours of incubation time. A cytostatic effect was observed at 10 µM and 100 µM of CP39 and CP53 respectively. ☆ vehicle, CP39/CP53 concentration: ■ 0.1 µM, ○ 1 µM, ◇ 10 µM, and □ 100 µM; ▼ paclitaxel 8 nM.

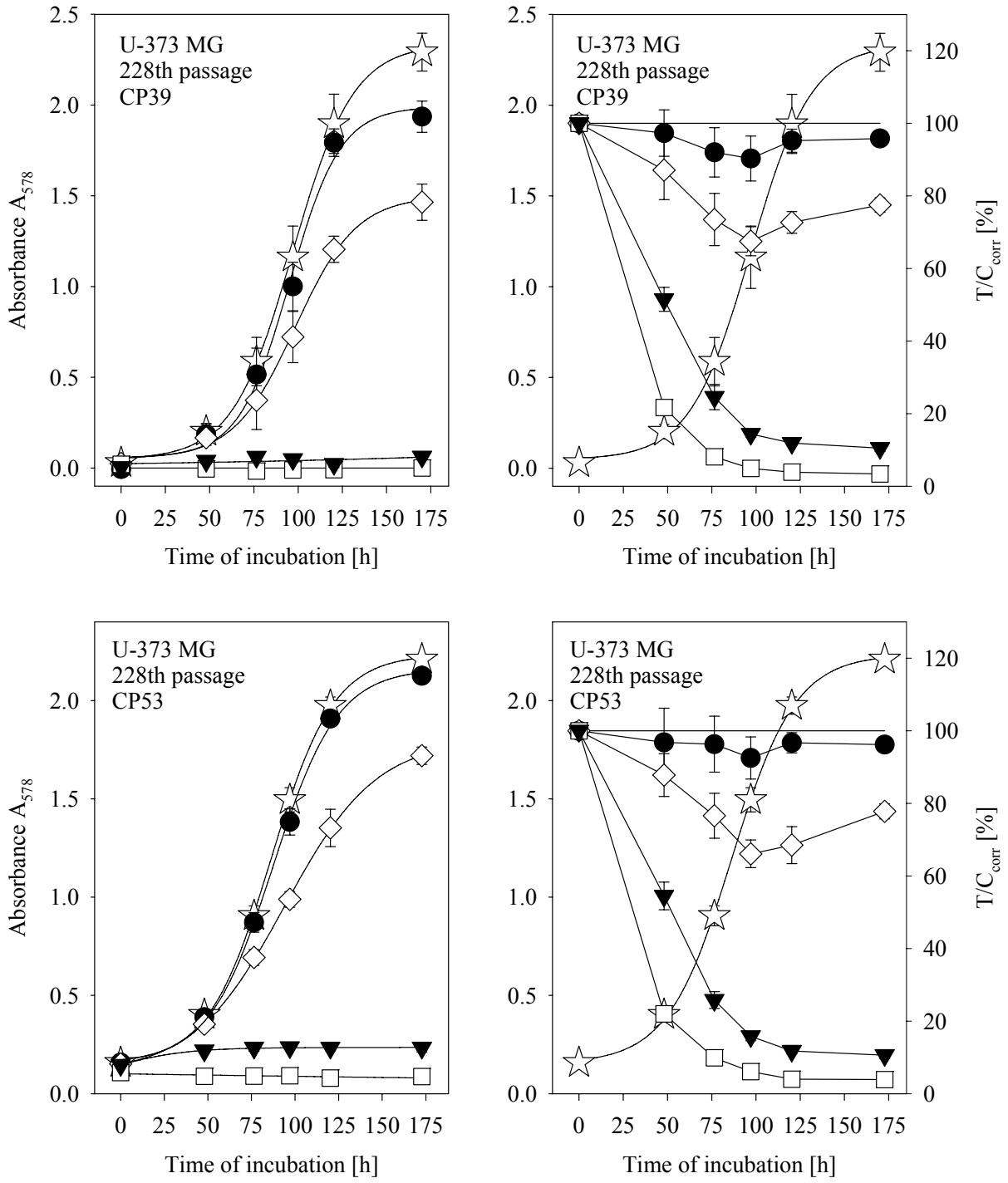

Figure 4-24: Effect of CP39 and CP53 (see also Fig. 4-4) on the proliferation of U-373 MG glioblastoma cells.. The cells showed a chemosensitivity similar to that of U-87 MG (Fig. 4-22). Both compounds were cytotoxic at a concentration of 10 µM, but the cells started to recover after about 100 hours. At 100 µM CP39 and CP53 exhibited a cytostatic effect on the cells. ☆ vehicle, CP39/CP53 concentration: ● 1 µM, ◇ 10 µM, and □ 100 µM; ▼ paclitaxel 8 nM.

4.4.5 Influence of pgp and bcrp on imatinib

4.4.5.1 Expression of pgp and bcrp in human glioblastoma cell variants

Since imatinib has been discussed to be a substrate of the pgp and the bcrp resistance transporter, respectively (Burger et al. 2004; Houghton et al. 2004; Illmer et al. 2004), the lack of the antiproliferative activity of imatinib against the human glioblastoma cell variants could be ascribed to the expression of these resistance proteins. Therefore the expression of pgp and bcrp was investigated on all of the three glioblastoma cell variants used in the chemosensitivity assays, using RT-PCR and immunostaining. Fig. 4-25 shows the results of the RT-PCR experiments.

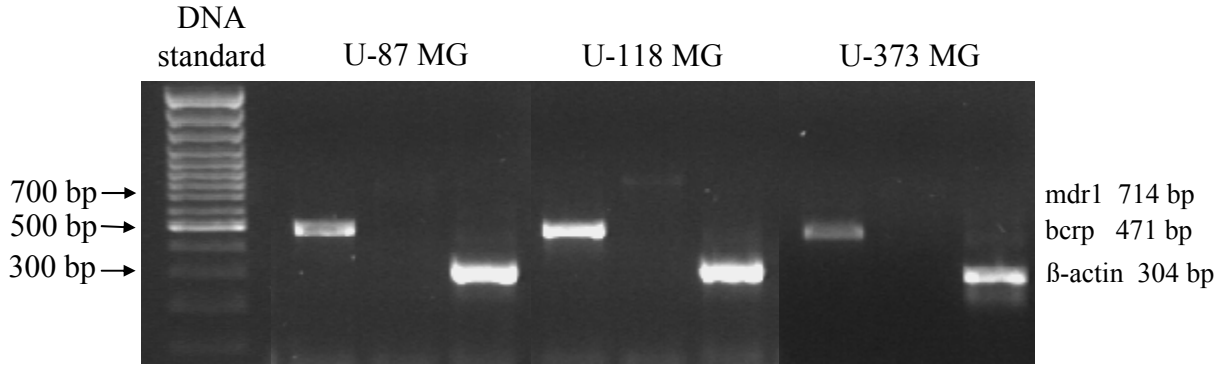

Figure 4-25: Agarose gel electrophoresis of RT-PCR products. All three glioblastoma cell variants show a band for the bcrp PCR-product, indicating the respective mRNA, but not for the mdr1 PCR-product (positive control β-actin).

Indicating the expression of bcrp but lack of expression of the pgp in all three cell variants, the results of the RT-PCR experiments were confirmed by immunostaining for the pgp expression (Fig. 4-26), but not for the bcrp expression (Fig. 4-27). The KBv1 cells showed high expression of pgp along the plasma membrane and a slight accumulation of FITC fluorescence emission in an organelle close to the nucleus, presumably the golgi apparatus, where the immature pgp is processed. The glioblastoma cells lacked pgp expression and only very weak fluorescence was detected in the cytoplasm, most likely derived from non-specific binding of the secondary antibody, since the nuclei remained completely non-fluorescent. Membranous bcrp was clearly detected in a high portion of MCF7 wild type breast cancer cells, whereas the identically labeled glioblastoma cells showed no appearance of bcrp.

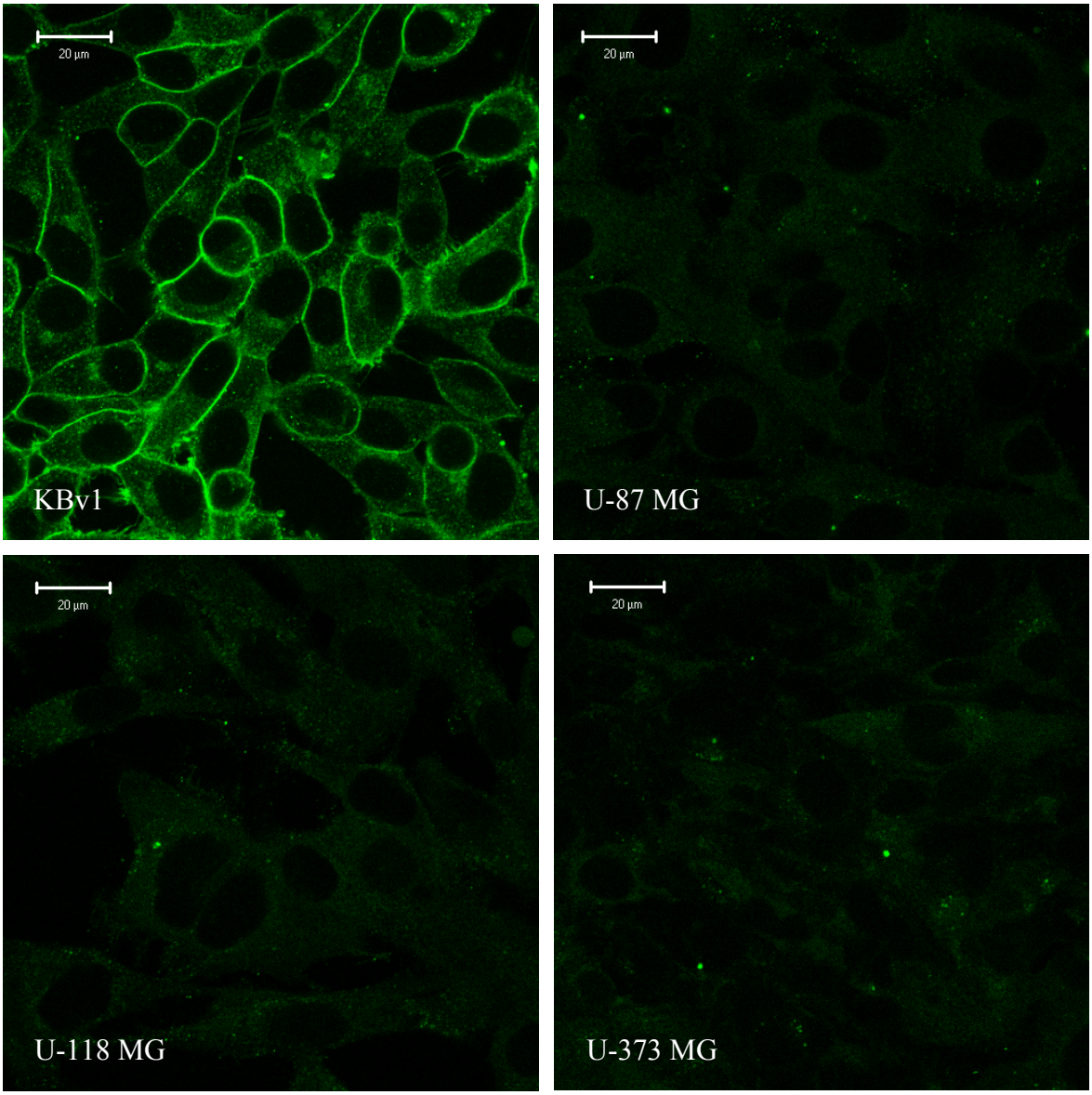

Figure 4-26: Human glioblastoma cells after immunostaining with anti-pgp primary antibody and FITC-conjugated secondary antibody. The positive control KBv1 shows expression of pgp at the cellular membrane, whereas the three glioblastoma variants lack pgp expression. Only weak, non-specific binding throughout the cells can be observed. Plan Apochromat 63x 1.4 Oil Ar laser 488 nm, LP505 nm.

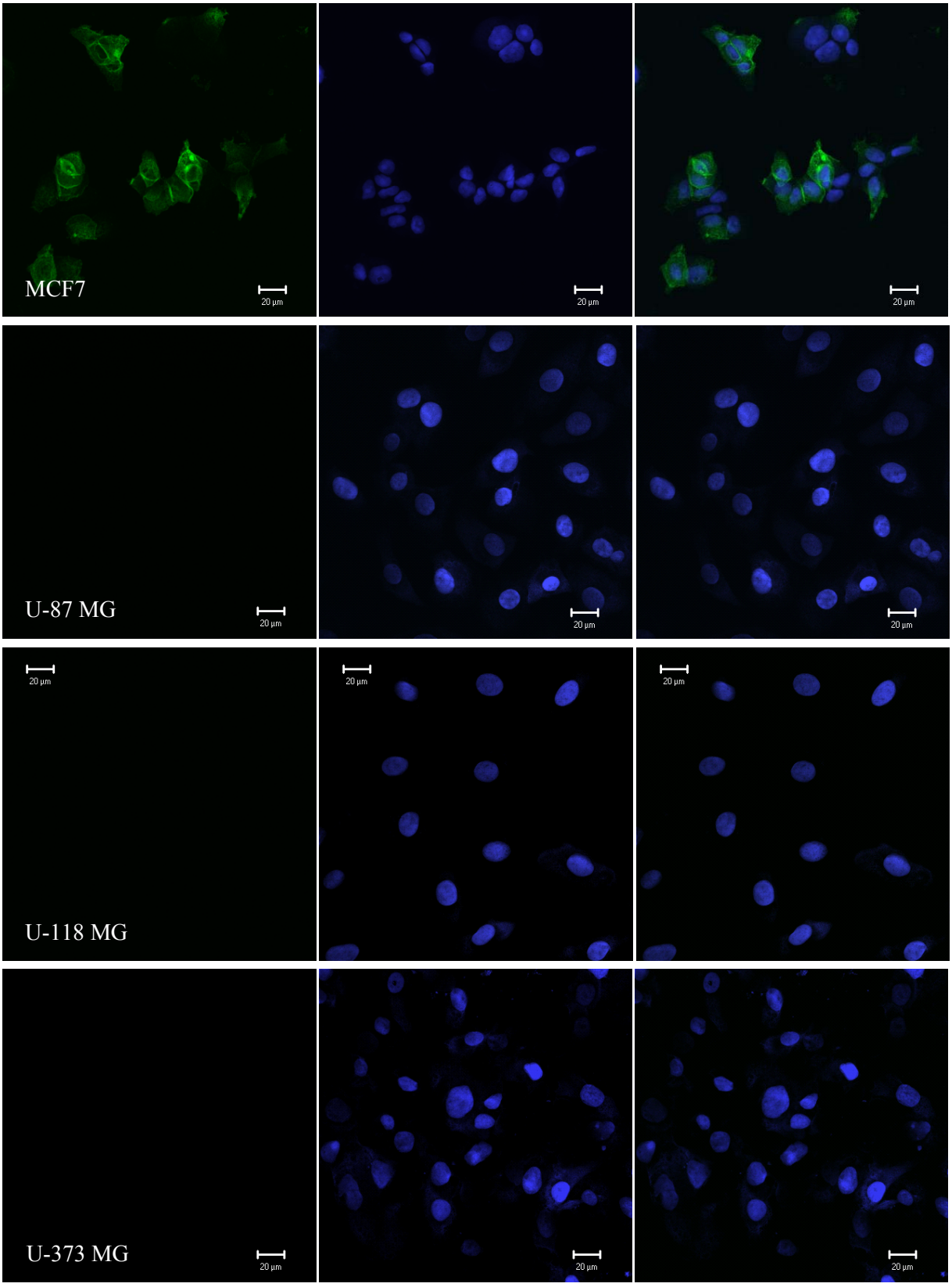

Figure 4-27: Human glioblastoma cells after immunostaining with anti-bcrp primary antibody and Cy5-conjugated secondary antibody. Most of the MCF7 wild type cells show membranous expression of bcrp, the three glioblastoma variants lack bcrp expression. Left: bcrp, HeNe laser 633 nm, LP650 nm, green false color; middle: nuclei, Ar laser 488 nm, LP505 nm, blue false color; right: merged detection channels. Plan Neofluar 40x 1.3 Oil.

4.4.5.2 Modulation of pgp and bcrp by imatinib

In addition to the determination of pgp and bcrp in the human glioblastoma cell variants imatinib was tested for its ability to modulate those two resistance proteins using the calcein-AM efflux assay for pgp (Homolya et al. 1996) and the mitoxantrone efflux assay for bcrp (Table 4-8).

As a lipophilic ester, the non-fluorescent calcein-AM rapidly permeates the plasma membrane of cells. Inside the cells highly fluorescent calcein is formed after calcein-AM cleavage by non-specific esterases. Calcein accumulates inside the cells due to its high hydrophilicity, leading to cytosolic trapping of the compound. Since calcein-AM is a substrate for the pgp and extruded by pgp-expressing cells, the increased intracellular calcein fluorescence correlates with a lowered expression of pgp and with an increased inhibition of pgp by tested compounds, respectively.

By analogy to the calcein-AM efflux assay, the ABCG2 assay works by loading of bcrp-expressing MCF7/Topo cells with the fluorescent bcrp substrate mitoxantrone. After a certain period of incubation with a potential bcrp modulator, the cell-associated mitoxantrone fluorescence is determined by a flow cytometer. High cell-associated fluorescence correlates with high mitoxantrone retention within the cells and consequently with a high inhibitory activity (bcrp inhibition) of the test compound.

Table 4-8: Pgp/ABCB1 and bcrp/ABCG2 modulation by imatinib. While imatinib starts modulation of the pgp at concentrations beyond therapeutically relevant levels (>10 µM), the bcrp function is not affected until an imatinib concentration of 10 µM, which is equivalent to the maximally suitable plasma concentration of imatinib.

Imatinib [µM]	Geometric mean (PGP170)	Geometric mean (BCRP)
0.0	5.69	300.24
0.1	6.29	286.51
0.3	6.30	290.80
1.0	6.40	313.37
3.0	6.43	354.82
10.0	7.42	513.77
30.0	13.47	982.74
100.0	234.20	1391.73

4.4.6 Effect of a combination of imatinib with paclitaxel on the proliferation of human glioblastoma cells

To investigate, if imatinib can enhances the cytotoxicity of the cytostatic agent paclitaxel, both compounds were administered in combination. As becomes obvious from the growth curves (Fig. 4-28), a combination of imatinib with paclitaxel did not increase the effect of paclitaxel.

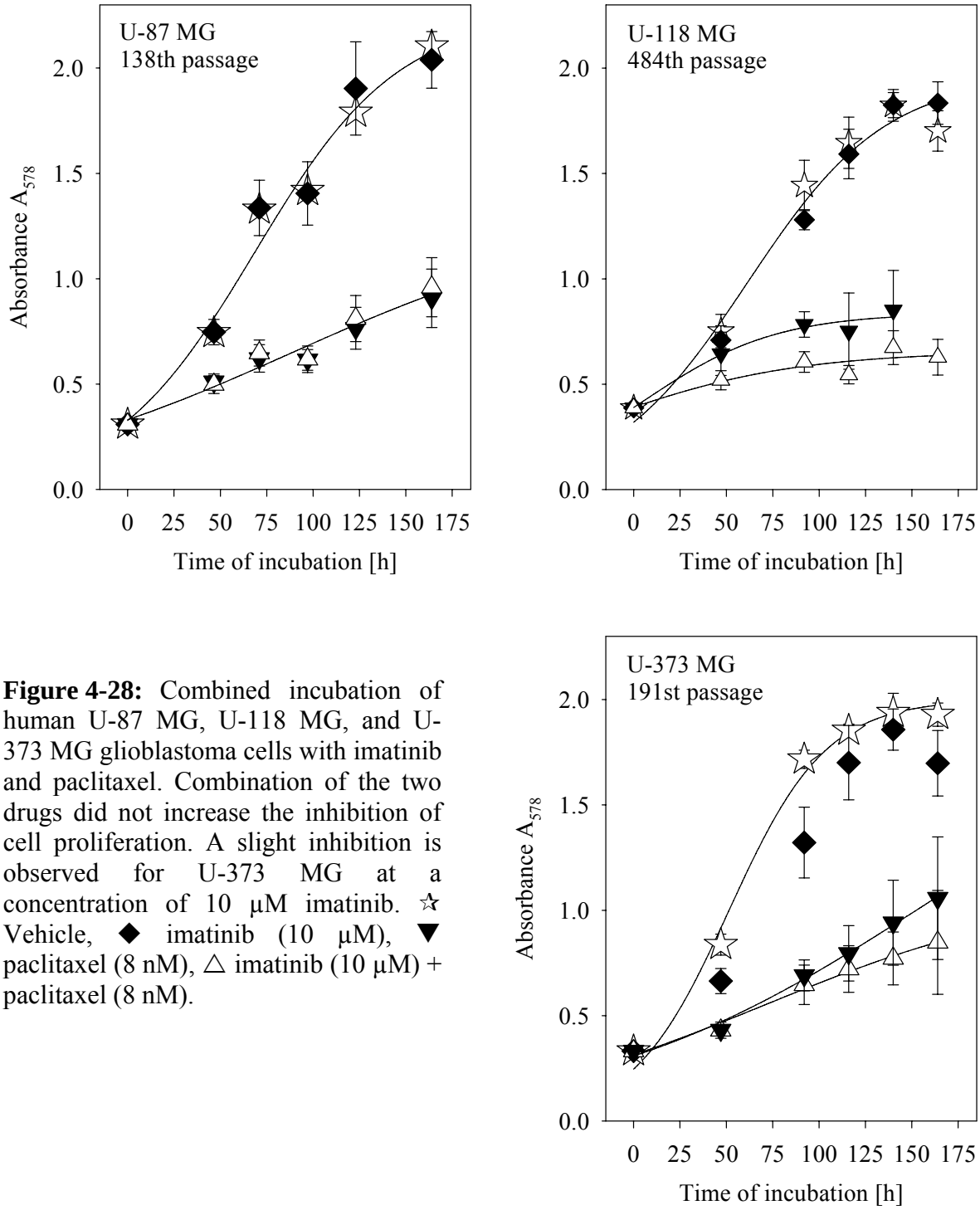

Figure 4-28: Combined incubation of human U-87 MG, U-118 MG, and U-373 MG glioblastoma cells with imatinib and paclitaxel. Combination of the two drugs did not increase the inhibition of cell proliferation. A slight inhibition is observed for U-373 MG at a concentration of 10 µM imatinib. ☆ Vehicle, ◆ imatinib (10 µM), ▼ paclitaxel (8 nM), △ imatinib (10 µM) + paclitaxel (8 nM).

4.4.7 Effect of imatinib on the proliferation of human glioblastoma cells in PDGF-free medium

To study the effect of imatinib in the absence of PDGF, experiments were carried out in serum-free HAMs F12 medium (Fig. 4-29). There was no increase in inhibition compared to that observed in serum-supplemented media. Only U-373 MG cells showed sensitivity at an imatinib concentration of 10 µM.

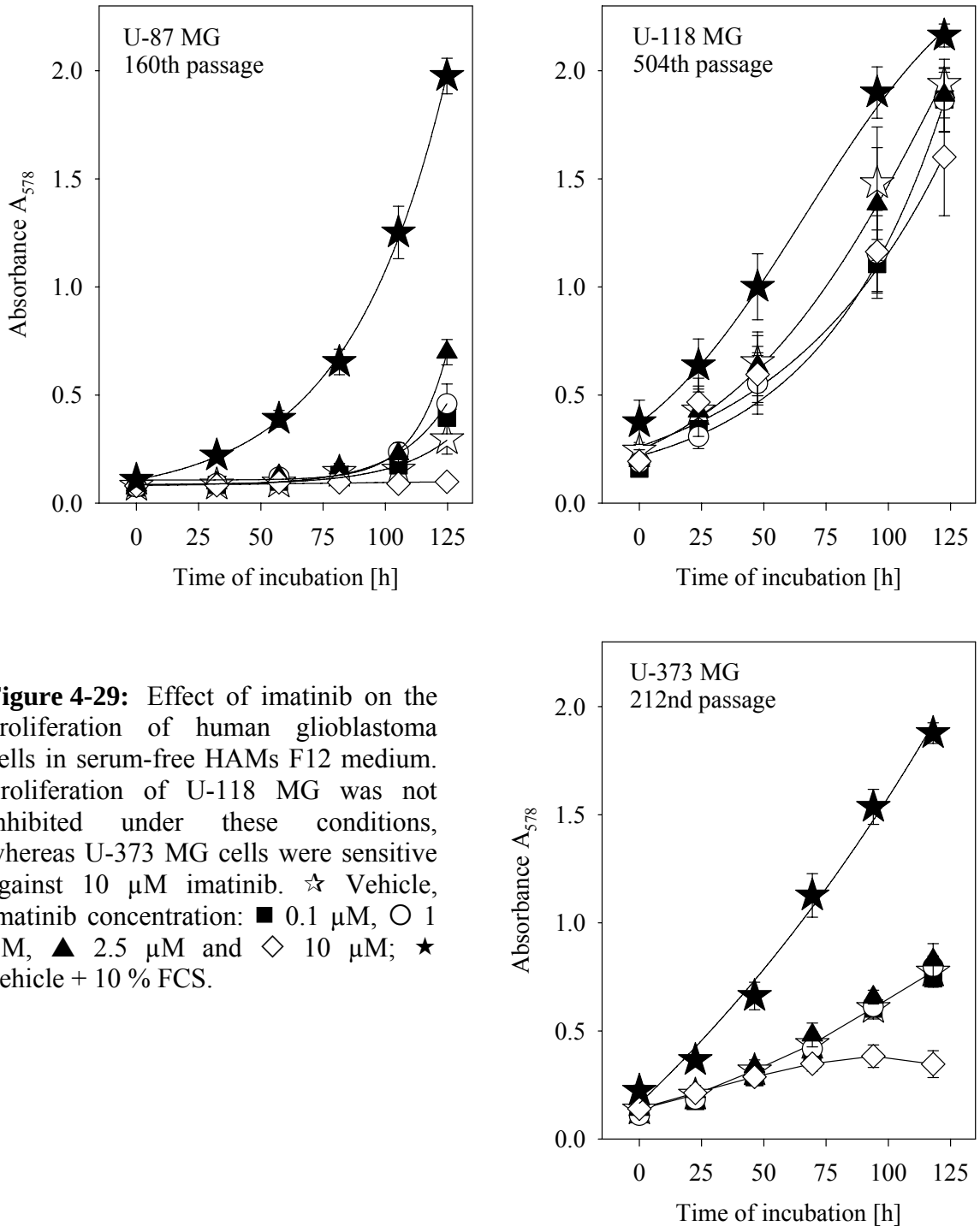

Figure 4-29: Effect of imatinib on the proliferation of human glioblastoma cells in serum-free HAMs F12 medium. Proliferation of U-118 MG was not inhibited under these conditions, whereas U-373 MG cells were sensitive against 10 µM imatinib. ☆ Vehicle, imatinib concentration: ■ 0.1 µM, ○ 1 µM, ▲ 2.5 µM and ◇ 10 µM; ★ vehicle + 10 % FCS.

4.4.8 Effect of imatinib on the proliferation of human K-562 CML cells

As imatinib is a registered drug for the treatment of chronic myelogenous leukemia, its activity against *bcr-abl* positive leukemia cells was investigated as a control. Total RNA of human K-562 cells was isolated and the *bcr-abl* oncogene mRNA was detected by RT-PCR (Fig. 4-31). Since the K-562 cells are non-adherent cells, but growing in suspension, the crystal violet method cannot be used for the determination of chemosensitivity. The suspension cells are lost during the initial removing step of culture medium prior to the fixation step. Thus the antiproliferative effect of imatinib against the *bcr-abl* positive K-562 CML cells was investigated by the MTT assay.

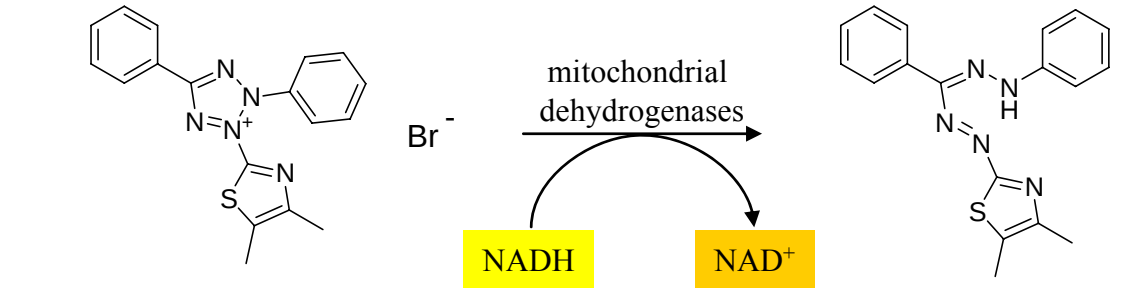

MTT (yellow)
(3-(4,5-Dimethylthiazol-2-yl)-
2,5-diphenyl-tetrazolium bromide)

MTT formazan (purple)

Figure 4-30: Chemical structures of MTT and its reduced form, the purple formazan. MTT is positively charged and water soluble, but sufficiently lipophilic to pass the plasma membrane of cells. After accumulation and reduction at the mitochondrial membrane, the purple MTT formazan precipitates and forms crystal needles inside the cell.

MTT is sensitive to chemical and enzymatic reduction. The yellow, water soluble tetrazolium bromide, is reduced to the purple formazan ($\lambda_{max\ (absorbance)}$ = 540 nm), which is not soluble in water, but in organic solvents such as DMSO. Incubation of cells with an aqueous MTT solution leads to an accumulation of the positively charged MTT at the inner membrane of mitochondria due to their high membrane potential. Thus the major part of the MTT present in the cytosol is reduced by mitochondrial dehydrogenases. After removal of the aqueous phase, the crystallized MTT formazan is redissolved in DMSO, and the absorbance of the solution is measured at 540 nm (A_{540}). A_{540} corresponds to the relative amount orthe the relative activity of mitochondrial dehydrogenases in treated cells compared to the cells of the control. It has to be pointed out that reducing or oxidizing agents may lead to an increase or

decrease in the measured A_{540} values. Furthermore, A_{540} not necessarily correlates with the number viable cells. For example, after cell lysis cellular dehydrogenases still can be active, pretending cell viability.

The results of the MTT assay with K-562 cells incubated with imatinib confirmed the antiproliferative effect of imatinib against CML cells at therapeutically relevant concentrations (Fig. 4-31).

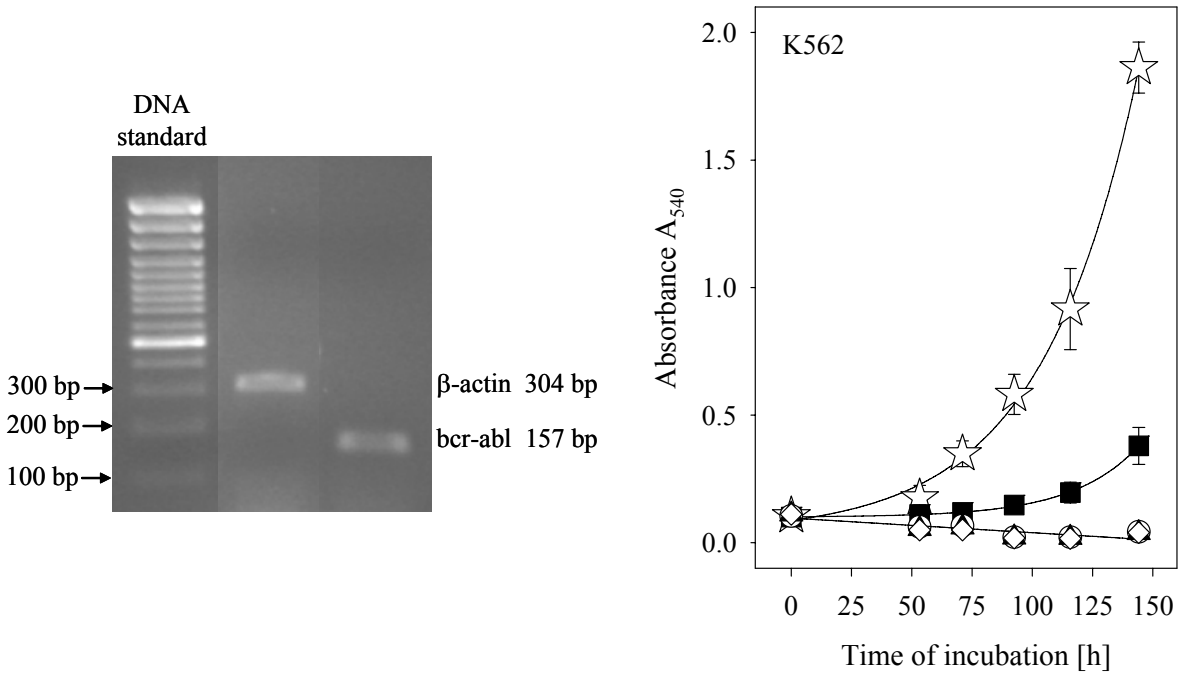

Figure 4-31: Left: agarose gel electrophoresis of RT-PCR products of K-562 mRNA. The band at 157 bp shows the presence of bcr-abl mRNA in human K-562 CML cells. Primers for β-actin (product band at 304 bp) were used as control. Right: MTT assay with human K-562 CML cells. The *bcr-abl* positive cells were incubated for 6 days with various concentrations of imatinib. Cell growth was clearly inhibited at a concentration of 0.1 µM. ☆ Vehicle, imatinib concentration: ■ 0.1 µM, ○ 1 µM, ▲ 2.5 µM, and ◇ 10 µM..

4.4.9 Effect of exogenous PDGF on the proliferation of human glioblastoma cells

In FCS-supplemented HAMs F12 medium the glioblastoma cells showed normal proliferation behaviour (Fig. 4-32). Addition of 10 ng/ml rhPDGF-BB did not increase cell proliferation in serum-free HAMs F12 medium, where the proliferation was generally very slow (Fig. 4-32). The experiment was also performed in serum-free MCDB105 medium (Pollack et al. 1990) and in serum-free standard culture media (EMEM and DMEM, respectively) with similar results (Fig. 4-33, 4-34). In serum-free MCDB105 medium even the maintenance of the

human glioblastoma cells failed, a result, which is contradictory to a report from the literature (Pollack et al. 1990). Up to 80 % of the cells detached and lost their characteristic morphology after the first 30 minutes in serum-free MCDB105 medium.

To investigate the relevancy of PDGF in cell proliferation, the human glioblastoma cells were incubated with exogenous PDGF-BB in serum-free HAMs F12 medium. The resulting growth curves are shown for U-87 MG, U-118 MG, and U-373 MG cells (Fig. 4-32). Exogenous PDGF-BB did not stimulate cell growth at the selected concentrations i. e. there was no difference in cell proliferation compared to the vehicle control.

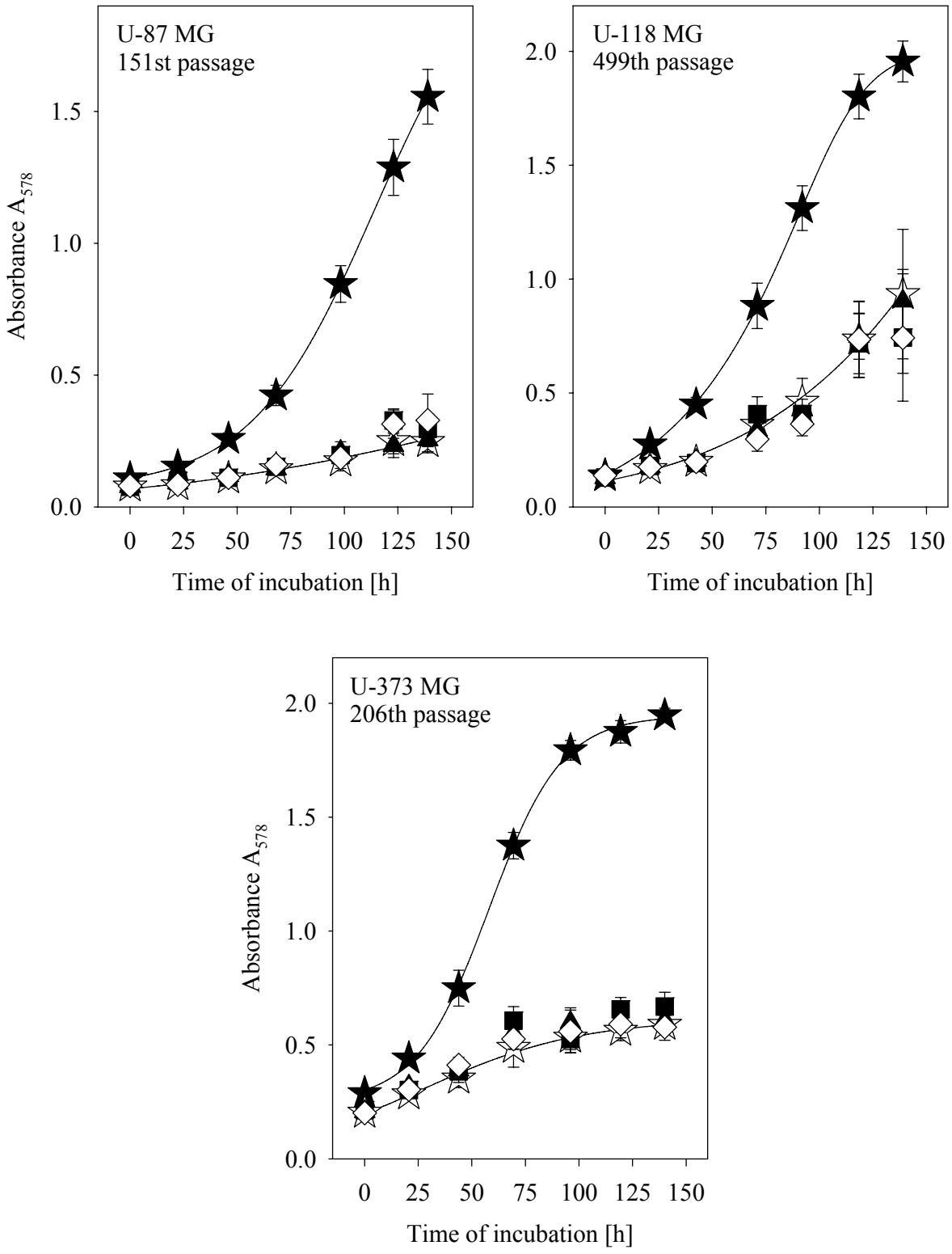

Figure 4-32: Incubation of human glioblastoma cell variants in the presence of recombinant human PDGF-BB in serum-free HAMs F12 medium. PDGF-BB had no effect on cell proliferation up to a concentration of 10 ng/ml. ☆ Vehicle, rhPDGF-BB concentration: ■ 0.1 ng/ml, ▲ 1 ng/ml, and ◇ 10 ng/ml, ★ vehicle +10 % FCS

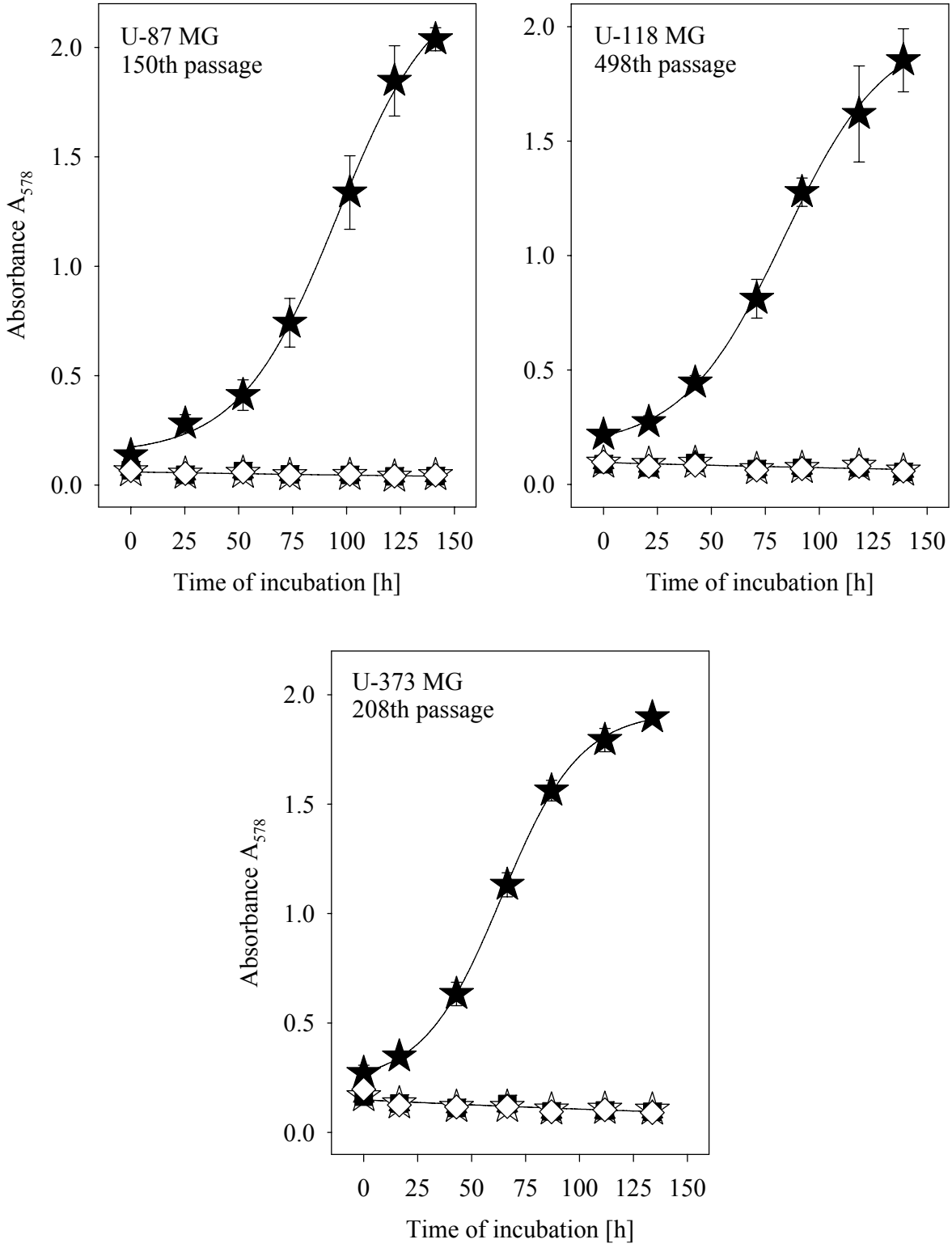

Figure 4-33: Incubation of human glioblastoma cell variants in the presence of recombinant human PDGF-BB in serum-free MCDB105 medium. Again, PDGF-BB had no effect on cell proliferation up to a concentration of 10 ng/ml. ☆ Vehicle, rhPDGF-BB concentration: ■ 0.1 ng/ml, ▲ 1 ng/ml, and ◇ 10 ng/ml, ★ vehicle + 10 % FCS.

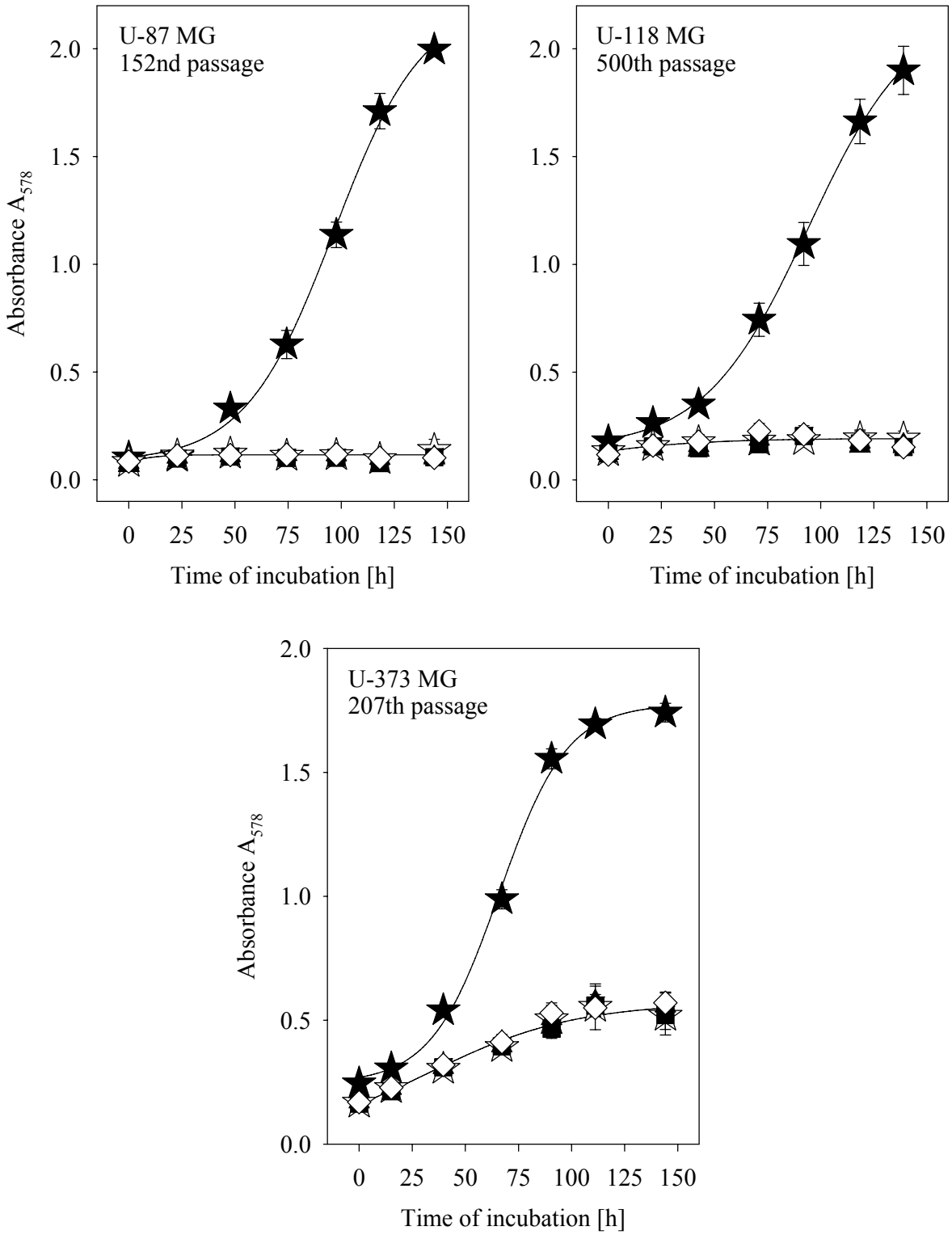

Figure 4-34: Incubation of human glioblastoma cell variants in the presence of recombinant human PDGF-BB in serum-free standard culture medium EMEM (U-87 MG, U-373 MG) respectively DMEM (U-118 MG). As observed in the experiments with serum-free HAMs F12 and MCDB105 medium, PDGF-BB had no effect on cell proliferation up to a concentration of 10 ng/ml. ☆ Vehicle, rhPDGF-BB concentration: ■ 0.1 ng/ml, ▲ 1 ng/ml, and ◇ 10 ng/ml, ★ vehicle + 10 % FCS.

4.5 Discussion

Expression and functionality of PDGFR in human glioblastoma cells.

The three human glioblastoma cell lines U-87 MG, U-118 MG, and U-373 MG show differential expression of the PDGF receptor subtypes (Fig. 4-5, 4-6, 4-8 – 4-10). These results are in agreement with the data of a report in the literature (Nister et al. 1991). The mRNA of the two major ligand subtypes (PDGF-A and –B) were also detected in all of the three cell variants (Fig. 4-7, Tab. 4-7).

After the demonstration of Ca^{2+} mobilization in A431 cells upon stimulation with various concentrations of EGF (Fig. 4-13) by the Fura-2 method (Takahashi et al. 1999), the functionality of PDGFRs was investigated in Swiss 3T3 mouse fibroblasts and in the human glioblastoma cells. In Swiss 3T3 cells the PDGF-BB triggered Ca^{2+} transients (Fig. 4-14) were inhibited by imatinib in a concentration-dependent manner (Fig. 4-15, 4-16), confirming its antagonistic activity on the PDGFR tyrosine kinase. In the three glioblastoma cell variants the mobilization of intracellular Ca^{2+} upon stimulation with PDGF-BB (Fig. 4-17) correlated with the expression of the PDGFRβ subtype, demonstrated by the flow cytometric experiments (Fig. 4-9, 4-10). The results of the fluorimetric Ca^{2+} measurements demonstrate the sensitivity of the glioblastoma variants to PDGF-BB as well as the functionality of the identified PDGF receptors. Considering the demonstrated expression of PDGFRs, together with the detection of PDGF-A and PDGF-B mRNA by RT-PCR, the proposed autocrine activation of the PDGF receptors (Hermanson et al. 1992; Guha et al. 1995; Yu et al. 1998; Lokker et al. 2002) seems possible.

Effect of selective tyrosine kinase inhibitors on human glioblastoma cells in vitro.

Kilic et al. reported on the inhibition of the proliferation of the human glioblastoma cell lines U-87 MG and U-343 MG at an imatinib concentration of 3 µM (Kilic et al. 2000). At concentrations of 6 and 10 µM the drug even reduced the number of seeded cells (Kilic et al. 2000). By contrast, the results of this work show that the incubation of the human glioblastoma cell variants U-87 MG, U-118 MG, and U-373 MG with the selective PDGFR tyrosine kinase inhibitor imatinib had no inhibitory effect on cell proliferation in serum-supplemented medium over standard and extended incubation period incubation (Fig. 4-18, 4-19). The compound also lacked antiproliferative activity when the cells were incubated in serum-free medium (Fig. 4-29). Although showing high activity against *bcr-abl* positive K-562 CML cells (Fig. 4-31) (Gambacorti-Passerini et al. 1997), imatinib was inactive against

the glioblastoma cells at therapeutically relevant concentrations (Lyseng-Williamson and Jarvis 2001). Moreover, a combination of imatinib with the cytostatic agent paclitaxel did not result in a noticeable effect (Fig. 4-28). Furthermore, tyrphostin AG-1296 (Kovalenko et al. 1994) had no inhibitory effect (Fig. 4-20). Leflunomide (Eckhardt et al. 1999) exhibited a cytotoxic and cytostatic effect on U-87 MG and U-373 MG cells respectively at a concentration of 100 µM (Fig. 4-21). Though leflunomide has been shown to inhibit PDGF receptor autophosphorylation with an IC_{50} value of 65 µM (Shawver et al. 1997), it has to be doubted whether the observed antiproliferative effect is caused by the disruption of the PDGF/PDGFR auto- or paracrine loop. More likely it may be ascribed to other toxic, but rather non-specific effects at such a high concentration of leflunomide. The bisindolylmethanone compounds CP39 and CP53 (Bohmer et al. 2003) showed similar effects on U-87 MG and U-373 MG. For both compounds concentrations above their IC_{50} value (PDGFR kinase inhibition) were needed to result into an antiproliferative effect (Fig. 4-22, 4-24). Though U-118 MG showed a higher chemosensitivity (Fig. 4-23) compared to U-87 MG and U-373 MG, the applied drug concentrations in the range of the IC_{50} value (PDGFR kinase inhibition) were not sufficient to yield an according inhibition of cell growth.

Referring to the results for imatinib, the contrast to the findings of Kilic et al. may be explained by the different conditions prevailing during the cytotoxicity assays. In this study the imatinib-containing culture media were not changed throughout the whole incubation period, whereas Kilic et al. replaced the culture medium every 48 hours. Bernhardt et al. showed that changes of the culture medium within a cytotoxicity assay affects cell proliferation leading to an overestimation of the activity of the tested drugs (Bernhardt et al. 1992). This might in part explain the reported antiproliferative activity of imatinib. Additionally, Kilic et al. used platelet-poor plasma, whereas serum-free media were used in this study to provide PDGF-free assay conditions.

Another explanation for the lack of the antiproliferative activity of imatinib would be prephosphorylation of the PDGF receptor protein at the activation loop within the receptor tyrosine kinase domain, which has been pointed out by Böhmer et al. (Bohmer et al. 2003) to be a critical determinant of imatinib inhibitory activity. At isolated receptors the phosphorylation of PDGFRβ at this site required one order of magnitude higher concentrations of STI-571 for inhibition of receptor kinase activity than non-activated PDGFRβ. But in intact cells imatinib inhibited preactivated and non-preactivated receptor kinases due to the regeneration of the inactive tyrosine kinase conformation by the action of protein tyrosine phosphatases (Bergsten et al. 2001). As a consequence the inhibitory activity

of imatinib should not depend on PDGF receptor stimulation, neither by endogenous PDGF (autocrine and paracrine stimulation) nor by exogenous PDGF present in FCS.

Influence of pgp/ABCB1 and bcrp/ABCG2 on the antiproliferative activity of imatinib against human glioblastoma cells.

Furthermore, a possible reason for the lack of the antiproliferative activity of imatinib against the glioblastoma cells, the influence of the drug resistance proteins pgp and bcrp, was also investigated. This included the detection of the pgp and bcrp mRNAs by RT-PCR, and the detection of the respective proteins by immunostaining, as well as the determination of pgp and bcrp modulation by imatinib using the flow cytometric Calcein-AM- (Homolya et al. 1996) and the mitoxantrone assay, respectively. Neither the pgp mRNA (Fig. 4-25) nor the pgp protein (Fig. 4-26) was detected in the three glioblastoma variants. Interestingly, although the bcrp mRNA was detected in all three glioma cell types (Fig. 4-25) the protein was not detected by the immunostaining method (Fig. 4-27). Consequently, the lack of antiproliferative efficacy of imatinib cannot be ascribed to those two resistance mechanisms. Moreover, the results from the calcein-AM- and mitoxantrone efflux-assays showed a very weak modulation of both resistance tranporters by imatinib at therapeutically relevant concentrations (Tab. 4-8). Considering these results, an expression of pgp and bcrp at the blood-brain barrier and in glioblastoma in vivo, should have a negligible effect on imatinib pharmacokinetics at the blood-brain barrier and on site of the intracranial tumor, respectively.

Effect of exogenous PDGF on the proliferation of human glioblastoma cells.

The proliferation of the glioblastoma cells was not increased by incubation with exogenous rhPDGF-BB under serum-free conditions (Fig. 4-32 - 4-34). The lacking response to exogenous PDGF is in contrast to the results in the literature (Pollack et al. 1990), where the effect of exogenous PDGF on human glioblastoma cells was investigated by [^{3}H]thymidine incorporation method. However, although commonly used, [^{3}H]thymidine incorporation seems to be inappropriate to investigate effects on cell proliferation, because changes in [^{3}H]thymidine incorporation may relate to changes in the size of the intracellular nucleotide pool rather than changes in DNA synthesis, and DNA synthesis continues in the absence of [^{3}H]thymidine incorporation (Wilson 2000).

Inhibition of human glioblastoma by imatinib.

Kilic et al. also reported on an inhibition of the growth of subcutaneously and intracranially implanted glioblastoma tumors in nude mice (Kilic et al. 2000). The observed efficacy in vivo may result from a high dose administration of 50 mg/kg of imatinib (i.p. and p.o.), leading to a plasma concentration beyond therapeutical levels (1.2-3 μM) in cumulative steady state after oral administration (Lyseng-Williamson et al. 2001).

Since PDGFRβ is expressed on vascular endothelial cells and PDGF has been shown to have angiogenic activity in various models (Bergsten et al. 2001) the reported in vivo effect may also be ascribed to an antiangiogenic activity of imatinib (Pollack et al. 1990; Cherrington et al. 2000; Morin 2000), which can take place at achievable intracranial drug concentrations. Buchdunger et al. showed that STI-571 potently inhibits serum-stimulated capillary sprouting from rat aorta in vitro at an IC_{50} value of 0.66 μM. Furthermore, imatinib was reported to inhibit PDGF-, VEGF- and bFGF-stimulated vascularization of a subcutaneous implant in mice (Buchdunger et al. 2002).

4.6 Summary

The results of this study suggest that the PDGF/PDGFR autocrine loop is not as relevant for malignancy and cell proliferation of human glioblastoma cells as has been proposed in the literature (Hermanson et al. 1992; Guha et al. 1995; Yu et al. 1998; Lokker et al. 2002). The reported induction of brain tumors in mice using a PDGF-B chain retrovirus (Uhrbom et al. 1998) is not indicative for a dominant role of PDGF in the proliferation and the survival of wild type tumors. The role of growth factors like nerve growth factor (Sultana et al. 1998; Singer et al. 1999), epidermal growth factor, transforming growth factor alpha, and others (Steck et al. 1986; Sultana et al. 1998; Yamada et al. 1998; Singer et al. 1999), that have also been identified in human astrocytoma, should be considered as well. The coexpression of a receptor and its ligand alone without proof of functional implications on tumor biology, as in case of PDGF receptors, is insufficient to provide a basis for a new therapeutic concept. This has, for instance, been shown for small cell lung cancer and Ewing sarcoma cells, both expressing c-KIT (Soria et al. 2003), and for melanoma in mice, expressing PDGFR (McGary et al. 2004).

A close look to the literature reveals that the current clinical trials (Dresemann 2003; Dresemann 2004; Raymond E 2004; National cancer institute 2005; U.S. National institutes

of health 2005; U.S. National institutes of health 2005) with glioblastoma and imatinib are mainly based on the report from Kilic et al. (Kilic et al. 2000). Beyond it there is only indirect indication of a major relevance of PDGF and PDGFR in the proliferation of human glioblastoma. Considering the poor outcome and prognosis of malignant glioma patients, the clinical evaluation of the efficacy of imatinib is of course warranted. However, the results of this study suggest that clinical antitumor effects of imatinib against glioblastoma are not mediated by PDGFR.

Bibliography

Ahlen K and Rubin K (1994). Platelet-derived growth factor-BB stimulates synthesis of the integrin alpha 2-subunit in human diploid fibroblasts. *Exp Cell Res* **215**: 347-53.

Andrae J, Molander C, Smits A, Funa K and Nister M (2002). Platelet-derived growth factor-B and -C and active alpha-receptors in medulloblastoma cells. *Biochem Biophys Res Commun* **296**: 604-11.

Antoniades H N, Scher C D and Stiles C D (1979). Purification of human platelet-derived growth factor. *Proc Natl Acad Sci U S A* **76**: 1809-13.

Assoian R K (1997). Anchorage-dependent cell cycle progression. *J Cell Biol* **136**: 1-4.

Bacus S S, Kiguchi K, Chin D, King C R and Huberman E (1990). Differentiation of cultured human breast cancer cells (AU-565 and MCF-7) associated with loss of cell surface HER-2/neu antigen. *Mol Carcinog* **3**: 350-62.

Beckman G, Beckman L, Ponten J and Westermark B (1971). G-6-PD and PGM phenotypes of 16 continuous human tumor cell lines. Evidence against cross-contamination and contamination by HeLa cells. *Hum Hered* **21**: 238-41.

Beckmann M P, Betsholtz C, Heldin C H, Westermark B, Di Marco E, Di Fiore P P, Robbins K C and Aaronson S A (1988). Comparison of biological properties and transforming potential of human PDGF-A and PDGF-B chains. *Science* **241**: 1346-9.

Bergsten E, Uutela M, Li X, Pietras K, Ostman A, Heldin C H, Alitalo K and Eriksson U (2001). PDGF-D is a specific, protease-activated ligand for the PDGF beta-receptor. *Nat Cell Biol* **3**: 512-6.

Bernhardt G, Reile H, Birnbock H, Spruss T and Schonenberger H (1992). Standardized kinetic microassay to quantify differential chemosensitivity on the basis of proliferative activity. *J Cancer Res Clin Oncol* **118**: 35-43.

Berridge M J, Heslop J P, Irvine R F and Brown K D (1984). Inositol trisphosphate formation and calcium mobilization in Swiss 3T3 cells in response to platelet-derived growth factor. *Biochem J* **222**: 195-201.

Besmer P, Snyder H W, Jr., Murphy J E, Hardy W D, Jr. and Parodi A (1983). The Parodi-Irgens feline sarcoma virus and simian sarcoma virus have homologous oncogenes, but in different contexts of the viral genomes. *J Virol* **46**: 606-13.

Betsholtz C, Johnsson A, Heldin C H, Westermark B, Lind P, Urdea M S, Eddy R, Shows T B, Philpott K, Mellor A L and et al. (1986). cDNA sequence and chromosomal localization of human platelet-derived growth factor A-chain and its expression in tumour cell lines. *Nature* **320**: 695-9.

Bishayee S, Majumdar S, Khire J and Das M (1989). Ligand-induced dimerization of the platelet-derived growth factor receptor. Monomer-dimer interconversion occurs independent of receptor phosphorylation. *J Biol Chem* **264**: 11699-705.

Bohmer F D, Karagyozov L, Uecker A, Serve H, Botzki A, Mahboobi S and Dove S (2003). A single amino acid exchange inverts susceptibility of related receptor tyrosine kinases for the ATP site inhibitor STI-571. *J Biol Chem* **278**: 5148-55.

Borkham-Kamphorst E, Meurer S K, Gressner A M and Weiskirchen R (2005). Disruption of intermolecular disulfide bonds in PDGF-BB dimers by N-acetyl-L-cysteine does not prevent PDGF signaling in cultured hepatic stellate cells. *Biochem Biophys Res Commun* **338**: 1711-8.

Buchdunger E, O'Reilly T and Wood J (2002). Pharmacology of imatinib (STI571). *Eur J Cancer* **38 Suppl 5**: S28-36.

Burger H, van Tol H, Boersma A W, Brok M, Wiemer E A, Stoter G and Nooter K (2004). Imatinib mesylate (STI571) is a substrate for the breast cancer resistance protein (BCRP)/ABCG2 drug pump. *Blood* **104**: 2940-2.

Carpenter G and Ji Q (1999). Phospholipase C-gamma as a signal-transducing element. *Exp Cell Res* **253**: 15-24.

Carroll M, Tomasson M H, Barker G F, Golub T R and Gilliland D G (1996). The TEL/platelet-derived growth factor beta receptor (PDGF beta R) fusion in chronic myelomonocytic leukemia is a transforming protein that self-associates and activates PDGF beta R kinase-dependent signaling pathways. *Proc Natl Acad Sci U S A* **93**: 14845-50.

Cherrington J M, Strawn L M and Shawver L K (2000). New paradigms for the treatment of cancer: the role of anti-angiogenesis agents. *Adv Cancer Res* **79**: 1-38.

Chomczynski P and Sacchi N (1987). Single-step method of RNA isolation by acid guanidinium thiocyanate-phenol-chloroform extraction. *Anal Biochem* **162**: 156-9.

Claesson-Welsh L, Eriksson A, Westermark B and Heldin C H (1989). cDNA cloning and expression of the human A-type platelet-derived growth factor (PDGF) receptor establishes structural similarity to the B-type PDGF receptor. *Proc Natl Acad Sci U S A* **86**: 4917-21.

Coussens L, Van Beveren C, Smith D, Chen E, Mitchell R L, Isacke C M, Verma I M and Ullrich A (1986). Structural alteration of viral homologue of receptor proto-oncogene fms at carboxyl terminus. *Nature* **320**: 277-80.

Dalla-Favera R, Gallo R C, Giallongo A and Croce C M (1982). Chromosomal localization of the human homolog (c-sis) of the simian sarcoma virus onc gene. *Science* **218**: 686-8.

de Bruin M, Miyake K, Litman T, Robey R and Bates S E (1999). Reversal of resistance by GF120918 in cell lines expressing the ABC half-transporter, MXR. *Cancer Lett* **146**: 117-26.

Denk P O and Knorr M (2002). [Differential regulation of expression of PDGF receptors on corneal epithelial cells]. *Ophthalmologe* **99**: 15-9.

Deuel T F, Huang J S, Proffitt R T, Baenziger J U, Chang D and Kennedy B B (1981). Human platelet-derived growth factor. Purification and resolution into two active protein fractions. *J Biol Chem* **256**: 8896-9.

Devare S G, Reddy E P, Law J D, Robbins K C and Aaronson S A (1983). Nucleotide sequence of the simian sarcoma virus genome: demonstration that its acquired cellular sequences encode the transforming gene product p28sis. *Proc Natl Acad Sci U S A* **80**: 731-5.

Diliberto P A, Gordon G W, Yu C L, Earp H S and Herman B (1992). Platelet-derived growth factor (PDGF) alpha receptor activation modulates the calcium mobilizing activity of the PDGF beta receptor in Balb/c3T3 fibroblasts. *J Biol Chem* **267**: 11888-97.

Dolle R E, Dunn J A, Bobko M, Singh B, Kuster J E, Baizman E, Harris A L, Sawutz D G, Miller D, Wang S and et al. (1994). 5,7-Dimethoxy-3-(4-pyridinyl)quinoline is a potent and selective inhibitor of human vascular beta-type platelet-derived growth factor receptor tyrosine kinase. *J Med Chem* **37**: 2627-9.

Doolittle R F, Hunkapiller M W, Hood L E, Devare S G, Robbins K C, Aaronson S A and Antoniades H N (1983). Simian sarcoma virus onc gene, v-sis, is derived from the gene (or genes) encoding a platelet-derived growth factor. *Science* **221**: 275-7.

Dresemann G (2003). STI 571/hydroxyurea in progressive, pretreated glioblastoma (GB) patients (pts.). *39th ASCO Annual Meeting*: Abstract No. 465.

Dresemann G (2004). Imatinib (STI571) plus hydroxyurea: Safety and efficacy in pre-treated, progressive glioblastoma multiforme (GBM) patients (pts). *40th ASCO Annual Meeting*: Abstract No.1550.

Duan D S, Pazin M J, Fretto L J and Williams L T (1991). A functional soluble extracellular region of the platelet-derived growth factor (PDGF) beta-receptor antagonizes PDGF-stimulated responses. *J Biol Chem* **266**: 413-8.

Eagle H (1955). Propagation in a fluid medium of a human epidermoid carcinoma, strain KB. *Proc Soc Exp Biol Med* **89**: 362-4.

Eckhardt S G, Rizzo J, Sweeney K R, Cropp G, Baker S D, Kraynak M A, Kuhn J G, Villalona-Calero M A, Hammond L, Weiss G, Thurman A, Smith L, Drengler R, Eckardt J R, Moczygemba J, Hannah A L, Von Hoff D D and Rowinsky E K (1999). Phase I and pharmacologic study of the tyrosine kinase inhibitor SU101 in patients with advanced solid tumors. *J Clin Oncol* **17**: 1095-104.

Ekman S, Thuresson E R, Heldin C H and Ronnstrand L (1999). Increased mitogenicity of an alphabeta heterodimeric PDGF receptor complex correlates with lack of RasGAP binding. *Oncogene* **18**: 2481-8.

Ferns G A, Raines E W, Sprugel K H, Motani A S, Reidy M A and Ross R (1991). Inhibition of neointimal smooth muscle accumulation after angioplasty by an antibody to PDGF. *Science* **253**: 1129-32.

Fleming T P, Saxena A, Clark W C, Robertson J T, Oldfield E H, Aaronson S A and Ali I U (1992). Amplification and/or overexpression of platelet-derived growth factor receptors and epidermal growth factor receptor in human glial tumors. *Cancer Res* **52**: 4550-3.

Frisch S M and Ruoslahti E (1997). Integrins and anoikis. *Curr Opin Cell Biol* **9**: 701-6.

Gambacorti-Passerini C, le Coutre P, Mologni L, Fanelli M, Bertazzoli C, Marchesi E, Di Nicola M, Biondi A, Corneo G M, Belotti D, Pogliani E and Lydon N B (1997). Inhibition of the ABL kinase activity blocks the proliferation of BCR/ABL+ leukemic cells and induces apoptosis. *Blood Cells Mol Dis* **23**: 380-94.

Gazit A, App H, McMahon G, Chen J, Levitzki A and Bohmer F D (1996). Tyrphostins. 5. Potent inhibitors of platelet-derived growth factor receptor tyrosine kinase: structure-activity relationships in quinoxalines, quinolines, and indole tyrphostins. *J Med Chem* **39**: 2170-7.

Giard D J, Aaronson S A, Todaro G J, Arnstein P, Kersey J H, Dosik H and Parks W P (1973). In vitro cultivation of human tumors: establishment of cell lines derived from a series of solid tumors. *J Natl Cancer Inst* **51**: 1417-23.

Gilbertson D G, Duff M E, West J W, Kelly J D, Sheppard P O, Hofstrand P D, Gao Z, Shoemaker K, Bukowski T R, Moore M, Feldhaus A L, Humes J M, Palmer T E and Hart C E (2001). Platelet-derived growth factor C (PDGF-C), a novel growth factor that binds to PDGF alpha and beta receptor. *J Biol Chem* **276**: 27406-14.

Golub T R, Barker G F, Lovett M and Gilliland D G (1994). Fusion of PDGF receptor beta to a novel ets-like gene, tel, in chronic myelomonocytic leukemia with t(5;12) chromosomal translocation. *Cell* **77**: 307-16.

Graves L M, Bornfeldt K E, Sidhu J S, Argast G M, Raines E W, Ross R, Leslie C C and Krebs E G (1996). Platelet-derived growth factor stimulates protein kinase A through a mitogen-activated protein kinase-dependent pathway in human arterial smooth muscle cells. *J Biol Chem* **271**: 505-11.

Green L S, Jellinek D, Jenison R, Ostman A, Heldin C H and Janjic N (1996). Inhibitory DNA ligands to platelet-derived growth factor B-chain. *Biochemistry* **35**: 14413-24.

Grynkiewicz G, Poenie M and Tsien R Y (1985). A new generation of Ca2+ indicators with greatly improved fluorescence properties. *J Biol Chem* **260**: 3440-50.

Guha A, Dashner K, Black P M, Wagner J A and Stiles C D (1995). Expression of PDGF and PDGF receptors in human astrocytoma operation specimens supports the existence of an autocrine loop. *Int J Cancer* **60**: 168-73.

Gupta M, Naik S, Pandey C M and Dabadghao S (2002). Drug sensitivity assay for leukaemic cells by flow cytometry. *Indian J Med Res* **115**: 260-4.

Hammacher A, Mellstrom K, Heldin C H and Westermark B (1989). Isoform-specific induction of actin reorganization by platelet-derived growth factor suggests that the functionally active receptor is a dimer. *Embo J* **8**: 2489-95.

Hammacher A, Nister M, Westermark B and Heldin C H (1988). A human glioma cell line secretes three structurally and functionally different dimeric forms of platelet-derived growth factor. *Eur J Biochem* **176**: 179-86.

Haniu M, Hsieh P, Rohde M F and Kenney W C (1994). Characterization of disulfide linkages in platelet-derived growth factor AA. *Arch Biochem Biophys* **310**: 433-7.

Haniu M, Rohde M F and Kenney W C (1993). Disulfide bonds in recombinant human platelet-derived growth factor BB dimer: characterization of intermolecular and intramolecular disulfide linkages. *Biochemistry* **32**: 2431-7.

Hart C E, Bailey M, Curtis D A, Osborn S, Raines E, Ross R and Forstrom J W (1990). Purification of PDGF-AB and PDGF-BB from human platelet extracts and identification of all three PDGF dimers in human platelets. *Biochemistry* **29**: 166-72.

Hart C E, Forstrom J W, Kelly J D, Seifert R A, Smith R A, Ross R, Murray M J and Bowen-Pope D F (1988). Two classes of PDGF receptor recognize different isoforms of PDGF. *Science* **240**: 1529-31.

Hay R J (1988). The seed stock concept and quality control for cell lines. *Anal Biochem* **171**: 225-37.

Heidaran M A, Pierce J H, Yu J C, Lombardi D, Artrip J E, Fleming T P, Thomason A and Aaronson S A (1991). Role of alpha beta receptor heterodimer formation in beta platelet-derived growth factor (PDGF) receptor activation by PDGF-AB. *J Biol Chem* **266**: 20232-7.

Heldin C H, Ernlund A, Rorsman C and Ronnstrand L (1989). Dimerization of B-type platelet-derived growth factor receptors occurs after ligand binding and is closely associated with receptor kinase activation. *J Biol Chem* **264**: 8905-12.

Heldin C H and Westermark B (1999). Mechanism of action and in vivo role of platelet-derived growth factor. *Physiol Rev* **79**: 1283-316.

Heldin C H, Westermark B and Wasteson A (1979). Platelet-derived growth factor: purification and partial characterization. *Proc Natl Acad Sci U S A* **76**: 3722-6.

Hermanson M, Funa K, Hartman M, Claesson-Welsh L, Heldin C H, Westermark B and Nister M (1992). Platelet-derived growth factor and its receptors in human glioma tissue: expression of messenger RNA and protein suggests the presence of autocrine and paracrine loops. *Cancer Res* **52**: 3213-9.

Hermanson M, Funa K, Koopmann J, Maintz D, Waha A, Westermark B, Heldin C H, Wiestler O D, Louis D N, von Deimling A and Nister M (1996). Association of loss of heterozygosity on chromosome 17p with high platelet-derived growth factor alpha receptor expression in human malignant gliomas. *Cancer Res* **56**: 164-71.

Holdhoff M, Kreuzer K A, Appelt C, Scholz R, Na I K, Hildebrandt B, Riess H, Jordan A, Schmidt C A, Van Etten R A, Dorken B and le Coutre P (2005). Imatinib mesylate radiosensitizes human glioblastoma cells through inhibition of platelet-derived growth factor receptor. *Blood Cells Mol Dis* **34**: 181-5.

Hollo Z, Homolya L, Davis C W and Sarkadi B (1994). Calcein accumulation as a fluorometric functional assay of the multidrug transporter. *Biochim Biophys Acta* **1191**: 384-8.

Homolya L, Hollo M, Muller M, Mechetner E B and Sarkadi B (1996). A new method for a quantitative assessment of P-glycoprotein-related multidrug resistance in tumour cells. *Br J Cancer* **73**: 849-55.

Homolya L, Hollo Z, Germann U A, Pastan I, Gottesman M M and Sarkadi B (1993). Fluorescent cellular indicators are extruded by the multidrug resistance protein. *J Biol Chem* **268**: 21493-6.

Houghton P J, Germain G S, Harwood F C, Schuetz J D, Stewart C F, Buchdunger E and Traxler P (2004). Imatinib mesylate is a potent inhibitor of the ABCG2 (BCRP) transporter and reverses resistance to topotecan and SN-38 in vitro. *Cancer Res* **64**: 2333-7.

Illmer T, Schaich M, Platzbecker U, Freiberg-Richter J, Oelschlagel U, von Bonin M, Pursche S, Bergemann T, Ehninger G and Schleyer E (2004). P-glycoprotein-mediated drug efflux is a resistance mechanism of chronic myelogenous leukemia cells to treatment with imatinib mesylate. *Leukemia* **18**: 401-8.

Johnsson A, Betsholtz C, Heldin C H and Westermark B (1985). Antibodies against platelet-derived growth factor inhibit acute transformation by simian sarcoma virus. *Nature* **317**: 438-40.

Kanakaraj P, Raj S, Khan S A and Bishayee S (1991). Ligand-induced interaction between alpha- and beta-type platelet-derived growth factor (PDGF) receptors: role of receptor heterodimers in kinase activation. *Biochemistry* **30**: 1761-7.

Kazlauskas A and Cooper J A (1989). Autophosphorylation of the PDGF receptor in the kinase insert region regulates interactions with cell proteins. *Cell* **58**: 1121-33.

Kenney W C, Haniu M, Herman A C, Arakawa T, Costigan V J, Lary J, Yphantis D A and Thomason A R (1994). Formation of mitogenically active PDGF-B dimer does not require interchain disulfide bonds. *J Biol Chem* **269**: 12351-9.

Kilic T, Alberta J A, Zdunek P R, Acar M, Iannarelli P, O'Reilly T, Buchdunger E, Black P M and Stiles C D (2000). Intracranial inhibition of platelet-derived growth factor-mediated glioblastoma cell growth by an orally active kinase inhibitor of the 2-phenylaminopyrimidine class. *Cancer Res* **60**: 5143-50.

Klinghoffer R A and Kazlauskas A (1995). Identification of a putative Syp substrate, the PDGF beta receptor. *J Biol Chem* **270**: 22208-17.

Koeffler H P and Golde D W (1980). Human myeloid leukemia cell lines: a review. *Blood* **56**: 344-50.

Kohler N and Lipton A (1974). Platelets as a source of fibroblast growth-promoting activity. *Exp Cell Res* **87**: 297-301.

Kovalenko M, Gazit A, Bohmer A, Rorsman C, Ronnstrand L, Heldin C H, Waltenberger J, Bohmer F D and Levitzki A (1994). Selective platelet-derived growth factor receptor kinase blockers reverse sis-transformation. *Cancer Res* **54**: 6106-14.

Kovalenko M, Ronnstrand L, Heldin C H, Loubtchenkov M, Gazit A, Levitzki A and Bohmer F D (1997). Phosphorylation site-specific inhibition of platelet-derived growth factor beta-receptor autophosphorylation by the receptor blocking tyrphostin AG1296. *Biochemistry* **36**: 6260-9.

Kumabe T, Sohma Y, Kayama T, Yoshimoto T and Yamamoto T (1992). Amplification of alpha-platelet-derived growth factor receptor gene lacking an exon coding for a portion of the extracellular region in a primary brain tumor of glial origin. *Oncogene* **7**: 627-33.

LaRochelle W J, Jeffers M, Corvalan J R, Jia X C, Feng X, Vanegas S, Vickroy J D, Yang X D, Chen F, Gazit G, Mayotte J, Macaluso J, Rittman B, Wu F, Dhanabal M, Herrmann J and Lichenstein H S (2002). Platelet-derived growth factor D: tumorigenicity in mice and dysregulated expression in human cancer. *Cancer Res* **62**: 2468-73.

LaRochelle W J, Jeffers M, McDonald W F, Chillakuru R A, Giese N A, Lokker N A, Sullivan C, Boldog F L, Yang M, Vernet C, Burgess C E, Fernandes E, Deegler L L, Rittman B, Shimkets J, Shimkets R A, Rothberg J M and Lichenstein H S (2001). PDGF-D, a new protease-activated growth factor. *Nat Cell Biol* **3**: 517-21.

LaRochelle W J, Jensen R A, Heidaran M A, May-Siroff M, Wang L M, Aaronson S A and Pierce J H (1993). Inhibition of platelet-derived growth factor autocrine growth

stimulation by a monoclonal antibody to the human alpha platelet-derived growth factor receptor. *Cell Growth Differ* **4**: 547-53.

Larose L, Gish G, Shoelson S and Pawson T (1993). Identification of residues in the beta platelet-derived growth factor receptor that confer specificity for binding to phospholipase C-gamma 1. *Oncogene* **8**: 2493-9.

Leal F, Williams L T, Robbins K C and Aaronson S A (1985). Evidence that the v-sis gene product transforms by interaction with the receptor for platelet-derived growth factor. *Science* **230**: 327-30.

Li X, Ponten A, Aase K, Karlsson L, Abramsson A, Uutela M, Backstrom G, Hellstrom M, Bostrom H, Li H, Soriano P, Betsholtz C, Heldin C H, Alitalo K, Ostman A and Eriksson U (2000). PDGF-C is a new protease-activated ligand for the PDGF alpha-receptor. *Nat Cell Biol* **2**: 302-9.

Liu P, Ying Y, Ko Y G and Anderson R G (1996). Localization of platelet-derived growth factor-stimulated phosphorylation cascade to caveolae. *J Biol Chem* **271**: 10299-303.

Lokker N A, O'Hare J P, Barsoumian A, Tomlinson J E, Ramakrishnan V, Fretto L J and Giese N A (1997). Functional importance of platelet-derived growth factor (PDGF) receptor extracellular immunoglobulin-like domains. Identification of PDGF binding site and neutralizing monoclonal antibodies. *J Biol Chem* **272**: 33037-44.

Lokker N A, Sullivan C M, Hollenbach S J, Israel M A and Giese N A (2002). Platelet-derived growth factor (PDGF) autocrine signaling regulates survival and mitogenic pathways in glioblastoma cells: evidence that the novel PDGF-C and PDGF-D ligands may play a role in the development of brain tumors. *Cancer Res* **62**: 3729-35.

Lyseng-Williamson K and Jarvis B (2001). Imatinib. *Drugs* **61**: 1765-74; discussion 1775-6.

Maguire M P, Sheets K R, McVety K, Spada A P and Zilberstein A (1994). A new series of PDGF receptor tyrosine kinase inhibitors: 3-substituted quinoline derivatives. *J Med Chem* **37**: 2129-37.

Maliepaard M, van Gastelen M A, de Jong L A, Pluim D, van Waardenburg R C, Ruevekamp-Helmers M C, Floot B G and Schellens J H (1999). Overexpression of the BCRP/MXR/ABCP gene in a topotecan-selected ovarian tumor cell line. *Cancer Res* **59**: 4559-63.

Matsui T, Heidaran M, Miki T, Popescu N, La Rochelle W, Kraus M, Pierce J and Aaronson S (1989). Isolation of a novel receptor cDNA establishes the existence of two PDGF receptor genes. *Science* **243**: 800-4.

Matsui T, Pierce J H, Fleming T P, Greenberger J S, LaRochelle W J, Ruggiero M and Aaronson S A (1989). Independent expression of human alpha or beta platelet-derived growth factor receptor cDNAs in a naive hematopoietic cell leads to functional coupling with mitogenic and chemotactic signaling pathways. *Proc Natl Acad Sci U S A* **86**: 8314-8.

McGary E C, Onn A, Mills L, Heimberger A, Eton O, Thomas G W, Shtivelband M and Bar-Eli M (2004). Imatinib mesylate inhibits platelet-derived growth factor receptor phosphorylation of melanoma cells but does not affect tumorigenicity in vivo. *J Invest Dermatol* **122**: 400-5.

Moolenaar W H, Tertoolen L G and de Laat S W (1984). Growth factors immediately raise cytoplasmic free Ca2+ in human fibroblasts. *J Biol Chem* **259**: 8066-9.

Mori S, Tanaka K, Omura S and Saito Y (1995). Degradation process of ligand-stimulated platelet-derived growth factor beta-receptor involves ubiquitin-proteasome proteolytic pathway. *J Biol Chem* **270**: 29447-52.

Morin M J (2000). From oncogene to drug: development of small molecule tyrosine kinase inhibitors as anti-tumor and anti-angiogenic agents. *Oncogene* **19**: 6574-83.

Muller Y A, Li B, Christinger H W, Wells J A, Cunningham B C and de Vos A M (1997). Vascular endothelial growth factor: crystal structure and functional mapping of the kinase domain receptor binding site. *Proc Natl Acad Sci U S A* **94**: 7192-7.

Mullins D E, Hamud F, Reim R and Davis H R (1994). Inhibition of PDGF receptor binding and PDGF-stimulated biological activity in vitro and of intimal lesion formation in vivo by 2-bromomethyl-5-chlorobenzene sulfonylphthalimide. *Arterioscler Thromb* **14**: 1047-55.

Murray-Rust J, McDonald N Q, Blundell T L, Hosang M, Oefner C, Winkler F and Bradshaw R A (1993). Topological similarities in TGF-beta 2, PDGF-BB and NGF define a superfamily of polypeptide growth factors. *Structure* **1**: 153-9.

National cancer institute N (2005). Phase II Study of Imatinib Mesylate in Patients With Gliomas; http://cancer.gov/clinicaltrials/EORTC-16011.

Nister M, Claesson-Welsh L, Eriksson A, Heldin C H and Westermark B (1991). Differential expression of platelet-derived growth factor receptors in human malignant glioma cell lines. *J Biol Chem* **266**: 16755-63.

Oefner C, D'Arcy A, Winkler F K, Eggimann B and Hosang M (1992). Crystal structure of human platelet-derived growth factor BB. *Embo J* **11**: 3921-6.

Ostman A, Andersson M, Hellman U and Heldin C H (1991). Identification of three amino acids in the platelet-derived growth factor (PDGF) B-chain that are important for binding to the PDGF beta-receptor. *J Biol Chem* **266**: 10073-7.

Palmer B D, Smaill J B, Boyd M, Boschelli D H, Doherty A M, Hamby J M, Khatana S S, Kramer J B, Kraker A J, Panek R L, Lu G H, Dahring T K, Winters R T, Showalter H D and Denny W A (1998). Structure-activity relationships for 1-phenylbenzimidazoles as selective ATP site inhibitors of the platelet-derived growth factor receptor. *J Med Chem* **41**: 5457-65.

Pech M, Gazit A, Arnstein P and Aaronson S A (1989). Generation of fibrosarcomas in vivo by a retrovirus that expresses the normal B chain of platelet-derived growth factor and mimics the alternative splice pattern of the v-sis oncogene. *Proc Natl Acad Sci U S A* **86**: 2693-7.

Pollack I F, Randall M S, Kristofik M P, Kelly R H, Selker R G and Vertosick F T (1990). Response of malignant glioma cell lines to epidermal growth factor and platelet-derived growth factor in a serum-free medium. *J Neurosurg* **73**: 106-12.

Prestrelski S J, Arakawa T, Duker K, Kenney W C and Narhi L O (1994). The conformational stability of a non-covalent dimer of a platelet-derived growth factor-B mutant lacking the two cysteines involved in interchain disulfide bonds. *Int J Pept Protein Res* **44**: 357-63.

Raines E W and Ross R (1982). Platelet-derived growth factor. I. High yield purification and evidence for multiple forms. *J Biol Chem* **257**: 5154-60.

Ramakrishnan V, Escobedo M A, Fretto L J, Seroogy J J, Tomlinson J E and Wolf D L (1993). A novel monoclonal antibody dependent on domain 5 of the platelet-derived growth factor beta receptor inhibits ligand binding and receptor activation. *Growth Factors* **8**: 253-65.

Raymond E B A, Van Oosterom A, et al (2004). Multicentre phase II study of imatinib mesylate in patients with recurrent glioblastoma: an EORTC: NDDG/BTG Intergroup study. *J Clin Oncol* . **22**: A-1501.

Reigstad L J, Varhaug J E and Lillehaug J R (2005). Structural and functional specificities of PDGF-C and PDGF-D, the novel members of the platelet-derived growth factors family. *Febs J* **272**: 5723-41.

Robbins K C, Antoniades H N, Devare S G, Hunkapiller M W and Aaronson S A (1983). Structural and immunological similarities between simian sarcoma virus gene product(s) and human platelet-derived growth factor. *Nature* **305**: 605-8.

Roberts W G, Whalen P M, Soderstrom E, Moraski G, Lyssikatos J P, Wang H F, Cooper B, Baker D A, Savage D, Dalvie D, Atherton J A, Ralston S, Szewc R, Kath J C, Lin J, Soderstrom C, Tkalcevic G, Cohen B D, Pollack V, Barth W, Hungerford W and Ung E (2005). Antiangiogenic and antitumor activity of a selective PDGFR tyrosine kinase inhibitor, CP-673,451. *Cancer Res* **65**: 957-66.

Roberts W M, Look A T, Roussel M F and Sherr C J (1988). Tandem linkage of human CSF-1 receptor (c-fms) and PDGF receptor genes. *Cell* **55**: 655-61.

Robey R W, Honjo Y, van de Laar A, Miyake K, Regis J T, Litman T and Bates S E (2001). A functional assay for detection of the mitoxantrone resistance protein, MXR (ABCG2). *Biochim Biophys Acta* **1512**: 171-82.

Ronnstrand L, Mori S, Arridsson A K, Eriksson A, Wernstedt C, Hellman U, Claesson-Welsh L and Heldin C H (1992). Identification of two C-terminal autophosphorylation sites in the PDGF beta-receptor: involvement in the interaction with phospholipase C-gamma. *Embo J* **11**: 3911-9.

Ross R, Glomset J, Kariya B and Harker L (1974). A platelet-dependent serum factor that stimulates the proliferation of arterial smooth muscle cells in vitro. *Proc Natl Acad Sci U S A* **71**: 1207-10.

Rupp E, Siegbahn A, Ronnstrand L, Wernstedt C, Claesson-Welsh L and Heldin C H (1994). A unique autophosphorylation site in the platelet-derived growth factor alpha receptor from a heterodimeric receptor complex. *Eur J Biochem* **225**: 29-41.

Sargent J M (2003). The use of the MTT assay to study drug resistance in fresh tumour samples. *Recent results in cancer research* **161**: 13-25.

Schneller M, Vuori K and Ruoslahti E (1997). Alphavbeta3 integrin associates with activated insulin and PDGFbeta receptors and potentiates the biological activity of PDGF. *Embo J* **16**: 5600-7.

Seifert R A, Hart C E, Phillips P E, Forstrom J W, Ross R, Murray M J and Bowen-Pope D F (1989). Two different subunits associate to create isoform-specific platelet-derived growth factor receptors. *J Biol Chem* **264**: 8771-8.

Shawver L K, Schwartz D P, Mann E, Chen H, Tsai J, Chu L, Taylorson L, Longhi M, Meredith S, Germain L, Jacobs J S, Tang C, Ullrich A, Berens M E, Hersh E, McMahon G, Hirth K P and Powell T J (1997). Inhibition of platelet-derived growth factor-mediated signal transduction and tumor growth by N-[4-(trifluoromethyl)-phenyl]5-methylisoxazole-4-carboxamide. *Clin Cancer Res* **3**: 1167-77.

Simon M P, Pedeutour F, Sirvent N, Grosgeorge J, Minoletti F, Coindre J M, Terrier-Lacombe M J, Mandahl N, Craver R D, Blin N, Sozzi G, Turc-Carel C, O'Brien K P, Kedra D, Fransson I, Guilbaud C and Dumanski J P (1997). Deregulation of the platelet-derived growth factor B-chain gene via fusion with collagen gene COL1A1 in dermatofibrosarcoma protuberans and giant-cell fibroblastoma. *Nat Genet* **15**: 95-8.

Singer H S, Hansen B, Martinie D and Karp C L (1999). Mitogenesis in glioblastoma multiforme cell lines: a role for NGF and its TrkA receptors. *J Neurooncol* **45**: 1-8.

Soria J C, Johnson B E and Chevalier T L (2003). Imatinib in small cell lung cancer. *Lung Cancer* **41 Suppl 1**: S49-53.

Sorkin A, Westermark B, Heldin C H and Claesson-Welsh L (1991). Effect of receptor kinase inactivation on the rate of internalization and degradation of PDGF and the PDGF beta-receptor. *J Cell Biol* **112**: 469-78.

Spritz R A, Strunk K M, Lee S T, Lu-Kuo J M, Ward D C, Le Paslier D, Altherr M R, Dorman T E and Moir D T (1994). A YAC contig spanning a cluster of human type III receptor protein tyrosine kinase genes (PDGFRA-KIT-KDR) in chromosome segment 4q12. *Genomics* **22**: 431-6.

Steck P A, Gallick G E, Maxwell S A, Kloetzer W S, Arlinghaus R B, Moser R P, Gutterman J U and Yung W K (1986). Expression of epidermal growth factor receptor and associated glycoprotein on cultured human brain tumor cells. *J Cell Biochem* **32**: 1-10.

Sugarman B J, Aggarwal B B, Hass P E, Figari I S, Palladino M A, Jr. and Shepard H M (1985). Recombinant human tumor necrosis factor-alpha: effects on proliferation of normal and transformed cells in vitro. *Science* **230**: 943-5.

Sultana S, Zhou R, Sadagopan M S and Skalli O (1998). Effects of growth factors and basement membrane proteins on the phenotype of U-373 MG glioblastoma cells as determined by the expression of intermediate filament proteins. *Am J Pathol* **153**: 1157-68.

Sun P D and Davies D R (1995). The cystine-knot growth-factor superfamily. *Annu Rev Biophys Biomol Struct* **24**: 269-91.

Sundberg C and Rubin K (1996). Stimulation of beta1 integrins on fibroblasts induces PDGF independent tyrosine phosphorylation of PDGF beta-receptors. *J Cell Biol* **132**: 741-52.

Swan D C, McBride O W, Robbins K C, Keithley D A, Reddy E P and Aaronson S A (1982). Chromosomal mapping of the simian sarcoma virus onc gene analogue in human cells. *Proc Natl Acad Sci U S A* **79**: 4691-5.

Takahashi A, Camacho P, Lechleiter J D and Herman B (1999). Measurement of intracellular calcium. *Physiol Rev* **79**: 1089-125.

Todaro G J and Green H (1963). Quantitative studies of the growth of mouse embryo cells in culture and their development into established lines. *J Cell Biol* **17**: 299-313.

U.S. National institutes of health N (2005). Imatinib Mesylate in Treating Patients With Gliomas; http://www.clinicaltrials.gov/ct/gui/show/NCT00039364.

U.S. National institutes of health N (2005). Imatinib Mesylate With or Without Radiation Therapy in Treating Young Patients With Newly Diagnosed or Recurrent Glioma; http://www.clinicaltrials.gov/ct/show/NCT00021229.

Uhrbom L, Hesselager G, Nister M and Westermark B (1998). Induction of brain tumors in mice using a recombinant platelet-derived growth factor B-chain retrovirus. *Cancer Res* **58**: 5275-9.

Uren A, Merchant M S, Sun C J, Vitolo M I, Sun Y, Tsokos M, Illei P B, Ladanyi M, Passaniti A, Mackall C and Toretsky J A (2003). Beta-platelet-derived growth factor receptor mediates motility and growth of Ewing's sarcoma cells. *Oncogene* **22**: 2334-42.

Ustach C V and Kim H R (2005). Platelet-derived growth factor D is activated by urokinase plasminogen activator in prostate carcinoma cells. *Mol Cell Biol* **25**: 6279-88.

Ustach C V, Taube M E, Hurst N J, Jr., Bhagat S, Bonfil R D, Cher M L, Schuger L and Kim H R (2004). A potential oncogenic activity of platelet-derived growth factor d in prostate cancer progression. *Cancer Res* **64**: 1722-9.

Uutela M, Lauren J, Bergsten E, Li X, Horelli-Kuitunen N, Eriksson U and Alitalo K (2001). Chromosomal location, exon structure, and vascular expression patterns of the human PDGFC and PDGFC genes. *Circulation* **103**: 2242-7.

Valius M, Bazenet C and Kazlauskas A (1993). Tyrosines 1021 and 1009 are phosphorylation sites in the carboxy terminus of the platelet-derived growth factor receptor beta subunit and are required for binding of phospholipase C gamma and a 64-kilodalton protein, respectively. *Mol Cell Biol* **13**: 133-43.

Westermark B and Wasteson A (1976). A platelet factor stimulating human normal glial cells. *Exp Cell Res* **98**: 170-4.

Wilson A P (2000). Cytotoxicity and viability assays. *Animal cell culture (3rd edition)*: 175-219.

Xu X, Shen J, Mall J W, Myers J A, Huang W, Blinder L, Saclarides T J, Williams J W and Chong A S (1999). In vitro and in vivo antitumor activity of a novel immunomodulatory drug, leflunomide: mechanisms of action. *Biochem Pharmacol* **58**: 1405-13.

Yamada S M, Yamaguchi F, Morrison R S, Takahashi H and Teramoto A (1998). [Inhibition of fibroblast growth factor receptor 1 expression in human glioblastoma cell contributes to the cell growth suppression]. *No To Shinkei* **50**: 1101-5.

Yarden Y, Escobedo J A, Kuang W J, Yang-Feng T L, Daniel T O, Tremble P M, Chen E Y, Ando M E, Harkins R N, Francke U and et al. (1986). Structure of the receptor for platelet-derived growth factor helps define a family of closely related growth factor receptors. *Nature* **323**: 226-32.

Yarden Y, Kuang W J, Yang-Feng T, Coussens L, Munemitsu S, Dull T J, Chen E, Schlessinger J, Francke U and Ullrich A (1987). Human proto-oncogene c-kit: a new cell surface receptor tyrosine kinase for an unidentified ligand. *Embo J* **6**: 3341-51.

Yu S, Pu P and Jiang D (1998). [A study on the relationship among activity of PDGFBB autocrine loop, cell proliferation and apoptosis in human glioma cells]. *Zhonghua Bing Li Xue Za Zhi* **27**: 352-5.

Zwerner J P and May W A (2002). Dominant negative PDGF-C inhibits growth of Ewing family tumor cell lines. *Oncogene* **21**: 3847-54.

Chapter 5

Investigations on the mechanism of action of new monastrol analogs on human glioblastoma cells by confocal laser-scanning microscopy

5.1 Introduction

5.1.1 The mitotic spindle as a pharmacological target in cancer chemotherapy

Due to its crucial role in cell division the mitotic spindle has been targeted in the treatment of cancer for several decades. The mitotic spindle consists of dynamic structures, the microtubules, and of associated proteins, contributing to the assembly and functionality of the whole spindle complex.

5.1.1.1 The role of microtubules in the mitotic spindle

The microtubules are hollow cylindrical structures made up of 13 protofilaments, which are composed of alternating α- and β-tubulin along the microtubule longitudinal axis. The process of polymerization, which necessitates GTP, shows different dynamics at the both ends of the microtubules, giving them a polar character. Both ends grow and shorten alternately by polymerization and depolymerization, respectively. However, the plus- (+) end shows a net growth by rapid polymerization, and at the minus- (-) end net shortening occurs, due to a dominating depolymerization (Walker et al. 1988).

In the mitosis phase, all microtubules are associated at their (-)-ends with the microtubule-organizing centers, the centrosomes, from which they are nucleated (Bailly and Bornens 1992). Various classes of microtubules are distinguished in the mitotic spindle, serving different functions during mitosis (Fig. 5-3). At the early anaphase the daughter chromosomes

start to get separated polewards by a shortening of the kinetochore microtubules and by a contributing effect of motor proteins. In the later anaphase the spindle poles move apart from each other by the action of motor proteins, that connect and couple overlapping microtubules at the equator of the mitotic spindle. Furthermore, astral microtubules radiate away from the centrosomes in all directions, and stabilize the position of the spindle in the mitotic cell by contributing to the separation of the poles.

5.1.1.2 Microtubule-interfering agents

Microtubule-interfering agents, also named "spindle-poisons", represent an important class of anticancer drugs, and some of them have been used in the treatment of cancer for almost 40 years. The earliest class of compounds, which was identified of arresting cells in the mitosis phase with aberrant mitotic spindles, were the vinca alkaloids (Palmer et al. 1960). The two representatives vincristine and vinblastine were introduced into clinical practice in the 1960s. Still they are in use as important chemotherapeutic agents in combinative treatment regimen, e.g. for the curative therapy of testicular cancer, Hodgkin disease, and acute lymphocytic leukemia, or for the palliative therapy of solid tumors. Since the vinca alkaloids had derived from the periwinkle plant (*Vinca rosea* L.), many other compounds were identified to act as so-called "spindle poisons" after the intensive screening of natural compounds.

In 1986, paclitaxel entered into clinical trials. Due to its therapeutic success, the interest in microtubules as a pharmacological target structure increased dramatically, and led to extensive efforts put in the development of further, more potent, and better tolerated inhibitors of the microtubule function. Many other natural products were identified for their interfering activity with the microtubular dynamics. Amongst them, currently evaluated in preclinical investigations, are naturally derived compounds, such as epothilones, which are secondary metabolites from myxobacteria (Altmann et al. 2000), and coral-derived eleutherobin derivatives (Hamel et al. 1999; McDaid et al. 1999). By now, also many new taxanes, paclitaxel prodrugs, and new formulations of classical microtubule-interfering agents are in clinical development (Wood et al. 2001).

All of those drugs have a common principle in their mechanism of action. The microtubule function is maintained in a dynamic state of polymerization and depolymerization (Mitchison and Kirschner 1984; Desai and Mitchison 1997). Antimicrotubule drugs disrupt this dynamic process, leading to a breakdown of the integrative function of polymeric tubulin. In this way it also can be explained, how e.g. the taxanes and the vinca alkaloids cause mitotic arrest, although acting in reciprocal ways. While the vinca

alkaloids promote destabilization of microtubules, leading to depolymerization, paclitaxel and other taxanes block the microtubule depolymerization (Schiff et al. 1979; Schiff and Horwitz 1980). Both attacks to the mitotic spindle function lead to a blockade in the cell cycle progression from the prometaphase/metaphase to the anaphase (Jordan and Wilson 1998). Fig. 5-1 and Fig. 5-2 show the chemical structures of microtubule-interfering agents, inhibiting microtubule polymerization and depolymerization, respectively.

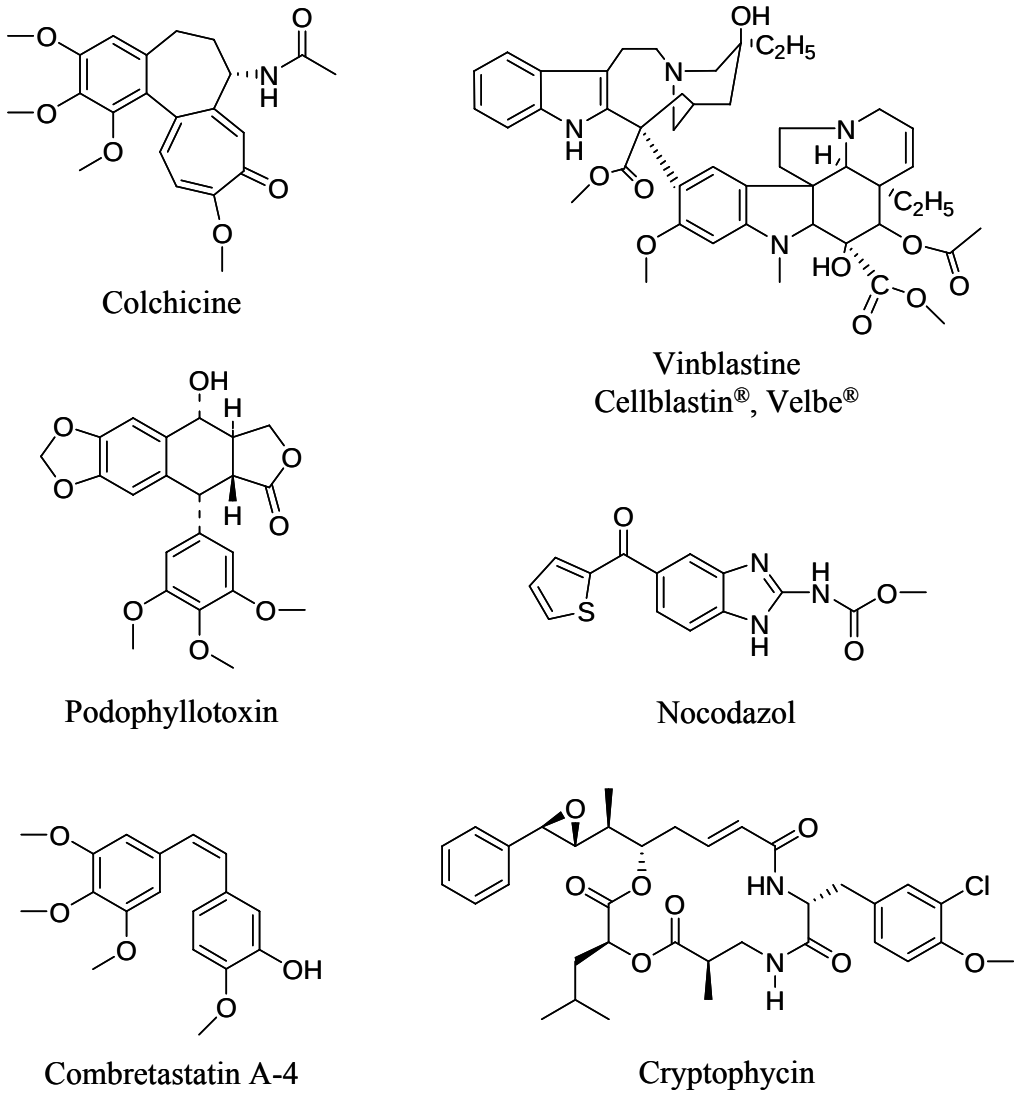

Figure 5-1: Chemical structures of compounds leading to microtubule depolymerization. Although producing depolymerization via a common mechanism, these compounds can be subdivided by their differing binding sites, whereas the vinca alkaloids and cryptophycin, as well as colchicine, podophyllotoxin, nocodazole, and combretastatin A-4 share common tubulin binding sites (Mollinedo and Gajate 2003).

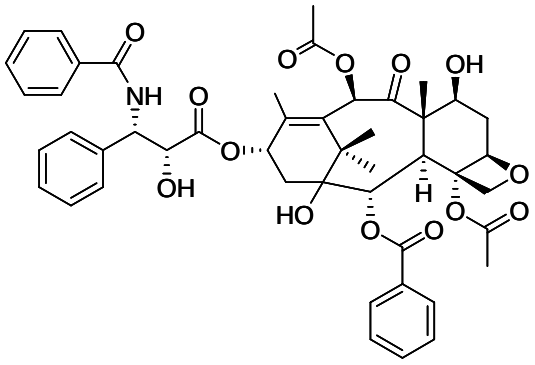

Paclitaxel
Taxol®

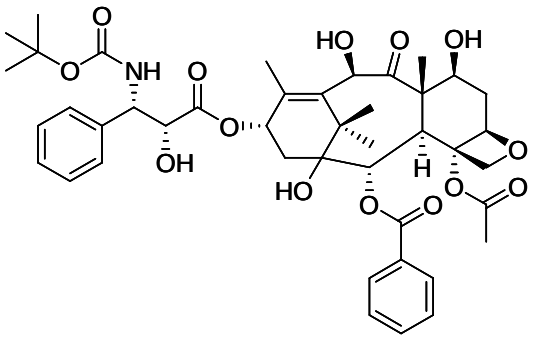

Docetaxel
Taxotere®

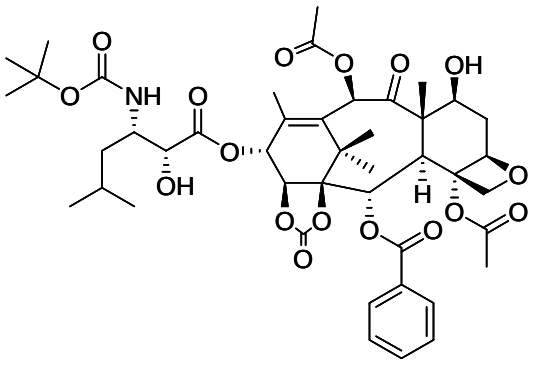

IDN 5109

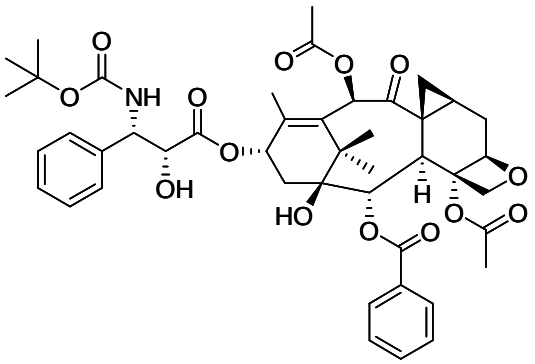

RPR 109881A

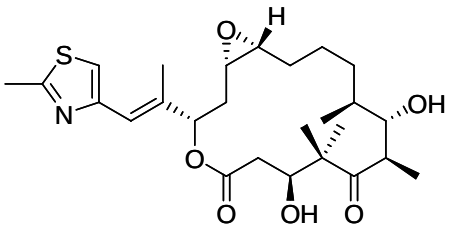

Epothilone A

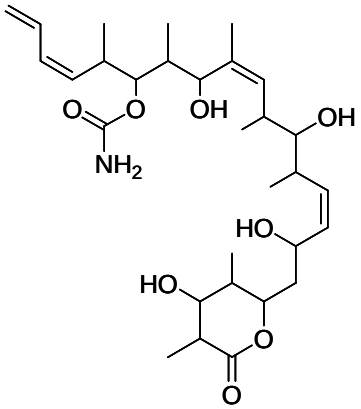

Discodermolide

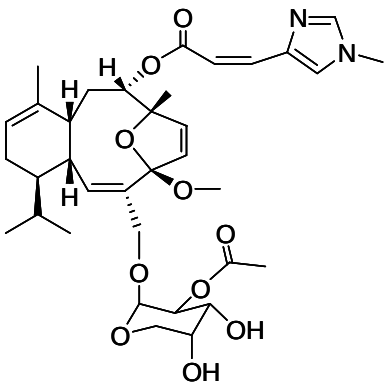

Eleutherobin

Figure 5-2: Inhibitors of microtubule depolymerization. The cellular target of paclitaxel, docetaxel, RPR 109881A, IDN 5109, and discodermolide is the β-tubulin in the microtubule polymer. The exact binding site for eleutherobin is not known yet (Wood et al. 2001; Mollinedo et al. 2003).

Figure 5-3 further illustrates the role of microtubules in mitosis. Destabilization of microtubules, e.g. by microtubule-interfering agents, leads to free kinetochore sites, which activate the mitotic spindle assembly checkpoint. This protein complex blocks the transition to the anaphase by inhibition of the anaphase-promoting complex. On the other hand, microtubule-stabilizing agents block the formation of spindle fibers even before mitosis is started. When cells are in mitosis already, these agents stabilize the spindle, finally preventing cytokinesis and cell cycle progression.

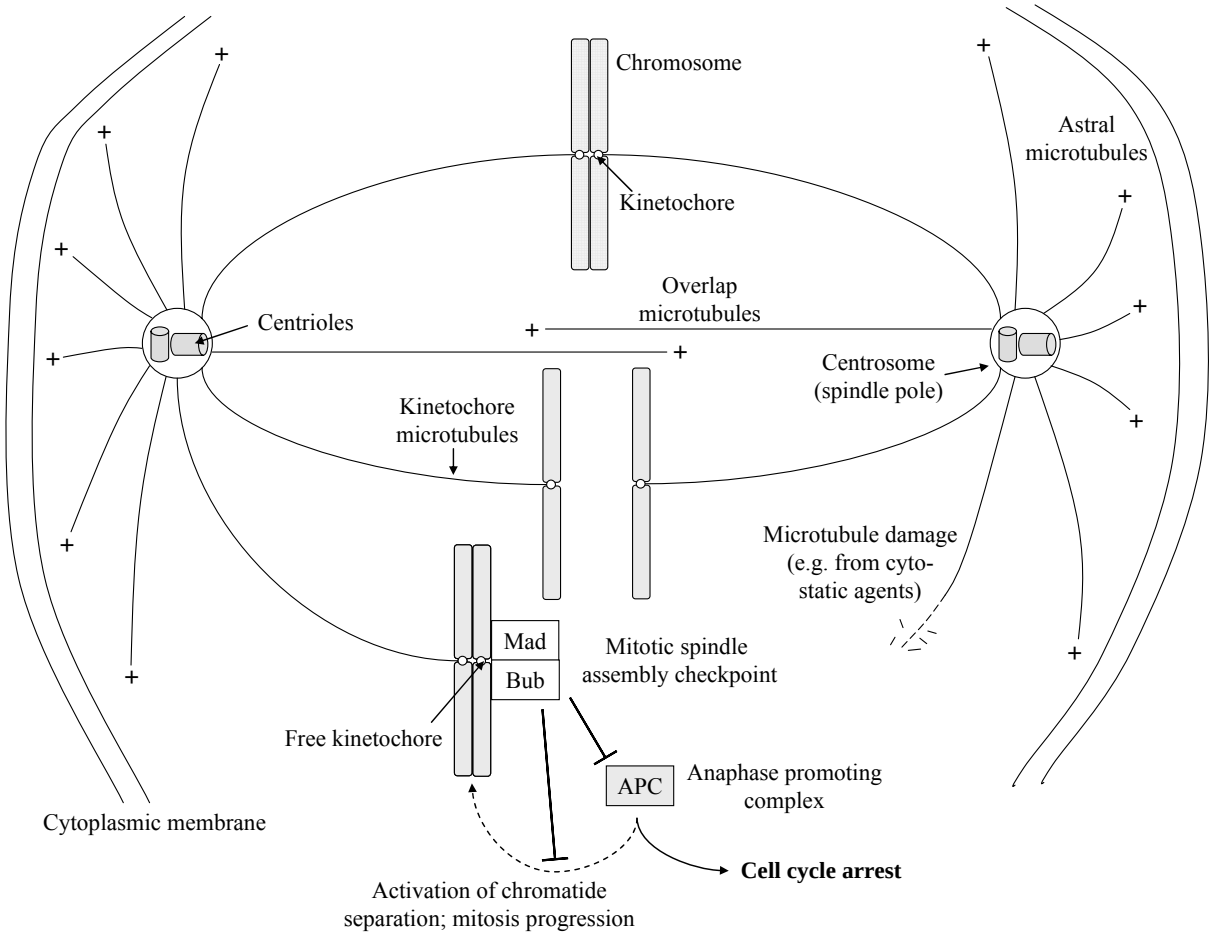

Figure 5-3: Schematic drawing of the mitotic spindle. Two so-called asters are formed by microtubules, radiating away from the microtubule-organizing centers (centrosomes), which contain a pair of centrioles each. The microtubules serve different functions during mitosis. The chromosomes are attached to the spindle via kinetochore microtubules, which contribute to the chromosome movement towards to spindle poles. The symmetrical respectively bipolar shape of the spindle complex is maintained by overlap microtubules, also responsible for spindle pole separation in the anaphase. The astral microtubules contribute to the positioning of the spindle and to the separation of the poles. Destabilization of microtubules, e.g. by microtubule-interfering agents, leads to free kinetochore sites, which activate the mitotic spindle assembly checkpoint. This protein complex blocks the transition to the anaphase by inhibition of the anaphase promoting complex (from Sorger et al. 1997, modified). Bub: budding uninhibited by benzimidazole; Mad: mitosis arrest deficient.

However, several interactions of drugs with tubulin provoke side effects, which are unrelated to the effect on the mitotic spindle. Tubulin polymers (microtubules) also play a crucial role in non-mitotic cytoskeletal functions, such as motility and cell-cell contacts. Thus, the disruption of the microtubule dynamics with drugs not only affects dividing cells, but also non-dividing cells.

New compounds are developed with a major emphasis to overcome common limitations in the clinical applicability. A major problem in the clinical use of current agents is the development of resistance due to p-glycoprotein (pgp) 170 expression in the tumor tissue or due to alterations in the tubulin binding sites, reducing the affinity and thereby the efficacy of current tubulin-binding drugs. The vinca alkaloids and the taxanes are both pgp substrates (Kohno et al. 1988; Hunter et al. 1991; Zacherl et al. 1994), and it has been shown that pgp expression causes resistance and reduced sensitivity, respectively, to those compounds in vitro (Izquierdo et al. 1996; Loe et al. 1996). The new compounds IDN 5109 (Bayer, Leverkusen, Germany) and RPR 109881A (Aventis, Strasbourg, France) are expected to circumvent the pgp-mediated multi-drug resistance in vivo, and already have shown promising preclinical effects when applied to pgp-overexpressing tumor cell lines (Polizzi et al. 1999; Gelmon et al. 2000). However, not only pgp is involved in the resistance to multiple antineoplastic agents, but also, for instance, the multi-drug resistance-associated protein (MRP) and the p110 major vault glycoprotein (Bosch and Croop 1996; Izquierdo et al. 1996; Loe et al. 1996).

In summary, despite the ongoing development of novel microtubule-interfering compounds it is likely, that they will suffer from the same severe side effects as the older classical drugs.

5.1.2 Control of the mitotic spindle assembly

The assembly and disassembly of microtubules is physiologically regulated by a balance of microtubule-stabilizing and destabilizing proteins, binding along the microtubules (Andersen 2000). Stabilizing proteins include the large group of the so-called microtubule-associated proteins (MAPs) (Mandelkow and Mandelkow 1995). These MAPs are substrates of the cyclin-dependent kinase 1 (CDK1), and, depending on their phosphorylation state, they control the microtubule dynamic properties in the transition from the G2 to the M phase of the cell cycle. During mitosis an increased phosphorylation reduces the affinity of the MAPs to microtubules, and thereby their promoting effect on tubulin-polymerization (Drechsel et al.

1992; Masson and Kreis 1995; Ookata et al. 1995). Destabilizing factors, promoting microtubule depolymerization, are oncoprotein 18/stathmin, and katanin (McNally and Vale 1993; Larsson et al. 1997; Ahmad et al. 1999; Andersen 2000). The *Xenopus* kinesin central motor 1 (XKCM1), a kinesin-related protein, particularly contributes to the microtubule depolymerization during mitotic spindle assembly (Walczak et al. 1996).

Furthermore, microtubule-binding motor proteins are essential for the microtubule function. These motor proteins can be subdivided into two major classes, the kinesins and dyneins. They move continuously along the microtubules, and thereby can carry various membrane-enclosed organelles, such as mitochondria, golgi stacks, and secretory vesicles, to their destination within the cell. Moreover, they serve important functions in the mitosis phase, e.g. movement of cytoskeletal filaments against each other, which is an indispensable process too. The N-terminal kinesins play a crucial role in mitotic spindle formation and in chromosome separation and transport. They move towards the (+)-end of the microtubules (Mandelkow and Hoenger 1999). However, another kinesin subfamily, the C-terminal motor domain type kinesins move towards the (-)-end (Noda et al. 2001; Xu et al. 2002). The dyneins are also (-)-end-directed motor proteins, contributing to vesicular trafficking, and to the positioning of cell organelles.

During mitosis, the chronology of interplay between microtubule-dynamics and motor proteins is controlled by several regulatory molecules, such as Bub, and Mad kinases. Those are essential components of the mitotic spindle assembly check point (Sorger et al. 1997; Skoufias et al. 2001), which monitors that all chromosomes are bivalently attached to microtubules via kinetochores, before the mitosis is moving from the metaphase to the anaphase (Li and Benezra 1996; Rudner and Murray 1996; Sorger et al. 1997).

Other proteins, such as the Aurora B family kinases, play an essential role in chromosome segregation and subsequent cytokinesis, the cytoplasmic division of the cell in the end of mitosis. They are also required for the orientation, condensation, and cohesion of chromosomes, and they are involved in microtubular dynamics (Shannon and Salmon 2002). Representing crucial elements in the progression of mitosis, the Aurora B family kinases and other regulatory proteins may provide new targets in cancer chemotherapy (Wood et al. 2001). Presently, the disruption of microtubule dynamics is of major clinical relevancy.

5.1.3 Motor protein-dependent mitotic spindle assembly and maintenance

Although tubulin is the most abundant protein within the mitotic spindle, numerous additional proteins contribute to its proper functionality. The most prominent proteins are the kinesins, microtubule-associated motor proteins.

Due to the cell cycle-dependent degradation of several kinesins, it has been suggested that the expression of certain subtypes is restricted to proliferating tissues, and crucial for mitosis progression (Brown et al. 1994; Funabiki and Murray 2000; Hill et al. 2000). Furthermore, these mitotic kinesins have been demonstrated to serve different functions during cell division (Tab. 5-1). Dysfunction of certain members of this protein family has been shown to result in mitotic arrest. For example, the kinesin CENP-E has been shown to be an essential component of the mitotic spindle assembly checkpoint in vitro (Abrieu et al. 2000). It connects the checkpoint complex to free kinetochores of microtubule-attached chromosomes (Schaar et al. 1997; Yao et al. 2000) and interacts with different kinetochore proteins (Chan et al. 1998). Playing a vital role in mitosis, this and other kinesins have been considered as potential new pharmacological targets for the treatment of malignancies.

Table 5-1: Role of various mitotic kinesins in mitosis (from Wood et al. 2001).

Mitotic kinesin type	Function	Experimental evaluation	Mitotic arrest(1)
Eg5 (2)	Spindle pole separation	Human cells	+
HSFT	Microtubule anchorage at the spindle poles	Human cells	-
MKLP1	Microtubule organization in metaphase spindle midzone	Human cells	+
	Late mitotic spindle microtubule organization and cytokinesis	*Drosophila, Caenorhabditis elegans*	-
Kif4	Metaphase chromosome alignment	*Xenopus* egg extracts and embryos	n.d.
CENP-E	Metaphase chromosome alignment	Human cells	+
Kid	Metaphase chromosome alignment	*Xenopus* egg extracts	n.d.
MCAK	Anaphase chromosome alignment	Human cells	-
RabK6	Cytokinesis	Human cells	-

(1) Dysfunction of kinesin causes mitotic arrest (+), dysfunction does not cause mitotic arrest (-). effect not determined (n.d.)

(2) Eg5 is the *Xenopus laevis* homolog of the human KSP kinesin.

The general structural features of the kinesin motors are similar throughout the whole protein superfamily (Vale and Fletterick 1997). The motor domain, which is the force-producing element of the protein, is divided into two major parts. The first part is a highly conserved globular catalytic core, whereas the second part, the neck region, has a length of ca. 40 amino acids, either adjacent at the N- or C-terminus of the catalytic core. Beyond the motor domain many kinesin proteins contain a long α-helical coiled-coil domain, which is termed the "stalk". Finally, an additional globular domain is often found at the end of the stalk. This tail domain is thought to target the motor to a particular cargo within the cell.

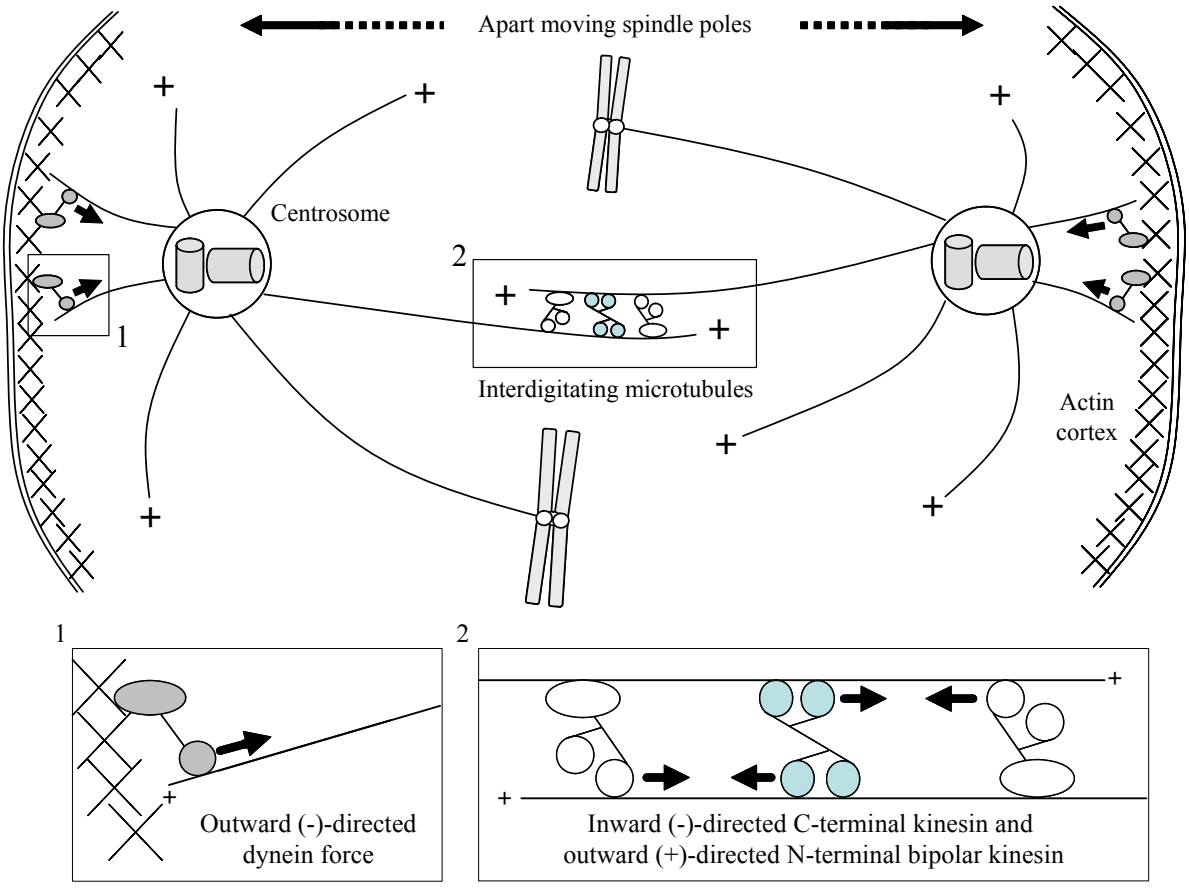

Figure 5-4: Schematic drawing of the prometaphase-metaphase transition. The spindle poles move apart from each other, due to the overweight of outward-directed forces. Dynein mediates the interaction between astral microtubules and the actin cortex (dynactin). The major contribution to the outward-directed forces is given by the bipolar kinesins, which enforce antiparallel sliding of the interdigitating microtubules of the spindle midzone. Together, these two forces overcome the inward-directed force, produced by C-terminal kinesins, also located at the spindle midzone. The short arrows indicate the moving direction of the motor proteins along the microtubules, which is opposite to the direction of the produced force.

Driven by ATP hydrolysis, the kinesins produce a directed force along microtubules.The N-terminal kinesins are (+)-directed, the C-terminal kinesins are (-)-directed. In mitosis, the N-terminal kinesins produce an outward-directed force, whereas the C-terminal kinesins act vice versa. A further (-)-directed force is exerted by the dynein motor proteins. The specific movement of the mitotic spindle is suggested, not to be driven by the sole action of one type of motor protein, but to be produced by multiple, complementary and antagonistic motors, which work simultaneously (Sharp et al. 2000).

In the interphase-prophase the centrosome doubles, and between the two future poles of the spindle slightly interdigitating microtubules are formed. This initial spindle assembly is balanced by dynein, mediating the interaction with the actin cortex at the cell membrane, and C-terminal kinesins in the midzone of the spindle. The dyneins pull the poles apart (outward-directed force) and the C-terminal kinesins push them towards each other (inward-directed force). The C-terminal kinesin force is limited due to the low extent of microtubule overlap in the midzone. With the continuous growth of the interdigitating microtubules, the kinesin force gradually increases until a steady state between the dynein and the kinesin forces is reached.

After the degradation of the nuclear envelope in the prometaphase, the length of the astral microtubules is decreased and the position of the bipolar spindle is determined and maintained by the action of the C-terminal kinesins and the bipolar kinesins (e.g. Eg5 kinesin). The bipolar kinesins generate an outward-directed force and are located in the spindle midzone too. The poles move further apart due to the overcome of the inward-directed C-terminal kinesin force by the action of bipolar kinesins and cortical dynein (Fig. 5-4). This further elongation of the spindle results in the “metaphase spindle steady state structure”, holding a tension between the spindle poles, generated by the competing inward and outward forces. After passing the metaphase-anaphase checkpoint (mitotic spindle assembly checkpoint) the tension is released by inactivation of the C-terminal kinesins. Right before the spindle disassembles again the final steady state is achieved in the telophase.

5.1.4 Mitotic arrest through Eg5 kinesin inhibition

The inhibition of Eg5 kinesin results in a characteristic spindle morphology, the monaster spindle (Fig. 5-5). This might be explained by an imbalance between the outward- and inward-directed forces, generated by dyneins and C- and N-terminal kinesins, after inhibition of Eg5. The C-terminal kinesins slide the antiparallel overlap microtubules vice versa to the

Eg5 kinesin-directed force, resulting in a net inward movement of the spindle poles (Fig. 5-5A). Thereby, the kinetochore microtubules, in part attached to chromosomes, are pushed apart from the spindle pole axis (Fig. 5-5B, 5-5C). Finally, free as well as chromosome-attached kinetochore microtubules radiate away from the maximally approached spindle poles (Fig. 5-5D). Since both centrosomes still consist of two intact and separate entities after this process, the term "monoastral spindle" seems incorrect, although this is the current denomination.

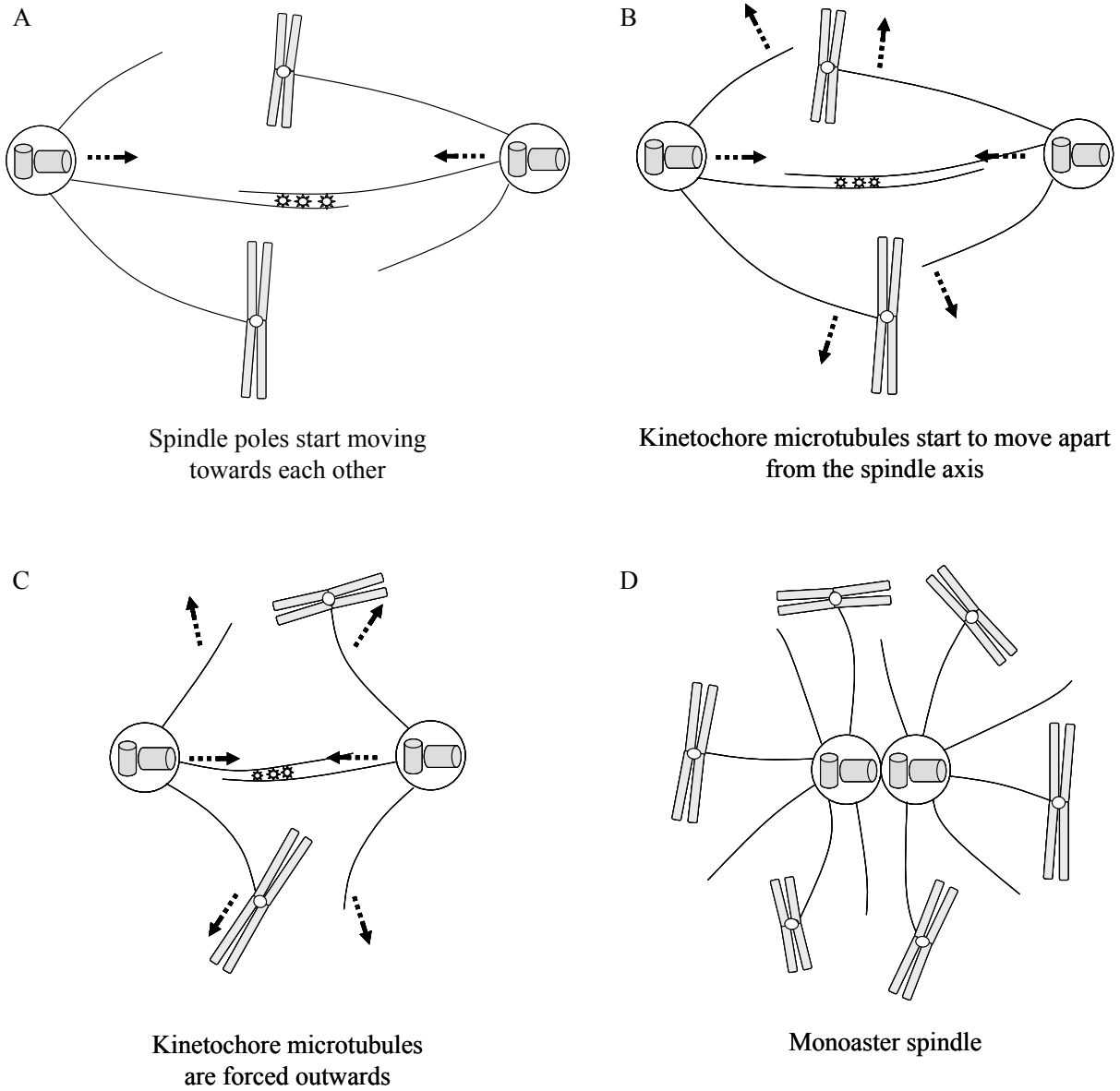

Figure 5-5: Schematic drawing of monaster spindle formation. The inhibition of bipolar Eg5 kinesin leads to an overweight of the inward-directed force of the C-terminal kinesins. The spindle poles are pulled towards each other (A). Due to the decreasing distance between the poles (B) the kinetochore microtubules are forced apart from the spindle axis (C). Finally, the spindle poles are situated right next to each other, and the microtubules originating from both poles form the characteristic so-called monaster spindle (D).

However, using fluorescence microscopic techniques, the centrosomes can hardly be distinguished from each other, unless they are specifically stained, distinctly different from tubulin. After the monaster spindle has completely formed, mitotic arrest may occur due to several free kinetochores of chromosomes, which are only partially connected to microtubules. As a consequence, the mitotic spindle assembly checkpoint cannot be satisfied and the transition from the metaphase to the anaphase is blocked. Since Eg5 is exclusively expressed during mitosis, this mechanism of inhibition is likely to leave other essential cellular functions unaffected, especially in non-mitotic cells. Due to this major difference to the commonly used microtubule-interfering agents, specific Eg5 kinesin inhibitors are considerd a very promising approach to the development of a new class of anticancer agents with minimal side effects on resting cells.

5.1.5 Eg5 kinesin inhibitors

In 1998, Sakowicz et al. screened a number of natural compounds for selective inhibition of kinesin (Sakowicz et al. 1998), and identified adociasulfate-2, which competitively inhibited the kinesin motor domain interaction with microtubules in vitro. However, this first kinesin inhibitor was not specific for a certain kinesin subtype.

Since only the Eg5 kinesin was known to be crucial for the formation of a bipolar mitotic spindle (Blangy et al. 1995), the formation of monopolar spindles was used as a determinant in the search for specific Eg5 inhibitors. Mayer et al. identified the first specific Eg5 kinesin inhibitor, monastrol, using a mitotic spindle phenotype-based screening method (Mayer et al. 1999). This compound, a 4-aryl-3,4-dihydro-pyrimidine-2(1H)-thione, led to the formation of a monopolar spindle, and also a direct inhibition of the Eg5 motor domain activity was confirmed in vitro. Moreover, Eg5 inhibition by monastrol did not affect the transition from the G2 cell cycle phase to mitosis, led to a reversible mitotic arrest, and had no effect on cellular processes involving other kinesins (Mayer et al. 1999; Kapoor et al. 2000). These results brought about the concept of the specific Eg5 kinesin inhibition as a new approach in cancer chemotherapy. However, racemic monastrol and its eutomer, (*S*)-monastrol, were determined to be only moderately potent allosteric inhibitors of Eg5 (Gartner et al. 2005), with IC_{50} values of 34 μM and 14 μM, respectively, determined in the microtubule-stimulated ATPase activity assay (Maliga et al. 2002). Therefore, new monastrol analogs were synthesized (Gartner et al. 2005; Sarli et al. 2005), in order to obtain more potent Eg5 kinesin

inhibitors. In 2003, Hotha et al. reported on the tetrahydro-β-carboline compound HR22C16, which selectively inhibited Eg5 kinesin with an IC_{50} value of 800 nM (Hotha et al. 2003). A derivative of HR22C16 showed an about one order of magnitude higher potency, with an IC_{50} value of 90 nM. However, it was not reported whether this compound was cell permeable or not. A series of β-carboline derivatives was synthesized by Sunder-Plassmann et al. (Sunder-Plassmann et al. 2005). After the screening of a small library of 60 compounds for Eg5 inhibitory activity, the most potent compound showed an IC_{50} value of 650 nM.

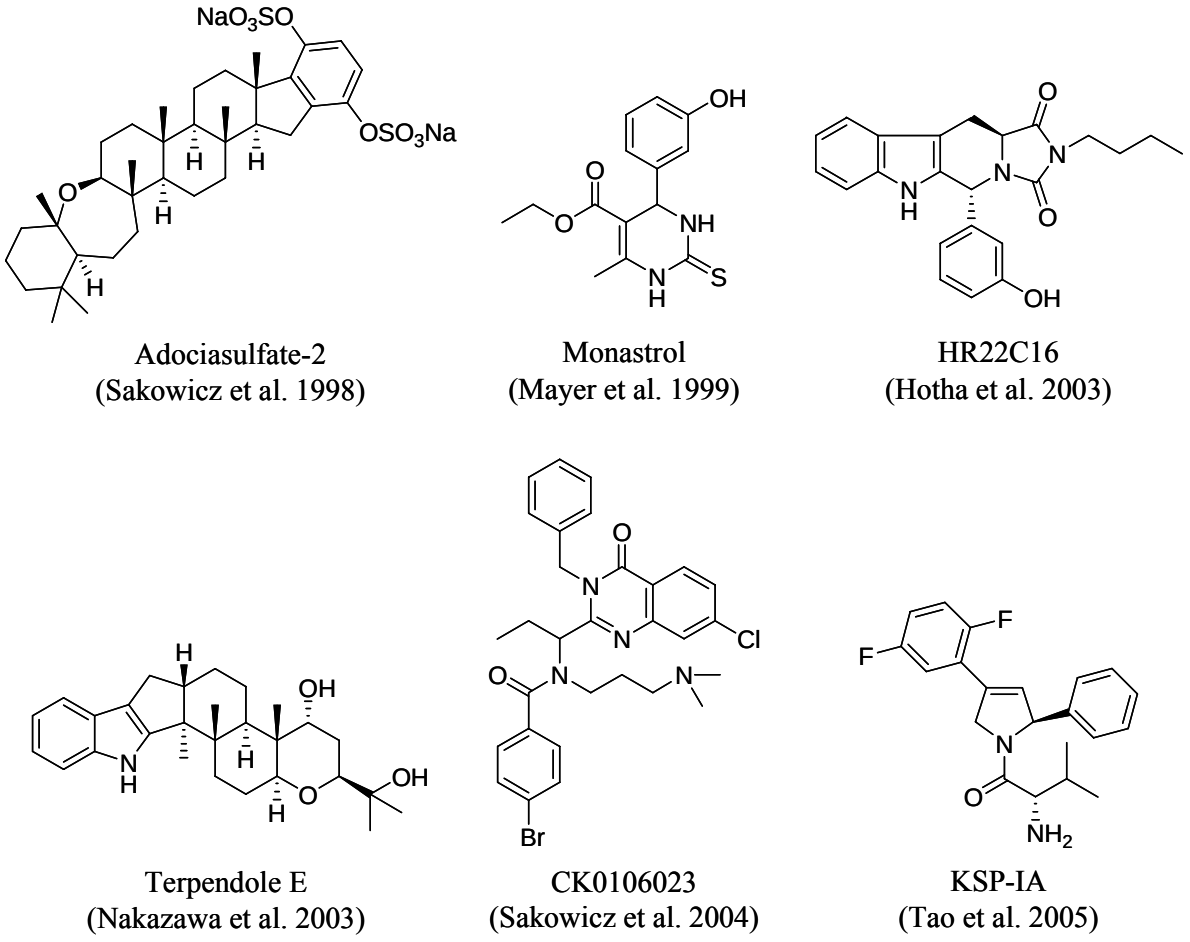

Figure 5-6: Chemical structures of various kinesin inhibitors. Adociasulfate-2, was isolated from a marine sponge, the genus *Haliclona* (also known as *Adocia*). Sakowicz et al. suggested kinesins as a useful pharmacological target for the first time (Sakowicz et al. 1998). The identification of the first specific Eg5 kinesin inhibitor monastrol (Mayer et al. 1999) initiated the development and the preclinical evaluation of further, more potent Eg5 inhibitors as potential new anticancer agents. Among the other lead compounds structural resemblance to monastrol is only observed for the β-carbolin derivative HR22C16 (Hotha et al. 2003). Terpendole E inhibits Eg5 kinesin specifically (Nakazawa et al. 2003), but with an even lower potency than monastrol. Based on CK0106023 (Sakowicz et al. 2004), a series of new 2-(aminomethyl)quinazolinone derivatives has been synthesized, of which one is in clinical phase II evaluation. The KSP-IA represents the most potent specific Eg5 kinesin inhibitor by now (Tao et al. 2005).

Further lead structures are currently considered for the development of more potent specific Eg5 kinesin inhibitors. Among them are terpendole E (IC_{50} = 23 μM) (Nakazawa et al. 2003), CK0106023 with a K_i value of 12 nM (Sakowicz et al. 2004), and KSP-IA, a compound derived from a dihydropyrazole lead structure (IC_{50} = 10 nM Tao et al. 2005).

5.2 Objective

The inhibition of kinesin Eg5 by small molecules, such as monastrol, is currently evaluated as an approach to develop a novel class of antiproliferative drugs for the treatment of malignant tumors. Due to the moderate potency of the lead compound monastrol, new monastrol analogs were synthesized by Giannis and coworkers at the University of Leipzig (Gartner et al. 2005; Sarli et al. 2005), in order to obtain more potent Eg5 kinesin inhibitors. With respect to the treatment of primary and secondary CNS tumors, several of those compounds were evaluated in our laboratory for their antiproliferative activity against human glioblastoma cell variants (Müller et al. 2006), using the crystal violet chemosensitivity assay (Bernhardt et al. 1992). Compared to monastrol, the antiproliferative potency of the investigated compounds was at least one order of magnitude higher. The compounds were neither inactivated by hydrolysis nor by binding to serum proteins. Furthermore, at effective antiproliferative concentrations, the compounds were neither substrates nor modulators of pgp in the flow cytometric calcein-AM assay (Homolya et al. 1993; Hollo et al. 1994; Homolya et al. 1996). The results have been published in part by Müller et al. (Müller et al. 2006).

The objective of this work was to investigate the effect of new monastrol analogs on human glioblastoma cells by means of confocal laser-scanning microscopy. The experiments were performed to investigate, whether the observed antiproliferative activity of the test compounds was accompanied by formation of monaster spindles and subsequent mitotic arrest of the treated cells. Since the common clinical side effects of classical microtubule-interfering agents are ascribed to the damage of the microtubule cytoskeleton (Quasthoff and Hartung 2002), the effect of the new monastrol analogs on the cytoskeleton of quiescent cells was also evaluated. The effects of the new compounds were compared to the classical tubulin-depolymerizing agent vinblastine. Furthermore, the effect on the β-actin cytoskeleton was investigated, which is also an essential component of the cytoskeleton of mitotic and quiescent cells.

5.3 Materials and methods

5.3.1 Tested compounds

The new monastrol analogs MG-Pr99-S, MG-Pr98-S, VS-17, VS-38, VS-48, and VS-54, were synthesized and characterized as described (Gartner et al. 2005; Sarli et al. 2005). These compounds as well as another substance from this series, VS-83, were provided by the workgroup of Prof. Giannis (University of Leipzig, Germany). S-Trityl-L-cysteine (Brier et al. 2004) was purchased from MP BIOMEDICALS (Eschwege, Germany), whereas monastrol, prepared as described (Gartner et al. 2005), also was provided by Prof. Giannis. 10 mM stock solutions were prepared in DMSO; a 1 mM stock solution of vinblastine (SIGMA, Munich, Germany) was made in 70 % ethanol. All compound stocks were stored at –20 °C.

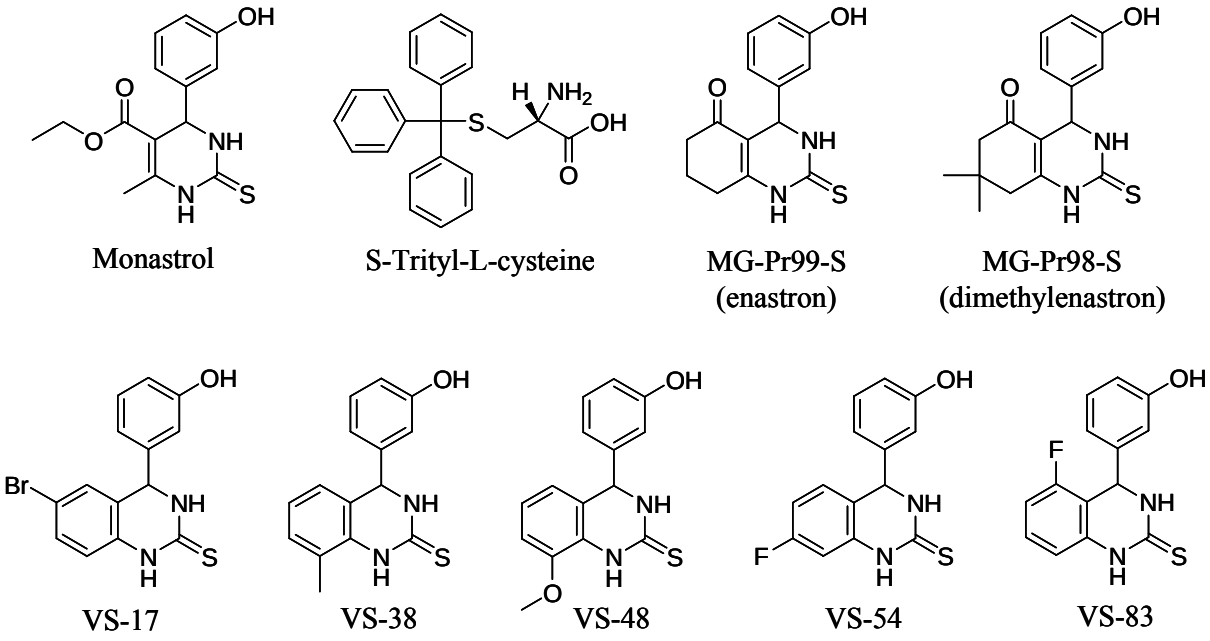

Figure 5-7: Chemical structures of the selective Eg5 inhibitor monastrol, the non-specific kinesin inhibitor S-trityl-L-cysteine, and the new monastrol analogs.

5.3.2 Culture of the human glioblastoma cells

The human U-87 MG (ATCC HTB 14, passage 126) glioblastoma/astrocytoma cell line (Beckman et al. 1971) was obtained from the American Type Culture Collection (ATCC).

Cell banking and quality control were performed according to the "seed stock concept" (Hay 1988). The cells were grown in Eagle´s minimum essential medium (EMEM, Sigma, Deisenhofen, Germany), containing L-glutamine, 2.2 g/l $NaHCO_3$, 110 mg/l sodium pyruvate, and 5 % fetal calf serum (FCS, Biochrom, Berlin, Germany). The cells were cultured in a water-saturated atmosphere of 95 % air and 5 % carbon dioxide at 37 °C in 25-cm² culture flasks (Nunc, Wiesbaden, Germany), and were serially passaged following trypsinization using trypsin (0.05 %)/EDTA(0.02 %) (Roche Diagnostics, Mannheim, Germany). Mycoplasma contamination was routinely monitored, and only mycoplasma-free cultures were used.

5.3.3 Confocal laser-scanning microscopy

5.3.3.1 Treatment of the cells

Cells were seeded into 8-well Lab-Tek Chamber Slides (NUNC, Wiesbaden, Germany). At 75 % confluence the culture medium was replaced with medium containing 50 µM monastrol, 1 µM S-trityl-L-cysteine, or 10 nM vinblastine. The concentrations of the new monastrol analogs were selected on the basis of the chemosensitivity data, obtained by the kinetic crystal violet assay: VS-17: 10 µM; VS-38: 5 µM; VS-48: 10 µM; VS-54: 5 µM; VS-83: 5 µM; MG-Pr99-S: 1 µM; MG-Pr98-S: 5 µM. Cells were incubated at 37 °C for 2 hours.

5.3.3.2 Fixation and permeabilization of the glioblastoma cells

After the incubation with drugs, the medium was carefully removed, and the cells were fixed with 4 % paraformaldehyde solution in phosphate buffered saline (PBS) for 20 minutes at room temperature. Thereafter, each well was washed 3 times with PBS containing 0.5 % bovine serum albumin (BSA, SERVA, Heidelberg, Germany). Cells were permeabilized by incubation with PBS, containing 0.5 % BSA and 1 % Triton-X 100 (SERVA, Heidelberg, Germany) for 10 minutes at room temperature, followed by three washing steps with PBS 0.5 % BSA.

5.3.3.3 Staining

Chromosomes were stained with SYTOXGreen® nucleic acid staining dye (MOLECULAR PROBES, Eugene, OR, USA). For double staining, microtubules were labeled using the mouse anti-human α-tubulin primary antibody (DIANOVA, Hamburg, Germany) and Cy5™-conjugated anti-mouse secondary antibody (DIANOVA). Triple staining of DNA,

microtubules, and Eg5 kinesin was performed using SYTOXGreen®, α-tubulin primary antibody, secondary labeled with the Alexa Fluor® 546-conjugated goat anti-mouse secondary antibody (MOLECULAR PROBES), and anti-human Eg5 antibody (BD Biosciences Pharmingen, Heidelberg, Germany). All antibodies were used as a 1:200 dilution in PBS, containing 0.5 % BSA. β-actin was stained with Alexa Fluor® 647 phalloidin (MOLECULAR PROBES). Microscopic images were acquired with a Carl Zeiss Axiovert 200M LSM510 confocal laser-scanning microscope. Multifluorescence image acquisition was performed in the multitrack acquisition mode. The acquisition parameters are given in the respective figure legends.

5.3.3.4 Image processing

False colours were used for β-actin and Eg5 kinesin (red), tubulin (green) and DNA (blue). Images (Fig. 5-8, 5-9, 5-11, 5-13, 5-15) were processed with the AutoDeBlur deconvolution software.

5.4 Results

5.4.1 Differential spindle formation in human glioblastoma cells

5.4.1.1 Effect of monastrol on the spindle formation of human glioblastoma cells

Fig. 5-8 shows the characteristic effects of monastrol and vinblastine on the spindle formation in human U-87 MG glioblastoma cells. Compared to the untreated cells, clear differences in the spindle formation were observed. The untreated control showed normal bipolar spindles. Monastrol induced a distinctly differing spindle, where the chromosomes surrounded the microtubules, radiating away from the spindle poles. The displayed image in Fig. 5-8 shows an earlier stage in monaster formation, according to Fig. 5-5C. The two spindle poles are still approaching towards each other and can be distinguished as separate entities. As expected, neither the integrity of the microtubular spindle fibers was affected, nor the condensed state of the chromatin. This indicates that the cell was not able to progress in mitosis, which finally would have led to the decondensation of the chromosomal DNA, suggesting that the cell was arrested at the mitotic spindle assembly checkpoint.

After treatment with the microtubule-destabilizing agent vinblastine, the DNA was still condensed to chromosomes. However, no microtubules were built up. The chromosomes were surrounded by depolymerized tubulin. Few brightly fluorescent spots within the labeled tubulin indicate the centrosomes, containing the centrioles, the microtubule-generating centers, with a high tubulin content. As becomes obvious, no mitotic checkpoint can be passed after treatment with vinblastine.

5.4.1.2 Effect of new monastrol derivatives on the spindle formation of human glioblastoma cells

The characteristic monaster formation was observed after incubation with monastrol as well as with the new monastrol derivatives VS-38, VS-54, VS-83, MG-Pr99-S (enastron), and MG-Pr98-S (dimethylenastron). No monasters, but normal spindle formation was observed with the compounds VS-17 and VS-48. The incubation of the cells with the non-specific kinesin inhibitor S-trityl-L-cysteine and the monastrol analog VS-83 induced spindles similar, but distinctly different from the type of monaster, which is induced by the selective Eg5 inhibitors (Fig. 5-9).

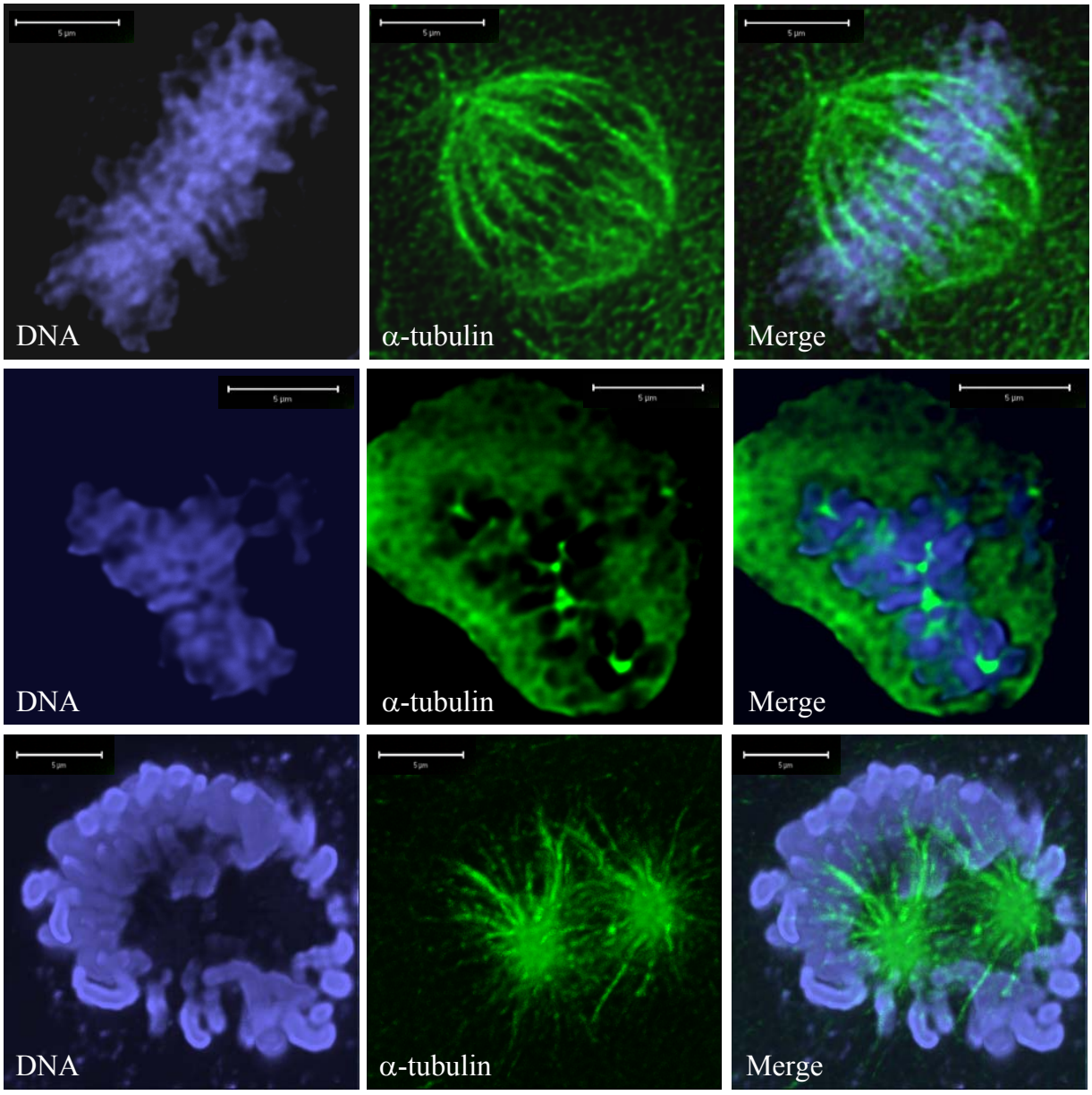

Figure 5-8: Mitotic U-87 MG cells, stained with SYTOXGreen® nucleic acid staining dye and immunofluorescently labeled α-tubulin. Upper row: control; the untreated cells show a normal mitosis metaphase, with arrangement of chromosomes in the middle plane perpendicular to the spindle axis. Middle row: vinblastine; the formation of the mitotic spindle is impeded by the microtubule-interfering agent vinblastine, leading to tubulin-embedded chromosomes. Lower row: treatment with monastrol. The displayed spindle formation after monastrol treatment shows the movement of the two spindle poles towards each other, due to the specific inhibition of the Eg5 kinesin. This results into an overweighted dynein action, leading to an approach of the spindle poles. In these pictures (lower row), the spindle formation is caught on its way to a characteristic monaster. Plan-Apochromat 63x/1.4 oil, Ar 488, HFT 488, LP505; HeNe 633, HFT UV/488/543/633, LP560. Upper and middle row images were processed with 2-D deconvolution; lower row images were obtained by 3-D deconvolution from a z-stack sum-projection.

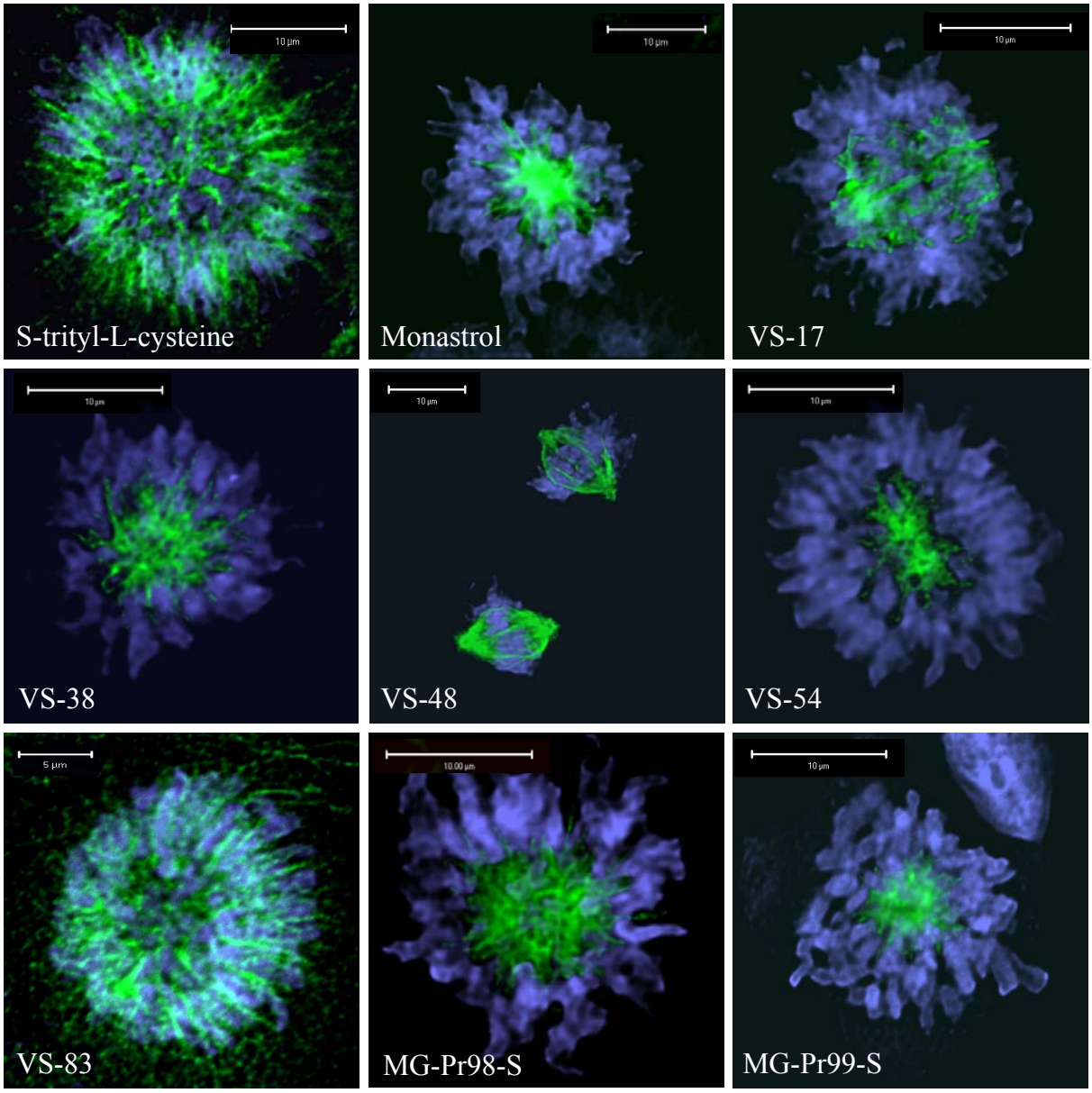

Figure 5-9: Mitotic U-87 MG cells after treatment with the specific Eg5 inhibitor monastrol, the non-specific inhibitor S-trityl-L-cysteine, and various new monastrol analogs. Except for VS-17 and VS-48 all other compounds produce the characteristic monaster spindles. Interestingly, with the non-specific kinesin inhibitor S-trityl-L-cystein, a different morphology is observed in the monaster. Compared to the characteristic spindle morphology after treatment with specific Eg5 inhibitors, a higher number of microtubules is observed, which are not attached to chromosomes yet. This suggests that S-trityl-L-cystein interacts in an earlier phase of mitosis, when only a few chromosomes are partially connected to kinetochore microtubules. Plan-Apochromat 63x/1.4 oil, Ar 488, HFT 488, LP505; HeNe 633, HFT UV/488/543/633, LP560. All images were processed with 2-D deconvolution.

5.4.2 Expression and distribution of Eg5 in human glioblastoma cells

For the determination of the expression and distribution of Eg5 kinesin in quiescent cells, U-87 MG were triple stained for Eg5, microtubules, and nuclei. Even though not in mitosis, the quiescent cells showed Eg5 kinesin expression (Fig. 5-10). The motor protein was observed to be widely distributed within the cytoplasm, forming dot-like clusters. Furthermore, it lacked significant colocalization with microtubules, their primary site of interaction in mitosis. During mitosis Eg5 was colocalized with tubulin at and between the spindle poles (Fig. 5-11). As expected, no colocalization with astral microtubules was observed.

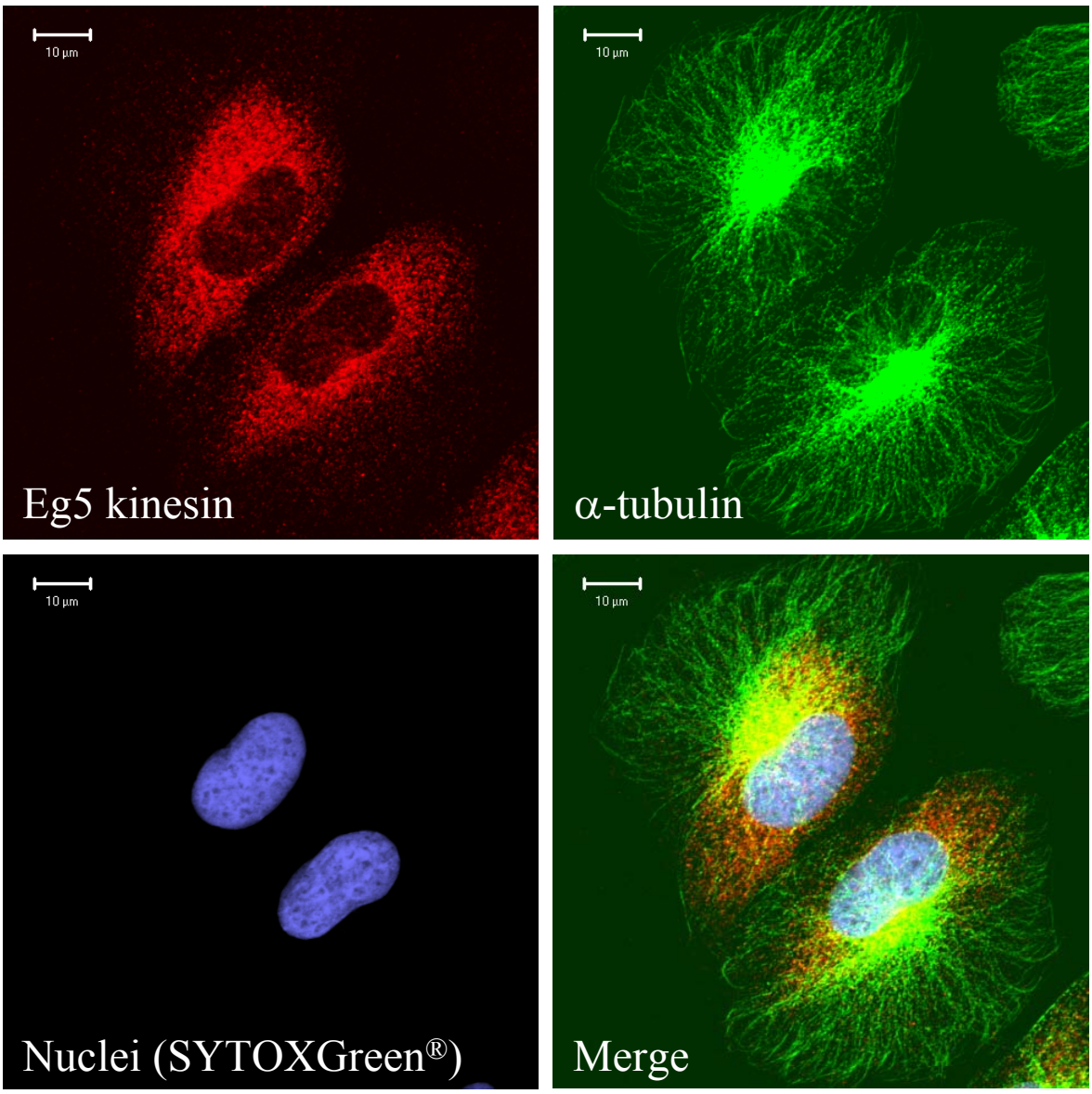

Figure 5-10: Multifluorescence image of fixed U-87 MG cells. In these quiescent cells Eg5 is distributed all over the cytoplasm with a perinuclear accumulation. Quantitative colocalization with microtubules is not observed. Plan-Apochromat 63x/1.4 oil; Ar 488, HFT 488, LP505; .HeNe 543, HFT 488/543, LP560; HeNe 633, UV/488/543/633, LP650.

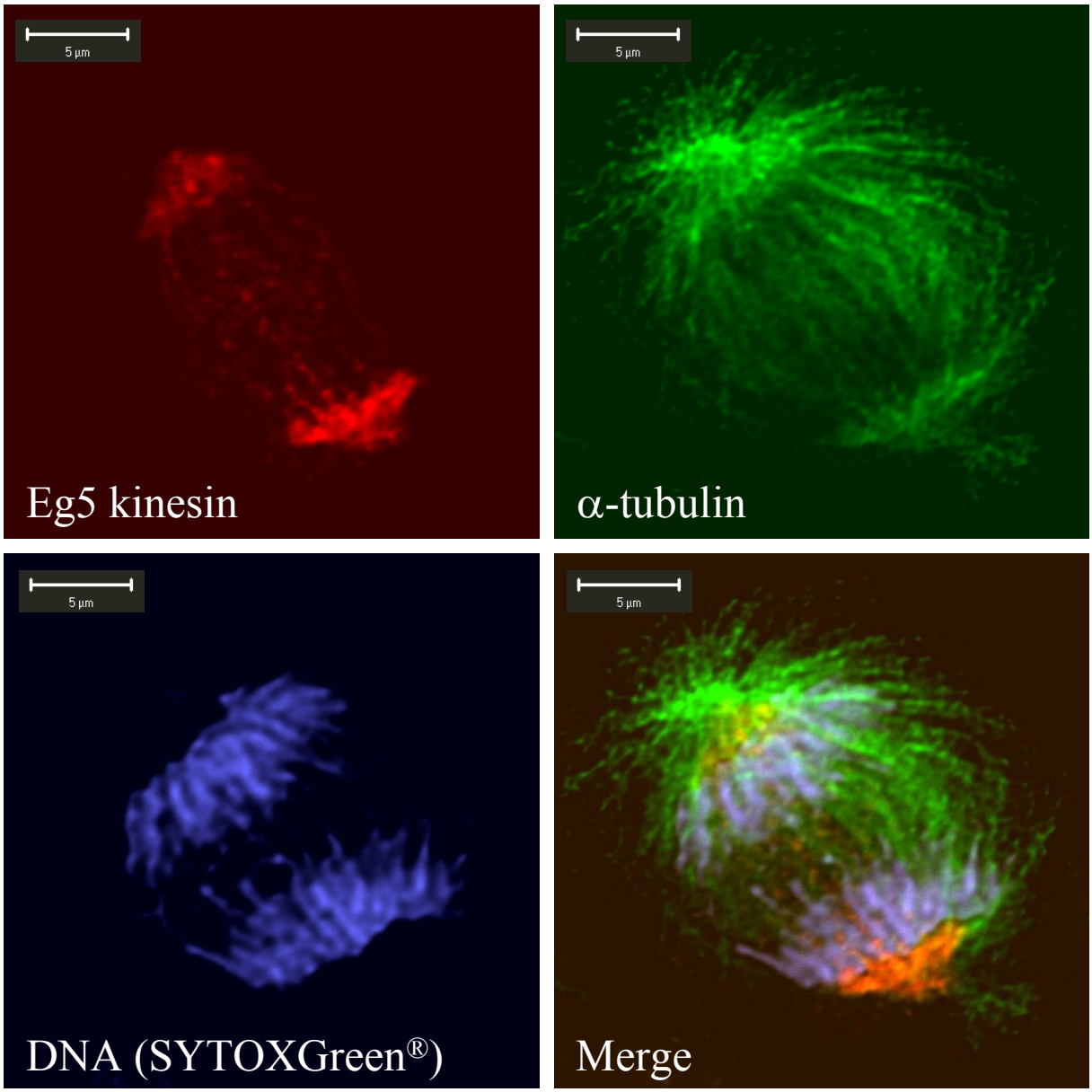

Figure 5-11: Multifluorescence image of a mitotic U-87 MG cell. Eg5 kinesin is colocalized with spindle microtubules, parallel to the spindle axis, representing interdigitating overlap microtubules. No colocalization was observed with astral microtubules. The images also indicate that Eg5 is not colocalized with the more outward-directed kinetochore microtubules, which are connected to the chromosomes. Plan-Apochromat 63x/1.4 oil; Ar 488, HFT 488, LP505; .HeNe 543, HFT 488/543, LP560; HeNe 633, UV/488/543/633, LP650. Images were processed with 2-D deconvolution.

5.4.3 Effect of vinblastine on Eg5 distribution in human glioblastoma cells

Vinblastine-treated non-dividing cells showed the same Eg5 distribution pattern, even though the microtubule cytoskeleton was collapsed due to the depolymerizing effect of the vinca alkaloid (Fig. 5-12). Again, a quantitative colocalization of the two proteins was not observed. After treatment with vinblastine, Eg5 showed a diffuse distribution in the mitotic cell, and partial colocalization with tubulin (Fig. 5-13).

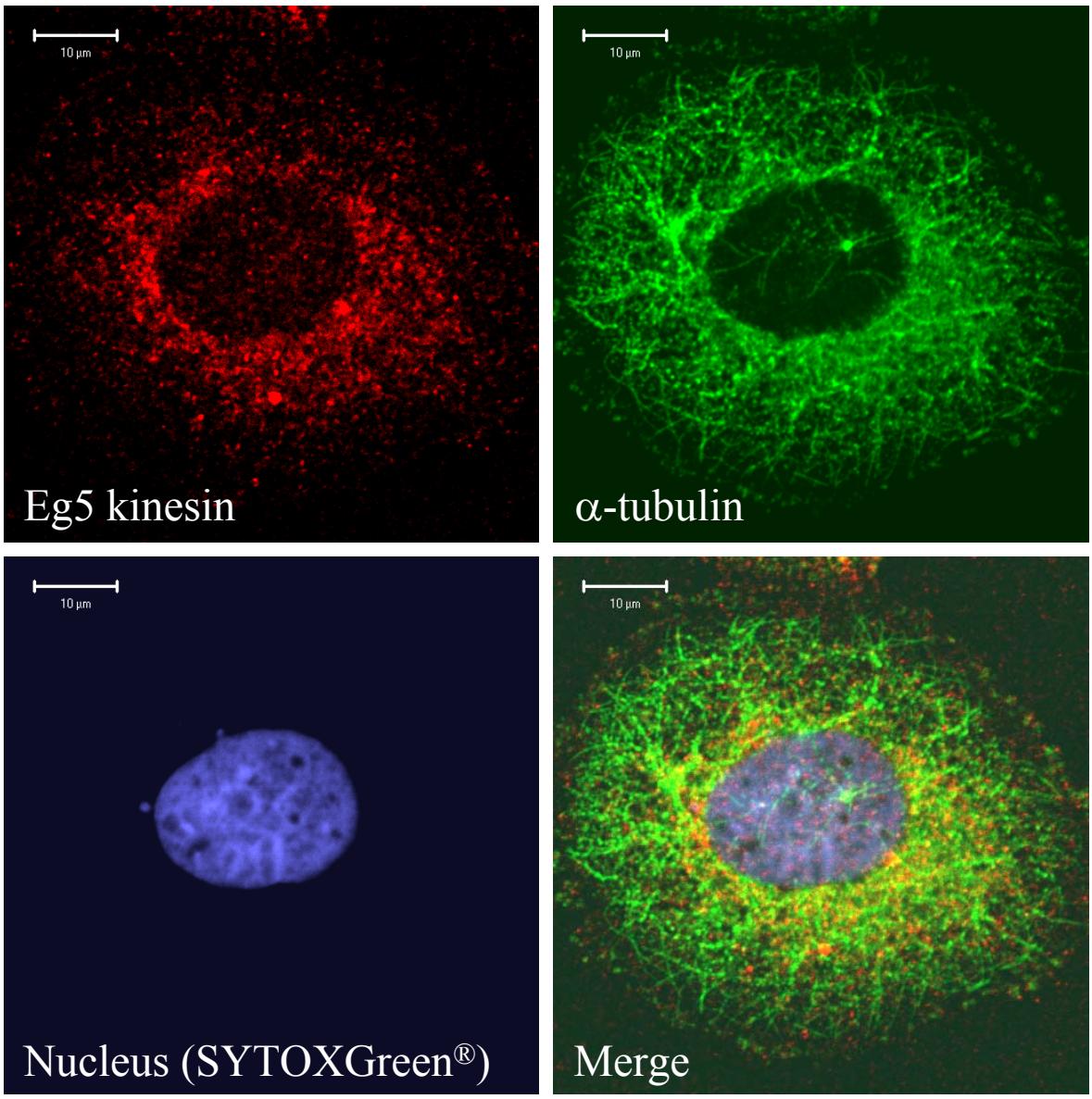

Figure 5-12: Effect of vinblastine on the Eg5 kinesin distribution in U-87 MG. The cell is rounded up due to the disrupted microtubule-cytoskeleton. However, the Eg5 distribution is not changed. The same dot-like clusters are observed as in the untreated control cells. Plan-Apochromat 63x/1.4 oil; Ar 488, HFT 488, LP505; .HeNe 543, HFT 488/543, LP560; HeNe 633, UV/488/543/633, LP650.

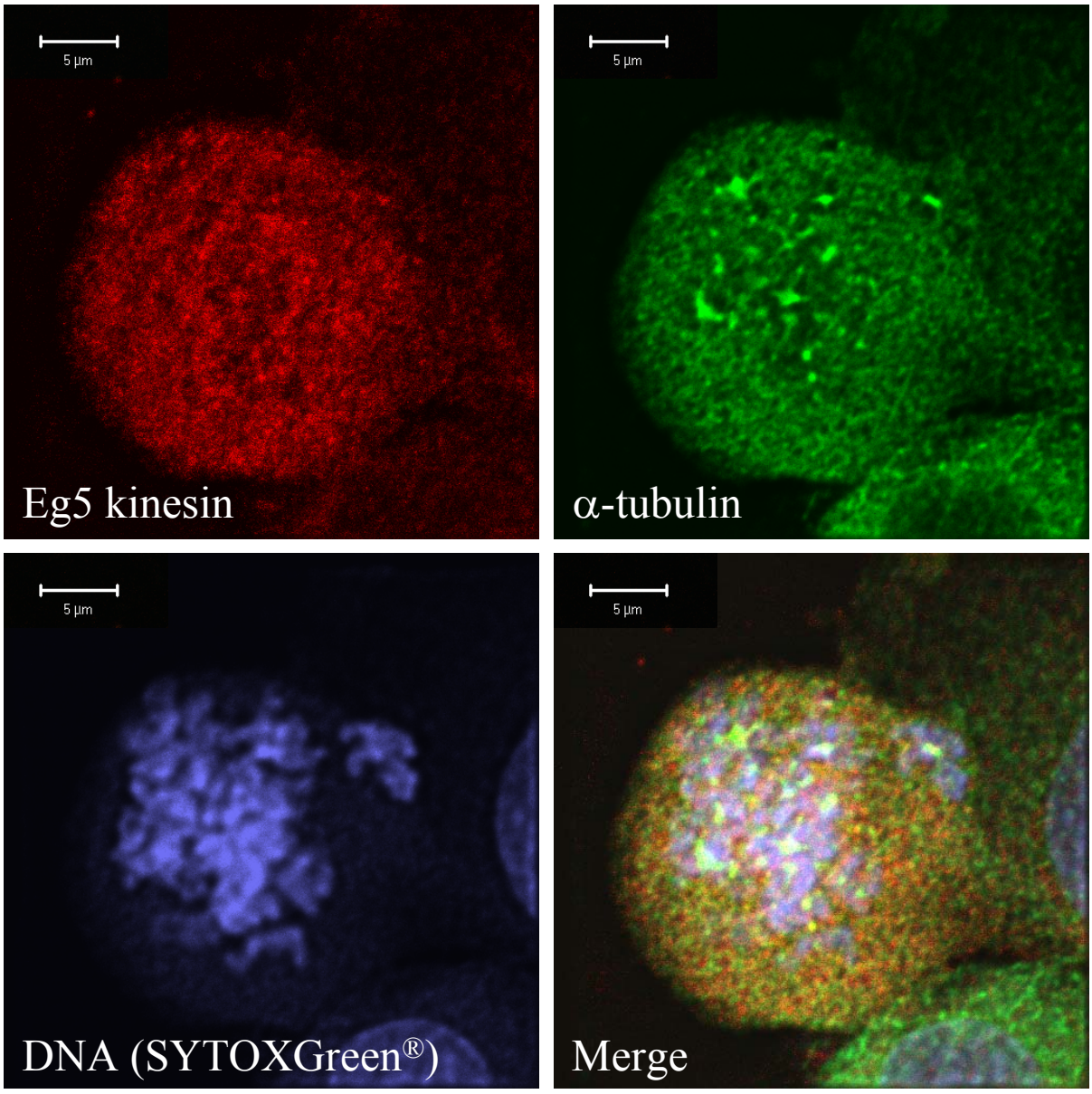

Figure 5-13: Mitotic U-87 MG cells after treatment with vinblastine. The Eg5 kinesin is distributed all over the cell. It does not form big clusters any more, but shows partial colocalization with the depolymerized tubulin. As becomes obvious from the adjacent cells, Eg5 expression is much lower in non-mitotic cells. Plan-Apochromat 63x/1.4 oil; Ar 488, HFT 488, LP505; .HeNe 543, HFT 488/543, LP560; HeNe 633, UV/488/543/633, LP650. Images were processed with 2-D deconvolution.

5.4.4 Effect of new monastrol analogs on Eg5 distribution in human glioblastoma cells

As exemplarily shown for MG-Pr99-S (Fig. 5-14), the incubation of the glioblastoma cells with the new monastrol analogs, did not change the cellular distribution of Eg5 in quiescent cells, compared to the untreated control (Fig. 5-10). In mitosis Eg5 mainly remained colocalized with the spindle microtubules (Fig. 5-15).

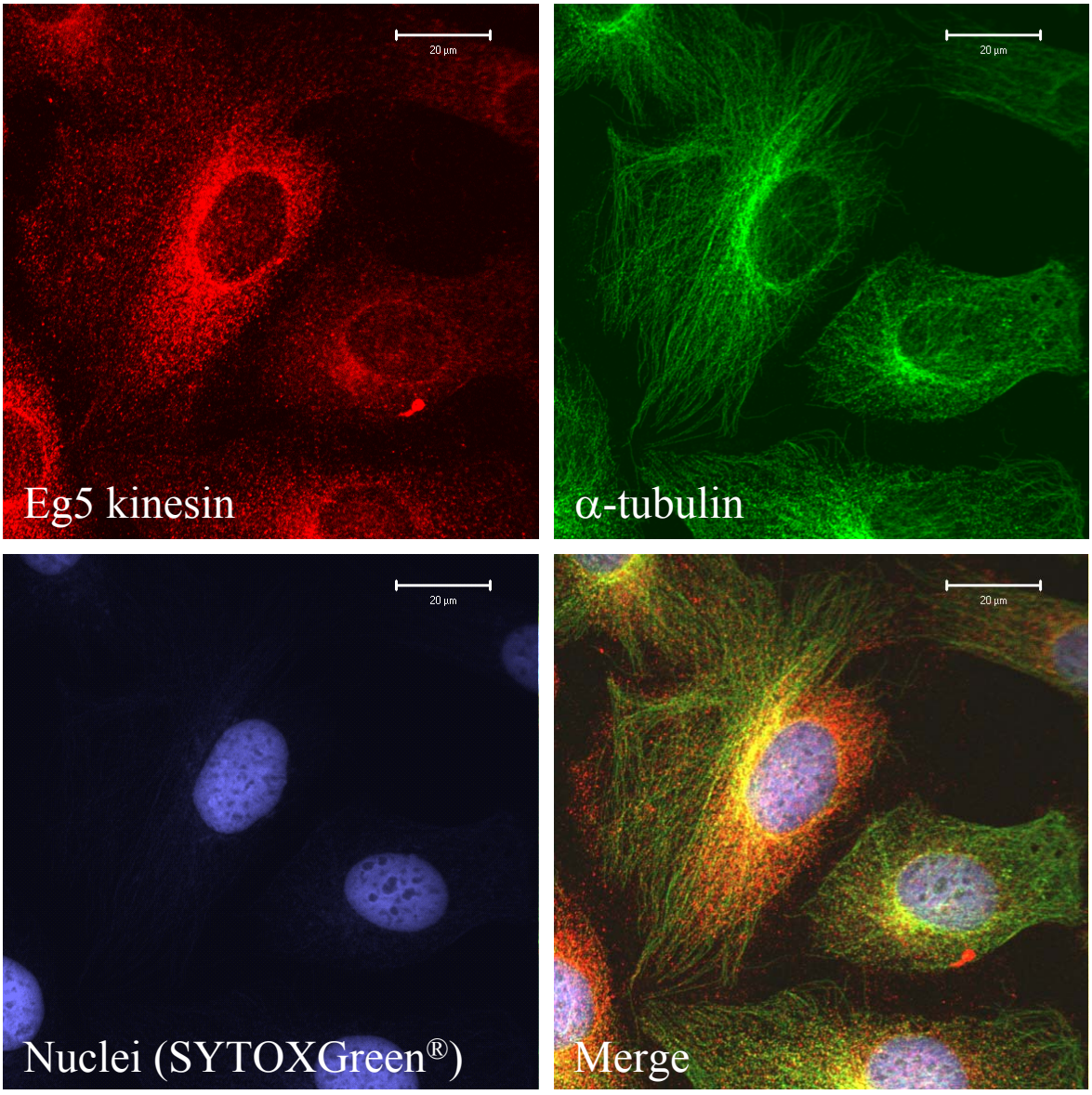

Figure 5-14: Quiescent U-87 MG cells after incubation with MG-Pr99-S. Compared to the untreated control (Fig. 5-10), the cellular Eg5 distribution is not altered. Plan-Apochromat 63x/1.4 oil; Ar 488, HFT 488, LP505; HeNe 543, HFT 488/543, LP560; HeNe 633, UV/488/543/633, LP650.

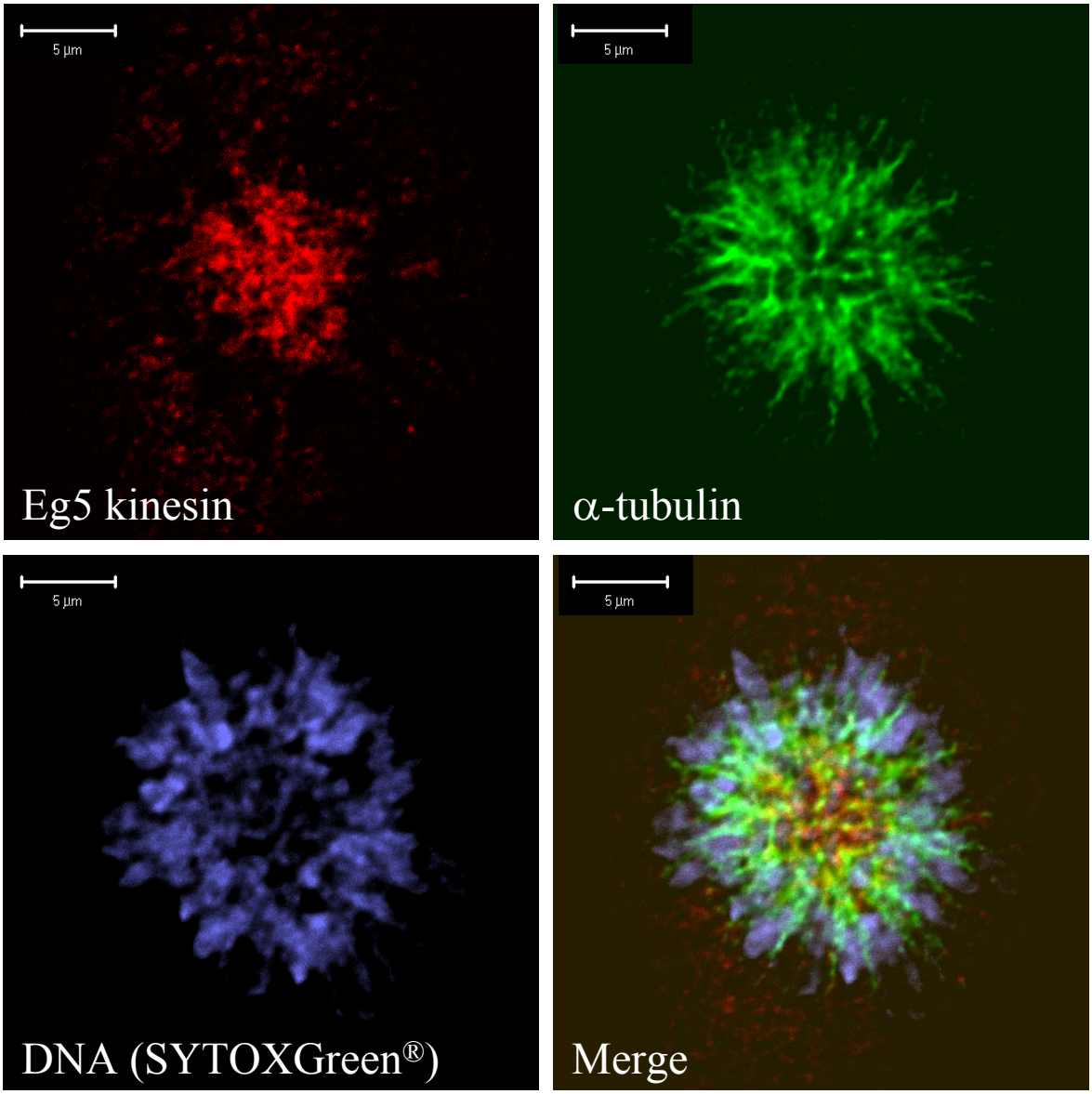

Figure 5-15: Mitotic U-87 MG cell after incubation with the monastrol analog MG-Pr99-S. A major portion of Eg5 is colocalized with tubulin, suggesting that the process of monaster formation does not significantly affect the connection between both proteins. Plan-Apochromat 63x/1.4 oil; Ar 488, HFT 488, LP505; .HeNe 543, HFT 488/543, LP560; HeNe 633, UV/488/543/633, LP650. Images were processed with 2-D deconvolution.

5.4.5 Effect of new monastrol derivatives on the cytoskeleton of quiescent glioblastoma cells

To investigate the effect of Eg5 inhibition on resting cells, again, human U-87 MG glioblastoma cells were incubated with selective Eg5 kinesin inhibitors. After fixation, the cells were triple stained for β-actin, microtubules, and nuclei. Untreated cells and vinblastine-treated cells were used as controls. Moreover, the cells were incubated with the non-specific kinesin inhibitor S-trityl-L-cystein.

The untreated glioblastoma cells showed a normal microtubule cytoskeleton phenotype. The microtubules formed a network throughout the cells with accumulation near the nucleus, where the centrosome, the microtubule generating and organizing center, is situated (Fig. 5-16). The β-actin cytoskeleton appeared as straight rigid fibers, arranged in a parallel manner, forming a cellular cortex (Fig. 5-16). As becomes obvious from the images, the β-actin cytoskeleton contributes to the cellular shape and expansion. The treatment with vinblastine disrupted the microtubule-system, and led to a characteristic appearance in the fluorescence image (Fig. 5-17). The cells lost their typical polygonal shape, and no intact microtubules, but small microtubule fragments were observed. However, the β-actin remained unchanged, showing the fiber clusters. The non-specific inhibition of kinesin motors by S-trityl-L-cysteine had no detectable effect, neither on the microtubules nor on the β-actin fibers (Fig. 5-18). The characteristic cell shape was maintained, and compared to the untreated cells (Fig. 5-16) no differences were observed. This kinesin inhibition may harm the treated cells in the long run, e.g. by blocking cellular transport processes. However, according to the intact cytoskeleton, an acute toxicity against non-mitotic cells was not observed. After incubation with the selective Eg5 kinesin inhibitors, exemplarily shown for dimethylenastron (MG-Pr98-S), no cytoskeletal damage was observed (Fig. 5-19).

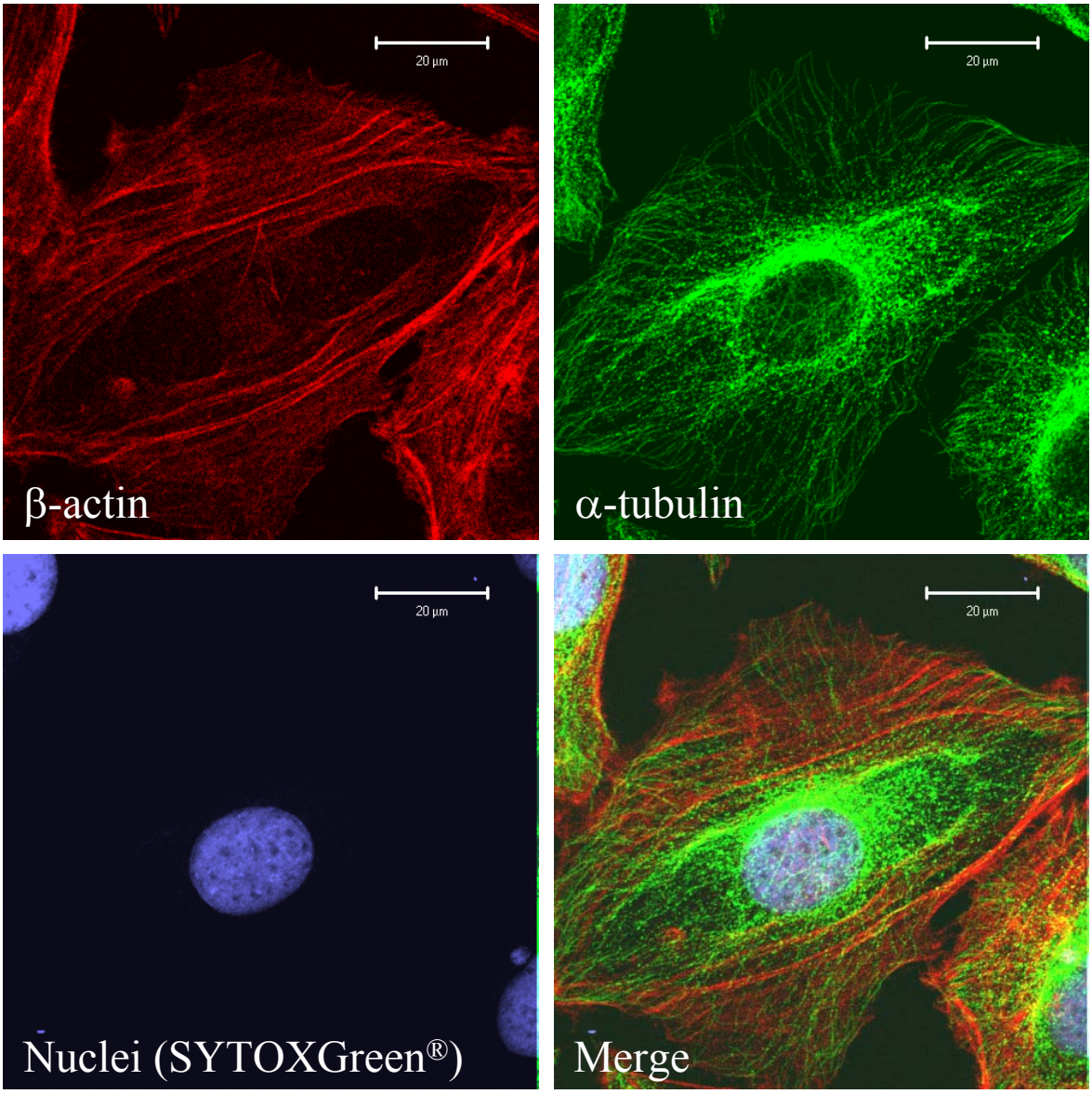

Figure 5-16: Multifluorescence image of fixed U-87 MG cells. The polygonal appearance of the cells, grown as a monolayer culture, is primarily coined by β-actin fiber clusters. The cytoplasm is spanned by the microtubule network, originating from the centrosome close to the nucleus. The image represents the bottom z-plane, in which the cell foots onto the microscopic slide. This explains the localization of a few microtubules within the nucleus. Plan-Apochromat 63x/1.4 oil; Ar 488, HFT 488, LP505; .HeNe 543, HFT 488/543, LP560; HeNe 633, UV/488/543/633, LP650.

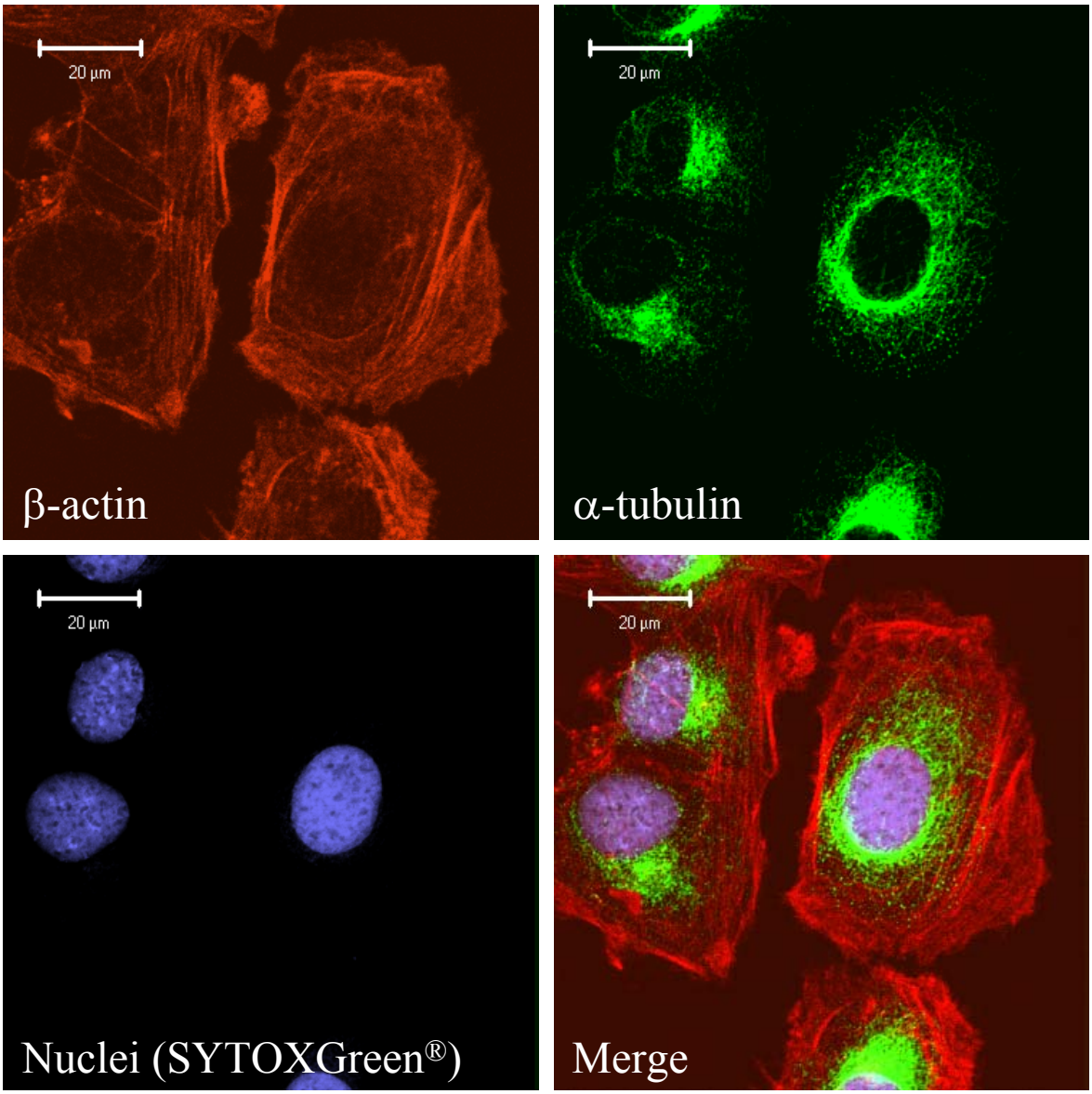

Figure 5-17: U-87 MG cells after incubation with the microtubule-destabilizing agent vinblastine. Although the microtubules are almost quantitatively disrupted, the cellular expansion is maintained, since the β-actin fibers are not affected by vinblastine. Plan-Apochromat 63x/1.4 oil; Ar 488, HFT 488, LP505; .HeNe 543, HFT 488/543, LP560; HeNe 633, UV/488/543/633, LP650.

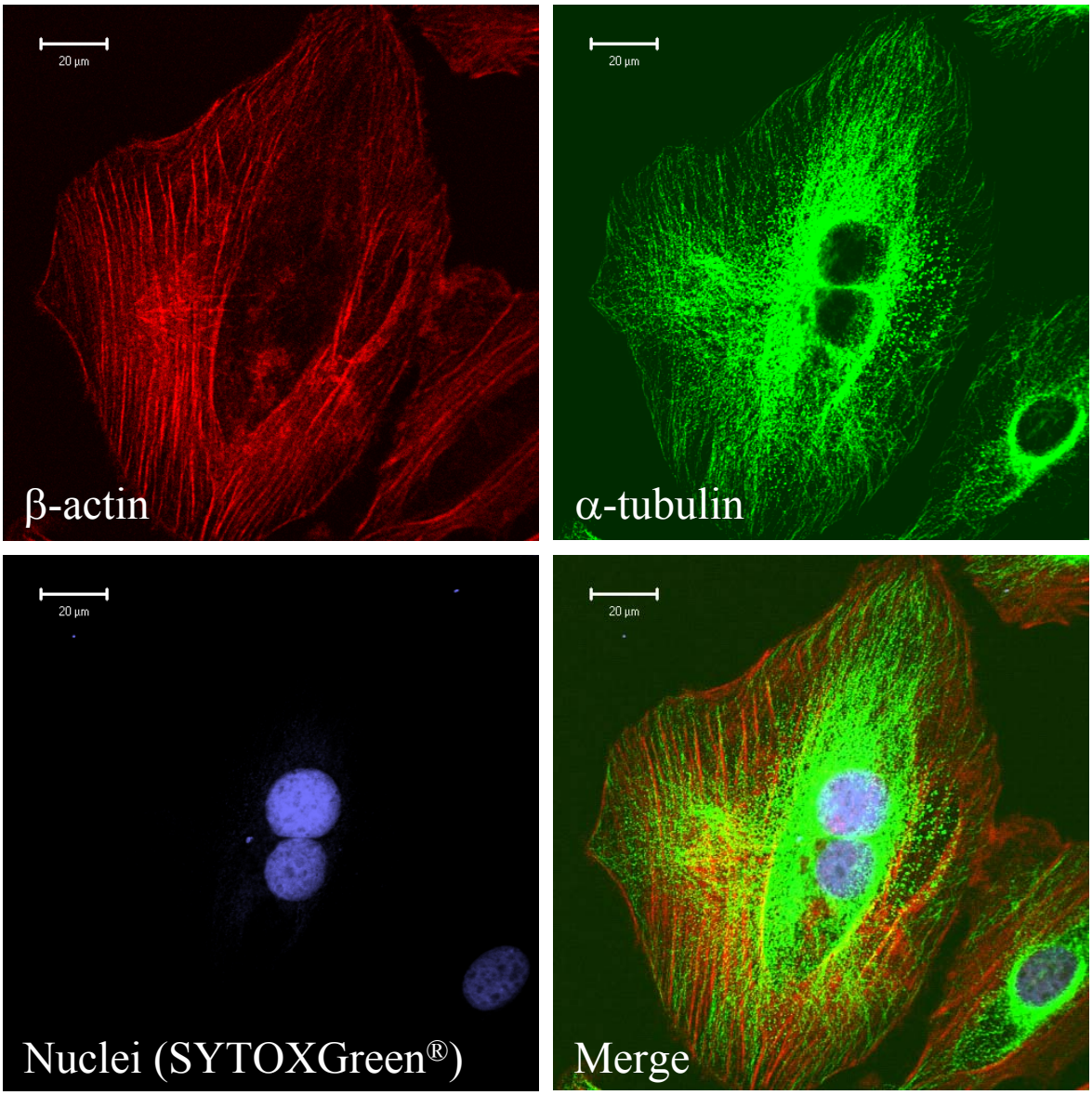

Figure 5-18: Human U-87 MG glioblastoma cells, incubated with the non-specific kinesin inhibitor S-trityl-L-cystein. The microtubule dynamics appear to be unaffected, as well as the β-actin cytoskeleton. Again, the image represents a plane near the cell footing on the microscopic slide. Plan-Apochromat 63x/1.4 oil; Ar 488, HFT 488, LP505; .HeNe 543, HFT 488/543, LP560; HeNe 633, UV/488/543/633, LP650.

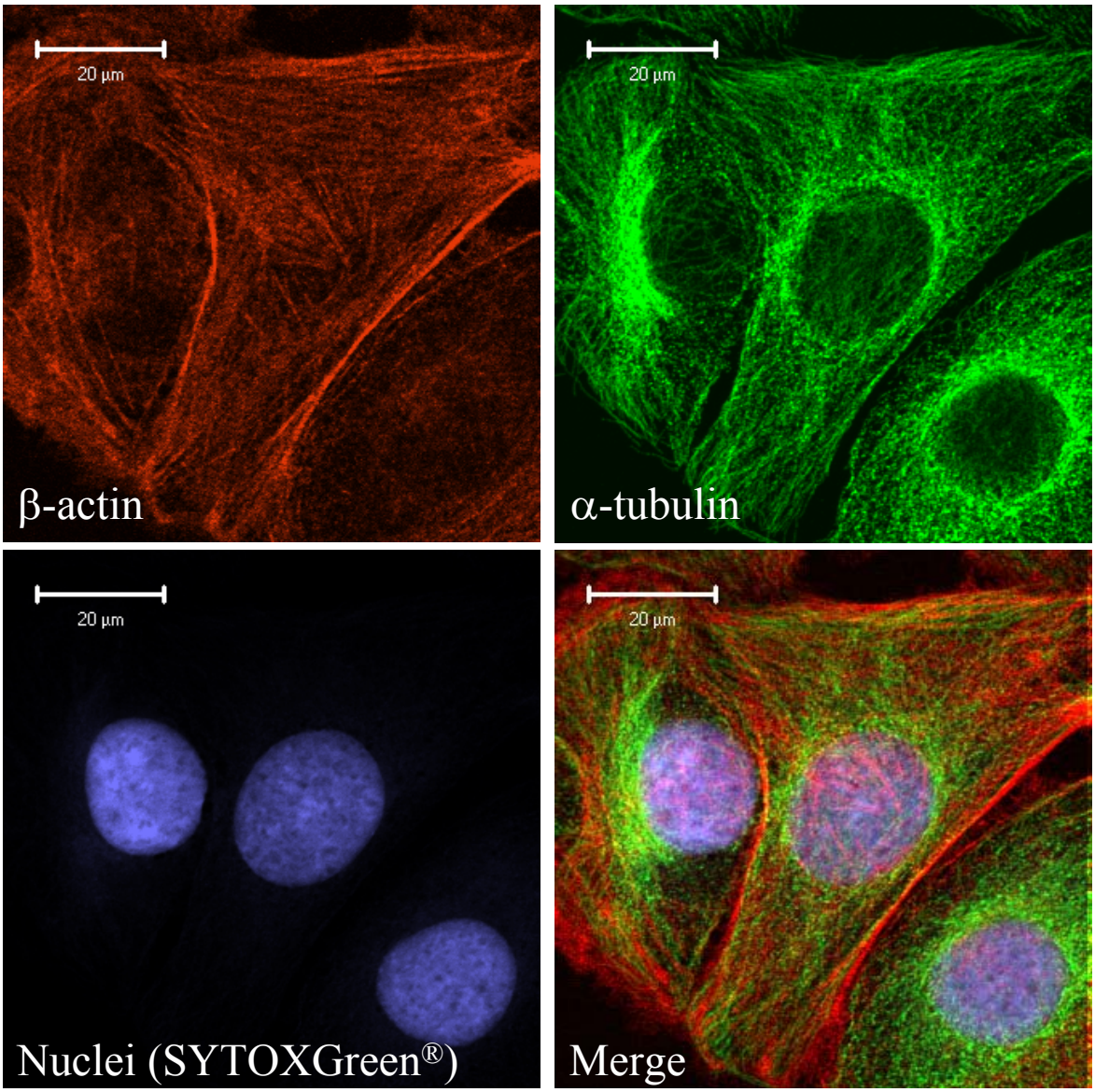

Figure 5-19: Incubation of human glioblastoma cells with the selective Eg5 kinesin inhibitor dimethylenastron (MG-Pr98-S). As observed in untreated cells and in cells treated with S-trityl-L-cystein, both, microtubules and β-actin remained unchanged. Plan-Apochromat 63x/1.4 oil; Ar 488, HFT 488, LP505; .HeNe 543, HFT 488/543, LP560; HeNe 633, UV/488/543/633, LP650.

5.5 Discussion

Effect of new monastrol analogs on the spindle formation in human U-87 MG glioblastoma cells.

The formation of the characteristic monaster spindle was demonstrated in human U-87 MG glioblastoma cells after incubation with the first identified specific Eg5 kinesin inhibitor monastrol (Fig. 5-8). Compared to tubulin-destabilizing agents, such as vinblastine (Fig. 5-8), the microtubule spindle fibers were shown to remain unaffected from treatment with monastrol (Fig. 5-8). According to the results of the chemosensitivity tests (Müller et al. 2006), human U-87 MG cells were incubated with the respective inhibitory concentrations of the new monastrol analogs. Except for VS-17 and VS-48, all compounds produced the same characteristic effect on the formation of the mitotic spindle, as the selective Eg5 kinesin inhibitor monastrol (Fig. 5-9). However, compared to the lead compound, the new monastrol analogs were more potent, and induced monasters at lower concentrations, confirming the observations in other cell types (Gartner et al. 2005). A monaster phenotype, distinctly different from the monastrol-induced monaster spindle, was observed after incubation with VS-83. This phenotype was similar to monaster formation induced by the non-selective kinesin inhibitor S-trityl-L-cysteine (Fig. 5-9). This observation is in contrast to the work of Sarli et al., reporting on similar effects of monastrol and VS-83 (Sarli et al. 2005). However, Sarli et al. applied 100 µM monastrol and 25 µM VS-83 to synchronized simian BSC-1 cells. In addition, the BSC-1 cells were treated for 10 hours, whereas the human U-87 MG glioblastoma cells were treated with monastrol (50 µM) and VS-83 (5 µM) for 2 hours.

Expression and distribution of Eg5-related kinesin in human glioblastoma cells.

Although being described as a mitotic kinesin (Sharp et al. 2000; Wood et al. 2001), the expression of Eg5 was observed in mitotic as well as in non-mitotic human U-87 MG glioblastoma cells. The motor protein was distributed all over the cytoplasm, forming dot-like clusters, without being quantitatively colocalized with the microtubule cytoskeleton (Fig. 5-10). The Eg5 expression level was observed to be much higher in mitotic than in resting cells (Fig. 5-13).

Compared to untreated cells, the incubation with vinblastine and selective Eg5 inhibitors (new monastrol analogs) did not alter the Eg5 distribution in quiescent cells (Fig. 5-10, 5-12, 5-14). In mitotic cells Eg5 was colocalized with overlap microtubules in untreated cells, and remained colocalized with tubulin after treatment with Eg5 inhibiting compounds (Fig 5-11,

5-15). Only partial colocalization in mitotic cells was observed after treatment with vinblastine, and Eg5 clusters were not observed any more (Fig. 5-13).

Effect of new monastrol analogs on the cytoskeleton of human glioblastoma cells.
The specific Eg5 inhibitors and the non-specific kinesin inhibitor S-trityl-L-cystein, neither did affect the β-actin cytoskeleton, nor did they disrupt the microtubule system in quiescent cells (Fig. 5-18, 5-19). These effects were compared to untreated cells (Fig. 5-16), and to the treatment of cells with vinblastine, which resulted in a major disruption of the microtubule structure, with an uprounding effect on the cell shape (Fig. 5-17). As expected, vinblastine treatment had no effect on the β-actin fibers (Fig. 5-17).

5.6 Summary

In summary, these results show, that in human U-87 MG glioblastoma cells, the newly synthesized monastrol analogs VS-38, VS-54, VS-83, enastron, and dimethylenastron induce the characteristic monaster spindle formation with higher potency, compared to the first selective small molecule Eg5 kinesin inhibitor monastrol. This supports the results from the chemosensitivity experiments (Müller et al. 2006), where the new monastrol analogs exhibited antiproliferative activity against human glioblastoma cells. The compounds gave rise to mitotic arrest in human glioblastoma cells by inducing the formation of monaster spindles, the characteristic effect of the specific Eg5 kinesin inhibition.

The microscopic investigations on the effect of the new monastrol analogs on the microtubules and on β-actin (cytoskeleton) of resting cells further support the results from the cytotoxicity assays. Compared to the antimicrotubular agent paclitaxel, the monastrol analogs lacked a cytocidal effect on the cells. As the monastrol analogs have been demonstrated to be neither substrates nor modulators of the multi-drug resistance p-glycoprotein 170 (Müller et al. 2006), these new Eg5 kinesin inhibitors not only are supposed to be less neurotoxic anticancer drugs in comparison to classical tubulin inhibitors, but also may be promising new agents for further preclinical studies, aiming at the treatment of primary and secondary CNS tumors.

Bibliography

Abrieu A, Kahana J A, Wood K W and Cleveland D W (2000). CENP-E as an essential component of the mitotic checkpoint in vitro. *Cell* **102**: 817-26.

Ahmad F J, Yu W, McNally F J and Baas P W (1999). An essential role for katanin in severing microtubules in the neuron. *J Cell Biol* **145**: 305-15.

Altmann K H, Wartmann M and O'Reilly T (2000). Epothilones and related structures--a new class of microtubule inhibitors with potent in vivo antitumor activity. *Biochim Biophys Acta* **1470**: M79-91.

Andersen S S (2000). Spindle assembly and the art of regulating microtubule dynamics by MAPs and Stathmin/Op18. *Trends Cell Biol* **10**: 261-7.

Bailly E and Bornens M (1992). Cell biology. Centrosome and cell division. *Nature* **355**: 300-1.

Beckman G, Beckman L, Ponten J and Westermark B (1971). G-6-PD and PGM phenotypes of 16 continuous human tumor cell lines. Evidence against cross-contamination and contamination by HeLa cells. *Hum Hered* **21**: 238-41.

Bernhardt G, Reile H, Birnbock H, Spruss T and Schonenberger H (1992). Standardized kinetic microassay to quantify differential chemosensitivity on the basis of proliferative activity. *J Cancer Res Clin Oncol* **118**: 35-43.

Blangy A, Lane H A, d'Herin P, Harper M, Kress M and Nigg E A (1995). Phosphorylation by p34cdc2 regulates spindle association of human Eg5, a kinesin-related motor essential for bipolar spindle formation in vivo. *Cell* **83**: 1159-69.

Bosch I and Croop J (1996). P-glycoprotein multidrug resistance and cancer. *Biochim Biophys Acta* **1288**: F37-54.

Brier S, Lemaire D, Debonis S, Forest E and Kozielski F (2004). Identification of the protein binding region of S-trityl-L-cysteine, a new potent inhibitor of the mitotic kinesin Eg5. *Biochemistry* **43**: 13072-82.

Brown K D, Coulson R M, Yen T J and Cleveland D W (1994). Cyclin-like accumulation and loss of the putative kinetochore motor CENP-E results from coupling continuous synthesis with specific degradation at the end of mitosis. *J Cell Biol* **125**: 1303-12.

Chan G K, Schaar B T and Yen T J (1998). Characterization of the kinetochore binding domain of CENP-E reveals interactions with the kinetochore proteins CENP-F and hBUBR1. *J Cell Biol* **143**: 49-63.

Desai A and Mitchison T J (1997). Microtubule polymerization dynamics. *Annu Rev Cell Dev Biol* **13**: 83-117.

Drechsel D N, Hyman A A, Cobb M H and Kirschner M W (1992). Modulation of the dynamic instability of tubulin assembly by the microtubule-associated protein tau. *Mol Biol Cell* **3**: 1141-54.

Funabiki H and Murray A W (2000). The Xenopus chromokinesin Xkid is essential for metaphase chromosome alignment and must be degraded to allow anaphase chromosome movement. *Cell* **102**: 411-24.

Gartner M, Sunder-Plassmann N, Seiler J, Utz M, Vernos I, Surrey T and Giannis A (2005). Development and biological evaluation of potent and specific inhibitors of mitotic Kinesin Eg5. *Chembiochem* **6**: 1173-7.

Gelmon K A, Latreille J, Tolcher A, Genier L, Fisher B, Forand D, D'Aloisio S, Vernillet L, Daigneault L, Lebecq A, Besenval M and Eisenhauer E (2000). Phase I dose-finding study of a new taxane, RPR 109881A, administered as a one-hour intravenous infusion days 1 and 8 to patients with advanced solid tumors. *J Clin Oncol* **18**: 4098-108.

Hamel E, Sackett D L, Vourloumis D and Nicolaou K C (1999). The coral-derived natural products eleutherobin and sarcodictyins A and B: effects on the assembly of purified tubulin with and without microtubule-associated proteins and binding at the polymer taxoid site. *Biochemistry* **38**: 5490-8.

Hay R J (1988). The seed stock concept and quality control for cell lines. *Anal Biochem* **171**: 225-37.

Hill E, Clarke M and Barr F A (2000). The Rab6-binding kinesin, Rab6-KIFL, is required for cytokinesis. *Embo J* **19**: 5711-9.

Hollo Z, Homolya L, Davis C W and Sarkadi B (1994). Calcein accumulation as a fluorometric functional assay of the multidrug transporter. *Biochim Biophys Acta* **1191**: 384-8.

Homolya L, Hollo M, Muller M, Mechetner E B and Sarkadi B (1996). A new method for a quantitative assessment of P-glycoprotein-related multidrug resistance in tumour cells. *Br J Cancer* **73**: 849-55.

Homolya L, Hollo Z, Germann U A, Pastan I, Gottesman M M and Sarkadi B (1993). Fluorescent cellular indicators are extruded by the multidrug resistance protein. *J Biol Chem* **268**: 21493-6.

Hotha S, Yarrow J C, Yang J G, Garrett S, Renduchintala K V, Mayer T U and Kapoor T M (2003). HR22C16: a potent small-molecule probe for the dynamics of cell division. *Angew Chem Int Ed Engl* **42**: 2379-82.

Hunter J, Hirst B H and Simmons N L (1991). Epithelial secretion of vinblastine by human intestinal adenocarcinoma cell (HCT-8 and T84) layers expressing P-glycoprotein. *Br J Cancer* **64**: 437-44.

Izquierdo M A, Scheffer G L, Flens M J, Schroeijers A B, van der Valk P and Scheper R J (1996). Major vault protein LRP-related multidrug resistance. *Eur J Cancer* **32A**: 979-84.

Jordan M A and Wilson L (1998). Microtubules and actin filaments: dynamic targets for cancer chemotherapy. *Curr Opin Cell Biol* **10**: 123-30.

Kapoor T M, Mayer T U, Coughlin M L and Mitchison T J (2000). Probing spindle assembly mechanisms with monastrol, a small molecule inhibitor of the mitotic kinesin, Eg5. *J Cell Biol* **150**: 975-88.

Kohno K, Kikuchi J, Sato S, Takano H, Saburi Y, Asoh K and Kuwano M (1988). Vincristine-resistant human cancer KB cell line and increased expression of multidrug-resistance gene. *Jpn J Cancer Res* **79**: 1238-46.

Larsson N, Marklund U, Gradin H M, Brattsand G and Gullberg M (1997). Control of microtubule dynamics by oncoprotein 18: dissection of the regulatory role of multisite phosphorylation during mitosis. *Mol Cell Biol* **17**: 5530-9.

Li Y and Benezra R (1996). Identification of a human mitotic checkpoint gene: hsMAD2. *Science* **274**: 246-8.

Loe D W, Deeley R G and Cole S P (1996). Biology of the multidrug resistance-associated protein, MRP. *Eur J Cancer* **32A**: 945-57.

Maliga Z, Kapoor T M and Mitchison T J (2002). Evidence that monastrol is an allosteric inhibitor of the mitotic kinesin Eg5. *Chem Biol* **9**: 989-96.

Mandelkow E and Hoenger A (1999). Structures of kinesin and kinesin-microtubule interactions. *Curr Opin Cell Biol* **11**: 34-44.

Mandelkow E and Mandelkow E M (1995). Microtubules and microtubule-associated proteins. *Curr Opin Cell Biol* **7**: 72-81.

Masson D and Kreis T E (1995). Binding of E-MAP-115 to microtubules is regulated by cell cycle-dependent phosphorylation. *J Cell Biol* **131**: 1015-24.

Mayer T U, Kapoor T M, Haggarty S J, King R W, Schreiber S L and Mitchison T J (1999). Small molecule inhibitor of mitotic spindle bipolarity identified in a phenotype-based screen. *Science* **286**: 971-4.

McDaid H M, Bhattacharya S K, Chen X T, He L, Shen H J, Gutteridge C E, Horwitz S B and Danishefsky S J (1999). Structure-activity profiles of eleutherobin analogs and their cross-resistance in Taxol-resistant cell lines. *Cancer Chemother Pharmacol* **44**: 131-7.

McNally F J and Vale R D (1993). Identification of katanin, an ATPase that severs and disassembles stable microtubules. *Cell* **75**: 419-29.

Mitchison T and Kirschner M (1984). Dynamic instability of microtubule growth. *Nature* **312**: 237-42.

Mollinedo F and Gajate C (2003). Microtubules, microtubule-interfering agents and apoptosis. *Apoptosis* **8**: 413-50.

Müller C, Gross D, Sarli V, Gartner M, Giannis A, Bernhardt G and Buschauer A (2006). Inhibitors of kinesin Eg5: antiproliferative activity of monastrol analogues against human glioblastoma cells. *Cancer Chemother Pharmacol*.

Nakazawa J, Yajima J, Usui T, Ueki M, Takatsuki A, Imoto M, Toyoshima Y Y and Osada H (2003). A novel action of terpendole E on the motor activity of mitotic Kinesin Eg5. *Chem Biol* **10**: 131-7.

Noda Y, Okada Y, Saito N, Setou M, Xu Y, Zhang Z and Hirokawa N (2001). KIFC3, a microtubule minus end-directed motor for the apical transport of annexin XIIIb-associated Triton-insoluble membranes. *J Cell Biol* **155**: 77-88.

Ookata K, Hisanaga S, Bulinski J C, Murofushi H, Aizawa H, Itoh T J, Hotani H, Okumura E, Tachibana K and Kishimoto T (1995). Cyclin B interaction with microtubule-associated protein 4 (MAP4) targets p34cdc2 kinase to microtubules and is a potential regulator of M-phase microtubule dynamics. *J Cell Biol* **128**: 849-62.

Palmer C G, Livengood D, Warren A K, Simpson P J and Johnson I S (1960). The action of the vincaleukolastine on mitosis in vitro. *Exp Cell Res* **20**: 198-201.

Polizzi D, Pratesi G, Tortoreto M, Supino R, Riva A, Bombardelli E and Zunino F (1999). A novel taxane with improved tolerability and therapeutic activity in a panel of human tumor xenografts. *Cancer Res* **59**: 1036-40.

Quasthoff S and Hartung H P (2002). Chemotherapy-induced peripheral neuropathy. *J Neurol* **249**: 9-17.

Rudner A D and Murray A W (1996). The spindle assembly checkpoint. *Curr Opin Cell Biol* **8**: 773-80.

Sakowicz R, Berdelis M S, Ray K, Blackburn C L, Hopmann C, Faulkner D J and Goldstein L S (1998). A marine natural product inhibitor of kinesin motors. *Science* **280**: 292-5.

Sakowicz R, Finer J T, Beraud C, Crompton A, Lewis E, Fritsch A, Lee Y, Mak J, Moody R, Turincio R, Chabala J C, Gonzales P, Roth S, Weitman S and Wood K W (2004). Antitumor activity of a kinesin inhibitor. *Cancer Res* **64**: 3276-80.

Sarli V, Huemmer S, Sunder-Plassmann N, Mayer T U and Giannis A (2005). Synthesis and biological evaluation of novel EG5 inhibitors. *Chembiochem* **6**: 2005-13.

Schaar B T, Chan G K, Maddox P, Salmon E D and Yen T J (1997). CENP-E function at kinetochores is essential for chromosome alignment. *J Cell Biol* **139**: 1373-82.

Schiff P B, Fant J and Horwitz S B (1979). Promotion of microtubule assembly in vitro by taxol. *Nature* **277**: 665-7.

Schiff P B and Horwitz S B (1980). Taxol stabilizes microtubules in mouse fibroblast cells. *Proc Natl Acad Sci U S A* **77**: 1561-5.

Shannon K B and Salmon E D (2002). Chromosome dynamics: new light on Aurora B kinase function. *Curr Biol* **12**: R458-60.

Sharp D J, Rogers G C and Scholey J M (2000). Microtubule motors in mitosis. *Nature* **407**: 41-7.

Skoufias D A, Andreassen P R, Lacroix F B, Wilson L and Margolis R L (2001). Mammalian mad2 and bub1/bubR1 recognize distinct spindle-attachment and kinetochore-tension checkpoints. *Proc Natl Acad Sci U S A* **98**: 4492-7.

Sorger P K, Dobles M, Tournebize R and Hyman A A (1997). Coupling cell division and cell death to microtubule dynamics. *Curr Opin Cell Biol* **9**: 807-14.

Sunder-Plassmann N, Sarli V, Gartner M, Utz M, Seiler J, Huemmer S, Mayer T U, Surrey T and Giannis A (2005). Synthesis and biological evaluation of new tetrahydro-beta-carbolines as inhibitors of the mitotic kinesin Eg5. *Bioorg Med Chem* **13**: 6094-111.

Tao W, South V J, Zhang Y, Davide J P, Farrell L, Kohl N E, Sepp-Lorenzino L and Lobell R B (2005). Induction of apoptosis by an inhibitor of the mitotic kinesin KSP requires both activation of the spindle assembly checkpoint and mitotic slippage. *Cancer Cell* **8**: 49-59.

Vale R D and Fletterick R J (1997). The design plan of kinesin motors. *Annu Rev Cell Dev Biol* **13**: 745-77.

Walczak C E, Mitchison T J and Desai A (1996). XKCM1: a Xenopus kinesin-related protein that regulates microtubule dynamics during mitotic spindle assembly. *Cell* **84**: 37-47.

Walker R A, O'Brien E T, Pryer N K, Soboeiro M F, Voter W A, Erickson H P and Salmon E D (1988). Dynamic instability of individual microtubules analyzed by video light microscopy: rate constants and transition frequencies. *J Cell Biol* **107**: 1437-48.

Wood K W, Cornwell W D and Jackson J R (2001). Past and future of the mitotic spindle as an oncology target. *Curr Opin Pharmacol* **1**: 370-7.

Xu Y, Takeda S, Nakata T, Noda Y, Tanaka Y and Hirokawa N (2002). Role of KIFC3 motor protein in Golgi positioning and integration. *J Cell Biol* **158**: 293-303.

Yao X, Abrieu A, Zheng Y, Sullivan K F and Cleveland D W (2000). CENP-E forms a link between attachment of spindle microtubules to kinetochores and the mitotic checkpoint. *Nat Cell Biol* **2**: 484-91.

Zacherl J, Hamilton G, Thalhammer T, Riegler M, Cosentini E P, Ellinger A, Bischof G, Schweitzer M, Teleky B, Koperna T and et al. (1994). Inhibition of P-glycoprotein-mediated vinblastine transport across HCT-8 intestinal carcinoma monolayers by verapamil, cyclosporine A and SDZ PSC 833 in dependence on extracellular pH. *Cancer Chemother Pharmacol* **34**: 125-32.

Chapter 6

Summary

The treatment of malignant brain tumors poses a basic challenge in todays cancer therapy. Since the quantitative resection is hardly possible due to the invasive growth of the tumor, prevention of relapse after resection by concomitant irradiation treatment and chemotherapy is of major importance for patient outcome. While the efficiency of surgery and irradiation therapy seem to be exploited, new approaches in the chemotherapy may provide hope for the future. Amongst them are the exploration of new transport pathways across the blood-brain barrier and the overcome of the p-glycoprotein (pgp)-mediated multi-drug resistance, respectively, and the evaluation of new pharmacological targets, allowing selective inhibition of tumor growth, while minimizing cytotoxic side effects.

The objective of this work was to investigate, whether doxorubicin-loaded polybutylcyanoacrylate (PBCA) nanoparticles are able to provide overcome of the pgp-mediated multi-drug resistance in vitro, and to investigate the mechanism of the enhanced antiproliferative activity of doxorubicin nanoparticles, compared to the efficiency of the drug in solution. The doxorubicin nanoparticle formulations exceeded the antiproliferative effect of the dissolved drug against pgp-overexpressing KBv1 cells. The flow cytometric determination of the cell-associated doxorubicin fluorescence after incubation with the different drug formulations indicated an enhanced drug uptake with the nanoparticle formulations in pgp-negative human glioblastoma cells as well as in KBwt cells with weak pgp expression. No differential fluorescence increase was observed in pgp-overexpressing KBv1 cells at a drug concentration equivalent 500 nM doxorubicin, but at a concentration of 2 µM doxorubicin KBv1 cells showed increased fluorescence after incubation with nanoparticle-bound doxorubicin. Confocal laser-scanning microscopic studies with living KBwt cells showed

similar cytoplasmic doxorubicin distribution after incubation with different doxorubicin formulations. A higher overall doxorubicin–related fluorescence was observed after incubation with the nanoparticle-bound drug, and the cells were hemmed by doxorubicin fluorescence. With a mixture of empty PBCA nanoparticles and lucifer yellow, pgp-negative U-373 MG were hemmed by lucifer yellow derived fluorescence. The results from CLSM studies indicate that the nanoparticles do not enter the cells. In conclusion, the enhanced antiproliferative effect of the nanoparticle-bound doxorubicin against pgp-overexpressing cells can be explained by a concentration gradient of drug, released from nanoparticles after adsorption to the cell surface, leading to saturation and overcome of the pgp-mediated drug efflux transport.

As a non-cytotoxic approach in the chemotherapy of malignant glioblastoma, the concept of platelet-derived growth factor (PDGF) receptor kinase inhibition was evaluated as the second part of this work. Therefore the PDGF receptor expression and activity were demonstrated in human glioblastoma cell lines. However, the inhibition of PDGF receptors in human glioblastoma cells, using various selective PDGF receptor kinase inhibitors, amongst them the registered drug imatinib, did not affect cell growth in therapeutically relevant concentrations. Moreover, no enhanced cytotoxicity was observed when imatinib was combined with the microtubule-interfering agent paclitaxel. Furthermore, the cells lacked expression of the resistance proteins pgp and breast cancer resistance protein (bcrp), demonstrating that lack of antiproliferative activity of the PDGF receptor inhibitors cannot be ascribed to these drug resistance mechanisms. Moreover glioblastoma cell proliferation was independent of PDGF. These results suggest that the single PDGF receptor inhibition by selective tyrosine kinase inhibitors, including imatinib, does not represent a suitable approach in the treatment of glioblastoma.

The selective inhibition of the Eg5 kinesin by small molecule inhibitors such as monastrol is currently preclinically evaluated as a new approach to the treatment of malignant tumors. However, the potency of the first identified selective Eg5 inhibitor monastrol is rather low. Several new monastrol analogs exhibited higher antiproliferative activity against human glioblastoma cells. In the last part of this work the effects of these new monastrol analogs on the spindle formation and the cytoskeleton of mitotic and quiescent glioblastoma cells were evaluated by confocal laser-scanning microscopy. Except for the two compounds VS-17 and VS-48 all other tested compounds led to the characteristic monoaster spindle formation with a potency of at least one order of magnitude higher than that of monastrol. Although the expression of the Eg5 kinesin in the human glioblastoma cells was not limited to the mitosis

phase, the microtubule and actin cytoskeleton remained unaffected by the new compounds, also in non-dividing cells.. These results support the hypothesis that selective Eg5 inhibitors may represent an interesting class of potential anticancer drugs, predicted to exhibit less cytotoxic side effects in comparison to classical tubulin inhibitors.

Abbreviations

ABCB1	ATP binding cassette B1
ABCG2	ATP binding cassette G2
ACE	automatic component extraction
AM	acetoxymethylester
Amp	ampicillin
APC	anaphase promoting complex
ATCC	American Type Culture Collection
ATP	adenosine triphosphate
AUC	area under the curve
BBB	blood-brain barrier
BCNU	carmustine
bcrp	breast cancer resistance protein
BCSFB	blood-cerebrospinal fluid barrier
bFGF	basic fibroblast growth factor
bp	base pairs
BP	bandpass filter
BSA	bovine serum albumin
Bub	budding uninhibited by benzimidazole
CCNU	lomustine
cDNA	complementary DNA
CDK	cycline-dependent kinase
c-KIT	cytosolic Hardy-Zuckerman 4 feline sarcoma viral oncogene homolog
CLSM	confocal laser-scanning microscopy
cm	cytoplasmic membrane
C_{max}	maximal plasma concentration
CML	chronic myelogenous leukemia
CS	citrate buffered saline
CSF-1	colony stimulating factor 1
CNS	central nervous system
Cy5	cyanine 5
Da	dalton
DEPC	diethyl pyrocarbonate
DMEM	Dulbecco´s modified Eagle medium
DMSO	dimethylsulfoxide
DNA	desoxyribonucleic acid
DoxoNP	doxorubicin-loaded nanoparticles
DoxoNPT80	polysorbate 80-coated DoxoNP
ECFP	enhanced cyan fluorescent protein
EGFP	enhanced green fluorescent protein
EDTA	ethylenediaminetetraacetic acid
EEG	electroencephalogram
EGFR	epidermal growth factor receptor
EMEM	Eagles minimum essential medium
ER	endoplasmic reticulum
FCS	fetal calf serum
FITC	fluorescein-5-isothiocyanate
G418	geneticin

GAP	GTPase activating protein
GDP	guanosine diphosphate
GIST	gastrointestinal stroma tumors
Grb2	growth factor receptor-bound protein 2
GTP	guanosine triphosphate
Gy	Gray
HAMs F12	Ham's nutrient mixture F-12
HEPES	N-(2-hydroxyethyl)piperazine-N´-(2-ethanesulfonic acid)
HER-2/c-ErB-2	erythroblastic leukemia cytosolic oncogene homolog 2
HFT	Hauptfarbteiler (main dichroic beam splitter)
HPLC	high performance liquid chromatography
IC_{50}	concentration of inhibitor required to give a 50 % inhibition of activity
IP3	inositol-1,4,5-trisphosphate
Kan	kanamycin
L15	Leibovitz L15 medium
LB	Luria Bertani broth
LDL	low density lipoprotein
LOH	loss of heterozygosity
LP	longpass filter
LY-CH	lucifer yellow carbohydrazide
MAB	monoclonal antibody
MAD	mitosis arrest deficient
MAP	mitogen activated protein kinase
MCS	multiple cloning site
MDM2	murine double minute 2
MGMT	O^6-methylguanine-DNA methyltransferase
M-MLV	moloney murine leukemia virus
mRNA	messenger RNA
MRP	multi-drug resistance-associated protein
MTT	3-(4,5-Dimethylthiazol-2-yl)-2,2-diphenyl-tetrazolium bromide
NADH	1,4-dihydronicotinamide adenine dinucleotide
NCBI	National Center for Biotechnology Information
Neo	neomycin
NFT	Nebenfarbteiler (secondary dichroic beam splitter)
NGF	nerve growth factor
NMDA	N-methyl-D-aspartic acid
NP	nanoparticles
nuc	nucleus
O6BG	O^6-benzylguanine
PBCA	polybutylcyanoacrylate
PBS	phosphate buffered saline
PDGF	platelet-derived growth factor
PDGFR	PDGF receptor
PFA	paraformaldehyde
PFS	progression-free survival
PKC	protein kinase C
PLC	phospholipase C
pgp	p-glycoprotein 170
pH	negative logarithm of the hydrogen ion concentration
Ph. Eur. 1997	European Pharmacopoeia 1997
PIP2	phosphatidylinositol-4,5-bisphosphate

PLGA	poly(lactid-co-glycolid)
$P_{o/w}$	octanol-water partition coefficient
PSC 833	valspodar
PTEN	phosphate and tensin homolog
Pur	puromycin
Raf	Raf protein kinase
Ras	Ras protein kinase
RES	reticuloendothelial system
rhPDGF	recombinant human PDGF
RNA	ribonucleic acid
RPMI-1640	Rosswell Park Memorial Institute-1640 medium
RT-PCR	reverse transcription-polymerase chain reaction
SCF	stem cell factor
SEM	scanning electron microscopy
SH2	Src homology 2 domain
Src	Src kinase (from v-src “viral sarcoma”)
SOC	salt optimized + carbon medium
SOS	son of sevenless
SRS	stereotactic radiosurgery
SSV	simian sarcoma virus
Taq-polymerase	*Thermus aquaticus* polymerase
TBE	tris-borat-EDTA-buffer
TGF-β	transforming growth factor beta
Topo	topotecan
TP53	tumor protein p53
UDP	uridin-5´-diphosphate
UV-vis	ultraviolet-visible
VEGF	vascular endothelial growth factor
WHO	World Health Organization
XKCM1	*Xenopus* kinesin central motor 1